

Adsorbents for the Removal of Naphthenic Acids from Oil Sands Process Water:  
Investigation of Reclamation Materials from Surface Mining of Oil Sands and  
Development of Biochars from Biological Sludge and Peat

by

Deborah Cristina Crominski da Silva Medeiros

A thesis submitted in partial fulfillment of the requirements for the degree of

Doctor of Philosophy  
in  
Environmental Engineering

Department of Civil and Environmental Engineering  
University of Alberta

## ABSTRACT

Oil sands process water (OSPW) is generated in high quantities during the extraction of the bitumen from the oil sands. Naphthenic acids (NAs) are recalcitrant compounds, corresponding more than 50% of all organics in OSPW. The efficient management of OSPW is of importance to guarantee efficient water reuse or safe discharge of OSPW to compel with the aggressive timeline on OSPW reclamation. This thesis investigates the adsorption NAs from OSPW using two types of materials: (1) reclamation materials from the surface mining of oil sands and (2) biochars produced from sludge (municipal wastewater treatment plant) and peat (surface mining of oil sands).

The reclamation materials peat-mineral mix (PT) and Pleistocene fluvial sands from different locations (PF-1 and PF-2) were investigated as adsorbents of decanoic acid (DA) and 5-phenylvaleric acid (PVA) as model NA compounds. Equilibrium of DA and PVA was reached at 2 days for PT, and 3 and 6 days for PF materials, respectively. Maximum adsorption capacities for DA and PVA were, respectively,  $16.8 \times 10^3$  and  $10^4$  mg kg<sup>-1</sup> for PT, 142.9 and 81.3 mg kg<sup>-1</sup> for PF-1, and 600 and 476.2 mg kg<sup>-1</sup> for PF-2. Hydrophobic interactions, hydrogen bonding, and  $\pi$ - $\pi$  interaction were the main adsorption mechanisms. Desorption of model compounds from post-adsorption materials was not observed for 14 days. Removal of NAs from real OSPW ranged from 20 to 54%. PT is the most promising adsorbent of NAs from OSPW because it partially removed NAs with a wide range of molecular weights and structures at very low dosage. Adsorption of NAs was affected by the total organic carbon of the materials, emphasizing the hydrophobic interaction as an important adsorption mechanism.

Pristine and zinc chloride (ZnCl<sub>2</sub>)-activated biochars produced from sludge were applied in the adsorption of NAs in real OSPW. By using ZnCl<sub>2</sub>-activated biochar instead of pristine

biochar, the adsorption capacity for total NAs (classical and oxidized species) increased from 2.3 to 26.6 mg g<sup>-1</sup>, respectively. Abundance of mesopores and oxygen-containing surface groups made the ZnCl<sub>2</sub>-activated biochar an excellent adsorbent of NAs. The rate of adsorption of NAs from OSPW was fast, reaching equilibrium at 2 h. The adsorption followed pseudo-second order kinetics and Freundlich isotherm. The adsorption mechanisms were pore-filling, hydrogen bonding, and  $\pi$ - $\pi$  interactions. ZnCl<sub>2</sub>-activated biochar has higher affinity for higher carbon and double bond equivalency (DBE) numbers, therefore, NAs with more hydrophobic, recalcitrant, and with higher cyclic characteristics. The spent biochar can be regenerated through thermal regeneration and reused efficiently. Adsorption treatment with activated biochar decreased the concentration of magnesium (7%), calcium (21%), strontium (27%), barium (60%), dissolved organic carbon (63%), and chemical oxygen demand (66%). Reduction of 66% of the acute toxicity towards *V. fischeri* and 91% of bioavailability of organics was observed after activated biochar treatment.

The effect of type of feedstock (sludge and peat) and the chemical activation (none, FeCl<sub>3</sub>- and FeCl<sub>3</sub>+ZnCl<sub>2</sub>-activated) on the changes in the characteristics of biochar was studied for adsorption of surrogate compounds of NAs and NAs from real OSPW. Higher inorganic fraction of sludge yielded in biochars with higher ash contents than peat-based biochars. After activation, the peat-based biochars presented higher porous properties and O/C ratios than sludge-based biochars. Chemical activation of biochar resulted in the enhancement of some functional groups, such as -OH stretching group and C=C of aromatic rings. The adsorption of NAs from real OSPW was impressive and better than surrogate compounds, in which the pristine biochars removed up to 23% of total NAs. Removal of classical and oxidized NAs surpassed 90% for FeCl<sub>3</sub>+ZnCl<sub>2</sub>-activated biochars. The biochar properties were correlated with the adsorption capacities obtained

for surrogate compounds of NAs and NAs from OSPW, emphasizing the importance of the mesopore fraction of biochar and H/C ratio in the adsorption.

The study of reclamation materials as adsorbents of NAs contributes to the understanding of the mobility potential of NAs from OSPW on reclamation materials used in oil sands reclamation landscapes. The research on biochars promotes circular economy by presenting efficient adsorbents for NAs in OSPW, reducing the environmental impact associated with waste disposal and allowing the efficient reclamation and reuse of OSPW. Further studies on biochar tailoring should focus on improving the mesopore volume and balancing the hydrophobicity and aromaticity of biochar.

## PREFACE

The research presented in this thesis is an original work designed, planned, performed and interpreted by myself under the supervision of Dr. Mohamed Gamal El-Din in the Department of Civil and Environmental Engineering at the University of Alberta. I conducted the majority of the experiments, data analysis, and preparation of the manuscripts. The researchers in Dr. Gamal El-Din's Research Group also contributed to the manuscript edits and sample analysis, in which some of them were co-authors of the manuscripts submitted or prepared for submission for publication. Contributions to each chapter are detailed as follows:

- Chapter 2: A version of this chapter was published as “Medeiros, D. C. C. S., Chelme-Ayala, P., Benally, C., Al-Anzi, B. S., and Gamal El-Din, M. Review on carbon-based adsorbents from organic feedstocks for removal of organic contaminants from oil and gas industry process water: Production, adsorption performance and research gaps. *Journal of Environmental Management*, 320, 2022. <https://doi.org/10.1016/j.jenvman.2022.115739>”. Dr. Pamela Chelme-Ayala, Dr. Chelsea Benally and Dr. Bader S. Al-Anzi contributed to the manuscript revision and editing. Dr. Mohamed Gamal El-Din contributed to the research, planning, final editing, and approval of manuscript.
- Chapter 3: A version of this chapter was published as “Medeiros, D. C. C. S., Chelme-Ayala, P., and Gamal El-Din, M. Sorption and desorption of naphthenic acids on reclamation materials: Mechanisms and selectivity of naphthenic acids from oil sands process water. *Chemosphere*, 2023. <https://doi.org/10.1016/j.chemosphere.2023.138462>”. I prepared the reclamation materials, performed the experiments discussed in Chapter 3, and analyzed the data. I conducted most of the characterization experiments of the reclamation materials. Dr. Mohamed Gamal El-Din contributed to the research, planning, final editing, and approval of

manuscript. Dr. Pamela Chelme-Ayala contributed to the research, planning, manuscript revision and editing. Dr. Zuo Tong How performed the analytical measurement of NAs in the samples. X-ray diffractograms (XRD) and Fourier transform infrared spectrometry (FTIR) that were performed in the EAS X-Ray Diffraction Laboratory and Analytical and Instrumentation Laboratory of the University of Alberta. Silt, sand and clay composition, and TOC content were determined in the Natural Resources Analytical Laboratory of the University of Alberta.

- Chapter 4: A version of this chapter was published as “Medeiros, D. C. C. S., Chelme-Ayala, P., and Gamal El-Din, M. Sludge-based activated biochar for adsorption treatment of real oil sands process water: Selectivity of naphthenic acids, reusability of spent biochar, leaching potential, and acute toxicity removal. *Chemical Engineering Journal*, 493, 2023. <https://doi.org/10.1016/j.cej.2023.142329>”. I prepared the pristine and activated biochars, performed the experiments discussed in Chapter 4, and analyzed the data. I conducted most of the characterization experiments of the biochars and feedstock. Dr. Mohamed Gamal El-Din contributed to the research, planning, final editing, and approval of manuscript. Dr. Pamela Chelme-Ayala contributed to the research, planning, manuscript revision and editing. Dr. Lingling Yang conducted the analytical measurement of NAs in the OSPW samples and the bioavailability of organics in the OSPW. Ms. Foroough Mehravaran assisted in the Microtox bioassay. XRD and FTIR analysis were performed in the EAS X-Ray Diffraction Laboratory and Analytical and Instrumentation Laboratory of the University of Alberta, respectively.
- Chapter 5: A version of this chapter will be submitted to Bioresource Technology as “Medeiros, D. C. C. S., Chelme-Ayala, P., and Gamal El-Din, M. The role of feedstock type and chemical activation on biochar synthesis for the adsorption of naphthenic acids: Implications in the tailoring of activated biochars”. I prepared the biochars, performed the

experiments discussed in Chapter 5, and analyzed the data. I conducted most of the characterization experiments of the biochars and feedstocks. Dr. Mohamed Gamal El-Din contributed to the research, planning, and manuscript revision. Dr. Pamela Chelme-Ayala contributed to the research, planning, manuscript revision and editing. Dr. Lingling Yang conducted the analytical measurement of NAs in the OSPW samples and Dr. Zuo Tong How conducted the analytical measurement of model compounds of NAs. XRD and FTIR analysis were performed in the EAS X-Ray Diffraction Laboratory and Analytical and Instrumentation Laboratory of the University of Alberta, respectively.

## DEDICATION

*To my amazing husband who has never failed to cheer me up. You have been my source of strength, love, and motivation. This endeavor would not have been possible without you.*

*To my wonderful parents who worked very hard in life to provide for their daughters. You have taught me to be honest, determined, and to always persevere.*

*To my little sister who supported me through my journeys. You have always been there looking at the stars while I'm away.*



*“Not a single one of us here today has done it alone. We are each a patchwork quilt of those who have loved us, those who have believed in our futures, those who showed us empathy and kindness or told us the truth even when it wasn’t easy to hear. (...) I hope you’ll find your own way to express your gratitude for all the steps and missteps that have led us to this common destination.”*

**Taylor Swift**  
**Honorary Doctor of Fine Arts**  
Commencement Speech  
New York University, 2022

## **ACKNOWLEDGEMENTS**

First and foremost, I would like to express my gratitude to my supervisor, Dr. Mohamed Gamal El-Din, for giving me the opportunity to work on water projects under his tutelage. His invaluable guidance supported me on this journey and his challenges have led me to excel as an environmental researcher. It has been an honor to be part of his research group.

My heartfelt gratitude goes to Dr. Pamela Chelme-Ayala for her treasured word of encouragement at every stage of the research. Her endless support of the students and the staff with her knowledge and kindness inspires me. Her dedication does not go unnoticed.

I would like to thank Dr. Lingling Yang and Dr. Zuo Tong How for the numerous analytical analyses of OSPW throughout my projects. My appreciation also goes to the postdoctoral fellows and graduate students that helped me gain better understanding of the water treatment processes, especially Dr. Chelsea Benally for helping with the revision of my thesis, and Foroogh Mehravaran for her assistance in the toxicity aspects of OSPW.

I would like to acknowledge the financial support of the University of Alberta's Future Energy Systems research initiative, supported by the Canada First Research Excellence Fund, the Natural Sciences and Engineering Research Council of Canada (NSERC) Senior Industrial Research Chair (IRC) in Oil Sands Tailings Water Treatment.

Finally, I would like to express my sincere gratitude towards my family for their support on my endeavors. Thank you to my husband who always had my back and gave me strength to persevere with his infinite love, patience, and support. Thank you to my parents who had to endure the hardships of life to raise their daughters with love and utmost support. Thank you to my sister who has never failed to give me words of encouragement and love. All my accomplishments are dedicated to them.

## TABLE OF CONTENTS

<b>CHAPTER 1 INTRODUCTION AND RESEARCH OBJECTIVES</b> .....	<b>1</b>
<b>1.1 Background and Motivation</b> .....	<b>1</b>
1.1.1 Oil Sands Process Water .....	1
1.1.2 Naphthenic acids .....	2
1.1.3 OSPW treatments .....	3
<b>1.2 Research scope and objectives</b> .....	<b>5</b>
1.2.1 Study of reclamation materials from surface mining of oil sands .....	5
1.2.2 Study on activated biochars from sludge and peat .....	7
<b>1.3 Hypothesis</b> .....	<b>10</b>
<b>1.4 Thesis organization</b> .....	<b>11</b>
<b>1.5 References</b> .....	<b>12</b>
<b>CHAPTER 2 LITERATURE REVIEW</b> .....	<b>18</b>
<b>2.1 Adsorption fundamentals</b> .....	<b>18</b>
2.1.1 Physical and chemical adsorption .....	18
2.1.2 Critical parameters in adsorption.....	19
2.1.3 Adsorption kinetics.....	21
2.1.4 Adsorption isotherms.....	24
<b>2.2 Carbon-based adsorbents for adsorption of organic compounds</b> .....	<b>25</b>
2.2.1 Activated carbon and biochar definitions .....	25
2.2.2 Production of carbon-based adsorbents from biomasses to enhance adsorption of organic compounds.....	27
2.2.3 Research gaps on carbon-based adsorbents for adsorption of organic compounds.....	31
<b>2.3 Adsorbent materials for removal of naphthenic acids from OSPW</b> .....	<b>33</b>
<b>2.4 References</b> .....	<b>37</b>
<b>CHAPTER 3 INVESTIGATION OF RECLAMATION MATERIALS FROM SURFACE MINING OF OIL SANDS FOR ADORPTION OF NAPHTHENIC ACIDS</b> ...	<b>50</b>
<b>3.1 Introduction</b> .....	<b>50</b>
<b>3.2 Methodology</b> .....	<b>52</b>
3.2.1 Chemicals .....	52

3.2.2	Preparation and characterization of reclamation materials.....	53
3.2.3	Instrumentation of adsorption and desorption experiments .....	55
3.2.4	Adsorption and desorption of model compounds of NAs .....	56
3.2.5	Adsorption of classical NAs from raw OSPW .....	58
3.2.6	Data analysis.....	59
<b>3.3</b>	<b>Results and discussion .....</b>	<b>60</b>
3.3.1	Characterization of reclamation materials.....	60
3.3.2	Effect of adsorbent dosage on adsorption of model compounds of NAs .....	65
3.3.3	Adsorption kinetics.....	68
3.3.4	Adsorption equilibrium modelling .....	73
3.3.5	Adsorption mechanisms .....	77
3.3.6	Desorption of model compounds of NAs from post-adsorption reclamation materials.....	78
3.3.7	Adsorption performance of classical NAs from raw OSPW by reclamation materials: Effect of structure of NAs on adsorption.....	79
3.3.8	Evaluation of adsorption distribution coefficients .....	83
3.3.9	Effect of the properties of reclamation materials on adsorption of NAs.....	84
<b>3.4</b>	<b>Conclusions .....</b>	<b>86</b>
<b>3.5</b>	<b>References .....</b>	<b>87</b>
<b>CHAPTER 4</b>	<b>SLUDGE-BASED ACTIVATED BIOCHAR FOR ADSORPTION TREATMENT OF OIL SANDS PROCESS WATER.....</b>	<b>97</b>
<b>4.1</b>	<b>Introduction .....</b>	<b>97</b>
<b>4.2</b>	<b>Methodology.....</b>	<b>100</b>
4.2.1	OSPW, biological sludge, and chemicals.....	100
4.2.2	Biochar synthesis and characterization .....	102
4.2.3	Biochar characterization.....	103
4.2.4	Adsorption experiments.....	105
4.2.5	Regeneration and reuse of spent biochar.....	106
4.2.6	Leaching study.....	107
4.2.7	Study of acute toxicity and bioavailability of organics .....	107

<b>4.3</b>	<b>Results and discussion</b> .....	<b>108</b>
4.3.1	Properties of sludge and sludge-based biochars .....	108
4.3.2	Performance of pristine and activated biochars in the adsorption of classical and oxidized NAs from OSPW .....	117
4.3.3	Adsorption kinetics of classical NAs from raw OSPW on activated biochar: Selectivity of NAs as a function of time .....	119
4.3.1	Equilibrium modelling of classical NAs from raw OSPW on activated biochar	125
4.3.2	Adsorption mechanisms .....	128
4.3.3	Regeneration and reuse ability of spent biochar.....	130
4.3.4	Leaching of metals from activated biochar to the OSPW during treatment.....	132
4.3.5	Water quality of raw OSPW after adsorption treatment with activated biochar .	134
4.3.6	Toxicity and bioavailability of organics in OSPW after adsorption treatment with activated biochar.....	136
<b>4.4</b>	<b>Conclusions</b> .....	<b>138</b>
<b>4.5</b>	<b>References</b> .....	<b>141</b>
<b>CHAPTER 5 THE ROLE OF FEEDSTOCK TYPE AND CHEMICAL ACTIVATION ON BIOCHAR SYNTHESIS FROM SLUDGE AND PEAT FOR THE ADSORPTION OF NAPHTHENIC ACIDS .....</b>		
<b>5.1</b>	<b>Introduction</b> .....	<b>154</b>
<b>5.2</b>	<b>Methodology</b> .....	<b>156</b>
5.2.1	Chemicals and OSPW .....	156
5.2.2	Feedstock preparation.....	157
5.2.3	Biochar synthesis.....	158
5.2.4	Characterization of feedstocks and biochars .....	159
5.2.5	Adsorption experiments.....	160
5.2.6	Data analysis.....	160
<b>5.3</b>	<b>Results and discussion</b> .....	<b>161</b>
5.3.1	pH <sub>pzc</sub> , surface area and pore volume of biochars from sludge and peat.....	161
5.3.2	Proximate analysis and elemental content of biochars from sludge and peat .....	164
5.3.3	Functional surface groups and crystallinity of biochars from sludge and peat ...	168

5.3.4	Thermostability of biochars from sludge and peat .....	171
5.3.5	Adsorption performance of surrogate compounds of NAs on biochars from sludge and peat.....	173
5.3.6	Adsorption performance of NAs from raw OSPW on biochars from sludge and peat: Competitive adsorption in real process water.....	176
5.3.7	Effect of biochar properties on adsorption of NAs .....	182
<b>5.4</b>	<b>Conclusions</b> .....	<b>184</b>
<b>5.5</b>	<b>References</b> .....	<b>186</b>
<b>CHAPTER 6</b>	<b>CONCLUSIONS AND RECOMMENDATIONS</b> .....	<b>194</b>
<b>6.1</b>	<b>Thesis overview</b> .....	<b>194</b>
<b>6.2</b>	<b>Conclusions</b> .....	<b>196</b>
<b>6.3</b>	<b>Recommendations</b> .....	<b>201</b>
<b>BIBLIOGRAPHY</b> .....		<b>204</b>
<b>APPENDIX: SUPPORTING INFORMATION</b> .....		<b>237</b>
<b>Analytical methods for the measurement of model compounds of NAs in solution and classical and oxidized NAs in OSPW</b> .....		<b>237</b>
<b>Figures</b> .....		<b>238</b>
<b>Tables</b> .....		<b>250</b>

## LIST OF TABLES

<b>Table 2.1:</b> Adsorption kinetic models.....	23
<b>Table 2.2:</b> Adsorption isotherm models. ....	25
<b>Table 2.3:</b> Adsorption conditions and capacity for removal of naphthenic acids by different types of adsorbents.....	36
<b>Table 3.1:</b> Characteristics of selected model compounds of naphthenic acids.....	53
<b>Table 3.2:</b> Properties of studied reclamation materials. ....	64
<b>Table 3.3:</b> Summary of modeling kinetics parameters obtained for adsorption of model NA compounds on reclamation materials. ....	73
<b>Table 3.4:</b> Summary of modeling equilibrium parameters obtained for adsorption of model NA compounds on reclamation materials. ....	77
<b>Table 3.5:</b> Results of adsorption of classical NAs from real OSPW.....	82
<b>Table 3.6:</b> Adsorption distribution coefficients ( $K_d$ ) and adsorption distribution coefficients normalized for organic carbon ( $K_{OC}$ ) of DA, PVA and classical NAs on reclamation materials. ....	84
<b>Table 4.1:</b> Characteristics of raw OSPW.....	102
<b>Table 4.2:</b> Properties of biological sludge, pristine biochar (SB-600), and activated biochar (SB-Zn). ....	110
<b>Table 4.3:</b> Modeling kinetic parameters obtained for the adsorption of classical NAs from raw OSPW on SB-Zn. ....	125
<b>Table 4.4:</b> Modeling isotherm parameters obtained for the adsorption of classical NAs from raw OSPW on SB-Zn. ....	128
<b>Table 4.5:</b> Concentration of metals in the raw and SB-Zn-treated OSPW.....	134
<b>Table 4.6:</b> Water quality of raw OSPW and OSPW treated with SB-Zn at $2 \text{ g L}^{-1}$ for 24 h. ....	136
<b>Table 5.1:</b> Properties of model compounds of NAs. ....	157
<b>Table 5.2:</b> Surface properties of the feedstocks and their respective biochars.....	163
<b>Table 5.3:</b> Proximate, elemental composition, and atomic ratio properties of sludge and peat as feedstocks and their respective biochars. ....	167
<b>Table 5.4:</b> Adsorption conditions and capacity for removal of naphthenic acids by different types of adsorbents.....	182

<b>Table 5.5:</b> Pearson correlation coefficient between adsorption capacity ( $q_t$ values) obtained from the adsorption of model compounds of NAs and NAs in raw OSPW and physicochemical properties of pristine and activated biochars from sludge and peat. ....	184
<b>Table S1:</b> Adsorption capacity of classical NAs from raw OSPW in terms of carbon and $-Z$ numbers by the reclamation materials PT ( $5 \text{ g L}^{-1}$ ), PF-1 ( $500 \text{ g L}^{-1}$ ), and PF-2 ( $100 \text{ g L}^{-1}$ ). Adsorption conditions: Initial concentration of classical NAs in OSPW: $46.3 \text{ mg L}^{-1}$ ; contact time of 2 days for PT and 6 days for PF-1 and PF-2 materials. ....	250
<b>Table S2:</b> Pearson correlation coefficient between adsorption properties ( $K_d$ , $K_{OC}$ , $q_{max}$ , and $q_t$ values) and physicochemical properties of reclamation materials obtained from an oil sands extraction site.....	251
<b>Table S3:</b> Properties of biological sludge.....	252
<b>Table S4:</b> Summary of modeling kinetics parameters obtained for adsorption of classical NAs from raw OSPW on SB-Zn as a function of carbon and DBE numbers. ....	253



## LIST OF FIGURES

<b>Figure 1.1:</b> Research overview for reclamation materials from surface mining of oil sands.....	7
<b>Figure 1.2:</b> Research overview for development of biochars as adsorbents of NAs.....	9
<b>Figure 3.1:</b> Air-dried, crushed, and sieved (a) PEAT-1, (b) PF-1 and (c) PF-2 reclamation materials received from an oil and gas industry located in Alberta. ....	55
<b>Figure 3.2:</b> FTIR spectra of (a) PT, (b) PF-1, and (c) PF-2 materials before and after adsorption of model compounds of NAs.....	65
<b>Figure 3.3:</b> Effect of adsorbent dosage for adsorption of model NA compounds on (a) PT, (b) PF-1, and (c) PF-2 materials. Conditions: 25 mg L <sup>-1</sup> initial model NA compound concentration at pH 8.5; 48 h of contact time. ....	67
<b>Figure 3.4:</b> (a) Adsorption capacity of PT and the fittings of (b) PFO, (c) PSO, and (d) Elovich kinetic models for adsorption of model NA compounds from 30 min to 14 days of contact time using 3 and 5 g L <sup>-1</sup> PT for DA and PVA, respectively.....	70
<b>Figure 3.5:</b> (a) Adsorption capacity of PF-1 and the fittings of (b) PFO, (c) PSO, and (d) Elovich kinetic models for adsorption of model NA compounds from 30 min to 14 days of contact time using 500 g L <sup>-1</sup> PF-1.....	71
<b>Figure 3.6:</b> (a) Adsorption capacity of PF-2 and the fittings of (b) PFO, (c) PSO, and (d) Elovich kinetic models for adsorption of model NA compounds from 30 min to 14 days of contact time using 100 g L <sup>-1</sup> PF-2.....	72
<b>Figure 3.7:</b> Adsorption of model NA compounds at initial concentrations from 30 to 100 mg L <sup>-1</sup> and its respective fitting of Langmuir isotherm for the adsorbents (a,b) PT, (c,d) PF-1, and (e,f) PF-2. ....	76
<b>Figure 3.8:</b> Concentration profile of NAs depicted by (a) carbon and (b) -Z numbers in the raw OSPW and OSPW after adsorption for the contact time of 2 days for PT and 6 days for PF materials. ....	82
<b>Figure 4.1:</b> (a) FTIR spectra and (b) XPS survey spectra of biological sludge feedstock, pristine biochar (SB-600), activated biochar (SB-Zn), and SB-Zn collected after adsorption. ....	114
<b>Figure 4.2:</b> Deconvoluted C1s XPS spectra for (a) sludge, (b) SB-600, (c) SB-Zn, and (d) SB-Zn collected after adsorption. ....	115

<b>Figure 4.3:</b> Deconvoluted O1s XPS spectra for (a) sludge, (b) SB-600, (c) SB-Zn, and (d) SB-Zn collected after adsorption. ....	116
<b>Figure 4.4:</b> (a) Thermogravimetric (TGA) and the first derivative of thermogravimetric (DTG) curves and (b) XRD diffractograms of sludge, SB-600, and ZB-Zn.....	117
<b>Figure 4.5:</b> Final concentration of NAs in OSPW after adsorption on pristine (SB-600) and activated (SB-Zn) biochars.....	118
<b>Figure 4.6:</b> Concentration of classical NAs in raw OSPW and OSPW treated with 2 g L <sup>-1</sup> of SB-Zn for different times partitioned by (a) different carbon numbers and (b) different DBE numbers. Total classical NAs in the raw OSPW: 40.4 mg L <sup>-1</sup> .....	123
<b>Figure 4.7:</b> (a) Adsorption capacity of classical NAs from raw OSPW treated with 2 g L <sup>-1</sup> of SB-Zn for different times, and fittings of (b) intraparticle diffusion model, (c) pseudo-first order and (d) pseudo-second order kinetics models. ....	124
<b>Figure 4.8:</b> (a) Adsorption capacity of SB-Zn for adsorption of NAs from raw OSPW, and fittings of (b) Langmuir and (c) Freundlich isotherms. ....	127
<b>Figure 4.9:</b> Adsorption of NAs from raw OSPW on activated biochar from sludge (SB-Zn)...	130
<b>Figure 4.10:</b> Adsorption efficiency of regenerated and reused SB-Zn for the removal of NAs from raw OSPW. Adsorption conditions: 2 g L <sup>-1</sup> biochar dosage; 24 h of contact time; raw OSPW. ....	132
<b>Figure 4.11:</b> (a) Toxicity of raw and treated OSPW towards Microtox® <i>Vibrio fischeri</i> and (b) biomimetic extraction using solid-phase microextraction (BE-SPME) of OSPW before and after 24 h treatment with 2 g L <sup>-1</sup> activated-biochar. ....	138
<b>Figure 4.12:</b> The circular economy concept envisioned for the waste management of sludge from municipal wastewater treatment plant and the treatment of OSPW from oil sands industries. ..	140
<b>Figure 5.1:</b> Nitrogen adsorption and desorption isotherms of (a) sludge and (b) peat, and their respective pristine and activated biochars. ....	164
<b>Figure 5.2:</b> FTIR spectra of (a) sludge and (b) peat, and their respective pristine and activated biochars.....	169
<b>Figure 5.3:</b> XRD diffractograms of (a) sludge and (b) peat, followed by their respective pristine and activated biochars. ....	170
<b>Figure 5.4:</b> (a,b) Thermogravimetric (TGA) and (c,d) first derivative of thermogravimetric (DTG) curves of sludge and peat, and their respective biochars.....	172

<b>Figure 5.5:</b> (a) Final concentration of model compound and (b) adsorption capacity of model compounds obtained for the adsorption using pristine and activated biochars from sludge and peat. Adsorption conditions: 2 g L <sup>-1</sup> biochar dosage; 24 h of contact time; 25 mg L <sup>-1</sup> initial concentration of NA. ....	175
<b>Figure 5.6:</b> (a) Final concentration and (b) adsorption capacity of NAs from OSPW on pristine and activated biochars. Adsorption conditions: 2 g L <sup>-1</sup> biochar dosage; 24 h of contact time; raw OSPW. ....	179
<b>Figure 5.7:</b> Concentration of classical NAs in terms of carbon number in raw OSPW and OSPW treated with biochars from (a) sludge and (b) peat. Adsorption conditions: 2 g L <sup>-1</sup> biochar dosage; 24 h of contact time; raw OSPW; total classical NAs in the raw OSPW: 40.4 mg L <sup>-1</sup> . ....	180
<b>Figure 5.8:</b> Concentration of classical NAs in terms of DBE number in raw OSPW and OSPW treated with biochars from (a) sludge and (b) peat. Adsorption conditions: 2 g L <sup>-1</sup> biochar dosage; 24 h of contact time; raw OSPW; total classical NAs in the raw OSPW: 40.4 mg L <sup>-1</sup> . ....	181
<b>Figure 6.1:</b> Carbon cycle of biochar for the OSPW treatment in the oil sands industries. ....	203
<b>Figure S1:</b> (a) SEM images of PT reclamation material before and after adsorption of model NA compounds at magnification from 500 to 5000 times. EDX spectra of PT reclamation material (b) before adsorption, and after adsorption of (c) DA and (d) PVA. ....	239
<b>Figure S2:</b> (a) SEM images of PF-1 reclamation material before and after adsorption of model NA compounds at magnification from 500 to 5000 times. EDX spectra of PF-1 reclamation material (b) before adsorption, and after adsorption of (c) DA and (d) PVA. ....	241
<b>Figure S3:</b> (a) SEM images of PF-2 reclamation material before and after adsorption of model NA compounds at magnification from 500 to 5000 times. EDX spectra of PF-2 reclamation material (b) before adsorption, and after adsorption of (c) DA and (d) PVA. ....	243
<b>Figure S4:</b> X-ray diffractograms obtained for (a) PT, (b) PF-1, and (c) PF-2 materials before and after adsorption. ....	245
<b>Figure S5:</b> Fittings of the Freundlich isotherm for the adsorption of model NA compounds at different initial concentrations using reclamation materials (a) PT, (b) PF-1, and (c) PF-2. ....	246
<b>Figure S6:</b> Adsorption capacity of classical NAs from raw OSPW treated with 2 g L <sup>-1</sup> of SB-Zn for different times partitioned by (a) carbon and (b) DBE numbers. ....	247

**Figure S7:** (a,b) PFO and (c,d) PSO kinetic modelling, and (e,f) IPD modelling for the adsorption of NAs on 2 g L<sup>-1</sup> SB-Zn for different adsorption times as a function of carbon numbers (n) 13 to 15 and DBE numbers 4, 6, and 12.....248

**Figure S8:** Adsorption capacity of classical NAs in terms of carbon and DBE numbers in raw OSPW and OSPW treated with biochars from sludge and peat. ....249

# **Chapter 1 Introduction and Research Objectives**

## **1.1 Background and Motivation**

### 1.1.1 Oil Sands Process Water

The fourth largest oil reserves in the world are located in Alberta as oil sands (Government of Alberta, 2022). The oil sands are composed of 10% bitumen, 5% water and 85% mineral solids (sand, clay and silt) (Zubot et al., 2012), and the bitumen extraction from the oil sands is performed through the Clark caustic hot water extraction process (Hao et al., 2005), requiring from 0.2 to 2.6 barrels of fresh water per barrel of bitumen (Natural Resources Canada, 2020). This process generates high volumes of oil sands process water (OSPW) that is stored in on-site tailings ponds as a requirement of the Alberta's zero discharge approach (Allen, 2008). The volume of fluid tailings in the Athabasca oil sands region has reached 1,360 Mm<sup>3</sup> in 2020, presenting approximately a 26% increase in volume since 2015 (Alberta Energy Regulator, 2021). To shed a light in the water volume being withheld in the tailings ponds, the average daily residential use of potable water by the population of Alberta in 2019 was of 0.64 Mm<sup>3</sup> (Statistics Canada, 2021).

The OSPW can be reused in the extraction process, but the reuse might involve the decrease of process water quality that leads to issues in bitumen recovery, scaling and corrosion of extraction plant infrastructure (Allen, 2008). In terms of composition, the OSPW will vary according to the types of OSPW (Li et al., 2017), which include raw OSPW collected from active settling basins, seepage drainage water collected from draining systems surrounding the active settling basins, consolidated tailings released water obtained from the treatment of fine tailings, and aged OSPW or OSPW undergoing biological treatment from wetlands and reclamation ponds (Mahaffey & Dubé, 2017). The characteristics include high alkalinity, inorganic constituents

(metals, anions), suspended particles (Allen, 2008), and some concentrations of organic compounds with recalcitrant characteristics, such as naphthenic acids (NAs) (Pourrezaei et al., 2014), polycyclic aromatic hydrocarbons, phenolic compounds, and xylenes (Lévesque, 2014). The presence of NAs is one of the most crucial contributors to the acute toxicity of OSPW (Li et al., 2017).

### 1.1.2 Naphthenic acids

NAs are molecules that originated in the petroleum deposits due to natural phenomena. They are amphiphilic compounds and saturated aliphatic and alicyclic carboxylic acids that are solubilized in the OSPW (alkaline mixture, pH ~ 8.5) during the extraction of bitumen from oil sands (Quinlan & Tam, 2015). The general chemical formula  $C_nH_{2n+Z}O_x$  represents the NAs, where the carbon number is indicated by “n” ( $7 \leq n \leq 26$ ), the hydrogen deficiency number resulting from a ring or double bond formation is represented by “Z” ( $0 \leq -Z \leq 24$ ), and the oxygen number is indicated by “x”, in which classical NAs are characterized by  $x = 2$  and oxidized NAs have x values ranging from 3 to 6 (Huang et al., 2015a; Meshref et al., 2017). Total NAs (classical and oxidized species) in the OSPW account for more than 50% of all organic compounds in OSPW (Grewer et al., 2010). As the total NAs are divided into classical and oxidized species, previous studies showed that the classical NAs are often the highest concentration of NAs in the total NAs. For example, the total NAs in the raw OSPW studied by Suara et al. (2022) had 55% of classical NAs, while the study of Huang et al. (2021) stated that classical NAs corresponded to 40% of total NAs in a raw OSPW, in which the remaining 60% was divided between oxidized NAs (3 to 6).

NAs are a source of toxicity of OSPW and even though the NAs can be naturally degraded over time, the degradation time is long and not practical. In addition, high molecular weight NAs

can have recalcitrant characteristics (Allen, 2008). Although NAs can facilitate the bitumen extraction from oil sands due to their surface-active characteristics, their presence could cause corrosion issues in the plant infrastructure (Quinlan & Tam, 2015). As reviewed by Li et al. (2017), NAs in OSPW are an environmental concern due to the acute and chronic toxicity to living organisms.

The quantification of NAs in OSPW can be performed using specific analytical techniques, such as ultraperformance liquid chromatography time-of-flight mass spectrometry (UPLC TOF-MS), Fourier transform ion cyclotron resonance (FT-ICR) MS, and ion mobility spectrometry (IMS) (Sun et al., 2014).

### 1.1.3 OSPW treatments

The complexity of the OSPW might require the application of several treatment steps, such as coagulation-flocculation to remove suspended solids and ozonation to improve the biodegradability of OSPW (Wang et al., 2015; Xue et al., 2016). Other techniques that can help to remove the organic matter can follow. Such techniques include supported biofilters (Arslan & Gamal El-Din, 2021), advanced oxidation through catalytic ozonation (Messele et al., 2021), electro-oxidation (Abdalrhman et al., 2020), UV/H<sub>2</sub>O<sub>2</sub> oxidation (Fang et al., 2019), photocatalysis (Liu et al., 2016), and adsorption (Benally et al., 2019).

Adsorption is a simple procedure that is effective at low and high pollutant concentrations. The advantages included enhanced selectivity to target specific pollutants depending on the adsorbent characteristics (engineered adsorbents) and regeneration ability of spent adsorbents (De Gisi et al., 2016; Kumari et al., 2020; Pourrezaei et al., 2014). A few adsorbents were previously studied for the adsorption of NAs, including: (1) waste materials, such as petroleum coke (Niasar

et al., 2019; Pourrezaei et al., 2014), blast furnace dust and sludge from steel factory, sludge from textile industry, and retained shale from shale industry (Hendges et al., 2021), (2) soil (Janfada et al., 2006), (3) commercial adsorbents, such as granular activated carbon (Islam et al., 2018) and resins (Hendges et al., 2021), and (4) engineered adsorbents, such as carbon xerogel (Benally et al., 2019) and biochar (Bhuiyan et al., 2017; Singh et al., 2020). Efficient adsorbents that come from natural or waste materials can reduce the environmental impact associated with production or disposal. For instance, biochar is a carbon-based material derived from organic sources (natural or wastes) that can function very well as adsorbent due to its characteristics and it is comparable to activated carbon (AC). The difference is that the energy required to produce biochars is about 15 times lower than required to produce AC (Alhashimi & Aktas, 2017). The feedstock used to produce activated biochars can yield different properties that may or may not benefit the adsorption of NAs (Bhuiyan et al., 2017). Sludge and peat have not yet been used as feedstock of engineered biochar to target NAs. The application of sludge as biochar might be an economical alternative (Tomczyk et al., 2020), since sludge has been associated with high toxicity for some aquatic microorganisms (da Silva Souza et al., 2020) and its disposal usually involves composting or incineration. Peat is obtained as a reclamation material at virtually no-cost. Additionally, the biochar production techniques can be optimized to improve functional groups, surface area and porous properties of the biochar surface to increase the adsorption capacity of organic compounds (Luo et al., 2018; Qu et al., 2021; Wang et al., 2017b).

On the other hand, the surface mining techniques of oil sands demand the excavation of the layers located above the oil sands called muskeg (closer to surface) and overburden (between muskeg and oil sands): muskeg is characteristic of peatland, and the overburden is a layer mostly composed of sand and clay (Speight, 2013). After excavation, the muskeg and the overburden are



stored for use in land reclamation. The study of such reclamation materials from an oil sands extraction site as adsorbents of NAs from OSPW is important to provide data on the transport of NAs in oil sands reclamation landscape where these materials may be used.

## **1.2 Research scope and objectives**

The high volume of OSPW generated by the oil sands industries must be treated to ensure efficient water reuse or safe discharge of OSPW to the environment to compel with the aggressive timeline on OSPW reclamation. Therefore, this project aimed at investigating the adsorption behavior of two types of adsorbents to target naphthenic acids in OSPW. The first part of this project focused on adsorption studies using different reclamation materials from oil sands surface mining. The second part of this project focused on development of biochars from sludge and peat and their use in adsorption studies.

### **1.2.1 Study of reclamation materials from surface mining of oil sands**

The main objective of this portion of the project is to investigate the adsorptive characteristics of reclamation materials obtained from mining excavation of oil sands. The study of such reclamation materials from an oil sands extraction site as adsorbents of NAs from OSPW is important to provide data on the transport of NAs in an oil sands reclamation landscape where these materials may be used. Therefore, the purpose of this study was to investigate three reclamation materials from oil sands excavation sites (peat-mineral mix named PT and Pleistocene fluvial sands sourced from different locations named PF-1 and PF-2) as adsorbents of NAs to evaluate the adsorption characteristics. Since the reclamation materials have not yet been used in the adsorption of NAs, model NA compound solutions were used to eliminate the interferences

between the complex matrix of OSPW and complex matrix of reclamation materials and to gain an understanding of the adsorption mechanisms according to the type of NA compounds used. The research overview is depicted in Figure 1.1. The objectives of the adsorption study are to:

(i) Determine the effect of adsorbent dosage and the equilibrium time required for adsorption of model NA compounds,

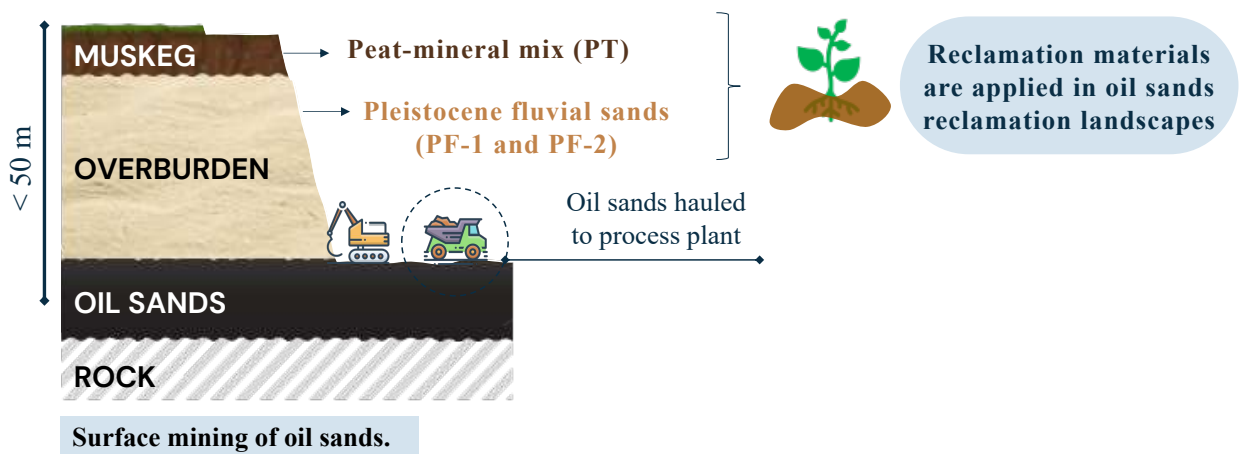
(ii) Gain understanding of the adsorption kinetics and adsorption mechanisms for the adsorption of model NA compounds on reclamation materials,

(iii) Evaluate the adsorption performance of the three reclamation materials for adsorption of three model NA compounds in terms of their distinct structures and characteristics,

(iv) Assess the leaching potential of the reclamation materials post-adsorption through desorption studies,

(v) Determine the adsorption capacity of reclamation materials to adsorb classical NAs from real OSPW, and

(vi) Determine the relationship between the uptake of NAs and the properties of the reclamation materials.



**Research question:**  
 What are the adsorption characteristics of reclamation materials for adsorption of NAs?

◇ **Potential applicability of these materials based on their properties**

- Characterization of materials
- Adsorption and desorption studies using model compounds of NAs
- Adsorption mechanisms
- Adsorption efficiency towards NAs in raw OSPW
- Effect of properties of reclamation materials on adsorption distribution coefficients

**Figure 1.1:** Research overview for reclamation materials from surface mining of oil sands.

### 1.2.2 Study on activated biochars from sludge and peat

The main objective of this portion of the project is to develop activated biochars from biological sludge and peat to target the adsorption of NAs in OSPW. The biological sludge was sourced from an anaerobic digester of a municipal wastewater treatment plant and the peat was procured from an oil and gas field as a material from the surface mining of oil sands. The effect of feedstock type (biological sludge or peat), chemical activation agents, and temperature of pyrolysis were studied, especially as they can add important characteristics to the biochar that could favor

the adsorption of NAs. The advantages of studying biochars as adsorbents include the conversion of waste into valuable materials, and they can effectively target NAs in OSPW at low dosages.

The biochar study is divided in two main sections (Figure 1.2) with their respective objectives:

(1) The development of biochar from sludge using zinc chloride as the chemical activation agent for adsorption of NAs from OSPW, in which the specific objectives were to:

(i) Evaluate the adsorption of classical and oxidized species of NAs from OSPW using pristine and activated biochars,

(ii) Characterize the sludge, pristine and the best activated biochar to identify the properties enhanced with biochar activation,

(iii) Gain an understanding of the adsorption kinetics and mechanisms for the adsorption of NAs from raw OSPW,

(iv) Evaluate the adsorption selectivity of NAs by biochar considering the diverse NA composition within OSPW,

(v) Study the potential leaching of metals from the produced biochar to the treated OSPW often associated with sludge-based biochars,

(vi) Evaluate the regeneration and reuse ability of spent biochars for NAs adsorption to reduce the risk of secondary pollution, and

(vii) Evaluate the effects of biochar adsorption on the acute toxicity and bioavailability of organics in OSPW after treatment.

(2) Study the effects of feedstock type (sludge or peat) and the chemical activation agents on the adsorption of NAs from OSPW, focusing on finding which biochar properties were the most important to target NAs. The specific objectives were to:

(i) Prepare biochars from sludge and peat using chemical activation agents (no activation, ferric chloride, and a combination of zinc chloride and ferric chloride) at pyrolysis temperature of 800°C,

(ii) Determine which production technique of biochar provided the best adsorption of model compounds of NAs with different structures,

(iii) Apply selected biochars in the adsorption of classical NAs from raw OSPW,

(iv) Characterize the feedstocks and produced biochars,

(v) Investigate the characteristics of activated biochars and their effects on the adsorption of NAs.

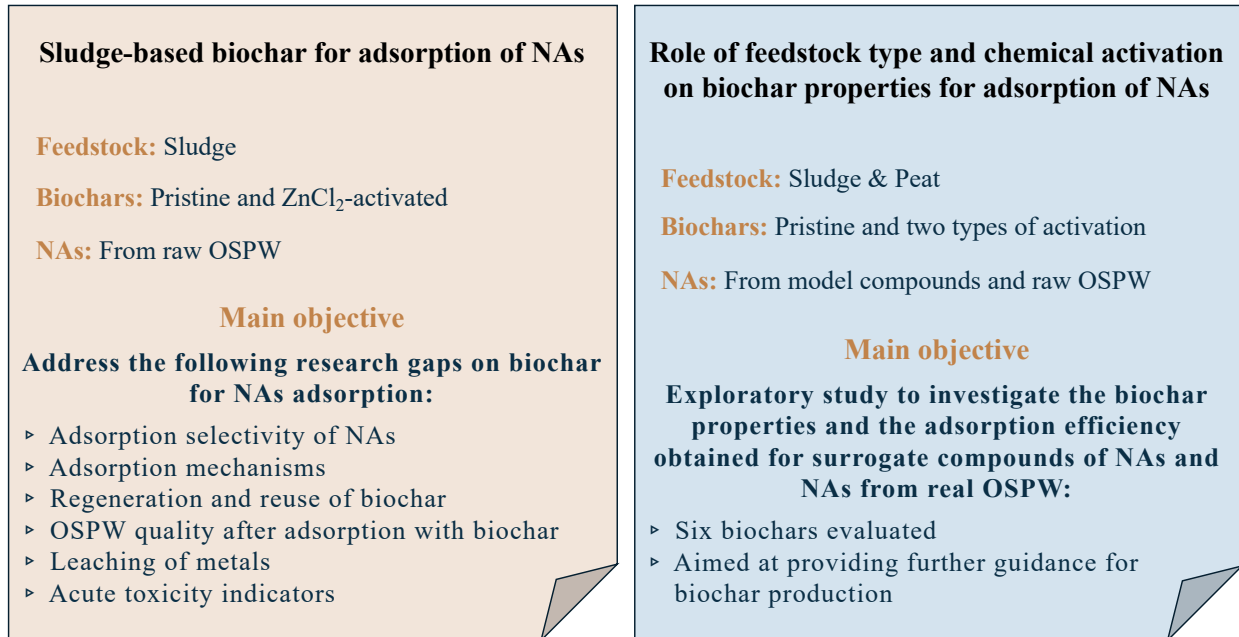


**Figure 1.2:** Research overview for development of biochars as adsorbents of NAs.

### 1.3 Hypothesis

Regarding the adsorption of NAs on the reclamation materials, it was hypothesized that high concentration of reclamation materials ( $>100 \text{ g L}^{-1}$ ) would be effective in removing NAs and the adsorption equilibrium would be reached at longer contact times than usual ( $>24 \text{ h}$ ). The leaching capacity would depend on the adsorption mechanisms (either physical or chemical adsorption). Considering the nature of PT, PF-1 and PF-2 materials and the nature of OSPW, it was hypothesized that the hydrophobic interactions would drive the adsorption and the highest removal of NAs would be observed for the material with the highest total organic carbon (TOC) content. Some mobility of NAs on the materials would be expected should the reclamation materials come in contact with OSPW, which might occur in an oil sands reclamation landscape.

Regarding the adsorption of NAs on biochars, it was hypothesized that the activated biochars produced with selected chemical activation agents will increase the biochar surface area, oxygen-containing functional groups, crystallinity and thermostability. Such improvement would lead to highly efficient biochars that could remove not only classical NAs, but oxidized NAs as well. It was hypothesized that hydrogen bonding and  $\pi$ - $\pi$  interactions would be the possible adsorption mechanisms and the adsorption would occur very fast. The thermal regeneration of the engineered biochars will allow reuse of adsorbent. Additionally, the engineered biochars will be able to reduce the organic load (NAs and other organic compounds) and the concentration of some metals in OSPW. Additionally, it is hypothesized that the study of biochar efficiency in the adsorption of NAs using surrogate compounds (i.e. model compounds, single compound solution) is not a proper approach to evaluate biochars as adsorbents considering the diverse composition of NAs in the OSPW.

## **1.4 Thesis organization**

Chapter 1 provides a general introduction and background information on the oil sands and the OSPW generated in the extraction of bitumen, as well as the target contaminant (NAs) in the OSPW. The OSPW treatment techniques are briefly presented with the with motivation for the research, which includes the study of adsorption processes using reclamation materials from surface mining of oil sands and activated biochars from sludge and peat. The research objectives and the hypotheses for the studies are presented. And finally, the thesis organization is provided for the reader.

Chapter 2 is the literature review for adsorption. The adsorption fundamentals are presented, focusing on the nature of adsorption, the critical parameters in adsorption processes, and the adsorption kinetics and isotherms. Then, the review on biochar production and properties for adsorption of organic compounds is presented. Lastly, the chapter concludes with the adsorbent materials used for adsorption of NAs in OSPW and the current research gaps on the field.

Chapter 3 presents the results of the investigation of reclamation materials obtained from mining excavation of oil sands as adsorbents of model compounds of NAs and NAs in OSPW. For the model compounds of NAs, the results of the effect of adsorbent dosage, adsorption kinetics and equilibrium experiments, and desorption experiments are presented. Then, the adsorption capacity for classical NAs is studied. Lastly, the adsorption distribution coefficients and the relationship between the properties of the reclamation materials and the adsorption capacities are presented.

Chapter 4 presents the results of the development of biochar from sludge using zinc chloride as the chemical activation agent for adsorption of NAs from OSPW. The results of the evaluation of the adsorption of classical and oxidized species of NAs from OSPW using pristine and activated

biochars and characterization of sludge, pristine and the best activated biochar are presented. For the classical NAs, the results of the adsorption kinetics, isotherms, adsorption mechanisms, and regeneration and reuse ability of spent biochars for the adsorption of NAs from raw OSPW are presented. Additionally, the chapter reports the study on the potential leaching of metals from biochar to the treated OSPW and the reduction of acute toxicity and bioavailability of organics of OSPW after adsorption treatment with biochar.

Chapter 5 presents the results of the study on the effects of feedstock type and the chemical activation agents on the adsorption of NAs from OSPW. In detail, the chapter reports the preliminary assessment of biochar produced with different activation agents and their efficiency for the adsorption of four NA model compounds. Then, the results of the characterization of the best activated biochars and their respective pristine biochar are presented. Lastly, the chapter reports the results of the investigation of the characteristics of the activated biochars and their effects on the adsorption of NAs from raw OSPW.

Chapter 6 provides a general overview of the thesis and summarizes the major conclusions from the previous chapters. The chapter concludes with the future recommendations for further research.

## 1.5 References

Abdalrhman, A. S., Zhang, Y., Arslan, M., & Gamal El-Din, M. (2020). Low-current electro-oxidation enhanced the biodegradation of the recalcitrant naphthenic acids in oil sands process water. *Journal of Hazardous Materials*, 398, 122807. <https://doi.org/10.1016/j.jhazmat.2020.122807>



- Alberta Energy Regulator. (2021). *State of Fluid Tailings Management for Mineable Oil Sands, 2020* <https://static.aer.ca/prd/documents/reports/2020-State-Fluid-Tailings-Management-Mineable-OilSands.pdf>
- Alhashimi, H. A., & Aktas, C. B. (2017). Life cycle environmental and economic performance of biochar compared with activated carbon: A meta-analysis. *Resources, Conservation and Recycling, 118*, 13-26. <https://doi.org/10.1016/j.resconrec.2016.11.016>
- Allen, E. W. (2008). Process water treatment in Canada's oil sands industry: I. Target pollutants and treatment objectives. *Journal of Environmental Engineering & Science, 7*(2), 123-138. <https://doi.org/10.1139/S07-038>
- Arslan, M., & Gamal El-Din, M. (2021). Bacterial diversity in petroleum coke based biofilters treating oil sands process water. *Science of the Total Environment, 782*, 146742. <https://doi.org/10.1016/j.scitotenv.2021.146742>
- Benally, C., Messele, S. A., & Gamal El-Din, M. (2019). Adsorption of organic matter in oil sands process water (OSPW) by carbon xerogel. *Water Research, 154*, 402-411. <https://doi.org/10.1016/j.watres.2019.01.053>
- Bhuiyan, T. I., Tak, J. K., Sessarego, S., Harfield, D., & Hill, J. M. (2017). Adsorption of acid-extractable organics from oil sands process-affected water onto biomass-based biochar: Metal content matters. *Chemosphere, 168*, 1337-1344. <https://doi.org/10.1016/j.chemosphere.2016.11.126>
- da Silva Souza, T., Lacerda, D., Aguiar, L. L., Martins, M. N. C., & Augusto de Oliveira David, J. (2020). Toxic potential of sewage sludge: Histopathological effects on soil and aquatic bioindicators. *Ecological Indicators, 111*, 105980. <https://doi.org/10.1016/j.ecolind.2019.105980>
- De Gisi, S., Lofrano, G., Grassi, M., & Notarnicola, M. (2016). Characteristics and adsorption capacities of low-cost sorbents for wastewater treatment: A review. *Sustainable Materials and Technologies, 9*, 10-40. <https://doi.org/10.1016/j.susmat.2016.06.002>
- Fang, Z., Huang, R., Chelme-Ayala, P., Shi, Q., Xu, C., & Gamal El-Din, M. (2019). Comparison of UV/Persulfate and UV/H<sub>2</sub>O<sub>2</sub> for the removal of naphthenic acids and acute toxicity towards *Vibrio fischeri* from petroleum production process water. *Science of the Total Environment, 694*, 133686. <https://doi.org/10.1016/j.scitotenv.2019.133686>

- Government of Alberta. (2022). Oil sands facts and statistics. <https://www.alberta.ca/oil-sands-facts-and-statistics.aspx>
- Grewer, D. M., Young, R. F., Whittal, R. M., & Fedorak, P. M. (2010). Naphthenic acids and other acid-extractables in water samples from Alberta: What is being measured? *Science of the Total Environment*, 408(23), 5997-6010. <https://doi.org/10.1016/j.scitotenv.2010.08.013>
- Hao, C., Headley, J. V., Peru, K. M., Frank, R., Yang, P., & Solomon, K. R. (2005). Characterization and pattern recognition of oil–sand naphthenic acids using comprehensive two-dimensional gas chromatography/time-of-flight mass spectrometry. *Journal of Chromatography A*, 1067(1), 277-284. <https://doi.org/10.1016/j.chroma.2005.01.041>
- Hendges, L. T., Costa, T. C., Temochko, B., Gómez González, S. Y., Mazur, L. P., Marinho, B. A., da Silva, A., Weschenfelder, S. E., de Souza, A. A. U., & de Souza, S. M. A. G. U. (2021). Adsorption and desorption of water-soluble naphthenic acid in simulated offshore oilfield produced water. *Process Safety and Environmental Protection*, 145, 262-272. <https://doi.org/10.1016/j.psep.2020.08.018>
- Huang, R., McPhedran, K. N., & Gamal El-Din, M. (2015a). Ultra Performance Liquid Chromatography Ion Mobility Time-of-Flight Mass Spectrometry Characterization of Naphthenic Acids Species from Oil Sands Process-Affected Water. *Environmental Science & Technology*, 49(19), 11737-11745. <https://doi.org/10.1021/acs.est.5b03178>
- Huang, R., Yang, L., How, Z. T., Fang, Z., Bekele, A., Letinski, D. J., Redman, A. D., & Gamal El-Din, M. (2021). Characterization of raw and ozonated oil sands process water utilizing atmospheric pressure gas chromatography time-of-flight mass spectrometry combined with solid phase microextractionun. *Chemosphere*, 266, 129017. <https://doi.org/10.1016/j.chemosphere.2020.129017>
- Islam, M. S., McPhedran, K. N., Messele, S. A., Liu, Y., & Gamal El-Din, M. (2018). Isotherm and kinetic studies on adsorption of oil sands process-affected water organic compounds using granular activated carbon. *Chemosphere*, 202, 716-725. <https://doi.org/10.1016/j.chemosphere.2018.03.149>
- Janfada, A., Headley, J. V., Peru, K. M., & Barbour, S. L. (2006). A Laboratory Evaluation of the Sorption of Oil Sands Naphthenic Acids on Organic Rich Soils. *Journal of Environmental Science and Health, Part A*, 41(6), 985-997. <https://doi.org/10.1080/10934520600620105>

- Kumari, U., Behera, S. K., Siddiqi, H., & Meikap, B. C. (2020). Facile method to synthesize efficient adsorbent from alumina by nitric acid activation: Batch scale defluoridation, kinetics, isotherm studies and implementation on industrial wastewater treatment. *Journal of Hazardous Materials*, 381, 120917. <https://doi.org/10.1016/j.jhazmat.2019.120917>
- Lévesque, C. M. (2014). *Oil sands process water and tailings pond contaminant transport and fate : physical, chemical and biological processes*, University of British Columbia]. <https://open.library.ubc.ca/collections/24/items/1.0165952>
- Li, C., Fu, L., Stafford, J., Belosevic, M., & Gamal El-Din, M. (2017). The toxicity of oil sands process-affected water (OSPW): A critical review. *Science of the Total Environment*, 601-602, 1785-1802. <https://doi.org/10.1016/j.scitotenv.2017.06.024>
- Liu, J., Wang, L., Tang, J., & Ma, J. (2016). Photocatalytic degradation of commercially sourced naphthenic acids by TiO<sub>2</sub>-graphene composite nanomaterial. *Chemosphere*, 149, 328-335. <https://doi.org/10.1016/j.chemosphere.2016.01.074>
- Luo, J., Li, X., Ge, C., Müller, K., Yu, H., Huang, P., Li, J., Tsang, D. C. W., Bolan, N. S., Rinklebe, J., & Wang, H. (2018). Sorption of norfloxacin, sulfamerazine and oxytetracycline by KOH-modified biochar under single and ternary systems. *Bioresource Technology*, 263, 385-392. <https://doi.org/10.1016/j.biortech.2018.05.022>
- Mahaffey, A., & Dubé, M. (2017). Review of the composition and toxicity of oil sands process-affected water. *Environmental Reviews*, 25(1), 97-114. <https://doi.org/10.1139/er-2015-0060>
- Meshref, M. N. A., Chelme-Ayala, P., & Gamal El-Din, M. (2017). Fate and abundance of classical and heteroatomic naphthenic acid species after advanced oxidation processes: Insights and indicators of transformation and degradation. *Water Research*, 125, 62-71. <https://doi.org/10.1016/j.watres.2017.08.007>
- Messele, S. A., Chelme-Ayala, P., & Gamal El-Din, M. (2021). Catalytic ozonation of naphthenic acids in the presence of carbon-based metal-free catalysts: Performance and kinetic study. *Catalysis Today*, 361, 102-108. <https://doi.org/10.1016/j.cattod.2020.01.042>
- Natural Resources Canada. (2020). *Crude oil facts*. <https://www.nrcan.gc.ca/science-data/data-analysis/energy-data-analysis/energy-facts/crude-oil-facts/20064#L4>

- Niasar, H. S., Das, S., Xu, C., & Ray, M. B. (2019). Continuous column adsorption of naphthenic acids from synthetic and real oil sands process-affected water (OSPW) using carbon-based adsorbents. *Chemosphere*, 214, 511-518. <https://doi.org/10.1016/j.chemosphere.2018.09.078>
- Pourrezaei, P., Alpatova, A., Chelme-Ayala, P., Perez-Estrada, L. A., Jensen-Fontaine, M., Le, X. C., & Gamal El-Din, M. (2014). Impact of petroleum coke characteristics on the adsorption of the organic fractions from oil sands process-affected water. *International Journal of Environmental Science and Technology*, 11(7), 2037-2050. <https://doi.org/10.1007/s13762-013-0406-x>
- Qu, J., Wang, Y., Tian, X., Jiang, Z., Deng, F., Tao, Y., Jiang, Q., Wang, L., & Zhang, Y. (2021). KOH-activated porous biochar with high specific surface area for adsorptive removal of chromium (VI) and naphthalene from water: Affecting factors, mechanisms and reusability exploration. *Journal of Hazardous Materials*, 401, 123292. <https://doi.org/10.1016/j.jhazmat.2020.123292>
- Quinlan, P. J., & Tam, K. C. (2015). Water treatment technologies for the remediation of naphthenic acids in oil sands process-affected water. *Chemical Engineering Journal*, 279, 696-714. <https://doi.org/10.1016/j.cej.2015.05.062>
- Singh, R., Naik, D. V., Dutta, R. K., & Kanaujia, P. K. (2020). Biochars for the removal of naphthenic acids from water: A prospective approach towards remediation of petroleum refinery wastewater. *Journal of Cleaner Production*, 266, 121986. <https://doi.org/10.1016/j.jclepro.2020.121986>
- Speight, J. G. (2013). Chapter 3 - Oil Sand Mining. In J. G. Speight (Ed.), *Oil Sand Production Processes* (pp. 59-79). Gulf Professional Publishing. <https://doi.org/https://doi.org/10.1016/B978-0-12-404572-9.00003-6>
- Statistics Canada. (2021). *Table 38-10-0271-01 Potable water use by sector and average daily use*. <https://doi.org/10.25318/3810027101-eng>
- Suara, M. A., Ganiyu, S. O., Paul, S., Stafford, J. L., & Gamal El-Din, M. (2022). Solar-activated zinc oxide photocatalytic treatment of real oil sands process water: Effect of treatment parameters on naphthenic acids, polyaromatic hydrocarbons and acute toxicity removal.

- Science of the Total Environment*, 819, 153029.  
<https://doi.org/10.1016/j.scitotenv.2022.153029>
- Sun, N., Chelme-Ayala, P., Klamerth, N., McPhedran, K. N., Islam, M. S., Perez-Estrada, L., Drzewicz, P., Blunt, B. J., Reichert, M., Hagen, M., Tierney, K. B., Belosevic, M., & Gamal El-Din, M. (2014). Advanced Analytical Mass Spectrometric Techniques and Bioassays to Characterize Untreated and Ozonated Oil Sands Process-Affected Water. *Environmental Science & Technology*, 48(19), 11090-11099.  
<https://doi.org/10.1021/es503082j>
- Tomczyk, B., Siatecka, A., Jędruchniewicz, K., Sochacka, A., Bogusz, A., & Oleszczuk, P. (2020). Polycyclic aromatic hydrocarbons (PAHs) persistence, bioavailability and toxicity in sewage sludge- or sewage sludge-derived biochar-amended soil. *Science of the Total Environment*, 747, 141123. <https://doi.org/10.1016/j.scitotenv.2020.141123>
- Wang, C., Alpatova, A., McPhedran, K. N., & Gamal El-Din, M. (2015). Coagulation/flocculation process with polyaluminum chloride for the remediation of oil sands process-affected water: Performance and mechanism study. *Journal of Environmental Management*, 160, 254-262. <https://doi.org/10.1016/j.jenvman.2015.06.025>
- Wang, P., Tang, L., Wei, X., Zeng, G., Zhou, Y., Deng, Y., Wang, J., Xie, Z., & Fang, W. (2017b). Synthesis and application of iron and zinc doped biochar for removal of p-nitrophenol in wastewater and assessment of the influence of co-existed Pb(II). *Applied Surface Science*, 392, 391-401. <https://doi.org/10.1016/j.apsusc.2016.09.052>
- Xue, J., Zhang, Y., Liu, Y., & Gamal El-Din, M. (2016). Effects of ozone pretreatment and operating conditions on membrane fouling behaviors of an anoxic-aerobic membrane bioreactor for oil sands process-affected water (OSPW) treatment. *Water Research*, 105, 444-455. <https://doi.org/10.1016/j.watres.2016.09.011>
- Zubot, W., MacKinnon, M. D., Chelme-Ayala, P., Smith, D. W., & Gamal El-Din, M. (2012). Petroleum coke adsorption as a water management option for oil sands process-affected water. *Science of the Total Environment*, 427-428, 364-372.  
<https://doi.org/10.1016/j.scitotenv.2012.04.024>

## Chapter 2 Literature Review<sup>1</sup>

### 2.1 Adsorption fundamentals

#### 2.1.1 Physical and chemical adsorption

Adsorption is a mass transfer process where a substance of interest moves from the liquid phase to the surface of a solid phase through diffusion. The substance of interest and the solid phase are called adsorbate and adsorbent, respectively. The binding of the adsorbate to the adsorbent surface occurs by either physical adsorption or chemical adsorption (Crittenden, 2012). The physical or chemical nature of adsorption can be determined by the heat of adsorption, in which values between 5 and 50 kJ mol<sup>-1</sup> indicate physical adsorption and 40 and 800 kJ mol<sup>-1</sup> indicate chemical adsorption (Banerjee et al., 1997).

Physical adsorption is characterized by the weak intermolecular forces between the adsorbate and the adsorbent, such as van der Waals forces, and it is assumed the adsorption is non-specific, meaning that the adsorbate is not attached to a specific site of the adsorbent and thus the surface of adsorbent might present a mono- or multi-layer of adsorbates. Additionally, since the heat of adsorption associated with physical adsorption is low, the physical adsorption is usually a reversible adsorption process (Ruthven, 1984).

---

<sup>1</sup> A version of this chapter has been published as: Medeiros, D. C. C. S., Chelme-Ayala, P., Benally, C., Al-Anzi, B. S., and Gamal El-Din, M. Review on carbon-based adsorbents from organic feedstocks for removal of organic contaminants from oil and gas industry process water: Production, adsorption performance and research gaps. *Journal of Environmental Management*, 320, 2022. <https://doi.org/10.1016/j.jenvman.2022.115739>

Chemical adsorption occurs when chemical bonds are formed between the adsorbate and the adsorbent (Ruthven, 1984). Such chemical bonds can be covalent or ionic bonds. It is assumed that chemical adsorption occurs in specific sites, in which monolayer adsorption is observed (Crittenden, 2012). Since the heat of adsorption is high, this process is defined as irreversible adsorption unless high energy is applied for regeneration (Kwon et al., 2011).

Co-occurrence of physical and chemical adsorption processes in wastewater treatment technologies is not unusual because the adsorption itself might be a result of several different adsorption processes, and the dominant adsorption process will depend on the type of adsorbent and adsorbate, wastewater composition, and other factors (Hu & Xu, 2020).

#### 2.1.2 Critical parameters in adsorption

The efficiency of an adsorption process depends on the proper selection of certain parameters, and they are distributed in two categories: (1) operational parameters, such as solution pH, temperature, initial concentration of pollutant, and adsorbent dosage; and (2) adsorbent characteristics, such as surface functional groups, surface area, and pore characteristics.

The solution pH affects the solubility of adsorbate, the electrostatic and dispersive interactions between the adsorbent and adsorbate, the existing form of the organic compound in solution and the surface charge of adsorbent (Lv et al., 2020; Park et al., 2010; Shi et al., 2013). The effect of solution pH on adsorption capacity can vary depending mainly on the surface charge of adsorbent, usually stated by the  $\text{pH}_{\text{pzc}}$ , and on the dissociated or undissociated form of the molecules of the organic compound. The organic compound molecules could ionize and become positively or negatively charged with  $\text{H}^+$  or  $\text{OH}^-$  concentrations in solution – behavior that can also be estimated by the  $\text{pK}_a$  value (Hairuddin et al., 2019; Kumar & Jena, 2016; Singh &

Balomajumder, 2016). In the case of NAs, NAs have pKa values between 5 and 6, and since the OSPW is an alkaline solution with pH around 8.5, the NAs will be in the deprotonated form (Quinlan & Tam, 2015).

The adsorbent dosage is an important parameter to optimize because insufficient adsorbent dosages will result in inadequate pollutant removal rates and exceeding the adsorbent dosage may have negative effects on adsorption, such as adsorbent aggregation issues. Adsorbent aggregation issues can reduce the number of binding sites because some binding sites are not accessible for the pollutant molecules (Qiao et al., 2018; Rodrigues et al., 2011; Zhu & Kolar, 2014), and can also promote desorption (Rodrigues et al., 2011). The initial concentration of the pollutant in adsorption studies should fall within the range of the pollutant concentrations found in the real wastewater of interest. The concentration of NAs in OSPW has been reported to reach up to 80 mg L<sup>-1</sup>, as reviewed by Li et al. (2017).

The adsorbent surface area and porous properties are considered the most important physical properties attained by the engineered biochar, and the adsorption capacity of an adsorbent is intrinsically related to those properties, since the interaction between the pollutant and the adsorbent results in adsorption of pollutant within the pore sites of the adsorbent material (Negara et al., 2019). The pore sizes are classified as micropores (<2 nm), mesopores (2–50 nm) and macropores (>50 nm) according to the IUPAC (Shabir et al., 2020). The adsorption capacity could be predicted by evaluating both adsorbate and adsorbent properties, which include the surface area, pore size and volume for the adsorbent and the molecule size of pollutant/adsorbate (Wu et al., 2020). The increase in mesopore volume can lead to an increase in adsorption capacity because the presence of mesopores allows the pollutant to reach the micropores (Hsieh & Teng, 2000), and



also the adsorption of larger molecules, which could be impeded by smaller pores (Fan et al., 2011).

To evaluate any adsorption data, two equations are useful: the removal rate (Eq. 2.1) and the adsorption capacity (Eq. 2.2), in which  $q_t$  is the adsorption capacity at time  $t$  ( $\text{mg g}^{-1}$ ),  $C_0$  is the pollutant concentration at time 0 ( $\text{mg L}^{-1}$ ),  $C_t$  ( $\text{mg L}^{-1}$ ) is the pollutant concentration at time  $t$  ( $\text{mg L}^{-1}$ ),  $m$  is the mass of adsorbent material (g), and  $V$  is the volume of the aqueous phase (solution containing the pollutant) (L). The removal rate will determine how much of the pollutant was removed from the initial solution, i.e., the efficiency of adsorbent material to adsorb the pollutant. The adsorption capacity represents the amount of pollutant removed by the adsorbent.

$$\text{Removal (\%)} = \frac{(C_0 - C_t)}{C_0} \times 100\% \quad (\text{Eq. 2.1})$$

$$q_t = \frac{(C_0 - C_t)}{m} V \quad (\text{Eq. 2.2})$$

### 2.1.3 Adsorption kinetics

The design of an adsorption process and the adsorbent viability in targeting specific pollutants in wastewater are evaluated by the adsorption kinetics, which is defined by the time progress of an adsorption process. The kinetic parameters behind the mass transfer of adsorbate from aqueous phase to solid phase of adsorbent are evaluated based on the concentration of the adsorbate at different times until equilibrium is reached (equilibrium time), which provides an insight into the rate-limiting mass transfer mechanism (Worch, 2012). According to Worch (2012), the mass transfer mechanism involved in adsorption is initialized with the adsorbate being transported from the liquid phase to the hydrodynamic boundary layer located around the

adsorbent particle, and then followed by the three important steps of adsorption kinetics, in which the step 1 or 2 are usually the rate-limiting step, as follows:

(1) External diffusion: the adsorbate moves from the boundary layer to the external surface of the adsorbent;

(2) Intraparticle diffusion: the adsorbate is transported from the external surface to the internal structure of the adsorbent by diffusion in the pore liquid and/or diffusion in the adsorbed state along the internal surface (surface diffusion);

(3) Dynamic equilibrium: energetic interaction between the adsorbate molecules and the final occupation of the adsorption sites.

The most common adsorption kinetic models (Table 2.1) applied to describe the adsorption kinetics of organic compounds related to oil and gas industries are the pseudo-first order (PFO), pseudo-second order (PSO), Elovich, and intraparticle diffusion (IPD) kinetic models.

The PFO model was developed by Lagergren (1898) and considers that the rate of change of solute adsorbed with time is proportional to the difference in the adsorption equilibrium capacity and the amount adsorbed. On the other hand, the PSO kinetic model suggests that the limiting step of adsorption process is possibly chemisorption, which involves forces of sharing or exchange of electrons between the adsorbate and the adsorbent (Ho & McKay, 1999). The Elovich model, described by Turner (1975), is considered the most effective in defining the adsorption kinetics involving chemisorption.

To gain an understanding of the adsorption mechanisms and to identify the rate-limiting step, the IPD kinetic model (Morris et al., 1966) is applied to the adsorption data. If one single plot is present and the plot passes through the origin, then it indicates that intraparticle diffusion is the rate-limiting step of the adsorption process (Fan et al., 2011). However, if more than one linear

plot is present, more than one mass transfer process instead of just intraparticle diffusion may be playing an important role in the adsorption process (Hao et al., 2018). Therefore, the three steps of adsorption (external diffusion, intraparticle diffusion and equilibrium steps) are presented as three linear plots (Ren et al., 2011). The evaluation of a suitability of a kinetic model for an experimental data is done based on the correlation coefficient ( $R^2$ ) provided by the fitting of linear plot to the data, in which the highest  $R^2$  is desired (Foo & Hameed, 2010).

**Table 2.1:** Adsorption kinetic models.

<b>Model</b>	<b>Equation</b>	<b>Model parameters</b>
PFO	$\ln(q_e - q_t) = \ln q_e - K_{PFO}t$ (Eq. 2.3)	$q_e$ (mg g <sup>-1</sup> ): adsorption capacity at equilibrium; $q_t$ (mg g <sup>-1</sup> ): adsorption capacity at time $t$ ; $K_{PFO}$ (min <sup>-1</sup> ): pseudo-first order rate constant.
PSO	$\frac{t}{q_t} = \frac{1}{K_{PSO}q_e^2} + \frac{t}{q_e}$ (Eq. 2.4)	$K_{PSO}$ (g mg <sup>-1</sup> min <sup>-1</sup> ): pseudo-second order rate constant.
Elovich	$q_t = \frac{1}{\beta} \ln(\alpha\beta) + \frac{1}{\beta} \ln(t)$ (Eq. 2.5)	$\alpha$ (mg g <sup>-1</sup> min <sup>-1</sup> ): initial adsorption rate; $\beta$ (g mg <sup>-1</sup> ): constant related to the extent of surface coverage and activation energy for chemisorption.
IPD	$q_t = k_i t^{0.5} + c_i$ (Eq. 2.6)	$k_i$ (mg g <sup>-1</sup> min <sup>-0.5</sup> ): intraparticle diffusion constant; $c_i$ : thickness of the boundary layer.

#### 2.1.4 Adsorption isotherms

The adsorption equilibrium is described by a dynamic equilibrium between the amount of adsorbate adsorbed in the solid phase (adsorbent) and the remaining concentration in the solution at specific conditions (temperature, pH, etc.). The modeling of adsorption equilibrium data through the equilibrium isotherms is one of the crucial steps to understand the adsorption mechanisms involved in an adsorption process under study, since surface properties of adsorbent, affinity between adsorbent and adsorbate, and an indication of adsorption capacity over time can be determined (Foo & Hameed, 2010; Wang & Guo, 2020). Therefore, the isotherm models are applied to the experimental data to identify the best fit and describe the adsorption process.

There are several isotherm models available to access equilibrium data and they are classified as per the number of parameters that must be determined from the experimental data (Worch, 2012). The most common isotherm models applied for adsorption of organic compounds from a liquid phase to a solid phase were Langmuir and Freundlich isotherms, classified as two-parameter models. These equations are presented in Table 2.2.

The Langmuir model (Eq. 2.7) stipulates that the adsorption occurs only in specific sites, and is based on the following assumptions: (1) the adsorbent sites where the adsorption occurs are limited and homogeneous, (2) the adsorption occurs in monolayer adsorption, meaning that once an adsorbent site is occupied by the adsorbate, adsorption cannot overlap, (3) there is no interaction between the adsorbed molecules and the surrounding areas (Langmuir, 1918). On the other hand, the Freundlich model (Eq. 2.8) assumes that the adsorbent surface is heterogeneous, and adsorption can occur in multilayers, indicating several adsorption sites with distinguished energies (Freundlich, 1906).

**Table 2.2:** Adsorption isotherm models.

<b>Model</b>	<b>Linearized</b>	<b>Isotherm parameters</b>
Langmuir	$\frac{C_e}{q_e} = \frac{1}{b_L q_{max}} + \frac{1}{q_{max}} C_e$ (Eq. 2.7)	$b_L$ (L mg <sup>-1</sup> ): Langmuir affinity constant; $q_{max}$ (mg g <sup>-1</sup> ): maximum adsorption capacity; $C_e$ (mg L <sup>-1</sup> ): concentration of pollutant at equilibrium;
Freundlich	$\log q_e = \log K_f + n_f \log C_e$ (Eq. 2.8)	$K_f$ (mg <sup>1-n</sup> L <sup>n</sup> g <sup>-1</sup> ): Freundlich adsorption coefficient $n_f$ : Freundlich heterogeneity parameter.

## 2.2 Carbon-based adsorbents for adsorption of organic compounds

### 2.2.1 Activated carbon and biochar definitions

Activated carbon (AC) and biochar are carbon-based materials produced from the carbonization of carbon material (Crittenden, 2012; Hao et al., 2018). The transformation of biomasses into carbon-based adsorbent materials occurs during thermal processes such as hydrothermal methods (Li et al., 2020c; Prasannamedha et al., 2021), pyrolysis (Li et al., 2020c; Peng et al., 2016), gasification methods (Kumar et al., 2020), and torrefaction and microwave pyrolysis (Chen et al., 2020b). Further transformations can occur by the application of chemical modifications, like acidic, alkaline and impregnation techniques, to achieve even higher quality adsorbent material (Ahmed et al., 2016), or physical activation, such as steam activation and gas purging (Lawal et al., 2021; Lawal et al., 2020; Rajapaksha et al., 2015).

The difference between AC and biochar is not always clear in the literature and definitions frequently overlap. However, AC can be produced from any material – non-renewable fossil fuel sources, waste, or renewable materials (Hagemann et al., 2018). For example, rubber tires (Gupta et al., 2014; Karmacharya et al., 2016), coal slime (Zhang et al., 2021) and bituminous coal (Acevedo et al., 2015) were used as precursor materials of AC. On the other hand, biochars are always produced using biomasses (Hagemann et al., 2018). There is a wide variety of biomasses used to produce both AC and biochar, such as coconut shell (Baharum et al., 2020; Mishra et al., 2019), corn straw (Feng et al., 2020), industrial sludge (Islam et al., 2021; Liu et al., 2021), rice husk (Guo et al., 2018; Shen et al., 2020), sewage sludge (Godlewska et al., 2019; Sullivan et al., 2019), and wood (Aghababaei et al., 2017; Wang et al., 2016; Yang et al., 2018).

AC is one of the most popular adsorbents due to the large surface area and porous properties of those adsorbents (El-Naas et al., 2016), and it is available commercially as granular activated carbon (GAC) and powdered activated carbon (PAC). The surface area of GAC and PAC are high: 950-1050 m<sup>2</sup> g<sup>-1</sup> for GAC and 1500-1800 m<sup>2</sup> g<sup>-1</sup> (Crittenden, 2012). However, with the advances in research, some engineered AC achieved even higher surface areas, as for the fox nutshell-based AC with 2869 m<sup>2</sup> g<sup>-1</sup> (Kumar & Jena, 2016) and sewage sludge-based AC with 2189 m<sup>2</sup> g<sup>-1</sup> (Samara et al., 2017).

Nowadays, biochars have been studied as an alternative material to AC because the energy required to produce biochars is reasonably lower than AC: 6.1 MJ kg<sup>-1</sup> for biochar and 97 MJ kg<sup>-1</sup> for AC (Alhashimi & Aktas, 2017). Even though the surface area and pore volume of biochars are usually not as high as those obtained for AC, biochars have a fairly high surface area. As reviewed by Medeiros et al. (2022), surface area obtained for biochars produced to target organic compounds ranged from as low as 2.6 to 2183.8 m<sup>2</sup> g<sup>-1</sup>. Surface area and abundance of functional

groups on the biochar surface are characteristics that influence the adsorption of organic compounds, and those characteristics depend on the feedstock type and activation and functionalization techniques (Medeiros et al., 2022).

### 2.2.2 Production of carbon-based adsorbents from biomasses to enhance adsorption of organic compounds

The types of feedstocks used to produce the desired carbon-based adsorbents can be either lignocellulosic (Mary et al., 2016) or non-lignocellulosic biomasses (Li & Jiang, 2017). Lignocellulosic biomasses are plant-based materials that are mainly composed of lignin, cellulose, and hemicellulose. Non-lignocellulosic materials are biomasses derived from animals and a portion of plants, and are primarily composed of protein, lipids, saccharides, inorganics and a portion of lignin and cellulose (Li & Jiang, 2017). Some lignocellulosic biomasses are agricultural wastes, and sugarcane bagasse (Mubarik et al., 2016), straw from corn (Qu et al., 2021), rice fruit wastes such as coconut parts (Bispo et al., 2018), and orange waste (de Jesus et al., 2017) were previously studied as precursors of biochar and activated carbon for the adsorption of organic compounds of interest. Sewage sludge (Regkouzas & Diamadopoulos, 2019), manure (Thang et al., 2019), and algae (Cheng et al., 2020a) are examples of non-lignocellulosic materials from which carbon-based materials were produced from.

The transformation of biomasses into carbon-based adsorbent materials occurs during thermal processes, and the most common one is the pyrolysis because it is a straightforward technique with simple procedure and is already an established technique in the industry (Wang et al., 2019). Pyrolysis at temperatures between 300 and 700°C (or even higher temperatures) in the absence of oxygen is a very suitable method for the production of a high quality carbon-based

adsorbent (Chen et al., 2020b; Kumar et al., 2020). Pyrolysis conditions critically impact the quality of resulting adsorbent and must be carefully evaluated when designing a carbon-based adsorbent since it can directly affect the adsorption capacity, and previous studies showed that higher pyrolysis temperatures lead of better performance in sequestering hydrophobic organic contaminants. Mohammed et al. (2018) produced biochar from pine fruit shell for adsorption of phenol at different pyrolysis temperatures and higher quality biochar characteristics were observed with the increase in the temperature, which reflected on the adsorption capacity: 10.4, 16, and 26.7 mg g<sup>-1</sup> for biochar produced at 350, 450, and 550°C, respectively. This finding corroborates with other studies: Wang et al. (2016) evaluated biochars from different feedstocks produced at different pyrolysis temperature to target hydrophobic organic contaminants (PAHs) and found that higher pyrolysis temperatures are crucial to increase the adsorption capacity.

Many reactions are responsible for the transformation of biomass to carbon-based adsorbents, such as depolymerization, isomerization, dehydration, aromatization, decarboxylation, and charring. The reactions present in the transformation of biomass will depend mainly on the biomass composition (Kumar et al., 2020). Additionally, the pyrolysis purges the hydrophilic groups from the surface of the adsorbent, leading to an increase in surface hydrophobicity, which can be beneficial for adsorption of hydrophobic molecules (Ahmed et al., 2016). Volatile matters and impurities are also purged from the pores, developing more pores on the material's surface (Danish & Ahmad, 2018). Finally, the heating process increases or decreases certain functional groups on the surface, with polarity and aromaticity depending on the temperature applied, all of which can exert influence on the pollutant uptake (Xing et al., 2021).

In addition to single pyrolysis, chemical activation processes can be applied to result in higher quality carbonaceous materials: improvement of surface area, porous properties, and



functional groups of engineered adsorbents (Kazemi Shariat Panahi et al., 2020). The use of chemical activation agents can improve surface characteristics without the need to apply high temperatures ( $>1000^{\circ}\text{C}$ ) (Genuino et al., 2018), and can also promote better separation of the adsorbent from solution (Kazemi Shariat Panahi et al., 2020).

Acid treatment of biochar with hydrochloric acid (HCl) was widely reported since it is useful to promote demineralization and cleaning of biochar surface by releasing the impurities from the pores (Cheng et al., 2020a; Kumar & Jena, 2016; Peng et al., 2016). Furthermore, HCl can act as an oxidant and modify functional groups on the surface of adsorbent (Ahmed et al., 2016; Kazemi Shariat Panahi et al., 2020). The study of reed-based biochar with and without HCl treatment after pyrolysis for phenolic compounds removal determined that acid-treating biochar is a crucial step in biochar production to ensure great adsorption capacities (Peng et al., 2016).

The most common chemical activation agents applied for adsorbent development that targeted the toxic organic compounds of interest for this review were zinc chloride ( $\text{ZnCl}_2$ ), potassium hydroxide (KOH), and phosphoric acid ( $\text{H}_3\text{PO}_4$ ).  $\text{ZnCl}_2$ -activation was associated with increasing the number of functional groups that will bind specifically to a certain organic contaminant and increasing the adsorption selectivity for organic constituents (Wang et al., 2017a). KOH-activation was reported to not only increase the number of functional groups of biochar surface (Luo et al., 2018) due to surface oxidation properties (Yakout, 2015), but also to increase the surface area from 114.4 (corn straw based-biochar with no activation) to  $2184 \text{ m}^2 \text{ g}^{-1}$  (KOH-activated corn straw based-biochar), because the biochar structure shapes with crystal KOH particles (Qu et al., 2021).  $\text{H}_3\text{PO}_4$ -activation considerably increased the surface area by 125 times for pine sawdust biochar, which also benefited from increasing the hydrophobicity to remove organic compounds (Chu et al., 2018).  $\text{ZnCl}_2$ , KOH and  $\text{H}_3\text{PO}_4$  were advantageous chemical

activation agents used to produce carbon-based materials targeting adsorption of organic compounds of interest because they can increase the surface area, develop micropores, and increase the number of functional groups on the surface.

Furthermore, carbon-based adsorbents can be produced by one-step or two-step activation when chemical activation agents are involved. One-step activation means that the feedstock will be subjected to pyrolysis only once, which could be before or after chemical activation. On the other hand, two-step activation means that feedstock will undergo pyrolysis, followed by chemical activation process, and then pyrolysis again for the second time. Even though two-step activation is less common than one-step, two-step activation can provide better yield of biochar, followed by further development of larger volume microporous structure in comparison with one-step processes (Qu et al., 2021).

In conclusion, the selection of the chemical activation agent to produce the carbon-based material will depend on the nature of organic compound, considering that some compounds of interest are hydrophobic, such as polycyclic aromatic hydrocarbons, or amphipathic compounds, such as naphthenic acids. Therefore, some chemical activation agents might be preferred over others. Considering that the adsorption of hydrophilic compounds and amphipathic compounds through the hydrophilic regions can occur on the diverse polar functional groups on biochar, the increase in the polar oxygen-containing surface groups of adsorbent and certain decrease in adsorbent hydrophobicity might provide enough sites for the adsorption of such compounds. On the other hand, the adsorption of hydrophobic compounds and amphipathic compounds through the hydrophobic regions asks for increased hydrophobicity of adsorbent, which can be achieved through the increase in pyrolysis temperature for example.

### 2.2.3 Research gaps on carbon-based adsorbents for adsorption of organic compounds

The literature review conducted for this thesis shows that there is a severe literature gap with respect to:

- (i) reuse and regeneration of carbon-based adsorbents from biomasses,
- (ii) leaching capacity of spent carbon-based materials,
- (iii) techno-economic analysis to evaluate the economic feasibility of the production of carbon-based adsorbents, and
- (iv) life cycle assessment and the impact of production technique of carbon-based material on the environment.

The study of adsorbent performance after regeneration is imperative in assessing the feasibility of reusing such adsorbents. Only a few authors in the topic of adsorption of organics from aqueous solutions by carbon-based materials from organic sources examined the regeneration of the engineered adsorbent material. As an illustration, five cycles of regeneration studies were performed on chicken manure-based biochar using ethanol as the eluent and applied the regenerated biochar for phenol removal, and the regenerated adsorbent obtained high adsorption capacity during the first three cycles, and then decreased 20% after five cycles (Thang et al., 2019). Similarly, a decrease of 4% in phenol adsorption capacity after two regeneration cycles and a 60% decrease after the fifth cycle in the regeneration studies of AC from black wattle bark waste using pyrolysis as desorption technique (Lütke et al., 2019). No loss in adsorption capacity was observed after the second regeneration cycle of coconut shell biochar, but an increase in adsorption capacity by 70%, after the third regeneration cycle was noticed, likely because the organic regeneration solvent used (hexane) might have cleaned the biochar surface (de Jesus et al., 2017). After the first regeneration cycle of walnut shells-based AC for phenanthrene using ethanol as eluent solution,

the adsorption capacity only reached 80% of original adsorption capacity (Zheng et al., 2018). Bioregeneration is another technique to promote regeneration of spent adsorbent, in which microorganisms can degrade the organic contaminants in the adsorbent. However, process waters are often hypersaline and might inhibit biological processes (Roccaro et al., 2015). The study of Roccaro et al. (2015) was able to promote bioregeneration of spent granular activated carbon in the adsorption of benzene and toluene of produced water from petroleum extraction. Therefore, the regeneration of spent adsorbent must always take into consideration the characteristics of the process water.

Studies on the effects of long-term usage of carbon-based adsorbents in terms of the natural release of pollutants were not reported for the carbon-based materials from biomasses for adsorption of organic compounds. The investigation of desorption and leaching capacities of adsorbents post-adsorption using water or wastewater instead of eluents can simulate the exposure of spent adsorbent to rainfall and wastewater at longer times. This kind of study can anticipate the potential of secondary pollution associated with the release of the adsorbed pollutant or released of other pollutants already in the carbon-based material. For example, biochars from sewage sludge have been reported to leach PAHs depending on the pyrolysis temperature, as well as metals (aluminum, barium, and calcium) (Chen et al., 2019c).

The economic feasibility of production and modification of adsorbents, the life cycle assessment, and the impact that their choice of carbon-based adsorbent production technique can have on the environment were not yet evaluated. In terms of a geographical perspective, the location and climatic factors will likely play a crucial role in the operating conditions, the feedstock source and availability for carbon-based material production, and suitability of regeneration technique. For example, sludge is one of the most studied precursor materials of carbon-based

adsorbents and that might be because it is available worldwide in any wastewater treatment plant. The study of carbon-based adsorbents from biomasses allows the dissemination of knowledge around the world that can lead to applicability in diverse settings. The environmental policy pertinent to the location of oil and gas operations also affects the outcome of process water treatment depending on the regulations, and legislation governs all water use processes (Radelyuk et al., 2019).

### **2.3 Adsorbent materials for removal of naphthenic acids from OSPW**

NAs have been reported to be successfully removed from OSPW using natural adsorbents with minimal processing, such as soils and engineered adsorbents, for example AC, biochar, biopolymers, carbon xerogel, and petroleum coke. Comparison of adsorption conditions and performance for removal of NAs is illustrated in Table 2.3.

NAs are large organic molecules that are difficult to adsorb from OSPW. As presented in Table 2.3, the adsorption capacity for NAs from OSPW is much lower than the adsorption capacities obtained for model NA compounds, which is expected since OSPW is a complex wastewater. Therefore, the study of novel, efficient and low-cost adsorbents to target these compounds in real process waters are imperative in the design of fixed-bed columns, biofilm support material or passive treatment technologies, such as pit lakes and wetlands (Benally et al., 2019; Rashed et al., 2020). Some authors reported the application of adsorbents for removal of organic matter and/or NAs from real OSPW. Such adsorbents were petroleum coke, carbon xerogel, commercial AC, biopolymer, and soil.

Commercial AC was reported for the adsorption of NAs in OSPW, attaining the highest adsorption capacity observed in the adsorption using OSPW (Table 2.3). One of the main characteristics of AC is the high surface area ( $>900 \text{ m}^2 \text{ g}^{-1}$ ).

Petroleum coke (PC) is a carbon-based waste material obtained from the oil refining process, in which about 20 kg of this by-product is resulted from the production of one barrel of synthetic crude oil (Pourrezaei et al., 2014; Zubot et al., 2012). PC can be applied as an in-situ adsorbent to treat OSPW, which could reduce the operational costs because it is readily available and free of charge and transportation costs (Pourrezaei et al., 2014). Even though the adsorption capacity attained by the PC using OSPW was low ( $1 \text{ mg g}^{-1}$ ), the PC has the advantage of being a waste material that required minimal processing.

In contrast with the PC and the AC, carbon xerogel studied by Benally et al. (2019) was designed for the adsorption of organic matter and NAs from OSPW. Their carbon-based material had abundance of mesopores and large surface area ( $573 \text{ m}^2 \text{ g}^{-1}$ ) responsible to greatly remove the acid extractable fraction and the classical NAs from OSPW. The carbon xerogel had adsorption capacity for NAs of  $7.8 \text{ mg g}^{-1}$ .

In terms of the development of biochars for adsorption of NAs from real OSPW, it was noticed very few studies on the topic. Most studies focused on model compounds of NAs (Frankel et al., 2016; Iranmanesh et al., 2014; Singh et al., 2020) instead of real process water. Only one study used real OSPW for the evaluation of biochar as adsorbent of organic matter (Bhuiyan et al., 2017). The adsorption capacity of the acid-extractable fraction was  $0.59 \text{ mg g}^{-1}$  (Bhuiyan et al., 2017). In contrast, the carbon xerogel presented adsorption capacity of the acid-extractable fraction of  $15 \text{ mg g}^{-1}$  (Benally et al., 2019). The research gaps on biochars designed for NAs adsorption from OSPW include the studies on (i) application of biochars for adsorption of NAs using real process water, (ii) adsorption selectivity of NAs in OSPW by biochar considering the diverse NA composition on OSPW, (iii) adsorption of classical and oxidized species of NAs from OSPW, (iv) biochar modifications to have enhanced adsorption of NAs from real OSPW, (v) regeneration and

reuse ability of spent biochars for NAs adsorption to reduce the risk of secondary pollution, and vi) leaching of metals from biochar to the OSPW.

The study of adsorption performance of natural soils and reclamation materials as adsorbent can have two main goals: provide an alternative low-cost adsorbent or determine environmental aspects associated with the leaching capacity, groundwater contamination potential, and environmental fate of pollutants (Qisse et al., 2020; Rao et al., 2020; Smaranda et al., 2017; Zhou et al., 2019). Soil and reclamation materials are often heterogeneous materials with distinct soil properties that might benefit or not the adsorption of organic compounds. To date, three studies have reported the use of natural adsorbents with minimal processing (soil) in the adsorption of NAs from OSPW (Janfada et al., 2006; Peng et al., 2002; Rezanezhad et al., 2012). However, the studies mainly focused on organic rich soils and did not evaluate the relationship between the properties of the materials and the adsorption capacity to try to narrow down the characteristics of soil that might be better for land applications.

**Table 2.3:** Adsorption conditions and capacity for removal of naphthenic acids by different types of adsorbents.

<b>Adsorbent</b>	<b>Source of NAs</b>	<b>Adsorption conditions</b>	<b>q<sub>t</sub> (mg g<sup>-1</sup>)</b>	<b>Reference</b>
AC (granular)	Raw OSPW	Dosage: 0.4 g L <sup>-1</sup>	60	(Islam et al., 2018)
	Ozonated OSPW	Contact time: 24 h	37	
Commercial AC	Solution of mixture of model NA compounds at pH 8	Dosage: 0.4 g L <sup>-1</sup> C <sub>0</sub> : 40 mg L <sup>-1</sup> Contact time: 48 h	40 – 255	(Niasar et al., 2016)
Biochar	Acid-extractable organics from OSPW	Dosage: 20 g L <sup>-1</sup> Contact time: 24 h	0.59	(Bhuiyan et al., 2017)
	Model NA compounds	Column study: Dosage: 0.1 g C <sub>0</sub> : 100 mg L <sup>-1</sup>	0.46 – 7.97	(Singh et al., 2020)
Biopolymer	OSPW	Dosage: 10 g L <sup>-1</sup> C <sub>0</sub> : 20.3 – 101.8 mg L <sup>-1</sup> Contact time: 24 h	–	(Arshad et al., 2016)
Carbon xerogel	Classical NAs from OSPW	Dosage: 3 g L <sup>-1</sup> C <sub>0</sub> : 26.3 mg L <sup>-1</sup> Contact time: 24 h	7.8	(Benally et al., 2019)
Petroleum coke	Solution of mixture of model NA compounds at pH 8	Dosage: 0.4 g L <sup>-1</sup> C <sub>0</sub> : 40 mg L <sup>-1</sup> Contact time: 48 h	63 – 330	(Niasar et al., 2016)
	OSPW	Dosage: 200 g L <sup>-1</sup> C <sub>0</sub> : 60.3 mg L <sup>-1</sup> Contact time: 16 h	1	(Pourrezaei et al., 2014)
Soil and reclamation material	OSPW	Dosage: 200 g L <sup>-1</sup> Contact time: 48 h	–	(Janfada et al., 2006)



## 2.4 References

- Acevedo, B., Barriocanal, C., Lupul, I., & Gryglewicz, G. (2015). Properties and performance of mesoporous activated carbons from scrap tyres, bituminous wastes and coal. *Fuel*, *151*, 83-90. <https://doi.org/10.1016/j.fuel.2015.01.010>
- Aghababaei, A., Ncibi, M. C., & Sillanpää, M. (2017). Optimized removal of oxytetracycline and cadmium from contaminated waters using chemically-activated and pyrolyzed biochars from forest and wood-processing residues. *Bioresource Technology*, *239*, 28-36. <https://doi.org/10.1016/j.biortech.2017.04.119>
- Ahmed, M. B., Zhou, J. L., Ngo, H. H., Guo, W., & Chen, M. (2016). Progress in the preparation and application of modified biochar for improved contaminant removal from water and wastewater. *Bioresource Technology*, *214*, 836-851. <https://doi.org/10.1016/j.biortech.2016.05.057>
- Alhashimi, H. A., & Aktas, C. B. (2017). Life cycle environmental and economic performance of biochar compared with activated carbon: A meta-analysis. *Resources, Conservation and Recycling*, *118*, 13-26. <https://doi.org/10.1016/j.resconrec.2016.11.016>
- Arshad, M., Khosa, M. A., Siddique, T., & Ullah, A. (2016). Modified biopolymers as sorbents for the removal of naphthenic acids from oil sands process affected water (OSPW). *Chemosphere*, *163*, 334-341. <https://doi.org/10.1016/j.chemosphere.2016.08.015>
- Baharum, N. A., Nasir, H. M., Ishak, M. Y., Isa, N. M., Hassan, M. A., & Aris, A. Z. (2020). Highly efficient removal of diazinon pesticide from aqueous solutions by using coconut shell-modified biochar. *Arabian Journal of Chemistry*, *13*(7), 6106-6121. <https://doi.org/10.1016/j.arabjc.2020.05.011>
- Banerjee, K., Cheremisinoff, P. N., & Cheng, S. L. (1997). Adsorption kinetics of o-xylene by flyash. *Water Research*, *31*(2), 249-261. [https://doi.org/10.1016/S0043-1354\(96\)00003-6](https://doi.org/10.1016/S0043-1354(96)00003-6)
- Benally, C., Messele, S. A., & Gamal El-Din, M. (2019). Adsorption of organic matter in oil sands process water (OSPW) by carbon xerogel. *Water Research*, *154*, 402-411. <https://doi.org/10.1016/j.watres.2019.01.053>
- Bhuiyan, T. I., Tak, J. K., Sessarego, S., Harfield, D., & Hill, J. M. (2017). Adsorption of acid-extractable organics from oil sands process-affected water onto biomass-based biochar:

- Metal content matters. *Chemosphere*, 168, 1337-1344.  
<https://doi.org/10.1016/j.chemosphere.2016.11.126>
- Bispo, M. D., Schneider, J. K., da Silva Oliveira, D., Tomasini, D., da Silva Maciel, G. P., Schena, T., Onorevoli, B., Bjerck, T. R., Jacques, R. A., Krause, L. C., & Caramão, E. B. (2018). Production of activated biochar from coconut fiber for the removal of organic compounds from phenolic. *Journal of Environmental Chemical Engineering*, 6(2), 2743-2750.  
<https://doi.org/10.1016/j.jece.2018.04.029>
- Chen, X., Yang, L., Myneni, S. C. B., & Deng, Y. (2019c). Leaching of polycyclic aromatic hydrocarbons (PAHs) from sewage sludge-derived biochar. *Chemical Engineering Journal*, 373, 840-845. <https://doi.org/10.1016/j.cej.2019.05.059>
- Chen, Y.-d., Wang, R., Duan, X., Wang, S., Ren, N.-q., & Ho, S.-H. (2020b). Production, properties, and catalytic applications of sludge derived biochar for environmental remediation. *Water Research*, 187, 116390. <https://doi.org/10.1016/j.watres.2020.116390>
- Cheng, H., Ji, R., Bian, Y., Jiang, X., & Song, Y. (2020a). From macroalgae to porous graphitized nitrogen-doped biochars – Using aquatic biota to treat polycyclic aromatic hydrocarbons-contaminated water. *Bioresource Technology*, 303, 122947.  
<https://doi.org/10.1016/j.biortech.2020.122947>
- Chu, G., Zhao, J., Huang, Y., Zhou, D., Liu, Y., Wu, M., Peng, H., Zhao, Q., Pan, B., & Steinberg, C. E. W. (2018). Phosphoric acid pretreatment enhances the specific surface areas of biochars by generation of micropores. *Environmental Pollution*, 240, 1-9.  
<https://doi.org/10.1016/j.envpol.2018.04.003>
- Crittenden, J. C. (2012). *MWH's water treatment : principles and design* (3rd ed. / rev. by John C. Crittenden [and others]. ed.) [eBook]. John Wiley and Sons.  
<https://doi.org/10.1002/9781118131473>
- Danish, M., & Ahmad, T. (2018). A review on utilization of wood biomass as a sustainable precursor for activated carbon production and application. *Renewable and Sustainable Energy Reviews*, 87, 1-21. <https://doi.org/10.1016/j.rser.2018.02.003>
- de Jesus, J. H. F., da C. Cunha, G., Cardoso, E. M. C., Mangrich, A. S., & Romão, L. P. C. (2017). Evaluation of waste biomasses and their biochars for removal of polycyclic aromatic

- hydrocarbons. *Journal of Environmental Management*, 200, 186-195. <https://doi.org/10.1016/j.jenvman.2017.05.084>
- El-Naas, M. H., Surkatti, R., & Al-Zuhair, S. (2016). Petroleum refinery wastewater treatment: A pilot scale study. *Journal of Water Process Engineering*, 14, 71-76. <https://doi.org/10.1016/j.jwpe.2016.10.005>
- Fan, J., Zhang, J., Zhang, C., Ren, L., & Shi, Q. (2011). Adsorption of 2,4,6-trichlorophenol from aqueous solution onto activated carbon derived from loosestrife. *Desalination*, 267(2), 139-146. <https://doi.org/10.1016/j.desal.2010.09.016>
- Feng, D., Guo, D., Zhang, Y., Sun, S., Zhao, Y., Shang, Q., Sun, H., Wu, J., & Tan, H. (2020). Functionalized construction of biochar with hierarchical pore structures and surface O-/N-containing groups for phenol adsorption. *Chemical Engineering Journal*, 127707. <https://doi.org/10.1016/j.cej.2020.127707>
- Foo, K. Y., & Hameed, B. H. (2010). Insights into the modeling of adsorption isotherm systems. *Chemical Engineering Journal*, 156(1), 2-10. <https://doi.org/10.1016/j.cej.2009.09.013>
- Frankel, M. L., Bhuiyan, T. I., Veksha, A., Demeter, M. A., Layzell, D. B., Helleur, R. J., Hill, J. M., & Turner, R. J. (2016). Removal and biodegradation of naphthenic acids by biochar and attached environmental biofilms in the presence of co-contaminating metals. *Bioresource Technology*, 216, 352-361. <https://doi.org/10.1016/j.biortech.2016.05.084>
- Freundlich, H. (1906). *Über die Adsorption in Lösungen*. Wilhelm Engelmann.
- Genuino, D. A. D., de Luna, M. D. G., & Capareda, S. C. (2018). Improving the surface properties of municipal solid waste-derived pyrolysis biochar by chemical and thermal activation: Optimization of process parameters and environmental application. *Waste Management*, 72, 255-264. <https://doi.org/10.1016/j.wasman.2017.11.038>
- Godlewska, P., Siatecka, A., Kończak, M., & Oleszczuk, P. (2019). Adsorption capacity of phenanthrene and pyrene to engineered carbon-based adsorbents produced from sewage sludge or sewage sludge-biomass mixture in various gaseous conditions. *Bioresource Technology*, 280, 421-429. <https://doi.org/10.1016/j.biortech.2019.02.021>
- Guo, W., Wang, S., Wang, Y., Lu, S., & Gao, Y. (2018). Sorptive removal of phenanthrene from aqueous solutions using magnetic and non-magnetic rice husk-derived biochars. *Royal Society Open Science*, 5(5), 172382. <https://doi.com/10.1098/rsos.172382>

- Gupta, V. K., Nayak, A., Agarwal, S., & Tyagi, I. (2014). Potential of activated carbon from waste rubber tire for the adsorption of phenolics: Effect of pre-treatment conditions. *Journal of Colloid and Interface Science*, 417, 420-430. <https://doi.org/10.1016/j.jcis.2013.11.067>
- Hagemann, N., Spokas, K., Schmidt, H.-P., Kägi, R., Böhler, M. A., & Bucheli, T. D. (2018). Activated Carbon, Biochar and Charcoal: Linkages and Synergies across Pyrogenic Carbon's ABCs. *Water*, 10(2), 182. <https://www.mdpi.com/2073-4441/10/2/182>
- Hairuddin, M. N., Mubarak, N. M., Khalid, M., Abdullah, E. C., Walvekar, R., & Karri, R. R. (2019). Magnetic palm kernel biochar potential route for phenol removal from wastewater. *Environmental Science and Pollution Research*, 26(34), 35183-35197. <https://doi.com/10.1007/s11356-019-06524-w>
- Hao, Z., Wang, C., Yan, Z., Jiang, H., & Xu, H. (2018). Magnetic particles modification of coconut shell-derived activated carbon and biochar for effective removal of phenol from water. *Chemosphere*, 211, 962-969. <https://doi.org/10.1016/j.chemosphere.2018.08.038>
- Ho, Y. S., & McKay, G. (1999). Pseudo-second order model for sorption processes. *Process Biochemistry*, 34(5), 451-465. [https://doi.org/10.1016/S0032-9592\(98\)00112-5](https://doi.org/10.1016/S0032-9592(98)00112-5)
- Hsieh, C.-T., & Teng, H. (2000). Influence of mesopore volume and adsorbate size on adsorption capacities of activated carbons in aqueous solutions. *Carbon*, 38(6), 863-869. [https://doi.org/10.1016/S0008-6223\(99\)00180-3](https://doi.org/10.1016/S0008-6223(99)00180-3)
- Hu, H., & Xu, K. (2020). Chapter 8 - Physicochemical technologies for HRP and risk control. In H. Ren & X. Zhang (Eds.), *High-Risk Pollutants in Wastewater* (pp. 169-207). Elsevier. <https://doi.org/https://doi.org/10.1016/B978-0-12-816448-8.00008-3>
- Iranmanesh, S., Harding, T., Abedi, J., Seyedeyn-Azad, F., & Layzell, D. B. (2014). Adsorption of naphthenic acids on high surface area activated carbons. *Journal of Environmental Science and Health, Part A*, 49(8), 913-922. <https://doi.org/10.1080/10934529.2014.894790>
- Islam, M. S., Kwak, J.-H., Nzediegwu, C., Wang, S., Palansuriya, K., Kwon, E. E., Naeth, M. A., El-Din, M. G., Ok, Y. S., & Chang, S. X. (2021). Biochar heavy metal removal in aqueous solution depends on feedstock type and pyrolysis purging gas. *Environmental Pollution*, 281, 117094. <https://doi.org/10.1016/j.envpol.2021.117094>

- Islam, M. S., McPhedran, K. N., Messele, S. A., Liu, Y., & Gamal El-Din, M. (2018). Isotherm and kinetic studies on adsorption of oil sands process-affected water organic compounds using granular activated carbon. *Chemosphere*, 202, 716-725. <https://doi.org/10.1016/j.chemosphere.2018.03.149>
- Janfada, A., Headley, J. V., Peru, K. M., & Barbour, S. L. (2006). A Laboratory Evaluation of the Sorption of Oil Sands Naphthenic Acids on Organic Rich Soils. *Journal of Environmental Science and Health, Part A*, 41(6), 985-997. <https://doi.org/10.1080/10934520600620105>
- Karmacharya, M. S., Gupta, V. K., Tyagi, I., Agarwal, S., & Jha, V. K. (2016). Removal of As(III) and As(V) using rubber tire derived activated carbon modified with alumina composite. *Journal of Molecular Liquids*, 216, 836-844. <https://doi.org/10.1016/j.molliq.2016.02.025>
- Kazemi Shariat Panahi, H., Dehghani, M., Ok, Y. S., Nizami, A.-S., Khoshnevisan, B., Mussatto, S. I., Aghbashlo, M., Tabatabaei, M., & Lam, S. S. (2020). A comprehensive review of engineered biochar: Production, characteristics, and environmental applications. *Journal of Cleaner Production*, 270, 122462. <https://doi.org/10.1016/j.jclepro.2020.122462>
- Kumar, A., & Jena, H. M. (2016). Removal of methylene blue and phenol onto prepared activated carbon from Fox nutshell by chemical activation in batch and fixed-bed column. *Journal of Cleaner Production*, 137, 1246-1259. <https://doi.org/10.1016/j.jclepro.2016.07.177>
- Kumar, A., Saini, K., & Bhaskar, T. (2020). Hydrochar and biochar: Production, physicochemical properties and techno-economic analysis. *Bioresource Technology*, 310, 123442. <https://doi.org/10.1016/j.biortech.2020.123442>
- Kwon, S., Fan, M., DaCosta, H. F. M., Russell, A. G., Berchtold, K. A., & Dubey, M. K. (2011). Chapter 10 - CO<sub>2</sub> Sorption. In D. A. Bell, B. F. Towler, & M. Fan (Eds.), *Coal Gasification and Its Applications* (pp. 293-339). William Andrew Publishing. <https://doi.org/10.1016/B978-0-8155-2049-8.10010-5>
- Lagergren, S. (1898). Zur theorie der sogenannten adsorption gelöster stoffe.
- Langmuir, I. (1918). The adsorption of gases on plane surfaces of glass, mica and platinum. *Journal of the American Chemical Society*, 40(9), 1361-1403. <https://doi.org/10.1021/ja02242a004>
- Lawal, A. A., Hassan, M. A., Ahmad Farid, M. A., Tengku Yasim-Anuar, T. A., Samsudin, M. H., Mohd Yusoff, M. Z., Zakaria, M. R., Mokhtar, M. N., & Shirai, Y. (2021). Adsorption

- mechanism and effectiveness of phenol and tannic acid removal by biochar produced from oil palm frond using steam pyrolysis. *Environmental Pollution*, 269, 116197. <https://doi.org/10.1016/j.envpol.2020.116197>
- Lawal, A. A., Hassan, M. A., Ahmad Farid, M. A., Yasim-Anuar, T. A. T., Mohd Yusoff, M. Z., Zakaria, M. R., Roslan, A. M., Mokhtar, M. N., & Shirai, Y. (2020). One-step steam pyrolysis for the production of mesoporous biochar from oil palm frond to effectively remove phenol in facultatively treated palm oil mill effluent. *Environmental Technology & Innovation*, 18, 100730. <https://doi.org/10.1016/j.eti.2020.100730>
- Li, C., Fu, L., Stafford, J., Belosevic, M., & Gamal El-Din, M. (2017). The toxicity of oil sands process-affected water (OSPW): A critical review. *Science of the Total Environment*, 601-602, 1785-1802. <https://doi.org/10.1016/j.scitotenv.2017.06.024>
- Li, D.-C., & Jiang, H. (2017). The thermochemical conversion of non-lignocellulosic biomass to form biochar: A review on characterizations and mechanism elucidation. *Bioresource Technology*, 246, 57-68. <https://doi.org/10.1016/j.biortech.2017.07.029>
- Li, Y., Xing, B., Ding, Y., Han, X., & Wang, S. (2020c). A critical review of the production and advanced utilization of biochar via selective pyrolysis of lignocellulosic biomass. *Bioresource Technology*, 312, 123614. <https://doi.org/10.1016/j.biortech.2020.123614>
- Liu, H., Xu, G., & Li, G. (2021). Preparation of porous biochar based on pharmaceutical sludge activated by NaOH and its application in the adsorption of tetracycline. *Journal of Colloid and Interface Science*, 587, 271-278. <https://doi.org/10.1016/j.jcis.2020.12.014>
- Luo, J., Li, X., Ge, C., Müller, K., Yu, H., Huang, P., Li, J., Tsang, D. C. W., Bolan, N. S., Rinklebe, J., & Wang, H. (2018). Sorption of norfloxacin, sulfamerazine and oxytetracycline by KOH-modified biochar under single and ternary systems. *Bioresource Technology*, 263, 385-392. <https://doi.org/10.1016/j.biortech.2018.05.022>
- Lütke, S. F., Igansi, A. V., Pegoraro, L., Dotto, G. L., Pinto, L. A. A., & Cadaval, T. R. S. (2019). Preparation of activated carbon from black wattle bark waste and its application for phenol adsorption. *Journal of Environmental Chemical Engineering*, 7(5), 103396. <https://doi.org/10.1016/j.jece.2019.103396>

- Lv, S., Li, C., Mi, J., & Meng, H. (2020). A functional activated carbon for efficient adsorption of phenol derived from pyrolysis of rice husk, KOH-activation and EDTA-4Na-modification. *Applied Surface Science*, 510, 145425. <https://doi.org/10.1016/j.apsusc.2020.145425>
- Mary, G. S., Sugumaran, P., Niveditha, S., Ramalakshmi, B., Ravichandran, P., & Seshadri, S. (2016). Production, characterization and evaluation of biochar from pod (*Pisum sativum*), leaf (*Brassica oleracea*) and peel (*Citrus sinensis*) wastes. *International Journal of Recycling of Organic Waste in Agriculture*, 5(1), 43-53. <https://doi.com/10.1007/s40093-016-0116-8>
- Medeiros, D. C. C. d. S., Nzediegwu, C., Benally, C., Messele, S. A., Kwak, J.-H., Naeth, M. A., Ok, Y. S., Chang, S. X., & Gamal El-Din, M. (2022). Pristine and engineered biochar for the removal of contaminants co-existing in several types of industrial wastewaters: A critical review. *Science of the Total Environment*, 809, 151120. <https://doi.org/10.1016/j.scitotenv.2021.151120>
- Mishra, S., Yadav, S. S., Rawat, S., Singh, J., & Koduru, J. R. (2019). Corn husk derived magnetized activated carbon for the removal of phenol and para-nitrophenol from aqueous solution: Interaction mechanism, insights on adsorbent characteristics, and isothermal, kinetic and thermodynamic properties. *Journal of Environmental Management*, 246, 362-373. <https://doi.org/10.1016/j.jenvman.2019.06.013>
- Mohammed, N. A. S., Abu-Zurayk, R. A., Hamadneh, I., & Al-Dujaili, A. H. (2018). Phenol adsorption on biochar prepared from the pine fruit shells: Equilibrium, kinetic and thermodynamics studies. *Journal of Environmental Management*, 226, 377-385. <https://doi.org/10.1016/j.jenvman.2018.08.033>
- Morris, J. C., Weber, W. J., Supply, U. S. D. o. W., & Control, P. (1966). *Adsorption of Biochemically Resistant Materials from Solution: 2*. Federal Water Pollution Control Administration, Basic and Applied Sciences Program. <https://books.google.ca/books?id=nDFSQAAMAAJ>
- Mubarik, S., Saeed, A., Athar, M. M., & Iqbal, M. (2016). Characterization and mechanism of the adsorptive removal of 2,4,6-trichlorophenol by biochar prepared from sugarcane baggase. *Journal of Industrial and Engineering Chemistry*, 33, 115-121. <https://doi.org/10.1016/j.jiec.2015.09.029>

- Negara, D. N. K. P., Nindhia, T. G. T., Surata, I. W., Hidajat, F., & Sucipta, M. (2019). Nanopore structures, surface morphology, and adsorption capacity of tabah bamboo-activated carbons. *Surfaces and Interfaces*, 16, 22-28. <https://doi.org/10.1016/j.surfin.2019.04.002>
- Niasar, H. S., Li, H., Kasanneni, T. V. R., Ray, M. B., & Xu, C. (2016). Surface amination of activated carbon and petroleum coke for the removal of naphthenic acids and treatment of oil sands process-affected water (OSPW). *Chemical Engineering Journal*, 293, 189-199. <https://doi.org/10.1016/j.cej.2016.02.062>
- Park, K.-H., Balathanigaimani, M. S., Shim, W.-G., Lee, J.-W., & Moon, H. (2010). Adsorption characteristics of phenol on novel corn grain-based activated carbons. *Microporous and Mesoporous Materials*, 127(1), 1-8. <https://doi.org/10.1016/j.micromeso.2009.06.032>
- Peng, J., Headley, J. V., & Barbour, S. L. (2002). Adsorption of single-ring model naphthenic acids on soils. *Canadian Geotechnical Journal*, 39(6), 1419-1426. <https://doi.org/10.1139/t02-098>
- Peng, P., Lang, Y.-H., & Wang, X.-M. (2016). Adsorption behavior and mechanism of pentachlorophenol on reed biochars: pH effect, pyrolysis temperature, hydrochloric acid treatment and isotherms. *Ecological Engineering*, 90, 225-233. <https://doi.org/10.1016/j.ecoleng.2016.01.039>
- Pourrezaei, P., Alpatova, A., Chelme-Ayala, P., Perez-Estrada, L. A., Jensen-Fontaine, M., Le, X. C., & Gamal El-Din, M. (2014). Impact of petroleum coke characteristics on the adsorption of the organic fractions from oil sands process-affected water. *International Journal of Environmental Science and Technology*, 11(7), 2037-2050. <https://doi.org/10.1007/s13762-013-0406-x>
- Prasannamedha, G., Kumar, P. S., Mehala, R., Sharumitha, T. J., & Surendhar, D. (2021). Enhanced adsorptive removal of sulfamethoxazole from water using biochar derived from hydrothermal carbonization of sugarcane bagasse. *Journal of Hazardous Materials*, 407, 124825. <https://doi.org/10.1016/j.jhazmat.2020.124825>
- Qiao, K., Tian, W., Bai, J., Dong, J., Zhao, J., Gong, X., & Liu, S. (2018). Preparation of biochar from *Enteromorpha prolifera* and its use for the removal of polycyclic aromatic hydrocarbons (PAHs) from aqueous solution. *Ecotoxicology and Environmental Safety*, 149, 80-87. <https://doi.org/10.1016/j.ecoenv.2017.11.027>



- Qisse, N., El Alouani, M., El Azzouzi, L., El Fadil, I., Saufi, H., Alaoui El Belghiti, M., Zrineh, A., & El Azzouzi, M. (2020). Adsorption of Imazalil herbicide onto Moroccan agricultural soils: Kinetic and isotherm adsorption studies. *Groundwater for Sustainable Development*, 11, 100468. <https://doi.org/10.1016/j.gsd.2020.100468>
- Qu, J., Wang, Y., Tian, X., Jiang, Z., Deng, F., Tao, Y., Jiang, Q., Wang, L., & Zhang, Y. (2021). KOH-activated porous biochar with high specific surface area for adsorptive removal of chromium (VI) and naphthalene from water: Affecting factors, mechanisms and reusability exploration. *Journal of Hazardous Materials*, 401, 123292. <https://doi.org/10.1016/j.jhazmat.2020.123292>
- Quinlan, P. J., & Tam, K. C. (2015). Water treatment technologies for the remediation of naphthenic acids in oil sands process-affected water. *Chemical Engineering Journal*, 279, 696-714. <https://doi.org/10.1016/j.cej.2015.05.062>
- Radelyuk, I., Tussupova, K., Zhapargazinova, K., Yelubay, M., & Persson, M. (2019). Pitfalls of Wastewater Treatment in Oil Refinery Enterprises in Kazakhstan—A System Approach. *Sustainability*, 11(6). <https://doi.org/10.3390/su11061618>
- Rajapaksha, A. U., Vithanage, M., Ahmad, M., Seo, D.-C., Cho, J.-S., Lee, S.-E., Lee, S. S., & Ok, Y. S. (2015). Enhanced sulfamethazine removal by steam-activated invasive plant-derived biochar. *Journal of Hazardous Materials*, 290, 43-50. <https://doi.org/10.1016/j.jhazmat.2015.02.046>
- Rao, L., Luo, J., Zhou, W., Zou, Z., Tang, L., & Li, B. (2020). Adsorption–desorption behavior of benzobicyclon hydrolysate in different agricultural soils in China. *Ecotoxicology and Environmental Safety*, 202, 110915. <https://doi.org/10.1016/j.ecoenv.2020.110915>
- Rashed, Y., Messele, S. A., Zeng, H., & Gamal El-Din, M. (2020). Mesoporous carbon xerogel material for the adsorption of model naphthenic acids: structure effect and kinetics modelling. *Environmental Technology*, 41(27), 3534-3543. <https://doi.org/10.1080/09593330.2019.1615130>
- Regkouzas, P., & Diamadopoulou, E. (2019). Adsorption of selected organic micro-pollutants on sewage sludge biochar. *Chemosphere*, 224, 840-851. <https://doi.org/10.1016/j.chemosphere.2019.02.165>

- Ren, L., Zhang, J., Li, Y., & Zhang, C. (2011). Preparation and evaluation of cattail fiber-based activated carbon for 2,4-dichlorophenol and 2,4,6-trichlorophenol removal. *Chemical Engineering Journal*, 168(2), 553-561. <https://doi.org/10.1016/j.cej.2011.01.021>
- Rezanezhad, F., Price, J. S., & Craig, J. R. (2012). The effects of dual porosity on transport and retardation in peat: A laboratory experiment. *Canadian Journal of Soil Science*, 92(5), 723-732. <https://doi.org/10.4141/cjss2011-050>
- Roccaro, P., Lombardo, G., & Vagliasindi, F. G. A. (2015). Offline bioregeneration of spent activated carbon loaded with real Produced Water and its adsorption capacity for benzene and toluene. *Desalination and Water Treatment*, 55(3), 756-766. <https://doi.org/10.1080/19443994.2014.964328>
- Rodrigues, L. A., da Silva, M. L. C. P., Alvarez-Mendes, M. O., Coutinho, A. d. R., & Thim, G. P. (2011). Phenol removal from aqueous solution by activated carbon produced from avocado kernel seeds. *Chemical Engineering Journal*, 174(1), 49-57. <https://doi.org/10.1016/j.cej.2011.08.027>
- Ruthven, D. M. (1984). *Principles of adsorption and adsorption processes*. John Wiley & Sons.
- Samara, F., Khamis, M., Sara, Z., & Elsayed, Y. (2017). Removal of benzo (a) anthracene from water using a novel UAE sludge-based activated adsorbent. *Desalination and Water Treatment*, 1-8. <https://doi.org/10.5004/dwt.2017.21422>
- Shabir, F., Sultan, M., Miyazaki, T., Saha, B. B., Askalany, A., Ali, I., Zhou, Y., Ahmad, R., & Shamshiri, R. R. (2020). Recent updates on the adsorption capacities of adsorbent-adsorbate pairs for heat transformation applications. *Renewable and Sustainable Energy Reviews*, 119, 109630. <https://doi.org/10.1016/j.rser.2019.109630>
- Shen, Y., Zhou, Y., Fu, Y., & Zhang, N. (2020). Activated carbons synthesized from unaltered and pelletized biomass wastes for bio-tar adsorption in different phases. *Renewable Energy*, 146, 1700-1709. <https://doi.org/10.1016/j.renene.2019.07.167>
- Shi, Q., Li, A., Zhu, Z., & Liu, B. (2013). Adsorption of naphthalene onto a high-surface-area carbon from waste ion exchange resin. *Journal of Environmental Sciences*, 25(1), 188-194. [https://doi.org/10.1016/S1001-0742\(12\)60017-5](https://doi.org/10.1016/S1001-0742(12)60017-5)
- Singh, N., & Balomajumder, C. (2016). Simultaneous removal of phenol and cyanide from aqueous solution by adsorption onto surface modified activated carbon prepared from

- coconut shell. *Journal of Water Process Engineering*, 9, 233-245.  
<https://doi.org/10.1016/j.jwpe.2016.01.008>
- Singh, R., Naik, D. V., Dutta, R. K., & Kanaujia, P. K. (2020). Biochars for the removal of naphthenic acids from water: A prospective approach towards remediation of petroleum refinery wastewater. *Journal of Cleaner Production*, 266, 121986.  
<https://doi.org/10.1016/j.jclepro.2020.121986>
- Smaranda, C., Popescu, M.-C., Bulgariu, D., Măluțan, T., & Gavrilesu, M. (2017). Adsorption of organic pollutants onto a Romanian soil: Column dynamics and transport. *Process Safety and Environmental Protection*, 108, 108-120. <https://doi.org/10.1016/j.psep.2016.06.027>
- Sullivan, G. L., Prigmore, R. M., Knight, P., & Godfrey, A. R. (2019). Activated carbon biochar from municipal waste as a sorptive agent for the removal of polyaromatic hydrocarbons (PAHs), phenols and petroleum based compounds in contaminated liquids. *Journal of Environmental Management*, 251, 109551.  
<https://doi.org/10.1016/j.jenvman.2019.109551>
- Thang, P. Q., Jitae, K., Giang, B. L., Viet, N. M., & Huong, P. T. (2019). Potential application of chicken manure biochar towards toxic phenol and 2,4-dinitrophenol in wastewaters. *Journal of Environmental Management*, 251, 109556.  
<https://doi.org/10.1016/j.jenvman.2019.109556>
- Turner, N. H. (1975). Kinetics of chemisorption: An examination of the Elovich equation. *Journal of Catalysis*, 36(3), 262-265. [https://doi.org/10.1016/0021-9517\(75\)90035-4](https://doi.org/10.1016/0021-9517(75)90035-4)
- Wang, F., Sun, H., Ren, X., & Zhang, K. (2017a). Sorption of naphthalene and its hydroxyl substitutes onto biochars in single-solute and bi-solute systems with propranolol as the co-solute. *Chemical Engineering Journal*, 326, 281-291.  
<https://doi.org/10.1016/j.cej.2017.05.159>
- Wang, J., & Guo, X. (2020). Adsorption isotherm models: Classification, physical meaning, application and solving method. *Chemosphere*, 258, 127279.  
<https://doi.org/10.1016/j.chemosphere.2020.127279>
- Wang, Y., Qiu, L., Zhu, M., Sun, G., Zhang, T., & Kang, K. (2019). Comparative Evaluation of Hydrothermal Carbonization and Low Temperature Pyrolysis of *Eucommia ulmoides*

- Oliver for the Production of Solid Biofuel. *Scientific Reports*, 9(1), 5535. <https://doi.org/10.1038/s41598-019-38849-4>
- Wang, Z., Han, L., Sun, K., Jin, J., Ro, K. S., Libra, J. A., Liu, X., & Xing, B. (2016). Sorption of four hydrophobic organic contaminants by biochars derived from maize straw, wood dust and swine manure at different pyrolytic temperatures. *Chemosphere*, 144, 285-291. <https://doi.org/10.1016/j.chemosphere.2015.08.042>
- Worch, E. (2012). *Adsorption Technology in Water Treatment*. De Gruyter. <https://doi.org/10.1515/9783110240238>
- Wu, W., Miao, G., Yan, X., Xing, B., & Yang, K. (2020). Correlations and prediction of adsorption capacity and affinity of aromatic compounds on activated carbons. *Science of the Total Environment*, 704, 135457. <https://doi.org/10.1016/j.scitotenv.2019.135457>
- Xing, J., Xu, G., & Li, G. (2021). Comparison of pyrolysis process, various fractions and potential soil applications between sewage sludge-based biochars and lignocellulose-based biochars. *Ecotoxicology and Environmental Safety*, 208, 111756. <https://doi.org/10.1016/j.ecoenv.2020.111756>
- Yakout, S. M. (2015). Monitoring the Changes of Chemical Properties of Rice Straw–Derived Biochars Modified by Different Oxidizing Agents and Their Adsorptive Performance for Organics. *Bioremediation Journal*, 19(2), 171-182. <https://doi.org/10.1080/10889868.2015.1029115>
- Yang, K., Jiang, Y., Yang, J., & Lin, D. (2018). Correlations and adsorption mechanisms of aromatic compounds on biochars produced from various biomass at 700 °C. *Environmental Pollution*, 233, 64-70. <https://doi.org/10.1016/j.envpol.2017.10.035>
- Zhang, G., Yang, H., Jiang, M., & Zhang, Q. (2021). Preparation and characterization of activated carbon derived from deashing coal slime with ZnCl<sub>2</sub> activation. *Colloids and Surfaces A: Physicochemical and Engineering Aspects*, 128124. <https://doi.org/10.1016/j.colsurfa.2021.128124>
- Zheng, X., Lin, H., Tao, Y., & Zhang, H. (2018). Selective adsorption of phenanthrene dissolved in Tween 80 solution using activated carbon derived from walnut shells. *Chemosphere*, 208, 951-959. <https://doi.org/10.1016/j.chemosphere.2018.06.025>

- Zhou, W., Zhang, Y., Li, W., Jia, H., Huang, H., & Li, B. (2019). Adsorption isotherms, degradation kinetics, and leaching behaviors of cyanogen and hydrogen cyanide in eight texturally different agricultural soils from China. *Ecotoxicology and Environmental Safety*, 185, 109704. <https://doi.org/10.1016/j.ecoenv.2019.109704>
- Zhu, Y., & Kolar, P. (2014). Adsorptive removal of p-cresol using coconut shell-activated char. *Journal of Environmental Chemical Engineering*, 2(4), 2050-2058. <https://doi.org/10.1016/j.jece.2014.08.022>
- Zubot, W., MacKinnon, M. D., Chelme-Ayala, P., Smith, D. W., & Gamal El-Din, M. (2012). Petroleum coke adsorption as a water management option for oil sands process-affected water. *Science of the Total Environment*, 427-428, 364-372. <https://doi.org/10.1016/j.scitotenv.2012.04.024>

## Chapter 3 Investigation of Reclamation Materials from Surface Mining of Oil Sands for Adsorption of Naphthenic Acids<sup>2</sup>

### 3.1 Introduction

The water consumption and production of process water in oil and gas industries mainly occur during the extraction and oil processing (Jafarinejad, 2017). One of the extraction techniques is the Clark caustic hot water extraction process (Clark & Pasternack, 1932), which is largely applied in the the extraction of bitumen by the Alberta oil sand industries. A high volume of oil sands process water (OSPW) is generated (Zubot et al., 2012) because 0.2 to 2.6 barrels of fresh water are required per barrel of bitumen (Natural Resources Canada, 2020). In terms of composition, OSPW is characterized by high alkalinity and contains some organic contaminants with recalcitrant characteristics that include naphthenic acids (NAs) (Pourrezaei et al., 2014), polycyclic aromatic hydrocarbons (PAHs), phenolic compounds, and xylenes (Lévesque, 2014). In fact, NAs account for more than 50% of all organic compounds in OSPW (Grewer et al., 2010).

NAs are amphiphilic compounds and saturated aliphatic and alicyclic carboxylic acids with recalcitrant characteristics that are solubilized in the OSPW during the extraction of bitumen from oil sands using the caustic hot water (Quinlan & Tam, 2015). The classical NAs are classified based on the carbon number ( $n$ ;  $7 \leq n \leq 26$ ), the hydrogen deficiency number ( $Z$ ;  $0 \leq -Z \leq 24$ ) resulted from ring or double bond formation, and the oxygen number ( $x$ ) through the chemical

---

<sup>2</sup> A version of this chapter was published as: Medeiros, D. C. C. S., Chelme-Ayala, P., and Gamal El-Din, M. Sorption and desorption of naphthenic acids on reclamation materials: Mechanisms and selectivity of naphthenic acids from oil sands process water. *Chemosphere*, 2023. <https://doi.org/10.1016/j.chemosphere.2023.138462>

formula  $C_nH_{2n+z}O_x$ . Classical NAs are represented by  $x = 2$  and oxidized NAs by  $x$  number from 3 to 6 (Huang et al., 2015a). There are several structures of NAs in the OSPW (Huang et al., 2018), and more branched and complex structures of NAs increase the difficulty of degradation (Wu et al., 2019). It was previously suggested that NAs are the primary source of OSPW toxicity (Hughes et al., 2017) and might cause environmental concerns due to the acute and chronic toxicity to living organisms (Li et al., 2017), such as mammals (Rogers et al., 2002), zebrafish (Scarlett et al., 2013), marine bacteria (Frank et al., 2008), and fathead minnow embryos (Marentette et al., 2015).

Several processes have been used to remove or degrade NAs including supported biofilters (Arslan & Gamal El-Din, 2021), adsorption (Benally et al., 2019), and advanced oxidation through catalytic ozonation (Messele et al., 2021), electro-oxidation (Abdalrhman et al., 2020), UV/H<sub>2</sub>O<sub>2</sub> oxidation (Fang et al., 2019), and photocatalysis (Liu et al., 2016). Adsorption is an important process in the fate and impact of organic contaminants in the environment and includes the adsorption process (Schwarzenbach et al., 2005), which has already proven effective in removing/isolating NAs from OSPW (Benally et al., 2019; Niasar et al., 2019; Pourrezaei et al., 2014). To date, three studies have reported the use of natural adsorbents with minimal processing (soil) in the adsorption of NAs (Janfada et al., 2006; Peng et al., 2002; Rezanezhad et al., 2012).

The oil sands are located below the layers called muskeg (top layer characteristic of peatland) and overburden (layer below muskeg and predominantly constituted of sand and clay). The surface mining of oil sands requires the excavation of such layers to reach the oil sands (Speight, 2013), and after excavation, the muskeg and the overburden are stored for use in land reclamation. The study of such reclamation materials from an oil sands extraction site as adsorbents of NAs from OSPW can provide data on the transport of NAs in oil sands reclamation landscape where these materials may be used.

Therefore, the purpose of this study was to investigate three reclamation materials from oil sands excavation sites (peat-mineral mix and Pleistocene fluvial sands sourced from different locations) as adsorbents of NAs to evaluate the adsorption characteristics. The specific objectives were to (1) evaluate the adsorption and desorption behavior of two model compounds of NAs on three reclamation materials and determine the possible adsorption mechanisms, (2) apply the reclamation materials in the adsorption of classical NAs from real OSPW, and (3) determine the relationship between the uptake of NAs and the properties of reclamation materials.

## **3.2 Methodology**

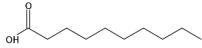
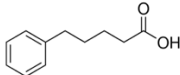
### **3.2.1 Chemicals**

Model NA compounds decanoic acid  $\geq 98\%$  (DA) and 5-phenylvaleric acid 99% (PVA) were purchased from Sigma Aldrich (Germany) and their characteristics are presented in Table 3.1. Solutions were prepared in 5 mM analytical grade sodium bicarbonate ( $\text{NaHCO}_3$ ) buffer to maintain pH 8.5 to mimic the pH of real OSPW.

Raw OSPW (pH = 8.5; classical NAs concentration =  $46.3 \text{ mg L}^{-1}$ ) was collected from an oil sands tailings pond in Fort McMurray, Alberta, Canada and stored in a cold room at  $4^\circ\text{C}$ .



**Table 3.1:** Characteristics of selected model compounds of naphthenic acids.

Compound	DA	PVA
Formula	C <sub>10</sub> H <sub>20</sub> O <sub>2</sub>	C <sub>11</sub> H <sub>14</sub> O <sub>2</sub>
Structure		
Molecular weight (g mol <sup>-1</sup> )	172.3	178.2
DBE <sup>1</sup>	1	5
-Z <sup>2</sup>	0	8
Solubility <sup>3,4</sup> (g L <sup>-1</sup> )	563	779
pKa <sup>3</sup>	4.8	4.7
Log P <sup>3</sup>	3.8	3.0
Log D <sup>3,4</sup>	0.65	-0.12

<sup>1</sup>Double bond equivalency.

<sup>2</sup>Hydrogen deficiency.

<sup>3</sup>Data source: SciFinder Scholar, Calculated using Advanced Chemistry Development(ACD/Labs) Software V11.02 (© 1994–2022 ACD/Labs). Parameters determined at 25°C.

<sup>4</sup>Solubility and log D at pH 8.

### 3.2.2 Preparation and characterization of reclamation materials

Three reclamation materials were received from an oil and gas industry located in Alberta, Canada (Figure 3.1). The materials were peat-mineral mix material (PT) and Pleistocene fluvial sands collected from different mines (PF-1 and PF-2). Samples were stored in a cold room at 4°C prior to preparation. Preparation involved air-drying the samples at room temperature (20°C) until the mass was constant (7 to 14 days), followed by crushing using a mortar and pestle, sieving to pass through a 2 mm mesh, and storing the prepared samples in sealed glass containers.

Characterization techniques were applied to understand the surface characteristics of the materials and their relationship with NAs. pH and electrical conductivity (EC) were measured

according to Rayment and Lyons (2011) using a pH/EC meter (Accumet™ Research AR20, Fisher Scientific, USA). Point of zero charge ( $\text{pH}_{\text{pzc}}$ ) was determined based on the salt addition method previously described in detail by Bakatula et al. (2018). The cation exchange capacity (CEC) of the materials was established based on  $\text{BaCl}_2$  method in Carter and Gregorich (2007) and the cations (Ca, Mg, K, Na, Al, Fe, and Mn) were measured using an inductively coupled plasma optical emission spectrometry (ICP-OES, Thermo iCAP6300 Duo, Thermo Scientific, United Kingdom). The determination of aluminum (Al), calcium (Ca), iron (Fe), magnesium (Mg), and silicon (Si) was performed through EPA 3051a digestion method followed by quantification using ICP-OES. The total organic carbon (TOC) was determined by adding 1 M HCl to remove inorganic carbon to a weighted amount of sample, followed by drying at  $70^\circ\text{C}$  overnight and analysis by combustion elemental analysis (Thermo Flash 2000, Thermo Fisher Scientific, Germany). The clay, silt and sand composition were determined by a laser particle analyzer (LS 13320, Beckman Coulter, USA). Surface area was determined by evaluation of  $\text{N}_2$  adsorption using a surface area analyzer (Autosorb-1MP Quantachrome, USA) and the Brunauer-Emmett-Teller (BET) method was applied to determine the surface area. Samples were outgassed at room temperature for 20 h before  $\text{N}_2$  adsorption. The surface was scanned for functional groups between  $400$  and  $4000\text{ cm}^{-1}$  at  $4\text{ cm}^{-1}$  resolution using Fourier transform infrared (FTIR) spectroscopy (Nicolet™ 8700 FT-IR Spectrometer, Thermo Scientific, USA). Prior to FTIR analysis, samples were pressed into KBr pellets. Surface morphology was studied using scanning electron microscopy equipped with energy dispersive X-ray spectrometer (SEM-EDX, EVO M10, Zeiss, Germany) at accelerating voltage of 20 kV in high vacuum mode at magnification from 500 to 5,000 times. Prior to surface morphology analysis, samples were sputtered with 16 nm layer of gold to improve image quality (Gold Sputter Unit, Denton Vacuum, USA). The crystal structure properties were evaluated by

means of an X-ray diffractometer (XRD Ultima IV, Rigaku, Japan) at scanning rate of  $3^{\circ} \text{ min}^{-1}$  between  $10$  and  $90^{\circ} 2\theta$  angles using Cobalt tube at  $38 \text{ kV}$  and  $38 \text{ mA}$ .



**Figure 3.1:** Air-dried, crushed, and sieved (a) PEAT-1, (b) PF-1 and (c) PF-2 reclamation materials received from an oil and gas industry located in Alberta.

### 3.2.3 Instrumentation of adsorption and desorption experiments

An analytical balance (APX-200, Denver Instrument, USA) was used to measure the mass of adsorbents. Adsorption and desorption experiments were performed in a platform shaker (New Brunswick™ Innova® 2100 platform shaker, Eppendorf Inc., USA) at agitation speed of  $200 \text{ rpm}$  and  $20^{\circ}\text{C}$ . The flasks used for the adsorption and desorption experiments were covered with parafilm. After contact time, samples were centrifuged at  $7000 \text{ rpm}$  for  $10 \text{ min}$  (Centrifuge 5810R, Eppendorf Inc., USA).  $0.45 \mu\text{m}$  filters (Basix™ Nylon Syringe Filters, Fisher Scientific, USA) were applied to separate the adsorbent material from solution and samples were stored at  $4^{\circ}\text{C}$  until analysis. The analytical methods for the measurement of the concentration of model compounds of NAs and NAs in OSPW are presented in the Supporting Information (Appendix).

### 3.2.4 Adsorption and desorption of model compounds of NAs

#### 3.2.4.1 *Effect of adsorbent dosage experiments*

Previous studies using similar adsorbents for adsorption of organic compounds indicated that adsorbent concentrations above 250 g L<sup>-1</sup> might be needed to achieve better adsorption efficiency rates (Li et al., 2019; Rao et al., 2020). On the other hand, very high adsorbent concentrations can impact on the mixing homogeneity due to the formation of a heavy slurry difficult to mix. Therefore, the effect of dosage of the reclamation materials consisted of evaluating the proper adsorbent dosage to perform the adsorption experiments, aiming at the concentration at which the mixing occurred properly and without difficulty. Sorbent dosage experiments using DA and PVA were performed to determine the concentration at which the removal of model compounds of NAs was maximize and the mixing was not compromised due to the high adsorbent dosage concentration.

The effect of adsorbent dosage was studied by varying the amount of reclamation material added to a specific volume of model NA compound solution at 48 h of adsorption contact time. The adsorbent dosages evaluated were as follows: 1 to 5 g L<sup>-1</sup>, 100 to 500 g L<sup>-1</sup>, and 20 to 100 g L<sup>-1</sup> for PT, PF-1, and PF-2 samples, respectively. Experiments were conducted in duplicate. Batch adsorption experiments were performed for each model NA compound solution at 25 mg L<sup>-1</sup>. Blank samples (reclamation materials, 5 mM NaHCO<sub>3</sub> buffer solution with no model NAs) passed through the same adsorption process to assess background contamination of reclamation materials, if any.

#### *3.2.4.2 Kinetic and equilibrium experiments*

Adsorption kinetics experiments were performed at different contact times from 30 min to 14 days, or until equilibrium was reached. Every single contact time required a single experiment. Experiments were performed using 25 mg L<sup>-1</sup> NA solution using 500 and 100 g L<sup>-1</sup> PF-1 and PF-2, respectively. For PT, dosage of 3 and 5 g L<sup>-1</sup> were used for DA and PVA, respectively. After the equilibrium time was determined by kinetics study, adsorption equilibrium experiments were performed at the equilibrium time using different initial concentration of model NA compound between 20 and 100 mg L<sup>-1</sup>. Experiments were performed in duplicate. After contact time, the contents of the flasks were centrifuged, filtered, and stored until analysis.

#### *3.2.4.3 Desorption experiments*

Adsorption equilibrium experiments were performed at the equilibrium time found based on the adsorption kinetic experiments. The initial concentration of model NA compound ranged from 20 to 100 mg L<sup>-1</sup>.

Erlenmeyer flasks containing the calculated amount of reclamation material at specific concentration (determined as the best adsorbent dosage) and 30 mL single NA solution in 5 mM NaHCO<sub>3</sub> buffer (pH 8.5) at concentrations ranging from 20 to 100 mg L<sup>-1</sup> were covered and placed in platform shaker for the contact time defined as the equilibrium time. Experiments were performed in duplicate. After contact time, the contents of the flasks were centrifuged, filtered, and stored at 4°C until analysis by LC-MS.

Post-adsorption adsorbents were collected from experiments performed at equilibrium time using 25 mg L<sup>-1</sup> NA solution by separating the supernatant from the adsorbent by centrifugation. The post-adsorption material was air-dried at 20°C until completely dry. The surface functional

groups, surface elemental composition, and crystal structure properties on the surface of materials obtained post-adsorption of DA and PVA were assessed by means of Fourier transform infrared (FTIR) spectra, SEM images, and X-ray diffractograms.

The objective of the desorption study was to evaluate the leaching capacity of model NA compounds from materials post-adsorption in natural settings. Three types of desorption solution were used:

- (i) buffer solution without model compounds (5 mM NaHCO<sub>3</sub> buffer, pH 8.5),
- (ii) 0.01 M CaCl<sub>2</sub> solution, and
- (iii) simulated soil solution, obtained by adding 50 g reclamation material in 1 L ultrapure water, shaking for 24 h at 200 rpm and 20°C, followed by centrifugation at 5000 rpm, according to procedure presented by Chen et al. (2021, pp. author-year). Each post-adsorption material was subjected to desorption experiments using its equivalent simulated soil solution.

The post-adsorption material was added to Erlenmeyer flasks containing the 30 mL of desorption solution. The dosage of post-adsorption material followed the best adsorbent dosage determined in the preliminary assessment according to the model compound (i.e., 500 g L<sup>-1</sup> PF-1 and 100 g L<sup>-1</sup> PF-2 for both DA and PVA, and 3 and 5 g L<sup>-1</sup> PT for DA and PVA, respectively). Flasks were covered and placed in the platform shaker for contact times between 30 min and 14 days. Every single contact time required a single batch experiment. Experiments were performed in duplicate. After contact time, the samples were centrifuged, filtered, and stored until analysis.

### 3.2.5 Adsorption of classical NAs from raw OSPW

Each reclamation material at concentration of 5, 500 and 100 g L<sup>-1</sup> for PT, PF-1, and PF-2 respectively, were added to flasks containing real OSPW. These concentrations were selected

based on the performance of reclamation materials for adsorption of model NA compounds from single solution. Flasks were covered and placed in the platform shaker for 2 days for PT material and 6 days for PF-1 and PF-2 materials. After contact time, the contents of flasks were centrifuged, filtered, and stored until analysis.

### 3.2.6 Data analysis

The removal rate (Eq. 2.1) and the adsorption capacity (Eq. 2.2) were applied to evaluate any adsorption data. For the kinetic study, the kinetic models PFO (Eq. 2.3), PSO (Eq. 2.4), and Elovich (Eq. 2.5) were used to understand the experimental data of kinetic study. The evaluation of a suitability of a kinetic model for an experimental data was done based on the correlation coefficient ( $R^2$ ) provided by the fitting of linear plot to the data and the comparison between the adsorption capacity calculated by the model ( $q_{e,model}$ ) and the adsorption capacity obtained experimentally ( $q_{e,exp}$ ) (Foo & Hameed, 2010). The experimental data of equilibrium study was evaluated based on the Langmuir (Eq. 2.7) and Freundlich (Eq. 2.8) isotherms.

From the fitting of the Langmuir isotherm to the experimental data, the dimensionless adsorption intensity ( $R_L$ ) was determined based on the following equation (Lei et al., 2013; Xiang et al., 2018):

$$R_L = \frac{1}{1+K_L C_0} \quad (\text{Eq. 3.1})$$

The thermodynamic parameter Gibbs free energy ( $\Delta G^\circ$ , kJ mol<sup>-1</sup>) was calculated from the Langmuir affinity constant ( $K_L$ , L mg<sup>-1</sup>) based on Eq. 3.2 and 3.3, where R is the Universal gas

constant ( $8.314 \cdot 10^{-3} \text{ kJ mol}^{-1} \text{ K}^{-1}$ ), T is the temperature (298 K), and MW is the molecular weight of the model NA compound (Tran et al., 2021; Zhou, 2020; Zhou & Zhou, 2014):

$$\Delta G^o = -R T \ln K^o \quad (\text{Eq. 3.2})$$

$$K^o = 10^3 K_L MW \quad (\text{Eq. 3.3})$$

The adsorption distribution coefficient ( $K_d$ , Eq. 3.4) is very important to evaluate the distribution of NA molecules in the materials (Shaheen et al., 2013). The  $K_d$  can be normalized in terms of the total organic carbon ( $K_{oc}$ , Eq. 3.5) (Qisse et al., 2020; Rao et al., 2020).

$$K_d = \frac{q_{eq}}{c_{eq}} \quad (\text{Eq. 3.4})$$

$$K_{oc} = \frac{K_d}{TOC(\%)} 100\% \quad (\text{Eq. 3.5})$$

The Pearson correlation (r) was applied to disclose the relationship between the main characteristics of reclamation materials and their adsorption properties ( $K_d$ ,  $K_{oc}$ ,  $q_{max}$ ,  $q_t$ ) (Boskovic et al., 2020). Microsoft Excel software was used to calculate the Pearson correlation values (r) using the functions =PEARSON and =TDIST.

### 3.3 Results and discussion

#### 3.3.1 Characterization of reclamation materials

Based on the physico-chemical properties of reclamation materials (Table 3.2), the electrical conductivity (EC), cation exchange capacity (CEC), and total organic carbon (TOC)



values were in the order of  $PT > PF-1 > PF-2$  and about 5, 17, and 24 times higher in PT than PF-1 and PF-2, respectively. The CEC originates from the organic matter and clay minerals and can suggest the adsorption capacity of cations via ionic interactions since higher CEC values indicate more electronegative sites (Liu et al., 2022). In terms of soil texture, PT has a silty characteristic (48.5%) while sand is the majority of PF-1 and PF-2 materials, which was expected for PF-1 and PF-2 materials, since they are Pleistocene fluvial sands. Clay accounts for the lowest portion of all materials. pH of materials was neutral for PT, and alkaline for PF-1 and PF-2. The  $pH_{pzc}$  range is around 6.5 for PT and PF-2 and 9.6 for PF-1. Considering that the OSPW pH is around 8.5, the surface of materials will be negatively charged ( $pH > pH_{pzc}$ ) for PT and PF-2 and positively charged ( $pH < pH_{pzc}$ ) for PF-1 (Peng et al., 2016). Since the  $pK_a$  of studied model NA compounds is 4.9 (Table S1), repulsion forces might occur between the materials and the NAs. The surface area of all materials was small and in the range of 2.30 to 5.97  $m^2 g^{-1}$ . The concentration of aluminum (Al) and silicon (Si) were in the order of  $PF-1 > PF-2 > PT$ . Ca and Fe contents were much higher for PT and were in the order of  $PT > PF-1 > PF-2$ . Mg content was in the order  $PF-1 > PT > PF-2$ .

Diversified particle shapes and sizes were observed in the SEM images of the materials before and after adsorption (Figure S1-3). Smaller particles are attached to larger particles, which is characteristic of soil materials (Chen et al., 2021) and might indicate different structural phases (Otieno et al., 2021). At magnification of 5000 times, the surface of PT was more homogeneous and smoother than PF-1 and PF-2. After the adsorption process, the PT surface (Figure S1a) changed from a smooth surface to a surface with irregular deposition for adsorption of DA and regular deposition for PVA. For PF-1 (Figure S2a) and PF-2 (Figure S3a) the surface became smoother and without less particle aggregation for adsorption of PVA, which was also observed

for adsorption of DA on PF-2. The EDX spectra obtained for the materials (Figure S1-3) indicated that PT was mainly composed of carbon (C) and oxygen (O), with 58 and 35.1%, respectively. Small amounts of Ca (2.3%), Fe (2.2%), and Si (1.5%) were found in PT material. The PF materials were again differentiated by their elemental composition. Both PF-1 and PF-2 materials were dominated by O (52.8 and 54%), C (22.8 and 20.1%), Si (17 and 20.1%), and small amounts of Al and Fe were observed for both. However, PF-1 presented small amounts of Ca (2.4%). Minimal changes were observed in the elemental composition detected by EDX in the materials after adsorption with DA and PVA.

The mineralogical analysis of the materials was performed by means of X-ray diffractograms to identify the mineral fractions present in these materials (Figure S4). The overall intensity of peaks for PT was much lower than PF-1 and PF-2. Quartz was the dominant peak for all materials, which agrees with the fact that the oil sands are enriched with quartz minerals (Entezari et al., 2017). Much lower intensity peaks indicated the presence of calcite and dolomite in PT and PF-1. Kaolinite was present in PF-1 and PF-2, while dolomite and albite were part of the mineral fraction of PF-1 and PF-2 only, respectively.

The FTIR readings of the materials before adsorption are presented in Figure 3.2. Similar spectra for PF-1 and PF-2 materials were observed, which was expected because they are both Pleistocene fluvial sands. For PF-1 (Figure 3.2b) and PF-2 (Figure 3.2c), the bands 3697 and 3620  $\text{cm}^{-1}$  were weak bands associated with the mineral presence of kaolinite with the OH-vibrations of AlOH (Li et al., 2020b; Madejová et al., 2017; Russell & Fraser, 1994), confirmed by the presence of kaolinite in the XRD diffractograms (Figure S4b,c). The materials have some bands in common: strong band around 3400  $\text{cm}^{-1}$  (Figure 3.2a) is characteristic of O-H stretching and indicates intermolecular hydrogen bonds formed by water molecules (Deng et al., 2022; Xing et al., 2019)

and the bands between 2960 and 2850  $\text{cm}^{-1}$  indicate the presence of organic contaminants (Russell & Fraser, 1994). The FTIR spectra can signal the hydrophobic and hydrophilic characteristic of organic matter at 3000-2800 and 1800-1600  $\text{cm}^{-1}$ , respectively (Xing et al., 2019), in which C-H stretching of aliphatic is linked to peaks in the hydrophobic region and C=C stretching of aromatic rings and C=O vibrations of carboxylic acids/anions and amides are linked to the peaks at 1630  $\text{cm}^{-1}$  (Fernandes et al., 2010; Wei et al., 2017; Xing et al., 2019). PT has strong peaks for both regions, highlighting the presence of hydrophobic and hydrophilic functional groups that might be desirable for adsorption of naphthenic acids. PF-1 and PF-2 also have peaks in those regions, but with much lower intensity. Additionally, bands around 1800-1600  $\text{cm}^{-1}$  are closely related to CEC (Xing et al., 2019). Considering that PT has much higher CEC than PF-1 and PF-2 materials, that can explain why the peak around 1630  $\text{cm}^{-1}$  is more intense for PT. The peak at 1439  $\text{cm}^{-1}$  in PF-1 spectra is linked to the presence of carbonates (Xing et al., 2019). The strong peak obtained at 1089  $\text{cm}^{-1}$  for PF-1 and PF-2 is indicative of O-H stretching of quartz band and Si-O stretching vibrations, such as Si-O-Si (Belkassa et al., 2021; Madejová et al., 2017; Volkov et al., 2021), agreeing with the XRD diffractograms in which quartz was the mineral with the strongest signal in the spectra (Figure S4). The peak at 1105  $\text{cm}^{-1}$  for PT is likely related to the C-O stretching, O-H deformation of polysaccharides, and silicate impurities (Grube et al., 2006).

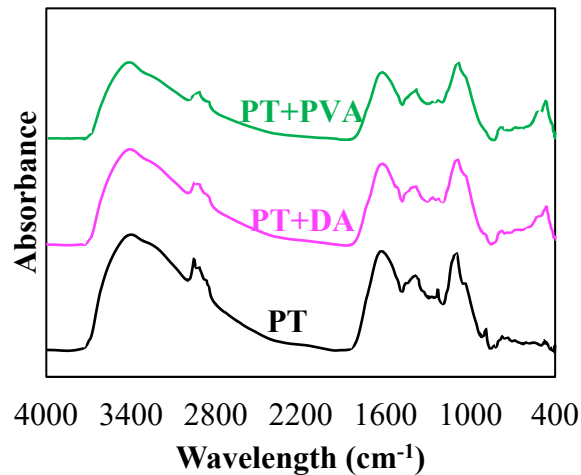
The band around 900  $\text{cm}^{-1}$  in PT spectra is due to calcite mineral (Russell & Fraser, 1994), also confirmed by the XRD diffractograms. Another indicative of kaolinite bands is the weak bands between 800-750  $\text{cm}^{-1}$  (Russell & Fraser, 1994), and Si-O-Al bending vibrations are represented by bands in the region of 700  $\text{cm}^{-1}$  (Madejová et al., 2017), both observed in PF-1 and PF-2 spectra. Iron oxide bands could be associated with the peaks observed at 512  $\text{cm}^{-1}$  for PF-1 (Kiskira et al., 2019) and at 540  $\text{cm}^{-1}$  for PT (Wei et al., 2017). The peaks observed at 462 and 475

cm<sup>-1</sup> are related to Si-O-Si bending vibrations and quartz, respectively (Chapman et al., 2001; Madejová et al., 2017). The albite characteristic was linked to sharp features around 400 cm<sup>-1</sup> as observed for PF-1 and PF-2 (Russell & Fraser, 1994).

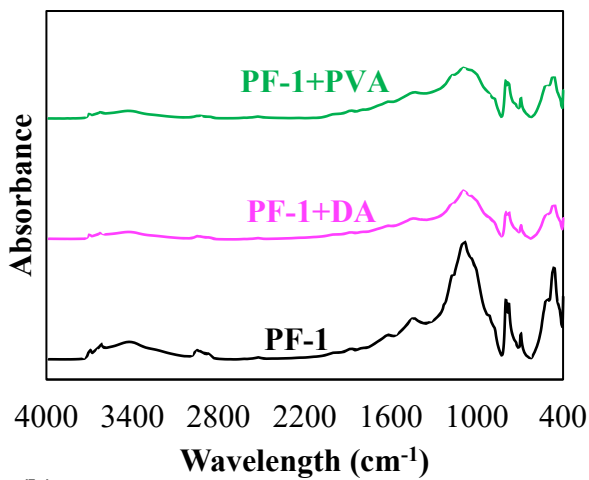
The changes observed in the FTIR spectra for the materials obtained after adsorption is discussed in the Section 3.3.4 (Adsorption mechanisms).

**Table 3.2:** Properties of studied reclamation materials.

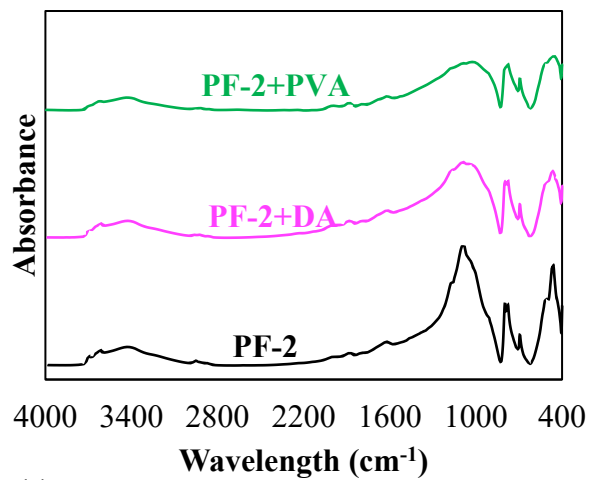
Parameter	Reclamation material			
	PT	PF-1	PF-2	
pH	7.02	8.94	8.16	
EC ( $\mu\text{S cm}^{-1}$ )	326.05	68.05	44.15	
CEC ( $\text{cmol}(+) \text{ kg}^{-1}$ )	157.41	9.30	7.83	
pH <sub>pzc</sub>	6.52	9.64	6.56	
TOC (%)	35.81	1.46	0.91	
Texture	Clay (%)	12.34	23.60	15.34
	Silt (%)	48.54	22.90	16.93
	Sand (%)	39.12	53.50	67.73
Surface area ( $\text{m}^2 \text{ g}^{-1}$ )	2.30	5.97	4.91	
Al ( $\text{g kg}^{-1}$ )	1.28	5.61	5.52	
Ca ( $\text{g kg}^{-1}$ )	33.62	20.4	1.84	
Fe ( $\text{g kg}^{-1}$ )	24.01	7.13	6.78	
Mg ( $\text{g kg}^{-1}$ )	3.91	7.42	1.16	
Si ( $\text{g kg}^{-1}$ )	0.88	2.90	2.20	



(a)



(b)



(c)

**Figure 3.2:** FTIR spectra of (a) PT, (b) PF-1, and (c) PF-2 materials before and after adsorption of model compounds of NAs.

### 3.3.2 Effect of adsorbent dosage on adsorption of model compounds of NAs

The effect of adsorbent dosage is a preliminary study to assess an unknown material as a potential adsorbent. When designing the appropriate amount of adsorbent dosage, the following were considered: the literature review of adsorbent dosages used for similar adsorbents (i.e., soils and sediments), the ratio between mass of adsorbent and volume of solution to ensure proper

mixing, and the percentage of pollutant removal. Based on that, 1 to 5, 100 to 500, and 20 to 100 g L<sup>-1</sup> were the range of adsorbent dosage evaluated for PT, PF-1, and PF-2, respectively. The results of the effect of adsorbent dosage on adsorption of DA and PVA (Figure 3.3) indicate that the application of higher adsorbent dosage ensured high rates of adsorption of DA and PVA, since the amount of model NA compounds adsorbed increased as the adsorbent dosage increased. Overall, the adsorption of DA was higher than PVA for all materials, indicating that compounds with lower  $-Z$  might be removed easily. However, the removal of NAs with higher  $-Z$  is desired, since higher  $-Z$  values in NAs infer more recalcitrant characteristic to the NAs (Islam et al., 2016).

3 g L<sup>-1</sup> PT for DA and 5 g L<sup>-1</sup> PT for PVA removed 100% of model compounds. The best adsorbent dosage for PF-1 and PF-2 were the highest evaluated concentration (500 and 100 g L<sup>-1</sup>, respectively), in which PF-1 removed 91 and 47% of DA and PVA, respectively and PF-2 removed 88 and 54% of DA and PVA, respectively.

Studies of adsorption of large organic compounds on soil also applied similar range of adsorbent dosages. For example, soil containing peat was used at 3 g L<sup>-1</sup> in the adsorption of naphthenic acids (Janfada et al., 2006; Peng et al., 2002) and 5 g L<sup>-1</sup> peat was used in the adsorption of a phenolic compound (Pei et al., 2007). The adsorption of perfluorinated acids and herbicides were achieved at 250 and 500 g L<sup>-1</sup> by Li et al. (2019) and Rao et al. (2020), respectively.

Based on the preliminary evaluation of adsorbent dosage for adsorption of model NA compounds, the optimal adsorbent dosage to be applied in the experiments that followed (kinetic, equilibrium and desorption experiments) were 3 and 5 g L<sup>-1</sup> PT for DA and PVA, respectively, and 500 g L<sup>-1</sup> PF-1 and 100 g L<sup>-1</sup> PF-2 for both DA and PVA.

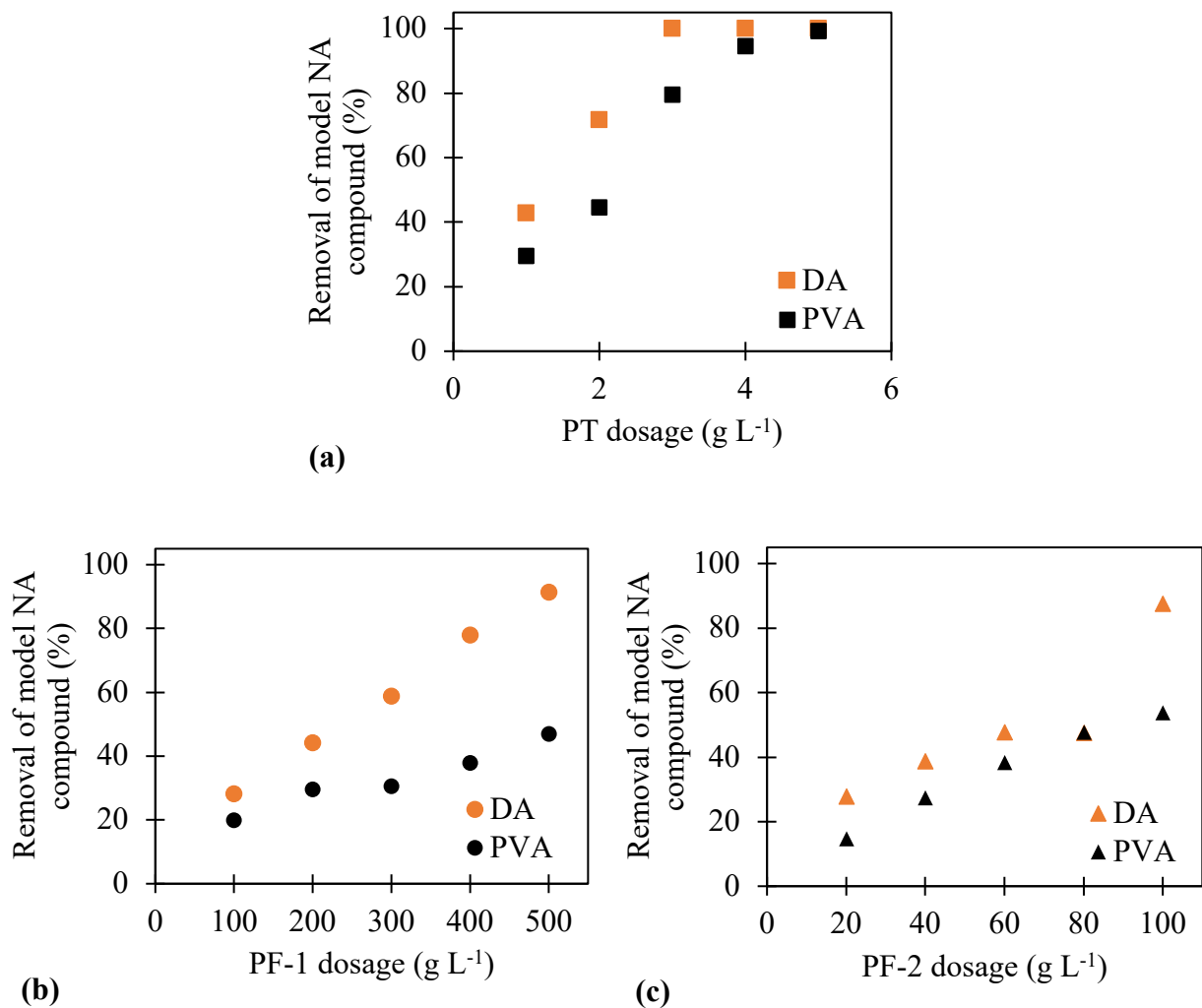


**Figure 3.3:** Effect of adsorbent dosage for adsorption of model NA compounds on (a) PT, (b) PF-1, and (c) PF-2 materials. Conditions: 25 mg L<sup>-1</sup> initial model NA compound concentration at pH 8.5; 48 h of contact time.

### 3.3.3 Adsorption kinetics

The kinetics study was performed between contact times 30 min and 14 days (Figure 3.4–3.6) and it was observed that there was no removal of model NA compounds in the first 8 h of contact time. For PT, 24 and 18 h was needed to obtain 7.6 and 9.4% removal of DA and PVA, respectively, while 16 and 8 h was needed to obtain approximately 6.5% removal for PF-1 for both compounds and 0.9 and 7.3% removal of DA and PVA for PF-2, respectively. Then, the adsorption advanced until 100% of DA and PVA were removed from solution, which occurred at 2 days using PT and 3 and 6 days for DA and PVA, respectively, using PF-1 and PF-2. Longer times to reach equilibrium is common in the adsorption of organic compounds in soil-like materials. For example, equilibrium was reached at 4 days for the adsorption of benzene and toluene on peat (Gharedaghloo & Price, 2021).

The kinetics models pseudo-first order (PFO), pseudo-second order (PSO), and Elovich models were applied to the experimental kinetics data to evaluate the adsorption of DA and PVA on PT (Figure 3.4), PF-1 (Figure 3.5), and PF-2 (Figure 3.6). The kinetics parameters obtained with the fitting are shown in Table 3.3. The higher values of  $R^2$  (0.90 – 0.95) and values of  $q_e$  predicted by the model closer to the experimental  $q_e$  suggest that the Elovich kinetics model described the adsorption of DA on all materials and the adsorption of PVA on PT. The adsorption of PVA on PF-1 and PF-2 was best described by the PFO kinetics model. The PSO kinetics model did not describe any of the adsorption processes.

The Elovich kinetics model indicates the predominance of chemical adsorption processes controlling the adsorption of DA on materials (Li et al., 2016; Tseng et al., 2003; Turner, 1975). The Elovich parameters can suggest important interactions between the pollutant and the adsorbent. The initial adsorption rate ( $\alpha$ ) can express the affinity between the pollutant and the



adsorbent (Rodríguez-Liébana & Peña, 2020). Among the three studied materials, PT was the one with the highest  $\alpha$ , implying that it has more affinity with DA, which was expected since the adsorption capacity of DA on PT was 165 and 33 times higher than PF-1 and PF-2, respectively, and the equilibrium time was reached earlier for PT. In comparison between the adsorption of DA and PVA on PT, there is higher affinity of PT with DA rather than PVA – the adsorption capacity is higher probably due to the less complex structure of DA. In terms of the adsorption of PVA on PF-1 and PF-2, the PFO kinetics model best described the process, indicating that the adsorption of NAs on materials is not a single-step phenomenon, but rather a multi-step mass transfer of pollutants that is affected by several factors such as physicochemical characteristics of adsorbent and nature of pollutant (Bian et al., 2022).

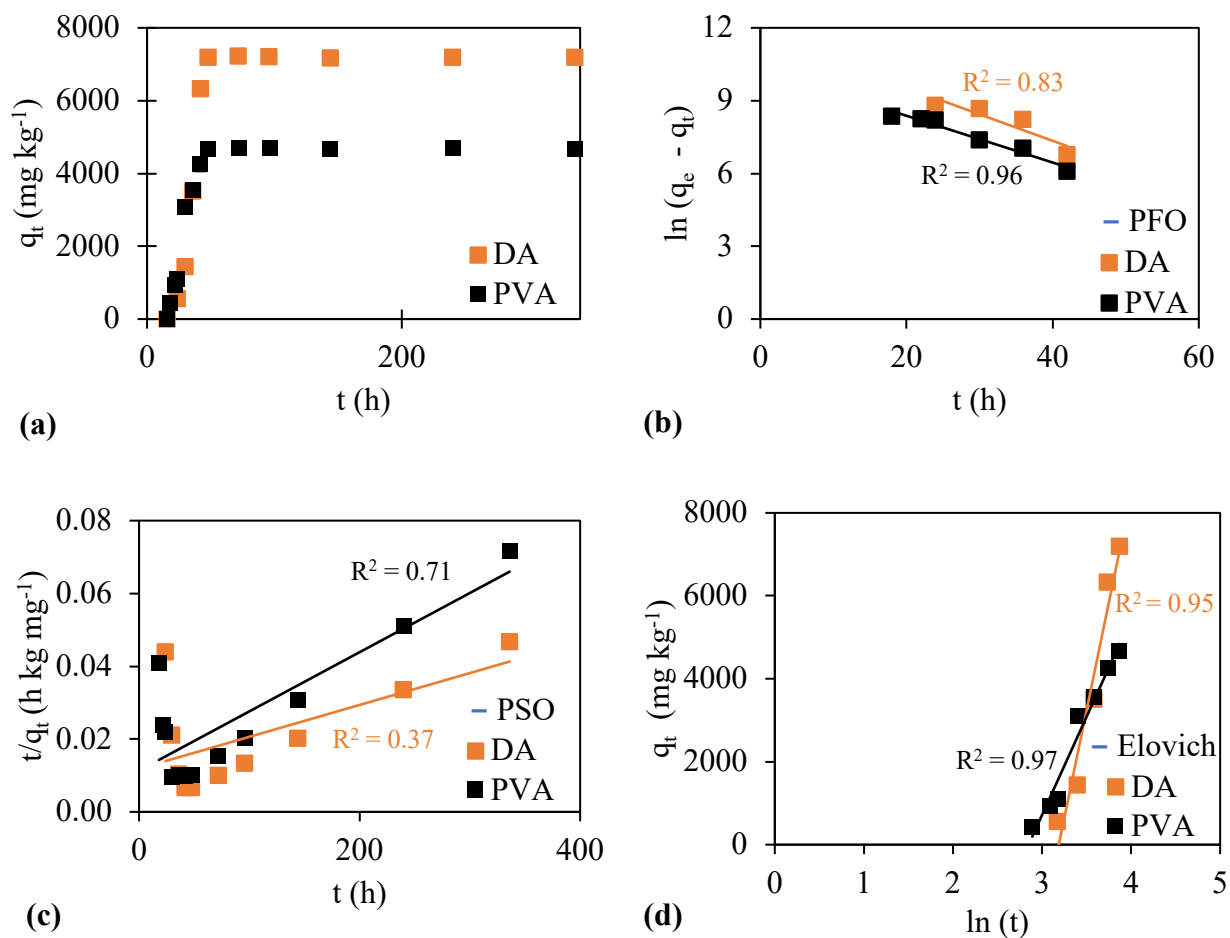


**Figure 3.4:** (a) Adsorption capacity of PT and the fittings of (b) PFO, (c) PSO, and (d) Elovich kinetic models for adsorption of model NA compounds from 30 min to 14 days of contact time using 3 and 5 g L<sup>-1</sup> PT for DA and PVA, respectively.

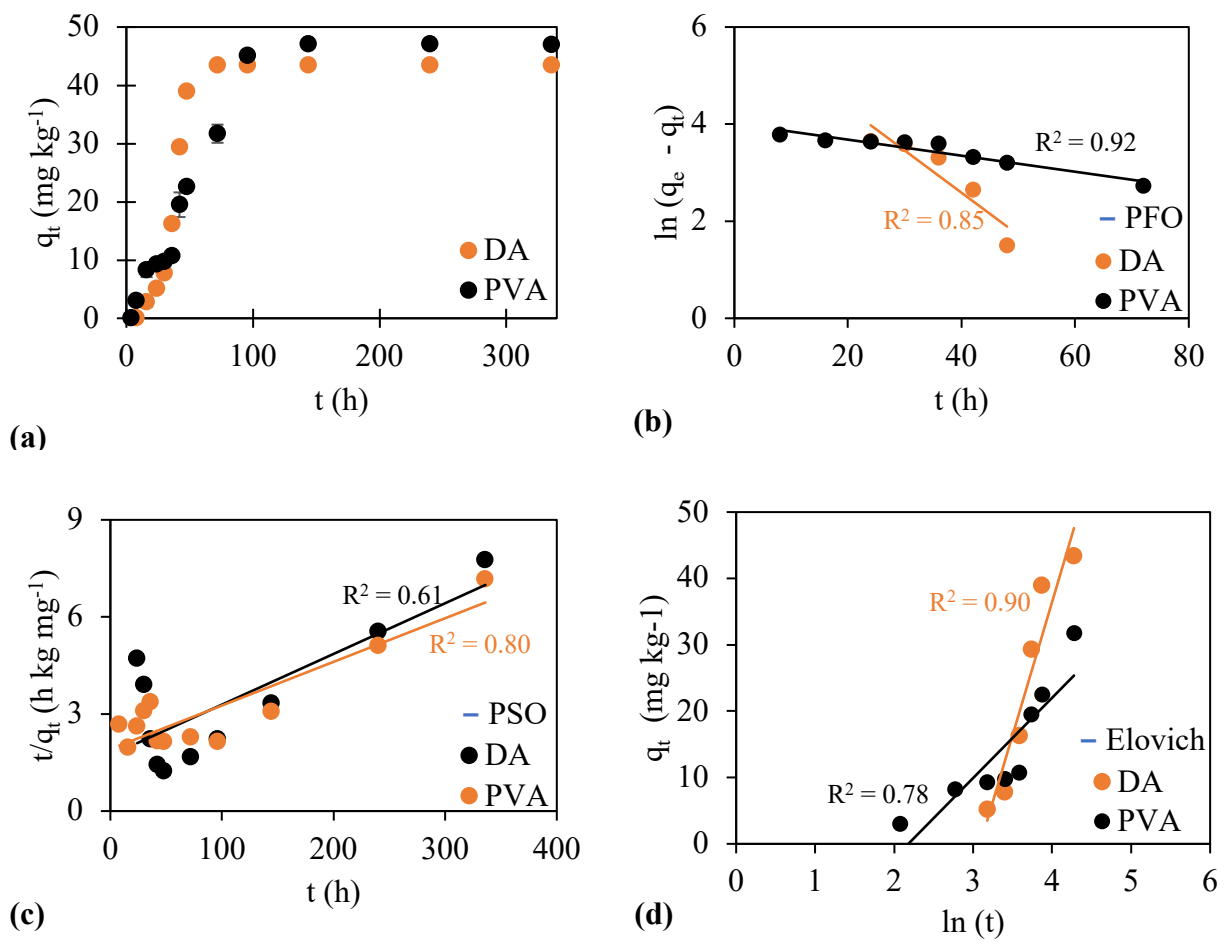


**Figure 3.5:** (a) Adsorption capacity of PF-1 and the fittings of (b) PFO, (c) PSO, and (d) Elovich kinetic models for adsorption of model NA compounds from 30 min to 14 days of contact time using 500 g L<sup>-1</sup> PF-1.

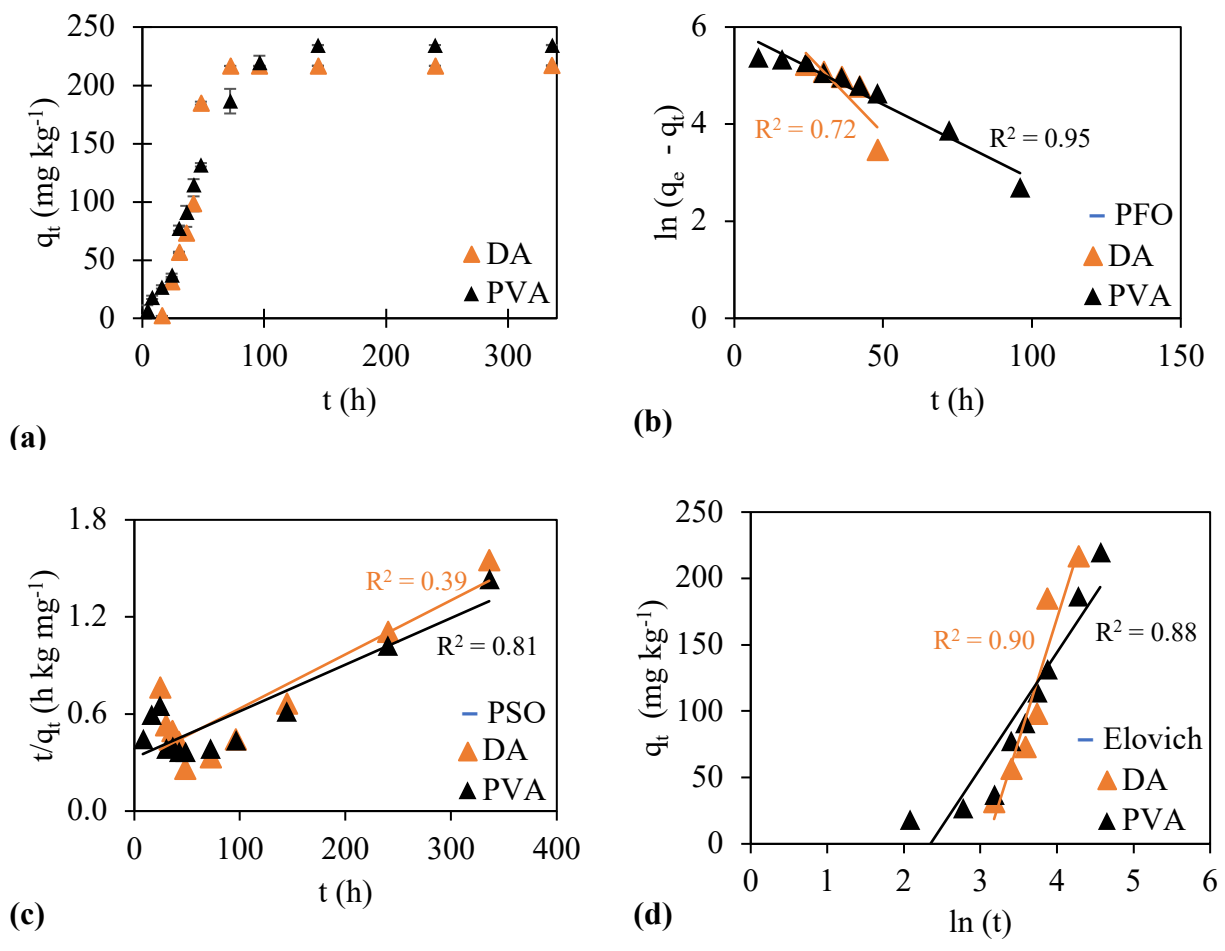


**Figure 3.6:** (a) Adsorption capacity of PF-2 and the fittings of (b) PFO, (c) PSO, and (d) Elovich kinetic models for adsorption of model NA compounds from 30 min to 14 days of contact time using 100 g L<sup>-1</sup> PF-2.

**Table 3.3:** Summary of modeling kinetics parameters obtained for adsorption of model NA compounds on reclamation materials.

Kinetics models and parameters		PT		PF-1		PF-2	
		DA	PVA	DA	PVA	DA	PVA
<b>q<sub>e,exp</sub><sup>a</sup> (mg kg<sup>-1</sup>)</b>		$7.2 \times 10^3$	$4.7 \times 10^3$	43.4	47.0	216.7	234.5
<b>PFO</b>	<b>q<sub>e,PFO</sub> (mg kg<sup>-1</sup>)</b>	$122 \times 10^3$	$30 \times 10^3$	429.9	55.2	1,091.2	378.53
	<b>K<sub>PFO</sub> (h<sup>-1</sup>)</b>	0.11	0.10	0.09	0.02	0.06	0.03
	<b>R<sup>2</sup></b>	0.83	0.96	0.85	0.92	0.72	0.95
<b>PSO</b>	<b>q<sub>e,PSO</sub> (mg kg<sup>-1</sup>)</b>	$111 \times 10^3$	$5 \times 10^3$	63.7	74.07	303	344.83
	<b>K<sub>PSO</sub> (kg mg<sup>-1</sup> h<sup>-1</sup>)</b>	$7 \times 10^{-7}$	$4 \times 10^{-6}$	$1.4 \times 10^{-4}$	$10^{-4}$	$4 \times 10^{-5}$	$3 \times 10^{-5}$
	<b>R<sup>2</sup></b>	0.37	0.71	0.61	0.80	0.39	0.81
<b>Elovich</b>	<b>q<sub>e,Elovich</sub> (mg kg<sup>-1</sup>)</b>	$7.1 \times 10^3$	$4.8 \times 10^3$	47.6	25.4	220.8	193.5
	<b>α (mg kg<sup>-1</sup> h<sup>-1</sup>)</b>	428.3	274.1	1.82	1.37	8.48	8.35
	<b>β (kg mg<sup>-1</sup>)</b>	$10^{-4}$	$2 \times 10^{-4}$	0.02	0.08	0.01	0.01
	<b>R<sup>2</sup></b>	0.95	0.97	0.90	0.78	0.90	0.88

### 3.3.4 Adsorption equilibrium modelling

The equilibrium study was performed at equilibrium time found in the kinetics study using initial concentrations of DA and PVA ranging from 20 to 100 mg L<sup>-1</sup> (Figure 3.7). The equilibrium adsorption capacity and the removal of DA and PVA increased with the increase in the initial concentration of pollutant.

The isotherm models Langmuir and Freundlich were applied to the experimental equilibrium data obtained at different initial concentrations to evaluate the adsorption of DA and PVA on materials (Figure 3.7 and S5) and the equilibrium parameters obtained with the fitting are shown in Table 3.4. The R<sup>2</sup> values obtained for the fitting of Langmuir isotherm to the adsorption

of NAs on materials were higher ( $R^2 = 0.99$ ) than the ones obtained for Freundlich isotherm, indicating that the adsorption processes follow the Langmuir model. The Langmuir isotherm assumes a monolayer adsorption on specific sites with homogeneously energies (Langmuir, 1918). Therefore, the adsorption of model NA compounds on materials might be of monolayer characteristic. Even though the adsorption of organic compounds usually fit the Freundlich isotherm due to the heterogenous characteristic of soils, Langmuir model has also described the adsorption of organic compounds on soils (Xiang et al., 2018). However, the adsorption of model compounds of NAs on soils by Peng et al. (2002) was best described by the linear isotherm instead of Langmuir or Freundlich isotherms.

The maximum adsorption capacity estimated by the Langmuir isotherm ranged from 81.3 to 16,800 mg kg<sup>-1</sup> (Table 3.4) and was in the order of PT > PF-2 > PF-1 for DA and PVA adsorption, and the  $q_{\max}$  was in the order of DA > PVA for all materials probably because of its lower double bond equivalency (DBE) and lower molecular weight (Rashed et al., 2020). PT is by far the best adsorbent of NAs probably because of its characteristics: high TOC content, CEC, and EC values.

The adsorption intensity parameter  $R_L$  was calculated for the experimental data. The  $R_L$  indicates if the adsorption is favorable ( $0 < R_L < 1$ ), irreversible ( $R_L = 0$ ), linear ( $R_L = 1$ ), or unfavorable ( $R_L > 1$ ) (Lei et al., 2013; Xiang et al., 2018). For the adsorption of NAs on materials, the  $R_L$  parameter for ranged from 0.003 to 0.16 for initial pollutant concentrations ranging from 20 to 100 mg L<sup>-1</sup>, in which the highest  $R_L$  values were observed for the lowest initial concentration. These results indicated that the adsorption of NAs on the studied materials was favorable. Nonetheless, all  $R_L$  values were all lower than 0.05 except for adsorption of DA on PT (0.16). The proximity with 0 might suggest a high degree of irreversibility (Vimonses et al., 2009). This fact

agrees with the previously findings: the best fitting to the Langmuir model for all adsorption processes and the fitting to the Elovich kinetics model for the adsorption of DA on all materials and PVA on PT, both of which could suggest chemisorption (Swenson & Stadie, 2019; Turner, 1975).

Additionally, the thermodynamic parameter Gibbs free energy ( $\Delta G^\circ$ ) can help distinguish an adsorption process from physisorption and chemisorption. Physisorption if  $-20 < \Delta G^\circ < 0$  kJ mol<sup>-1</sup>, chemisorption  $\Delta G^\circ < -40$  kJ mol<sup>-1</sup>, and a combination of both processes if  $-40 < \Delta G^\circ < -20$  kJ mol<sup>-1</sup> (Boskovic et al., 2020). For the adsorption of DA and PVA on materials, the  $\Delta G^\circ$  was within the range that characterizes the presence of physisorption and chemisorption. Also, based on the range, the adsorption mechanism could include H-bonding ( $-16 < \Delta G^\circ < -4$  kJ mol<sup>-1</sup>) and ligand exchange ( $\Delta G^\circ < -20$  kJ mol<sup>-1</sup>) (Boskovic et al., 2020).

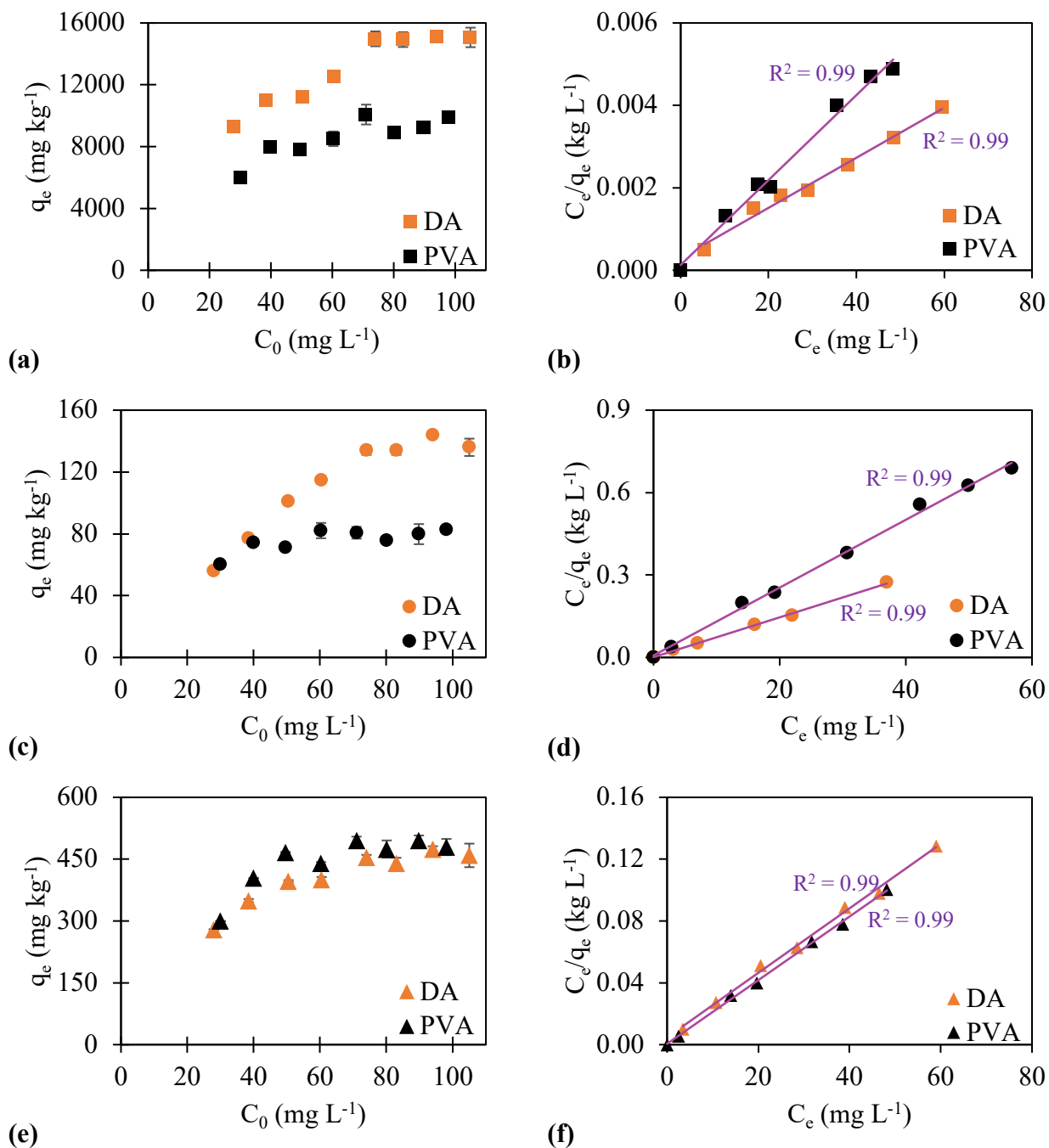


**Figure 3.7:** Adsorption of model NA compounds at initial concentrations from 30 to 100 mg L<sup>-1</sup> and its respective fitting of Langmuir isotherm for the adsorbents (a,b) PT, (c,d) PF-1, and (e,f) PF-2.



**Table 3.4:** Summary of modeling equilibrium parameters obtained for adsorption of model NA compounds on reclamation materials.

		PT		PF-1		PF-2	
Isotherms and parameters		DA	PVA	DA	PVA	DA	PVA
<b>Langmuir</b>	$q_{\max}$ (mg kg <sup>-1</sup> )	16.8 × 10 <sup>3</sup>	10 <sup>4</sup>	142.86	81.30	500	476.19
	$K_L$ (L mg <sup>-1</sup> )	0.30	1	7	1.71	0.67	3.50
	$R^2$	0.99	0.99	0.99	0.99	0.99	0.99
	$R_{L,20}$ <sup>a</sup>	0.16	0.05	0.008	0.03	0.08	0.01
	$R_{L,100}$ <sup>b</sup>	0.03	0.01	0.001	0.006	0.01	0.003
	$\Delta G^\circ$ (kJ mol <sup>-1</sup> )	-26.9	-29.9	-34.7	-31.3	-28.9	-33.0
<b>Freundlich</b>	$K_f$	8 × 10 <sup>3</sup>	6.4 × 10 <sup>3</sup>	114.29	70.81	306.90	450.71
	(mg <sup>1-n</sup> L <sup>n</sup> kg <sup>-1</sup> )						
	1/n	0.16	0.11	0.06	0.03	0.10	0.02
	$R^2$	0.79	0.46	0.89	0.32	0.91	0.18

<sup>a</sup>  $R_{L,20}$  obtained at the lowest initial concentration (20 mg L<sup>-1</sup>).

<sup>b</sup>  $R_{L,100}$  obtained at the highest initial concentration (100 mg L<sup>-1</sup>).

### 3.3.5 Adsorption mechanisms

The nature of adsorption mechanisms can be further elucidated using FTIR spectra (Figure 3.2) for materials before and after adsorption of model NA compounds with the assistance of the EDX (Figure S1–S3) and XRD (Figure S4) spectra of materials after adsorption.

Compared with the spectra obtained before adsorption, the wavenumber of some peaks of materials after adsorption of model NA compounds shifted (Figure 3.2), indicating that more than one adsorption mechanism is responsible for the adsorption of model NA compounds on the materials. Considering that the peaks at the region of 3400 cm<sup>-1</sup> shifted, hydrogen bonding is one of the adsorption mechanisms of DA and PVA on materials, indicating that the –OH containing

groups on adsorbent surface likely formed hydrogen bonds with the model NA compounds (Chen et al., 2019b). It was noticed that the peaks in the hydrophobic and hydrophilic groups shifted after adsorption, which could indicate that hydrophobic interactions are also a adsorption mechanism involved in the adsorption process (Xing et al., 2019). Another evidence of adsorption of DA and PVA (hydrophobic molecules) on hydrophobic sites is given by the shift in the siloxane (Si-O-Si) peaks (1089-1105 and 462-475  $\text{cm}^{-1}$ ) (Belkassa et al., 2021; Li et al., 2020b). The diffractograms obtained for the materials post-adsorption (Figure S4) supported the involvement of Si-O-Si groups in the adsorption since a slight modification in the intensity of quartz peaks was observed for PF-1 ( $2\theta = 24.3^\circ, 53.7^\circ, 58.9^\circ, 81.2^\circ$ ) and PF-2 ( $2\theta = 24.3^\circ, 31^\circ, 81.2^\circ, 81.4^\circ$ ), suggesting that the mineral phase (quartz) was involved in the adsorption (Cheng et al., 2020b), and Si content in the EDX spectra (Figure S2) was also modified after adsorption. Additionally,  $\pi$ - $\pi$  interaction could be evidenced by the shifts in peaks around 1630  $\text{cm}^{-1}$  (Tang et al., 2022).

### 3.3.6 Desorption of model compounds of NAs from post-adsorption reclamation materials

No desorption of DA and PVA from the three studied materials was observed from contact times from 30 min to 14 days for all three desorption solutions (buffer at pH 8.5, 0.1 M  $\text{CaCl}_2$ , simulated soil solution). The lack of desorption indicates that the molecules of NAs are tightly bound to the materials (Xu & Li, 2010) and that might be in the form of chemical bonds (Liang et al., 2022). Due to complexity of NAs, the adsorption of NAs on materials is likely irreversible, as suggested previously by the  $R_L$  constant calculated from the Langmuir affinity constant. Additionally, the low solubility of DA and PVA (Table 3.1) contributes to the low mobility of these compounds in the reclamation material and stronger adsorption affinity (Mutavdžić Pavlović

et al., 2014). Therefore, the leaching capacity of these model NA compounds from materials is considered low under the tested conditions.

### 3.3.7 Adsorption performance of classical NAs from raw OSPW by reclamation materials:

#### Effect of structure of NAs on adsorption

The reclamation materials were used independently as adsorbents of NAs from raw OSPW. The OSPW after application of PT, PF-1, or PF-2 materials and the concentration of classical NAs was determined. Samples of raw OSPW and OSPW after adsorption were analyzed to obtain classical NA concentration and the findings are presented in Figure 3.8. The adsorption capacity for classical NAs (Table 3.5) was much lower than the ones observed for the adsorption of representative compounds of NAs in buffered solution (DA and PVA). That was expected because the OSPW is a complex matrix containing thousand structures of NAs and other constituents that might affect adsorption (Wu et al., 2019). PT at dosage of 5 g L<sup>-1</sup> presented the highest adsorption capacity, followed by PF-2 and PF-1 materials, and this trend was also in accordance with the experiments with model compounds.

The classical NA concentration profiles in raw and post-adsorption OSPW as a function of carbon and  $-Z$  numbers (Figure 3.8) show that the classical NAs in the OSPW were in the range of carbon number 9–22 and  $-Z$  number 0–18. In terms of carbon number, the majority of NAs were found in the range of 12–19 and the highest peak was at 14, represented by 17.9% of all classical NAs in this particular OSPW, followed by carbon numbers 13 and 15 with 16 and 14.9% of all classical NAs. The most abundant NA species are the ones with  $-Z$  values as 4, 6, and 12, representing 35.4, 20.6, and 10.4% of NAs. The  $-Z$  values indicate that most of classical NAs in this raw OSPW were bicyclic, tricyclic, and hexacyclic. This trend was also observed by Benally et al. (2019). Additionally,  $-Z > 12$  represents 18.3% of classical NAs in the raw OSPW.

In general, removal was better achieved by PF-1, followed by PF-2 and PT, in which about 39, 27 and 20% removal classical NAs from real OSPW were observed, respectively. Even though PT had the lowest removal, PT remains the best adsorbent for classical NAs due to the low dosage required to achieve such removal ( $5 \text{ g L}^{-1}$ ), inferring higher adsorption capacities. In addition, PT dosage can be increased to more realistic values for real application, considering that better removal at higher adsorbent dosages concentrations is expected for real process water and this kind of natural adsorbent.

With respect to the  $-Z$  numbers, all  $-Z$  (0–18) were partially removed by all reclamation materials. This finding indicates the potential of these reclamation materials as natural adsorbents, since reduction of NAs with higher  $-Z$  numbers is desirable because of they have more recalcitrant characteristics and difficult degradation (Islam et al., 2016). PF-1 provided superior removal for  $-Z = 0$ ,  $4 \geq -Z \geq 8$ , and  $14 \geq -Z \geq 18$ . PF-2 had higher removal of  $-Z$  values 2, 10, and 12.

The removal of NAs from OSPW in terms of carbon numbers are also evaluated. Overall, following the trend presented by the  $-Z$  numbers, all the carbon numbers were partially removed by the materials. As expected, PF-1 material provided best removal for all except for carbon numbers 10–13 that were best removed by PF-2. As the carbon number increased further than 11, the removal also increased, indicated that adsorption was favorable due to the higher hydrophobicity of NAs (Zubot et al., 2012).

From the results presented in this section, one can conclude that the materials are a feasible option in the adsorption of NAs from OSPW, since it was able to remove NAs with diverse molecular weight (carbon numbers between 8 and 23) and ring structures ( $-Z$  from 0 to 18). Special attention is given to the PT material, which performed greatly at a very low concentration ( $5 \text{ g L}^{-1}$ ) in comparison with PF-1 and PF-2 materials that applied 500 and  $100 \text{ g L}^{-1}$ , respectively.

That illustrates the potential of PT as adsorbent of NAs from real OSPW. To illustrate this, 50 g L<sup>-1</sup> PT was applied to the adsorption of classical NAs from OSPW, and results are also presented in Figure 3.8. The total concentration of classical NAs using PT at 50 g L<sup>-1</sup> decreased by 54.4% and the final concentration reached 21.2 mg L<sup>-1</sup>. The removal of all carbon numbers increased significantly from the application of 5 g L<sup>-1</sup> PT and removals surpassed the ones observed for PF-1. The carbon numbers with highest concentration in OSPW (13–15) presented removal from 30.3 to 63.9% and the removal rate increased with carbon number > 15. By using 50 g L<sup>-1</sup> PT, the removal increased as the  $-Z$  values increased from 2 and 18 (37.8 to 87%), and the removals observed for each  $-Z$  value were higher than the ones obtained using 5 g L<sup>-1</sup> PT, 500 g L<sup>-1</sup> PF-1, and 100 g L<sup>-1</sup> PF-2 materials. This finding also indicates the adsorption was favorable due to the higher hydrophobicity of NAs (Zubot et al., 2012), which is desirable since complex NAs are more difficult to degrade as they are more recalcitrant.

Even though the materials were able to adsorb NAs from a wide range of carbon numbers and structures ( $-Z$ ), there is adsorption competitiveness, which can be evaluated based on the adsorption capacity (Table S1). The two highest adsorption capacities were observed for carbon numbers 13 and 16 for PT, 15 and 16 for PF-1, and 16 and 15 for PF-2 and  $-Z$  numbers 4 and 6. Lower carbon numbers (< 12) and lower  $-Z$  numbers (< 4) were the least adsorbed NAs. The study of Janfada et al. (2006) for adsorption of NAs on soil determined their studied soil had preference for  $-Z = 2$  at carbon number ranging from 13 to 17.

**Table 3.5:** Results of adsorption of classical NAs from real OSPW.

Material	Adsorption capacity (mg kg <sup>-1</sup> )	Removal (%)
PT at 5 g L <sup>-1</sup>	1.9 · 10 <sup>3</sup>	20.3
PF-1 at 500 g L <sup>-1</sup>	36.2	39.2
PF-2 at 100 g L <sup>-1</sup>	127.2	27.5

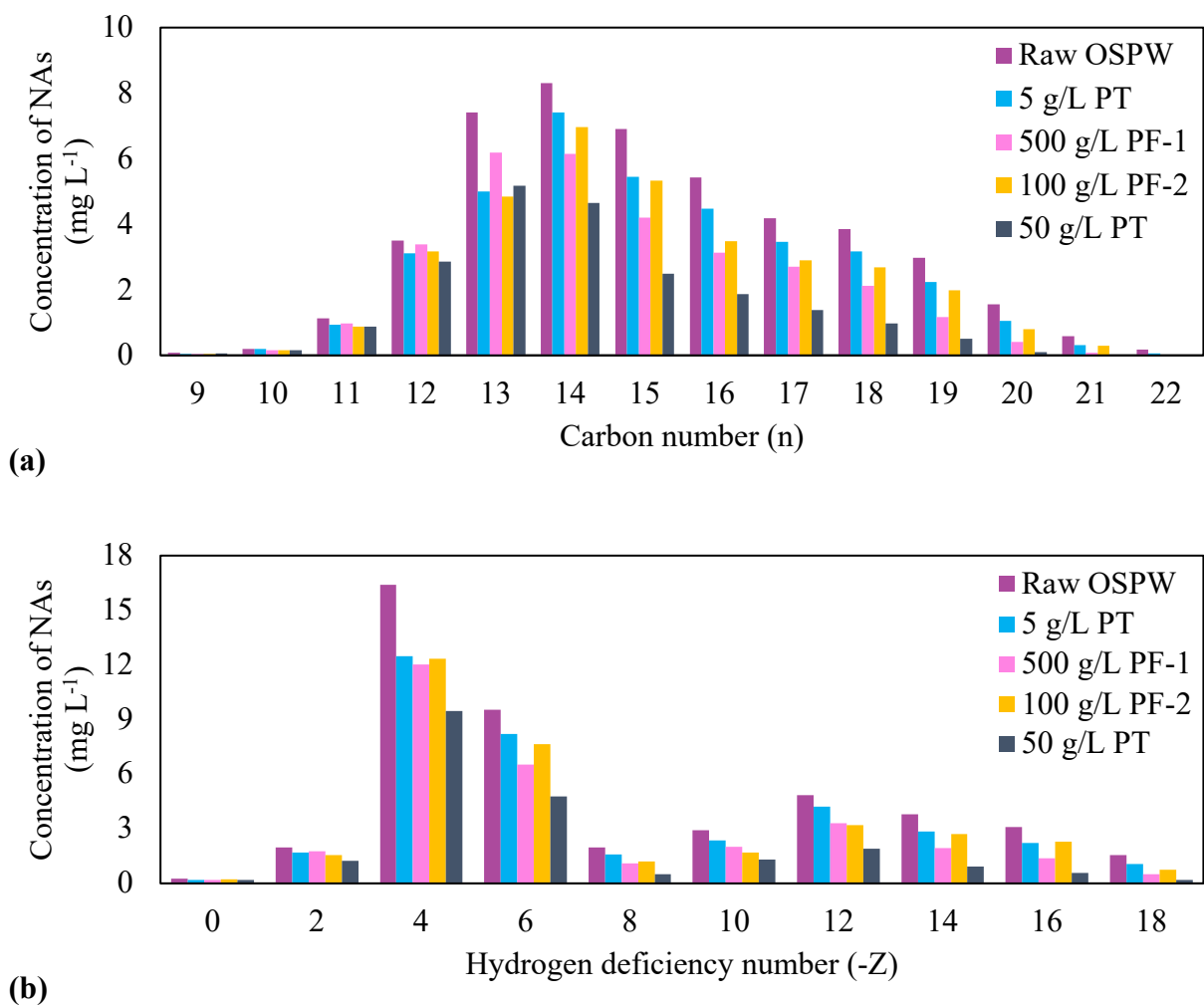


**Figure 3.8:** Concentration profile of NAs depicted by (a) carbon and (b) -Z numbers in the raw OSPW and OSPW after adsorption for the contact time of 2 days for PT and 6 days for PF materials.

### 3.3.8 Evaluation of adsorption distribution coefficients

The adsorption distribution coefficients ( $K_d$ ) and adsorption distribution coefficients normalized for organic carbon ( $K_{OC}$ ) were calculated for DA and PVA at 50 and 100 mg L<sup>-1</sup>, and classical NAs from real OSPW (Table 3.6). These coefficients  $K_d$  and  $K_{OC}$  are important to evaluate the affinity and distribution of organic compounds in the reclamation materials. Higher affinity is expected with higher  $K_d$  values (Qisse et al., 2020), and the coefficients were much lower for classical NAs from real OSPW in comparison with the ones obtained for adsorption of DA and PVA in buffered solution, indicating that the materials have more affinity with the model compounds than the NAs from real wastewater, most likely because of OSPW composition. In comparison with the study of Janfada et al. (2006), which found  $K_d$  of 3.7 and 17.8 L kg<sup>-1</sup> for adsorption of NAs on soil with 1.6 and 2.7% TOC, respectively, PT had a more affinity for classical NAs from real OSPW with  $K_d = 50.5$  L kg<sup>-1</sup>. PT had 35.8% TOC content, and its higher affinity with NAs might be associated with higher organic fraction (Janfada et al., 2006).

**Table 3.6:** Adsorption distribution coefficients ( $K_d$ ) and adsorption distribution coefficients normalized for organic carbon ( $K_{OC}$ ) of DA, PVA and classical NAs on reclamation materials.

Adsorption distribution coefficients ( $L\ kg^{-1}$ )										
RM*	$K_{d,50}^a$		$K_{d,100}^a$		$K_d^b$	$K_{OC,50}^c$		$K_{OC,100}^c$		$K_{OC}^b$
	DA	PVA	DA	PVA	O <sub>2</sub> - NAs	DA	PVA	DA	PVA	O <sub>2</sub> - NAs
PT <sup>d</sup>	668.3	760.6	253.2	204.5	50.5	1866.2	2123.9	707.0	571.0	141.1
PF-1 <sup>e</sup>	1007.	5.1	3.7	1.5	1.3	69016.5	346.5	251.7	99.6	88.2
PF-2 <sup>e</sup>	36.7	182.7	7.8	10.0	3.8	4032.7	20076.0	855.2	1093.1	416.5

\*Reclamation materials

<sup>a</sup>  $K_{d,50}$  and  $K_{d,100}$  are the adsorption distribution coefficients of model NA compounds at 50 and 100 mg L<sup>-1</sup>, respectively.

<sup>b</sup>  $K_d$  and  $K_{OC}$  of classical NAs obtained from adsorption of real OSPW at 2 days for PT and 6 days for PF-1 and PF-2.

<sup>c</sup>  $K_{OC,50}$  and  $K_{OC,100}$  are the adsorption distribution coefficients of model NA compounds at 50 and 100 mg L<sup>-1</sup>, respectively.

<sup>d</sup> PT was applied at 3 g L<sup>-1</sup> for adsorption of DA and 5 g L<sup>-1</sup> for adsorption of PVA and classical NAs from real OSPW.

<sup>e</sup> PF-1 and PF-2 were applied at 500 and 100 g L<sup>-1</sup>, respectively, for adsorption of DA, PVA, and classical NAs from real OSPW.

### 3.3.9 Effect of the properties of reclamation materials on adsorption of NAs

The adsorption of organic compounds on soil materials is often impacted depending on the material characteristics, such as TOC, CEC, and clay content (Conde-Cid et al., 2020; Liu et al., 2022; Xiang et al., 2018). The Pearson correlation can be applied to determine the correlation coefficient ( $r$ ) between the effect of the properties of materials (Table 1) and the adsorption properties obtained experimentally for the adsorption of representative compounds of NAs (DA and PVA) in buffered solution and classical NAs from real OSPW. The adsorption properties were  $K_d$  and  $K_{OC}$  determined for DA and PVA at 50 and 100 mg L<sup>-1</sup> ( $K_{d,50}$  and  $K_{d,100}$ ) and classical NAs



from real OSPW (Table 3.6),  $q_{\max}$  determined by the fitting of Langmuir isotherm (Table 3.4), and  $q_t$  determined for classical NAs adsorption from real OSPW at 2 days for PT and 6 days for PF-1 and PF-2 materials (Table 3.5). Based on the Pearson correlation coefficients (Table S2), the adsorption properties  $K_{d,100}$  for DA and PVA,  $K_d$  for classical NAs,  $q_{\max}$ , and  $q_t$  presented a perfect positive correlation ( $r = 1$ ) with CEC, TOC, and Fe content ( $p\text{-value} < 0.05$ ) and perfect negative correlation ( $r = -1$ ) with Al content ( $p\text{-value} < 0.05$ ). This finding shows that model compounds can be used to predict effects of adsorbent properties on adsorption, which is a more affordable choice regarding quantification (LC-MS for model compounds versus UPLC-TOF-MS for NAs in OSPW).

The  $K_d$  values were normalized in terms of the TOC ( $K_{OC}$ ) because  $K_{OC}$  is the standard parameter to convey adsorption of organic pollutants on soil materials and  $K_{OC}$  can be used to correlate the adsorption and adsorbent properties to remove the masking effect of TOC (Boskovic et al., 2020). Then, the  $K_{OC}$  was correlated with the adsorbent properties and none of the characteristics significantly affected the adsorption ( $p\text{-value} > 0.05$ ), indicating that the TOC might be the most important characteristic in the adsorption of NAs. This confirms that hydrophobic interaction was the main adsorption mechanism of NAs on reclamation materials, which was previously established by the evaluation of FTIR spectra of materials prior- and post-adsorption. Similar results were found for adsorption of other organic compounds on soils (Xiang et al., 2019; Xiang et al., 2018). Janfada et al. (2006) also determined that soils with higher organic fraction adsorbed more NAs.

### 3.4 Conclusions

This study investigated the potential application of reclamation materials (PT, PF-1, and PF-2) obtained from the mining excavation of oil sands as adsorbents of organic compounds such as NAs from OSPW. The materials were characterized, and it was noticed that PT have much higher TOC and CEC values, and silt is its major component. PF-1 and PF-2 differ in terms of  $\text{pH}_{\text{pzc}}$ , sand and clay contents. Representative compounds of NAs (DA and PVA) were used to determine adsorption kinetics and equilibrium, desorption capacity, and adsorption mechanisms. Desorption of DA and PVA from post-adsorption materials was not observed for up to 14 days of contact time with the evaluated desorption solutions. The adsorption mechanisms were assessed using FTIR, which concluded that hydrophobic interactions, hydrogen bonding, and  $\pi$ - $\pi$  interaction might be involved in the adsorption of NAs. The materials were applied in the adsorption of classical NAs from real OSPW, achieving removal of 39, 27 and 20% by PF-1, PF-2, and PT, respectively. All  $-Z$  numbers (0–18) and carbon numbers (8–23) were partially removed by the reclamation materials. PT was applied at  $5 \text{ g L}^{-1}$ , which is a very low dosage for this kind of adsorbent. By applying dosage of  $50 \text{ g L}^{-1}$  PT, the removal increased to 54.4% and increased with the  $-Z$  number, which is desirable since complex NAs are more recalcitrant. The physicochemical properties of materials and adsorption properties ( $K_d$ ,  $K_{OC}$ ,  $q_t$ ,  $q_{\text{max}}$ ) obtained for both representative compounds and classical NAs were correlated with TOC affecting adsorption of NAs the most; and that also highlights the hydrophobic interaction as an important adsorption mechanism of NAs on reclamation materials. Therefore, the reclamation materials obtained from the surface mining of oil sands have the ability to adsorb part of NAs from OSPW, allowing the materials to be applied on-site as part of reclamation approaches.

### 3.5 References

- Abdalrhman, A. S., Zhang, Y., Arslan, M., & Gamal El-Din, M. (2020). Low-current electro-oxidation enhanced the biodegradation of the recalcitrant naphthenic acids in oil sands process water. *Journal of Hazardous Materials*, 398, 122807. <https://doi.org/10.1016/j.jhazmat.2020.122807>
- Arslan, M., & Gamal El-Din, M. (2021). Bacterial diversity in petroleum coke based biofilters treating oil sands process water. *Science of the Total Environment*, 782, 146742. <https://doi.org/10.1016/j.scitotenv.2021.146742>
- Bakatula, E. N., Richard, D., Neculita, C. M., & Zagury, G. J. (2018). Determination of point of zero charge of natural organic materials. *Environmental Science and Pollution Research*, 25(8), 7823-7833. <https://doi.org/10.1007/s11356-017-1115-7>
- Belkassa, K., Khelifa, M., Batonneau-Gener, I., Marouf-Khelifa, K., & Khelifa, A. (2021). Understanding of the mechanism of crystal violet adsorption on modified halloysite: Hydrophobicity, performance, and interaction. *Journal of Hazardous Materials*, 415, 125656. <https://doi.org/10.1016/j.jhazmat.2021.125656>
- Benally, C., Messele, S. A., & Gamal El-Din, M. (2019). Adsorption of organic matter in oil sands process water (OSPW) by carbon xerogel. *Water Research*, 154, 402-411. <https://doi.org/10.1016/j.watres.2019.01.053>
- Bian, C., Wang, L., Cui, Z., Dong, Z., Shi, X., Li, Y., & Li, B. (2022). Adsorption-desorption and transport behavior of pydiflumetofen in eight different types of soil. *Ecotoxicology and Environmental Safety*, 234, 113378. <https://doi.org/10.1016/j.ecoenv.2022.113378>
- Boskovic, N., Brandstätter-Scherr, K., Sedláček, P., Bílková, Z., Bielská, L., & Hofman, J. (2020). Adsorption of epoxiconazole and tebuconazole in twenty different agricultural soils in relation to their properties. *Chemosphere*, 261, 127637. <https://doi.org/10.1016/j.chemosphere.2020.127637>
- Carter, M. R., & Gregorich, E. G. (2007). *Soil sampling and methods of analysis. [electronic resource]* (2nd ed. ed.). CRC Press. <https://www.taylorfrancis.com/books/9781420005271>
- Chapman, S. J., Campbell, C. D., Fraser, A. R., & Puri, G. (2001). FTIR spectroscopy of peat in and bordering Scots pine woodland: relationship with chemical and biological properties.

- Soil Biology and Biochemistry*, 33(9), 1193-1200. [https://doi.org/10.1016/S0038-0717\(01\)00023-2](https://doi.org/10.1016/S0038-0717(01)00023-2)
- Chen, H., Zhang, Y., Li, J., Zhang, P., & Liu, N. (2019b). Preparation of pickling-reheating activated alfalfa biochar with high adsorption efficiency for p-nitrophenol: characterization, adsorption behavior, and mechanism. *Environmental Science and Pollution Research*, 26(15), 15300-15313. <https://doi.com/10.1007/s11356-019-04862-3>
- Chen, X., Gu, X., Bao, L., Ma, S., & Mu, Y. (2021). Comparison of adsorption and desorption of triclosan between microplastics and soil particles. *Chemosphere*, 263, 127947. <https://doi.org/10.1016/j.chemosphere.2020.127947>
- Cheng, Y., Shiota, K., Kusakabe, T., Oshita, K., & Takaoka, M. (2020b). Characterizing the mechanisms of gas-phase elemental mercury adsorption with iodine-impregnated activated carbons using Brunauer-Emmett-Teller analysis, X-ray diffraction, X-ray photoelectron spectroscopy, and X-ray absorption near-edge structure analysis. *Chemical Engineering Journal*, 402, 126225. <https://doi.org/10.1016/j.cej.2020.126225>
- Clark, K. A., & Pasternack, D. S. (1932). Hot Water Separation of Bitumen from Alberta Bituminous Sand. *Industrial and Engineering Chemistry*, 24(12), 1410-1416. <https://doi.org/10.1021/ie50276a016>
- Conde-Cid, M., Fernández-Calviño, D., Núñez-Delgado, A., Fernández-Sanjurjo, M. J., Arias-Estévez, M., & Álvarez-Rodríguez, E. (2020). Estimation of adsorption/desorption Freundlich's affinity coefficients for oxytetracycline and chlortetracycline from soil properties: Experimental data and pedotransfer functions. *Ecotoxicology and Environmental Safety*, 196, 110584. <https://doi.org/10.1016/j.ecoenv.2020.110584>
- Deng, X., Jiang, Y., Zhang, M. a., Nan, Z., Liang, X., & Wang, G. (2022). Sorption properties and mechanisms of erythromycin and ampicillin in loess soil: Roles of pH, ionic strength, and temperature. *Chemical Engineering Journal*, 434, 134694. <https://doi.org/10.1016/j.cej.2022.134694>
- Entezari, I., Rivard, B., Geramian, M., & Lipsett, M. G. (2017). Predicting the abundance of clays and quartz in oil sands using hyperspectral measurements. *International Journal of Applied Earth Observation and Geoinformation*, 59, 1-8. <https://doi.org/10.1016/j.jag.2017.02.018>

- Fang, Z., Huang, R., Chelme-Ayala, P., Shi, Q., Xu, C., & Gamal El-Din, M. (2019). Comparison of UV/Persulfate and UV/H<sub>2</sub>O<sub>2</sub> for the removal of naphthenic acids and acute toxicity towards *Vibrio fischeri* from petroleum production process water. *Science of the Total Environment*, 694, 133686. <https://doi.org/10.1016/j.scitotenv.2019.133686>
- Fernandes, A. N., Giovanela, M., Esteves, V. I., & Sierra, M. M. d. S. (2010). Elemental and spectral properties of peat and soil samples and their respective humic substances. *Journal of Molecular Structure*, 971(1), 33-38. <https://doi.org/10.1016/j.molstruc.2010.02.069>
- Foo, K. Y., & Hameed, B. H. (2010). Insights into the modeling of adsorption isotherm systems. *Chemical Engineering Journal*, 156(1), 2-10. <https://doi.org/10.1016/j.cej.2009.09.013>
- Frank, R. A., Kavanagh, R., Kent Burnison, B., Arsenault, G., Headley, J. V., Peru, K. M., Van Der Kraak, G., & Solomon, K. R. (2008). Toxicity assessment of collected fractions from an extracted naphthenic acid mixture. *Chemosphere*, 72(9), 1309-1314. <https://doi.org/10.1016/j.chemosphere.2008.04.078>
- Gharedaghlou, B., & Price, J. S. (2021). Assessing benzene and toluene adsorption with peat depth: Implications on their fate and transport. *Environmental Pollution*, 274, 116477. <https://doi.org/10.1016/j.envpol.2021.116477>
- Grewer, D. M., Young, R. F., Whittal, R. M., & Fedorak, P. M. (2010). Naphthenic acids and other acid-extractables in water samples from Alberta: What is being measured? *Science of the Total Environment*, 408(23), 5997-6010. <https://doi.org/10.1016/j.scitotenv.2010.08.013>
- Grube, M., Lin, J. G., Lee, P. H., & Kokorevicha, S. (2006). Evaluation of sewage sludge-based compost by FT-IR spectroscopy. *Geoderma*, 130(3), 324-333. <https://doi.org/10.1016/j.geoderma.2005.02.005>
- Huang, R., Chen, Y., Meshref, M. N. A., Chelme-Ayala, P., Dong, S., Ibrahim, M. D., Wang, C., Klammerth, N., Hughes, S. A., Headley, J. V., Peru, K. M., Brown, C., Mahaffey, A., & Gamal El-Din, M. (2018). Characterization and determination of naphthenic acids species in oil sands process-affected water and groundwater from oil sands development area of Alberta, Canada. *Water Research*, 128, 129-137. <https://doi.org/10.1016/j.watres.2017.10.003>
- Huang, R., McPhedran, K. N., & Gamal El-Din, M. (2015a). Ultra Performance Liquid Chromatography Ion Mobility Time-of-Flight Mass Spectrometry Characterization of

- Naphthenic Acids Species from Oil Sands Process-Affected Water. *Environmental Science & Technology*, 49(19), 11737-11745. <https://doi.org/10.1021/acs.est.5b03178>
- Hughes, S. A., Mahaffey, A., Shore, B., Baker, J., Kilgour, B., Brown, C., Peru, K. M., Headley, J. V., & Bailey, H. C. (2017). Using ultrahigh-resolution mass spectrometry and toxicity identification techniques to characterize the toxicity of oil sands process-affected water: The case for classical naphthenic acids. *Environmental Toxicology and Chemistry*, 36(11), 3148-3157. <https://doi.org/10.1002/etc.3892>
- Islam, M. S., Zhang, Y., McPhedran, K. N., Liu, Y., & Gamal El-Din, M. (2016). Mechanistic investigation of industrial wastewater naphthenic acids removal using granular activated carbon (GAC) biofilm based processes. *Science of the Total Environment*, 541, 238-246. <https://doi.org/10.1016/j.scitotenv.2015.09.091>
- Jafarinejad, S. (2017). 2 - Pollutions and Wastes From the Petroleum Industry. In S. Jafarinejad (Ed.), *Petroleum Waste Treatment and Pollution Control* (pp. 19-83). Butterworth-Heinemann. <https://doi.org/https://doi.org/10.1016/B978-0-12-809243-9.00002-X>
- Janfada, A., Headley, J. V., Peru, K. M., & Barbour, S. L. (2006). A Laboratory Evaluation of the Sorption of Oil Sands Naphthenic Acids on Organic Rich Soils. *Journal of Environmental Science and Health, Part A*, 41(6), 985-997. <https://doi.org/10.1080/10934520600620105>
- Kiskira, K., Papirio, S., Mascolo, M. C., Fourdrin, C., Pechaud, Y., van Hullebusch, E. D., & Esposito, G. (2019). Mineral characterization of the biogenic Fe(III)(hydr)oxides produced during Fe(II)-driven denitrification with Cu, Ni and Zn. *Science of the Total Environment*, 687, 401-412. <https://doi.org/10.1016/j.scitotenv.2019.06.107>
- Langmuir, I. (1918). The adsorption of gases on plane surfaces of glass, mica and platinum. *Journal of the American Chemical Society*, 40(9), 1361-1403. <https://doi.org/10.1021/ja02242a004>
- Lei, C., Hu, Y.-y., & He, M.-z. (2013). Adsorption characteristics of triclosan from aqueous solution onto cetylpyridinium bromide (CPB) modified zeolites. *Chemical Engineering Journal*, 219, 361-370. <https://doi.org/10.1016/j.cej.2012.12.099>
- Lévesque, C. M. (2014). *Oil sands process water and tailings pond contaminant transport and fate : physical, chemical and biological processes*, University of British Columbia]. <https://open.library.ubc.ca/collections/24/items/1.0165952>

- Li, C., Fu, L., Stafford, J., Belosevic, M., & Gamal El-Din, M. (2017). The toxicity of oil sands process-affected water (OSPW): A critical review. *Science of the Total Environment*, 601-602, 1785-1802. <https://doi.org/10.1016/j.scitotenv.2017.06.024>
- Li, F., Fang, X., Zhou, Z., Liao, X., Zou, J., Yuan, B., & Sun, W. (2019). Adsorption of perfluorinated acids onto soils: Kinetics, isotherms, and influences of soil properties. *Science of the Total Environment*, 649, 504-514. <https://doi.org/10.1016/j.scitotenv.2018.08.209>
- Li, G., Zhu, W., Zhang, C., Zhang, S., Liu, L., Zhu, L., & Zhao, W. (2016). Effect of a magnetic field on the adsorptive removal of methylene blue onto wheat straw biochar. *Bioresource Technology*, 206, 16-22. <https://doi.org/10.1016/j.biortech.2015.12.087>
- Li, Y., Wei, M., Liu, L., Xue, Q., & Yu, B. (2020b). Adsorption of toluene on various natural soils: Influences of soil properties, mechanisms, and model. *Science of the Total Environment*, 740, 140104. <https://doi.org/10.1016/j.scitotenv.2020.140104>
- Liang, X., Liu, L., Jiang, Y., Nan, Z., Deng, X., Ma, F., Wang, G., & Wu, Y. (2022). Study of the sorption/desorption behavior of chlortetracycline on sediments in the upper reaches of the Yellow River. *Chemical Engineering Journal*, 428, 131958. <https://doi.org/10.1016/j.cej.2021.131958>
- Liu, B.-L., Li, Y.-W., Xie, L.-S., Guo, J.-J., Xiang, L., & Mo, C.-H. (2022). Sorption of microcystin-RR onto surface soils: Characteristics and influencing factors. *Journal of Hazardous Materials*, 431, 128571. <https://doi.org/10.1016/j.jhazmat.2022.128571>
- Liu, J., Wang, L., Tang, J., & Ma, J. (2016). Photocatalytic degradation of commercially sourced naphthenic acids by TiO<sub>2</sub>-graphene composite nanomaterial. *Chemosphere*, 149, 328-335. <https://doi.org/10.1016/j.chemosphere.2016.01.074>
- Madejová, J., Gates, W. P., & Petit, S. (2017). Chapter 5 - IR Spectra of Clay Minerals. In W. P. Gates, J. T. Klopogge, J. Madejová, & F. Bergaya (Eds.), *Developments in Clay Science* (Vol. 8, pp. 107-149). Elsevier. <https://doi.org/https://doi.org/10.1016/B978-0-08-100355-8.00005-9>
- Marentette, J. R., Frank, R. A., Bartlett, A. J., Gillis, P. L., Hewitt, L. M., Peru, K. M., Headley, J. V., Brunswick, P., Shang, D., & Parrott, J. L. (2015). Toxicity of naphthenic acid fraction components extracted from fresh and aged oil sands process-affected waters, and

- commercial naphthenic acid mixtures, to fathead minnow (*Pimephales promelas*) embryos. *Aquatic Toxicology*, 164, 108-117. <https://doi.org/10.1016/j.aquatox.2015.04.024>
- Messele, S. A., Chelme-Ayala, P., & Gamal El-Din, M. (2021). Catalytic ozonation of naphthenic acids in the presence of carbon-based metal-free catalysts: Performance and kinetic study. *Catalysis Today*, 361, 102-108. <https://doi.org/10.1016/j.cattod.2020.01.042>
- Mutavdžić Pavlović, D., Ćurković, L., Blažek, D., & Župan, J. (2014). The sorption of sulfamethazine on soil samples: Isotherms and error analysis. *Science of the Total Environment*, 497-498, 543-552. <https://doi.org/10.1016/j.scitotenv.2014.08.018>
- Natural Resources Canada. (2020). *Crude oil facts*. <https://www.nrcan.gc.ca/science-data/data-analysis/energy-data-analysis/energy-facts/crude-oil-facts/20064#L4>
- Niasar, H. S., Das, S., Xu, C., & Ray, M. B. (2019). Continuous column adsorption of naphthenic acids from synthetic and real oil sands process-affected water (OSPW) using carbon-based adsorbents. *Chemosphere*, 214, 511-518. <https://doi.org/10.1016/j.chemosphere.2018.09.078>
- Otieno, A. O., Home, P. G., Raude, J. M., Murunga, S. I., Ngumba, E., Ojwang, D. O., & Tuhkanen, T. (2021). Pineapple peel biochar and lateritic soil as adsorbents for recovery of ammonium nitrogen from human urine. *Journal of Environmental Management*, 293, 112794. <https://doi.org/10.1016/j.jenvman.2021.112794>
- Pei, Z.-g., Shan, X.-q., Liu, T., Xie, Y.-n., Wen, B., Zhang, S., & Khan, S. U. (2007). Effect of lead on the sorption of 2,4,6-trichlorophenol on soil and peat. *Environmental Pollution*, 147(3), 764-770. <https://doi.org/10.1016/j.envpol.2006.09.001>
- Peng, J., Headley, J. V., & Barbour, S. L. (2002). Adsorption of single-ring model naphthenic acids on soils. *Canadian Geotechnical Journal*, 39(6), 1419-1426. <https://doi.org/10.1139/t02-098>
- Peng, P., Lang, Y.-H., & Wang, X.-M. (2016). Adsorption behavior and mechanism of pentachlorophenol on reed biochars: pH effect, pyrolysis temperature, hydrochloric acid treatment and isotherms. *Ecological Engineering*, 90, 225-233. <https://doi.org/10.1016/j.ecoleng.2016.01.039>
- Pourrezaei, P., Alpatova, A., Chelme-Ayala, P., Perez-Estrada, L. A., Jensen-Fontaine, M., Le, X. C., & Gamal El-Din, M. (2014). Impact of petroleum coke characteristics on the adsorption



- of the organic fractions from oil sands process-affected water. *International Journal of Environmental Science and Technology*, 11(7), 2037-2050. <https://doi.org/10.1007/s13762-013-0406-x>
- Qisse, N., El Alouani, M., El Azzouzi, L., El Fadil, I., Saufi, H., Alaoui El Belghiti, M., Zrineh, A., & El Azzouzi, M. (2020). Adsorption of Imazalil herbicide onto Moroccan agricultural soils: Kinetic and isotherm adsorption studies. *Groundwater for Sustainable Development*, 11, 100468. <https://doi.org/10.1016/j.gsd.2020.100468>
- Quinlan, P. J., & Tam, K. C. (2015). Water treatment technologies for the remediation of naphthenic acids in oil sands process-affected water. *Chemical Engineering Journal*, 279, 696-714. <https://doi.org/10.1016/j.cej.2015.05.062>
- Rao, L., Luo, J., Zhou, W., Zou, Z., Tang, L., & Li, B. (2020). Adsorption–desorption behavior of benzobicyclon hydrolysate in different agricultural soils in China. *Ecotoxicology and Environmental Safety*, 202, 110915. <https://doi.org/10.1016/j.ecoenv.2020.110915>
- Rashed, Y., Messele, S. A., Zeng, H., & Gamal El-Din, M. (2020). Mesoporous carbon xerogel material for the adsorption of model naphthenic acids: structure effect and kinetics modelling. *Environmental Technology*, 41(27), 3534-3543. <https://doi.org/10.1080/09593330.2019.1615130>
- Rayment, G. E., & Lyons, D. J. (2011). *Soil chemical methods. [electronic resource] : Australasia*. CSIRO Pub. <https://doi.org/10.1071/9780643101364>
- Rezanezhad, F., Price, J. S., & Craig, J. R. (2012). The effects of dual porosity on transport and retardation in peat: A laboratory experiment. *Canadian Journal of Soil Science*, 92(5), 723-732. <https://doi.org/10.4141/cjss2011-050>
- Rodríguez-Liébana, J. A., & Peña, A. (2020). Differences in the sorption kinetics of various non-ionisable pesticides in a limited number of agricultural soils from the Mediterranean basin. *Journal of Environmental Management*, 276, 111336. <https://doi.org/10.1016/j.jenvman.2020.111336>
- Rogers, V. V., Wickstrom, M., Liber, K., & MacKinnon, M. D. (2002). Acute and Subchronic Mammalian Toxicity of Naphthenic Acids from Oil Sands Tailings. *Toxicological Sciences*, 66(2), 347-355. <https://doi.org/10.1093/toxsci/66.2.347>

- Russell, J. D., & Fraser, A. R. (1994). Infrared methods. In M. J. Wilson (Ed.), *Clay Mineralogy: Spectroscopic and Chemical Determinative Methods* (pp. 11-67). Springer Netherlands. [https://doi.org/10.1007/978-94-011-0727-3\\_2](https://doi.org/10.1007/978-94-011-0727-3_2)
- Scarlett, A. G., Reinardy, H. C., Henry, T. B., West, C. E., Frank, R. A., Hewitt, L. M., & Rowland, S. J. (2013). Acute toxicity of aromatic and non-aromatic fractions of naphthenic acids extracted from oil sands process-affected water to larval zebrafish. *Chemosphere*, *93*(2), 415-420. <https://doi.org/10.1016/j.chemosphere.2013.05.020>
- Schwarzenbach, R., Gschwend, P., & Imboden, D. (2005). Sorption I: General Introduction and Sorption Processes Involving Organic Matter ((pp. 275-330). <https://doi.org/https://doi.org/10.1002/0471649643.ch9>
- Shaheen, S. M., Tsadilas, C. D., & Rinklebe, J. (2013). A review of the distribution coefficients of trace elements in soils: Influence of sorption system, element characteristics, and soil colloidal properties. *Advances in Colloid and Interface Science*, *201-202*, 43-56. <https://doi.org/10.1016/j.cis.2013.10.005>
- Speight, J. G. (2013). Chapter 3 - Oil Sand Mining. In J. G. Speight (Ed.), *Oil Sand Production Processes* (pp. 59-79). Gulf Professional Publishing. <https://doi.org/https://doi.org/10.1016/B978-0-12-404572-9.00003-6>
- Swenson, H., & Stadie, N. P. (2019). Langmuir's Theory of Adsorption: A Centennial Review. *Langmuir*, *35*(16), 5409-5426. <https://doi.org/10.1021/acs.langmuir.9b00154>
- Tang, L., Gudda, F. O., Wu, C., Ling, W., El-Ramady, H., Mosa, A., & Wang, J. (2022). Contributions of partition and adsorption to polycyclic aromatic hydrocarbons sorption by fractionated soil at different particle sizes. *Chemosphere*, *301*, 134715. <https://doi.org/10.1016/j.chemosphere.2022.134715>
- Tran, H. N., Lima, E. C., Juang, R.-S., Bollinger, J.-C., & Chao, H.-P. (2021). Thermodynamic parameters of liquid-phase adsorption process calculated from different equilibrium constants related to adsorption isotherms: A comparison study. *Journal of Environmental Chemical Engineering*, *9*(6), 106674. <https://doi.org/10.1016/j.jece.2021.106674>
- Tseng, R.-L., Wu, F.-C., & Juang, R.-S. (2003). Liquid-phase adsorption of dyes and phenols using pinewood-based activated carbons. *Carbon*, *41*(3), 487-495. [https://doi.org/10.1016/S0008-6223\(02\)00367-6](https://doi.org/10.1016/S0008-6223(02)00367-6)

- Turner, N. H. (1975). Kinetics of chemisorption: An examination of the Elovich equation. *Journal of Catalysis*, 36(3), 262-265. [https://doi.org/10.1016/0021-9517\(75\)90035-4](https://doi.org/10.1016/0021-9517(75)90035-4)
- Vimonses, V., Lei, S., Jin, B., Chow, C. W. K., & Saint, C. (2009). Kinetic study and equilibrium isotherm analysis of Congo Red adsorption by clay materials. *Chemical Engineering Journal*, 148(2), 354-364. <https://doi.org/10.1016/j.cej.2008.09.009>
- Volkov, D. S., Rogova, O. B., & Proskurnin, M. A. (2021). Organic Matter and Mineral Composition of Silicate Soils: FTIR Comparison Study by Photoacoustic, Diffuse Reflectance, and Attenuated Total Reflection Modalities. *Agronomy*, 11(9). <https://doi.org/10.3390/agronomy11091879>
- Wei, C., Song, X., Wang, Q., & Hu, Z. (2017). Sorption kinetics, isotherms and mechanisms of PFOS on soils with different physicochemical properties. *Ecotoxicology and Environmental Safety*, 142, 40-50. <https://doi.org/10.1016/j.ecoenv.2017.03.040>
- Wu, C., De Visscher, A., & Gates, I. D. (2019). On naphthenic acids removal from crude oil and oil sands process-affected water. *Fuel*, 253, 1229-1246. <https://doi.org/10.1016/j.fuel.2019.05.091>
- Xiang, L., Wang, X.-D., Chen, X.-H., Mo, C.-H., Li, Y.-W., Li, H., Cai, Q.-Y., Zhou, D.-M., Wong, M.-H., & Li, Q. X. (2019). Sorption Mechanism, Kinetics, and Isotherms of Di-n-butyl Phthalate to Different Soil Particle-Size Fractions. *Journal of Agricultural and Food Chemistry*, 67(17), 4734-4745. <https://doi.org/10.1021/acs.jafc.8b06357>
- Xiang, L., Xiao, T., Mo, C.-H., Zhao, H.-M., Li, Y.-W., Li, H., Cai, Q.-Y., Zhou, D.-M., & Wong, M.-H. (2018). Sorption kinetics, isotherms, and mechanism of aniline aerofloat to agricultural soils with various physicochemical properties. *Ecotoxicology and Environmental Safety*, 154, 84-91. <https://doi.org/10.1016/j.ecoenv.2018.01.032>
- Xing, Z., Tian, K., Du, C., Li, C., Zhou, J., & Chen, Z. (2019). Agricultural soil characterization by FTIR spectroscopy at micrometer scales: Depth profiling by photoacoustic spectroscopy. *Geoderma*, 335, 94-103. <https://doi.org/10.1016/j.geoderma.2018.08.003>
- Xu, X.-R., & Li, X.-Y. (2010). Sorption and desorption of antibiotic tetracycline on marine sediments. *Chemosphere*, 78(4), 430-436. <https://doi.org/10.1016/j.chemosphere.2009.10.045>

- Zhou, X. (2020). Comments on “Efficient adsorption of Mn(II) by layered double hydroxides intercalated with diethylenetriaminepentaacetic acid and the mechanistic study. *J. Environ. Sci.* 85, 56–65”. *Journal of Environmental Sciences*, 90, 409-410. <https://doi.org/10.1016/j.jes.2020.01.015>
- Zhou, X., & Zhou, X. (2014). The unit problem in the thermodynamic calculation of adsorption using the Langmuir equation. *Chemical Engineering Communications*, 201(11), 1459-1467. <https://doi.org/10.1080/00986445.2013.818541>
- Zubot, W., MacKinnon, M. D., Chelme-Ayala, P., Smith, D. W., & Gamal El-Din, M. (2012). Petroleum coke adsorption as a water management option for oil sands process-affected water. *Science of the Total Environment*, 427-428, 364-372. <https://doi.org/10.1016/j.scitotenv.2012.04.024>

## Chapter 4      Sludge-Based Activated Biochar for Adsorption Treatment of Oil Sands Process Water<sup>3</sup>

### 4.1 Introduction

The oil sands process water (OSPW) is generated in the bitumen extraction from the oil sands using the process using the Clark caustic hot water extraction process (Hao et al., 2005). The OSPW must be stored in on-site tailings ponds as a requirement of the Alberta's zero discharge approach (Allen, 2008), resulting in large volume of fluid in the Athabasca oil sands region in the number of 1,360 million m<sup>3</sup> in 2020 (Alberta Energy Regulator, 2021). The OSPW is characterized by its high alkalinity and some concentration of organic contaminants with recalcitrant characteristics (Lévesque, 2014), in which the naphthenic acids (NAs) are one of the main concerns of OSPW because they account for more than 50% of all organic compounds in OSPW (Grewer et al., 2010) and are associated with acute and chronic toxicity to living organisms (Frank et al., 2008; Rogers et al., 2002; Scarlett et al., 2013). Additionally, the reuse of OSPW on-site might be limited by the presence of NAs as they are related to corrosion issues in the plant infrastructure (Quinlan & Tam, 2015).

There are several structures of NAs in the OSPW (Huang et al., 2018), and they are represented by the general chemical formula C<sub>n</sub>H<sub>2n+Z</sub>O<sub>x</sub>. “n” is the carbon number (7 ≤ n ≤ 26), “Z” is the hydrogen deficiency number resulted from ring or double bond formation (0 ≤ -Z ≤ 24)

---

<sup>3</sup> A version of this chapter was published as: Medeiros, D. C. C. S., Chelme-Ayala, P., and Gamal El-Din, M. Sludge-based activated biochar for adsorption treatment of real oil sands process water: Selectivity of naphthenic acids, reusability of spent biochar, leaching potential, and acute toxicity removal. *Chemical Engineering Journal*, 493, 2023. <https://doi.org/10.1016/j.cej.2023.142329>

and also described in terms of the double bond equivalency (DBE) where  $DBE = 1 - Z/2$ , and “x” is the oxygen number ( $2 \leq x \leq 6$ ) (Cancelli & Gobas, 2022; Huang et al., 2015a; Meshref et al., 2017). NAs with  $x = 2$  are named classical NAs, while NAs with  $x$  from 3 and 6 are named oxidized NAs (Huang et al., 2015a).

In the literature, there are some technologies reported for the treatment of OSPW in terms of NAs concentrations. Advanced oxidation was applied in the degradation of organics through ozonation and photocatalysis, while membrane nanofiltration and micellar-enhanced ultrafiltration were effective in decreasing the concentration of NAs in OSPW, as reviewed previously by Wu et al. (2019). Adsorption is one of the techniques to target NAs in OSPW. Carbon xerogel (Benally et al., 2019), biochar from agricultural wastes, energy crop residue, and woody biomass (Bhuiyan et al., 2017; Singh et al., 2020), granular activated carbon (Islam et al., 2018), and petroleum coke (Niasar et al., 2019; Pourrezaei et al., 2014) were reported as effective adsorbents of NAs. The advantages of adsorption include (1) straightforward procedure, (2) improved selectivity for specific pollutants depending on the adsorbent characteristics (engineered adsorbents), and (3) regeneration ability of spent adsorbents (De Gisi et al., 2016; Kumari et al., 2020; Pourrezaei et al., 2014).

Biochar is a promising adsorbent as it is a carbon-based material resulted from the pyrolysis of biomass under no oxygen conditions, and such feedstocks can be waste materials, also assisting in the waste management (Lehmann & Joseph, 2015). For instance, biological sludge from municipal wastewater treatment plants has been associated with high toxicity for some aquatic microorganisms (da Silva Souza et al., 2020) and the disposal of the sludge usually involves composting or incineration. However, the application of sludge as biochar might be an economical

alternative to those options, since even the application of sludge as composting material has led to soil contamination (Tomczyk et al., 2020).

There are two main categories of biochar: pristine biochar and activated biochar. Even though pristine biochar is resulted from the carbonization of biomass without further modifications and thus not requiring addition of chemicals, the pristine biochar can have limited adsorptive sites that can reduce the adsorption capacity, as highlighted by Qu et al. (2022). On the other hand, activated biochars can be designed through activation techniques, such as chemical activation (dos Reis et al., 2022) and steam activation (Chakraborty et al., 2018), to improve biochar properties, such as surface area, pore volume, and surface functional groups. The improvement of such properties leads to better adsorption performance to target one or more pollutants. For example, Qu et al. (Qu et al., 2023, pp. author-year) successfully prepared a magnetic bone-based biochar able to target a potentially toxic element and an antibiotic. Zinc chloride ( $ZnCl_2$ ) has been previously studied as chemical activation agent for biochar production, considering its role in improving the functional groups of biochar surface and increasing the adsorption capacity for organic constituents (Cheng et al., 2020a; Kong et al., 2014; Ma et al., 2020). Additionally, the  $ZnCl_2$  activation can significantly develop the pores in the biochar, yielding biochar with high fraction of mesopores (60 – 90% respective of mesopores) (Ding et al., 2021; Li et al., 2020d) that might be crucial in the adsorption of large organic compounds.

Very few studies have centered on the development of biochars for the adsorption of NAs from real OSPW. Most studies focused on model compounds of NAs (Frankel et al., 2016; Singh et al., 2020) instead of real process water, and to the date, only one study reported the use of biochar as adsorbent of the organic matter in real OSPW (Bhuiyan et al., 2017), in which the adsorption capacity of the acid-extractable fraction was low ( $0.56 \text{ mg g}^{-1}$ ) in comparison with other

designed carbon-based materials, such as carbon xerogel ( $15 \text{ mg g}^{-1}$ ) (Benally et al., 2019). The research gaps on biochars designed for NAs adsorption from OSPW include the studies on: (i) application of biochars for adsorption of NAs using real process water, (ii) adsorption selectivity of NAs by biochar considering the diverse NA composition on OSPW, (iii) adsorption of classical and oxidized species of NAs from OSPW, (iv) biochar modifications to have enhanced adsorption of NAs from real OSPW, (v) regeneration and reuse ability of spent biochars for NAs adsorption to reduce the risk of secondary pollution, and (vi) leaching of metals from biochar to the OSPW often associated with sludge-based biochars.

Therefore, this study reports, for the first time, a pristine and a  $\text{ZnCl}_2$ -activated biochar produced from sludge sourced from a municipal wastewater treatment plant in the adsorption of classical and oxidized species of NAs in real OSPW. As the NAs have hydrophilic and hydrophobic areas, it was imperative to create a biochar with amphiphilic surfaces where the adsorption of NAs could take place under different mechanisms. All the research gaps mentioned previously are addressed to fully describe the quality of the biochar, and the adsorption capacity and mechanisms were determined. Additionally, implications of biochar treatment of OSPW on toxicity by means Microtox® bioassay and bioavailability of organics were also evaluated. This study promotes circular economy as it focuses on the development of efficient adsorbents for NAs in OSPW by using sludge to reduce the environmental impact associated with the sludge disposal.

## **4.2 Methodology**

### **4.2.1 OSPW, biological sludge, and chemicals**

Raw OSPW was collected from oil sands tailing pond in Fort McMurray, Alberta, Canada by an oil and gas industry and stored in a cold room at  $4^\circ\text{C}$ . The raw OSPW properties are described



in Table 4.1. Prior to usage, the raw OSPW was mixed using a mechanical stirrer to homogenize the OSPW. The biological sludge used in this study is a mixture of primary and secondary sludge collected from the anaerobic digester of biosolids received from a municipal wastewater treatment plant (Edmonton, Alberta, Canada) and its pH, chemical oxygen demand (COD), and metal content are reported in Table S3. The sludge was stored at 4°C prior to preparation. For the biochar production, ZnCl<sub>2</sub> anhydrous >98% (Thermo Scientific™, USA) was purchased from Fisher Scientific (Canada). Ultra-pure water (Synergy UV, MilliporeSigma, USA) was used in the biochar production.

**Table 4.1:** Characteristics of raw OSPW.

<b>Parameter</b>		<b>Value</b>
pH		8.5
Dissolved organic carbon (mg L <sup>-1</sup> )		89.8
Chemical oxygen demand (mg L <sup>-1</sup> )		355.5
Total NAs (mg L <sup>-1</sup> )		61.8
Classical NAs	O <sub>2</sub> -NAs (mg L <sup>-1</sup> )	40.4
Oxidized NAs	O <sub>3</sub> -NAs (mg L <sup>-1</sup> )	11.5
	O <sub>4</sub> -NAs (mg L <sup>-1</sup> )	8.2
	O <sub>5</sub> -NAs (mg L <sup>-1</sup> )	1.3
	O <sub>6</sub> -NAs (mg L <sup>-1</sup> )	0.4
Extractable petroleum hydrocarbons (mg L <sup>-1</sup> )	F2 (C10-C16 HC)	0.71
	F3 (C16-C34 HC)	0.51
	F4 (C34-C50 HC)	<LOD
Polycyclic aromatic hydrocarbons (µg L <sup>-1</sup> )	Acridine	0.071
	Other PAHs	<LOD
Volatile compounds (µg L <sup>-1</sup> )	Benzene	<LOD
	Toluene	<LOD
	Ethylbenzene	<LOD
	Xylenes	<LOD
	F1 (C6-C10)	<LOD

LOD: limit of detection

#### 4.2.2 Biochar synthesis and characterization

Prior to biochar synthesis, the biological sludge was dried in an oven (Fisherbrand™ Isotemp™, Fisher Scientific, USA) at 105°C for 48 h. Dried sludge samples were crushed using a ball milling process at 30 s<sup>-1</sup> frequency for 50 s operation time (MM400, Retsch, Germany) to obtain a homogeneous powder and then stored in air-tight glass containers.

The pristine biochar SB-600, i.e., biochar without any activation, was produced at 600°C from sludge through pyrolysis in a closed system using a muffle furnace (Lindberg Blue M, Thermo Scientific™, USA) at the following conditions: 10°C min<sup>-1</sup> of heating rate, heating and cooling down under oxygen-free conditions achieved supplying 99% pure N<sub>2</sub> at 2 L min<sup>-1</sup>, and 2 h of retention time at 600°C.

The ZnCl<sub>2</sub>-activated biochar SB-Zn was produced by mixing the sludge with the chemical activation agent (0.5 M ZnCl<sub>2</sub>) in the ratio of 1 g dried biological sludge per 20 mL 0.5 M ZnCl<sub>2</sub> for 24 h using a magnetic stirring platform (Cimarec i, Thermo Scientific™, USA). The mass ratio of ZnCl<sub>2</sub> to sludge was 1.36, which was determined based on preliminary experiments. The typical mass ratio of feedstock to ZnCl<sub>2</sub> reported in the literature was 1 to 3 to produce biochar with high mesopore content (Guo et al., 2021; Kong et al., 2014; Li et al., 2020d; Nguyen et al., 2022; Uçar et al., 2009; Wang et al., 2021). The contents were further dried at 105°C for 24 h. Pyrolysis was done in a closed system using a muffle furnace at conditions listed previously at 600°C. After cooling time, the biochar was washed three times using ultra-pure water using a vacuum filtration system equipped with hydrophilic polycarbonate membrane of 8.0 µm pore size (TETP04700, Isopore™, Millipore, Germany), then dried in the oven at 105°C for 24 h. An agate mortar and pestle (Fisherbrand™, Fisher Scientific, USA) was used to finally crush the activated biochar.

#### 4.2.3 Biochar characterization

Characterization techniques were applied to understand the textural and surface characteristics of the feedstock and its respective pristine and activated biochars. Point of zero charge (pH<sub>pzc</sub>) was determined based on the method described in detail by Jang et al. (2018). Surface area and porous properties were determined by evaluating N<sub>2</sub> adsorption using a surface

area analyzer (Autosorb-iQ, Quantachrome, USA). Prior to N<sub>2</sub> adsorption, the samples were outgassed at 120°C for 4 h. The Brunauer–Emmett–Teller (BET) method was used to calculate the surface area ( $S_{\text{BET}}$ ) and the total pore volume ( $V_{\text{TOT}}$ ) of the samples (Brunauer et al., 1938). The micropore surface area ( $S_{\text{MICRO}}$ ), mesopore surface area ( $S_{\text{MESO}}$ ), and the micropore volume ( $V_{\text{MICRO}}$ ) were evaluated using the t-plot method (de Boer et al., 1966). The surface functional groups were determined between 400 and 4000 cm<sup>-1</sup> at 4 cm<sup>-1</sup> resolution using Fourier transform infrared (FTIR) spectroscopy (Nicolet™ 8700 FT-IR Spectrometer, Thermo Scientific, USA). Prior to FTIR analysis, samples were pressed into KBr pellets. The crystallographic properties were evaluated by means of X-ray diffractometer (XRD, Ultima IV, Rigaku, Japan) at scanning rate of 3° min<sup>-1</sup> between 10 and 90° 2 $\theta$  angles using Cobalt tube at 38 kV and 38 mA. The surface chemical composition and chemical states were characterized by X-ray photoelectron spectroscopy (XPS, Kratos AXIS 165, Kratos Analytical, UK). Proximate analysis was performed according to method presented by Crombie et al. (2013) to determine moisture, volatile matter, ash, and fixed carbon content by weight loss using a thermogravimetric analyzer (Discovery TGA, TA Instruments, USA) equipped with platinum pan. The thermogravimetric analyzer was also used to determine the thermostability of samples between 105 and 900°C at heating rate of 20°C min<sup>-1</sup>. The elemental composition in terms of carbon (C), nitrogen (N), hydrogen (H), and sulphur (S) concentrations was determined using an elemental analyzer (2400 Series II CHNOS analyzer, PerkinElmer, USA) in which the elemental oxygen content was estimated by difference (100 – C(%) – H(%) – N(%) – S(%) – Ash(%)) on a dry-mass basis.

Post-adsorption SB-Zn collected from experiments performed at equilibrium time using raw OSPW was dried at 50°C for 24 h and then characterized in terms of surface functional groups and surface chemical and electronic states of elements to identify the adsorption mechanisms.

#### 4.2.4 Adsorption experiments

The adsorption experiments consisted of adding covered flasks containing the biochar and the raw OSPW on a platform shaker (New Brunswick™ Innova® 2100 platform shaker, Eppendorf Inc., USA) at agitation speed of 200 rpm and temperature of 20°C for a certain period. 0.45 µm syringe filters (Basix™ Nylon Syringe Filters, Fisher Scientific, USA) were used to separate the biochar from OSPW after the adsorption process and samples were stored at 4°C until analysis. All experiments were performed in duplicates. Control experiments (no biochar on raw OSPW) were performed at same conditions to check if the adsorption of NAs on experimental apparatus (filter membranes, Erlenmeyer flasks and polypropylene tubes) or loss of NAs through the experiments were negligible (Li et al., 2020a; Wu et al., 2018). The analytical methods for the measurement of the concentration of classical and oxidized NAs in OSPW are presented in the Supporting Information (Appendix).

##### *4.2.4.1 Performance assessment of pristine and activated biochars*

Initially, pristine (SB-600) and activated (SB-Zn) biochars were evaluated as adsorbents of NAs from raw OSPW by performing adsorption experiments at biochar dosage of 2 g L<sup>-1</sup> and contact time of 24 h. Then, the initial and final concentration of classical and oxidized NAs were measured, and the removal rate and the adsorption capacity were calculated using Equations 2.1 and 2.2, respectively.

##### *4.2.4.2 Adsorption kinetics and equilibrium*

Adsorption kinetics experiments were performed using 2 g L<sup>-1</sup> SB-Zn and raw OSPW at different contact times from 5 min to 24 h to determine the equilibrium time and evaluate the

adsorption capacity for classical NAs over time. Every single contact time required a single batch experiment. The kinetics models PFO (Eq. 2.3), PSO (Eq. 2.4), and IPD (Eq. 2.6) were used to assess the experimental data of kinetics study, in which suitability of a certain model was determined based on the correlation coefficient ( $R^2$ ) provided by the fitting of linear plot to the data and the comparison between the adsorption capacity calculated by the model ( $q_{e,model}$ ) and the adsorption capacity obtained experimentally ( $q_{e,exp}$ ) (Foo & Hameed, 2010).

After determination of the equilibrium time, adsorption equilibrium experiments were performed at 24 h of contact time using SB-Zn and raw OSPW, in which the biochar dosage ranged from 0.25 to 2.5 g L<sup>-1</sup>. The experimental data of equilibrium study was evaluated based on the Langmuir (Eq. 2.7) and Freundlich (Eq. 2.8) isotherms.

#### 4.2.5 Regeneration and reuse of spent biochar

The spent biochar was obtained after the adsorption experiment using 2 g L<sup>-1</sup> SB-Zn and raw OSPW for contact time of 24 h. The spent biochar was dried at 50°C for 24 h prior to regeneration. The study of biochar reuse involved two distinguished steps that were called one cycle:

- (i) regeneration of spent biochar through thermal regeneration (pyrolysis at 600°C) and
- (ii) adsorption of NAs from real OSPW using the regenerated biochar.

The regeneration step for spent biochar was achieved by pyrolysis at 600°C under the conditions of 10°C min<sup>-1</sup> of heating rate, heating and cooling down under oxygen-free conditions achieved supplying 99% pure N<sub>2</sub> at 2 L min<sup>-1</sup>, and 2 h of retention time at 600°C. After pyrolysis of spent biochar, cool crucibles were taken out of the muffle furnace. The regenerated biochar was crushed using the mortar and pestle and stored in closed glass vials. The regenerated biochar was

applied in the adsorption of NAs from real OSPW at dosage of 2 g L<sup>-1</sup> and contact time of 24 h. All experiments were performed in duplicate. One cycle was respective of one spent biochar regeneration and one adsorption experiment using regenerated biochar. A total of five cycles was applied to determine the efficiency of biochar reuse.

#### 4.2.6 Leaching study

The leaching of metals from sludge-based biochars might present a concern in the application of such materials in water treatment. Therefore, a leaching study was conducted to identify the possible release of metals from the biochar into the raw OSPW during treatment. For that, adsorption experiments were performed using 2 g L<sup>-1</sup> SB-Zn and raw OSPW at the contact times 2 h and 30 days, and the concentrations of metals in raw and treated OSPW were determined by inductively coupled plasma optical emission spectrometry (ICP-OES, Thermo iCAP6300 Duo, Thermo Scientific, UK).

#### 4.2.7 Study of acute toxicity and bioavailability of organics

The acute toxicity of raw and SB-Zn-treated OSPW towards *Vibrio fischeri*, a luminescent marine bacterium, was determined using a modified Microtox® protocol based on the Microtox® 81.9% screening test. The suspension of *V. fischeri* was exposed to raw and treated OSPW at 15°C for 15 min and the luminescence intensity was determined using BioTek Synergy H1 microplate reader. The intensity was measured at time 0, 5 and 15 min for the control (diluent) and the OSPW to determine the percent of inhibition.

The biomimetic extraction by solid phase microextraction (BE-SPME) was used to determine the bioavailability of dissolved hydrocarbons for both neutral and ionizable organics

including acid extractable organics (AEO) in raw and treated OSPW. The method was previously described and discussed by Redman et al. (2018). Briefly, the samples were acidified with 50  $\mu\text{L}$  of phosphoric acid to pH 2.0 to 2.4, transferred to 20 mL glass vials with no headspace, and sealed with Teflon caps. The vials were placed in the SPME autosampler. The samples were equilibrated by adding 30  $\mu\text{m}$  polydimethylsiloxane (PDMS) fiber and agitating with orbital agitator (250 rpm) for 100 min at 30°C. Upon completion of equilibration time, the fiber was withdrawn and injected in the injection port at 280°C of the gas chromatograph equipped with a flame ionization detector (GC-FID). The fiber was thermally desorbed in the injection port for three minutes to fully desorb the organic components that partitioned into the PDMS. The results were normalized in terms of 2,3-dimethylnaphthalene (2,3-DMN) derived from liquid solvent injection of a series of aromatic hydrocarbon standards in dichloromethane.

### **4.3 Results and discussion**

#### **4.3.1 Properties of sludge and sludge-based biochars**

Table 4.2 provides the properties for the sludge (precursor material of biochars), pristine biochar SB-600 (biochar produced from sludge at 600°C without any activation) and activated biochar SB-Zn (biochar produced from sludge using  $\text{ZnCl}_2$  activation at 600°C). Of the two types of biochars produced, SB-Zn had surface area of 513.2  $\text{m}^2 \text{g}^{-1}$  and pore volume of 0.55  $\text{cm}^3 \text{g}^{-1}$ , which were 63 and 14 times higher than those of SB-600. About 76% of the surface area and 89% of the pore volume of the SB-Zn were respective of mesopores. The superior porous properties of SB-Zn are an indicative that the engineered biochar would perform better as adsorbent material of NAs from raw OSPW. The yield and the surface area of the biochar increased when the  $\text{ZnCl}_2$  was used as chemical activation agent, and that is because the  $\text{ZnCl}_2$  leads to superior decomposition



of carbonaceous material (Kumar & Mohan Jena, 2015) associated with the polymerization reactions (Mohanty et al., 2005).

The  $\text{pH}_{\text{pzc}}$  of biochar decreased when chemical activation was used. As the pH of OSPW is around 8.5, the engineered biochar will have negative charge ( $\text{pH} > \text{pH}_{\text{pzc}}$ ) (Peng et al., 2016) and the NAs in the OSPW will be mostly in the deprotonated form (Huang et al., 2017). Therefore, electrostatic repulsion might occur between the engineered biochar and NAs. However, the metal ions present in the raw OSPW could neutralize the negative charge and decrease the repulsion between the biochar and NAs in OSPW (Pourrezaei et al., 2014).

The content of C, H, N, O, and S decreased after the pyrolysis of sludge because of the thermo- and chemical- degradation of its organic constituents. One of the most important conclusions depicted from the elemental content is the associated ratios (H/C, O/C, (N+O)/C). The H/C is inversely proportional to the degree of aromaticity of biochar, while the O/C and (N+O)/C are proportional to the hydrophilicity and polarity (Chen et al., 2016; Nzediegwu et al., 2022). The comparison of atomic ratios of sludge and biochars showed that all atomic ratios decreased, indicating that the thermo- and chemical-decomposition of sludge resulted in higher aromaticity and hydrophobicity. On the other hand, the  $\text{ZnCl}_2$ -activation of biochar resulted in higher atomic ratios (H/C, O/C, (N+O)/C) than the respective pristine biochar, indicating that the activated biochar had lower aromaticity and higher affinity for water-soluble compounds than SB-600. Higher O/C ratio also relates to the abundance of oxygen-containing surface groups, which is due to the use of  $\text{ZnCl}_2$  as chemical activation agent. The  $\text{ZnCl}_2$  contributes to the retention of oxygen during pyrolysis, and that is why the O/C ratio in SB-Zn was 5 times higher than that of SB-600 (Yusuff et al., 2022). The ash content of the pristine and activated biochars is higher than that of the feedstock and might suggest high inorganic residue such as minerals (Yusuff et al., 2022). High

ash content in biochars produced from sludge is a common feature due to the nature of sludge (Fan et al., 2020; Zielińska et al., 2015).

**Table 4.2:** Properties of biological sludge, pristine biochar (SB-600), and activated biochar (SB-Zn).

<b>Properties</b>		<b>Sludge</b>	<b>SB-600</b>	<b>SB-Zn</b>
<b>Yield (%)</b>		–	58.3	64.3
<b>pH<sub>pzc</sub></b>		–	8.40	6.65
<b>Surface area (m<sup>2</sup> g<sup>-1</sup>)</b>	<b>S<sub>BET</sub></b>	1.4	7.87	513.2
	<b>S<sub>MESO</sub></b>	1.4	7.87	390.1
	<b>S<sub>MICRO</sub></b>	–	–	123.1
<b>Pore volume (cm<sup>3</sup> g<sup>-1</sup>)</b>	<b>V<sub>TOT</sub></b>	0.016	0.04	0.550
	<b>V<sub>MESO</sub></b>	0.016	0.04	0.492
	<b>V<sub>MICRO</sub></b>	–	–	0.058
<b>Proximate analysis (%)</b>	<b>Moisture</b>	3.4	2.7	5.3
	<b>Volatile matter</b>	53.3	10.6	15.7
	<b>Ash</b>	35.6	64.9	53.9
	<b>Fixed carbon</b>	7.7	21.8	24.1
<b>Elemental composition (%)</b>	<b>C</b>	32.9	27.8	28.3
	<b>H</b>	4.9	1.0	1.6
	<b>N</b>	5.3	3.9	2.3
	<b>O</b>	20.7	2.5	13.7
	<b>S</b>	0.6	0.0	0.3
<b>Atomic ratio</b>	<b>H/C</b>	1.78	0.42	0.66
	<b>O/C</b>	0.47	0.07	0.36
	<b>(N+O)/C</b>	0.61	0.19	0.43

The FTIR of feedstock, pristine and activated biochar (Figure 4.1a) indicates that the surface functional groups in the biological sludge changed after activation. The most noticeable change was observed in the peaks around 3400 and 1600  $\text{cm}^{-1}$ , which are characteristics of oxygen-containing functional groups. The pyrolysis temperature of sludge contributed to the degradation of oxygen-containing groups (Cybulak et al., 2019). The sludge also presented bands in the 2960 – 2850  $\text{cm}^{-1}$  region, which are associated with symmetric stretching of C–H vibrations (Chen et al., 2019a) and could indicate the presence of organic contaminants (Russell & Fraser, 1994). Since these peaks disappeared after pyrolysis, the compounds were degraded from sludge, as suggested by the first derivative of thermogravimetric (DTG) curves (Figure 4.3a).

The FTIR of SB-Zn biochar presented bands representative of oxygen-containing surface groups, such as –OH stretching (3200  $\text{cm}^{-1}$ ), C=O (2884  $\text{cm}^{-1}$ ), and C–O stretching vibration and –OH bending of carboxylic groups (1026  $\text{cm}^{-1}$ ) (Chen et al., 2015; Lin et al., 2019; Ma et al., 2021). The decrease in intensity of band around 1026  $\text{cm}^{-1}$  and absence of the other two bands of oxygen-containing groups in the SB-600 indicates that the thermo-degradation of sludge resulted in the release of such groups. This is in accordance with the elemental analysis (Table 4.2), considering that the atomic ratio O/C was much lower for SB-600 in comparison with SB-Zn. The band at 1567  $\text{cm}^{-1}$  is characteristic of aromatic C=C stretching vibrations (Vaughn et al., 2015). These results suggest that the activation with  $\text{ZnCl}_2$  led to aromatization of the carbon due to the dehydration trait of  $\text{ZnCl}_2$  (Liou, 2010) and allowed the abundance of oxygen-containing surface groups.

The changes in the chemical states and surface functional groups of biochar due to pyrolysis and activation can be investigated by means of the XPS survey spectra (Figure 4.1b) and the deconvoluted C1s (Figure 4.2) and O1s (Figure 4.3) XPS spectra. Based on the survey spectra,

it is possible to confirm that the Zn of ZnCl<sub>2</sub>-activation was successfully impregnated in the SB-Zn biochar. The deconvoluted C1s XPS spectra showed peaks for sludge, pristine, and activated biochar at 284.2 – 284.5 eV, 285.0 – 285.4 eV, and 287.8 – 288.0 eV that are assigned to C=O, C–OH, and C=O, respectively (dos Reis et al., 2022; Jieying et al., 2014). Sludge presented an additional the peak at 286.0 eV assigned to C–O/C–H (Cao et al., 2022). The deconvoluted O1s XPS spectra presented peaks at 531.8 – 532.1 eV assigned to either C–O or –OH for sludge, pristine and activated biochars (Cho et al., 2021) and the 534.3 eV peak of C–OH only for activated biochar (dos Reis et al., 2022). Additionally, the peak at 530.8 eV observed only for sludge and pristine biochar is due to C=O (Cao et al., 2022; Ullah et al., 2022). It is noticed that C=O peak decreased after pyrolysis for the pristine biochar, while the C–O/C–H peak disappeared for both pristine and activated biochar, and this occurrence can be associated with the loss of oxygen and hydrogen containing surface groups due to pyrolysis. On the other hand, the activated biochar presented increases in the C=O and C–OH groups, indicating that the ZnCl<sub>2</sub> activation was crucial to introduce oxygen-containing surface groups to the biochar that later on would participate in the adsorption of NAs. The discussion of the changes in the FTIR and XPS spectra after adsorption is presented in the section 4.3.5 Adsorption mechanisms.

The thermostability of feedstock and biochars was evaluated and the results (Figure 4.4b) indicated that the thermostability of biochars greatly increased after pyrolysis. In fact, the weight loss was 55, 10 and 17% for sludge, SB-600 and SB-Zn. The DTG curves of sludge showed major degradation step between 250 and 550°C, which indicates the degradation of volatile and organic compounds (Jerez et al., 2021; Xia et al., 2016). After biochar production, such compounds were released, and no major degradation steps were noticed for the biochars.

The XRD spectra of sludge and sludge-based biochars are presented in Figure 4.4c. The highest peak was due to graphite (peak at  $2\theta$  of  $31^\circ$ ), and the intensity of the peak was proportional to the carbon content (Li et al., 2020d) as presented in Table 4.2. The graphitic structure of biochars might assist the  $\pi$ - $\pi$  interaction between biochar surface and aromatic rings of pollutants (Ma et al., 2021). Quartz was also found in the sludge (peaks at  $2\theta$  of  $24.3^\circ$ ,  $42.1^\circ$ ,  $46.1^\circ$ ,  $58.9^\circ$ ,  $70.9^\circ$ ,  $80.6^\circ$ ,  $81.1^\circ$ ). After biochar production, some quartz peaks persisted in the pristine and activated biochars (peaks at  $2\theta$  of  $24.3^\circ$ ,  $58.9^\circ$ ,  $70.9^\circ$ ,  $80.6^\circ$ ,  $81.1^\circ$ ). The presence of quartz was also detected in the FTIR spectra with the presence of the band around  $450\text{ cm}^{-1}$  (Zhu et al., 2014). It was evidenced from the XRD spectra that the pyrolysis of sludge increased the crystallinity of biochar and the increase of mineralogical phases, which was expected considering that the biochars from sludge had high ash content, i.e., high inorganic residue such as minerals (Yusuff et al., 2022). For the activated biochar, it was noticed the addition of peaks associated with Zn, indicating that the sludge was restructured after pyrolysis, the crystallinity improved because of  $\text{ZnCl}_2$  activation, and the Zn was successfully impregnated in the biochar.

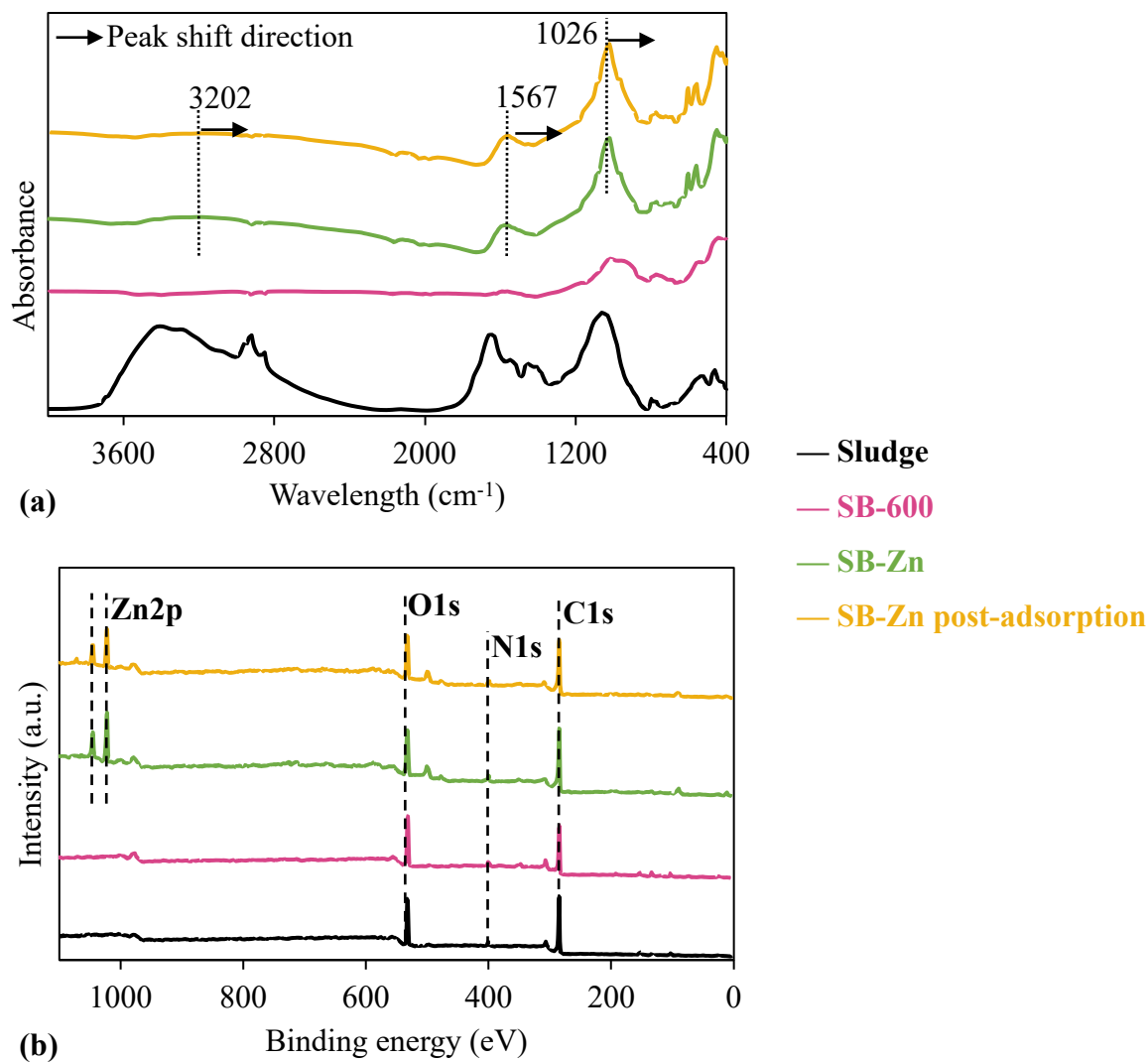


**Figure 4.1:** (a) FTIR spectra and (b) XPS survey spectra of biological sludge feedstock, pristine biochar (SB-600), activated biochar (SB-Zn), and SB-Zn collected after adsorption.

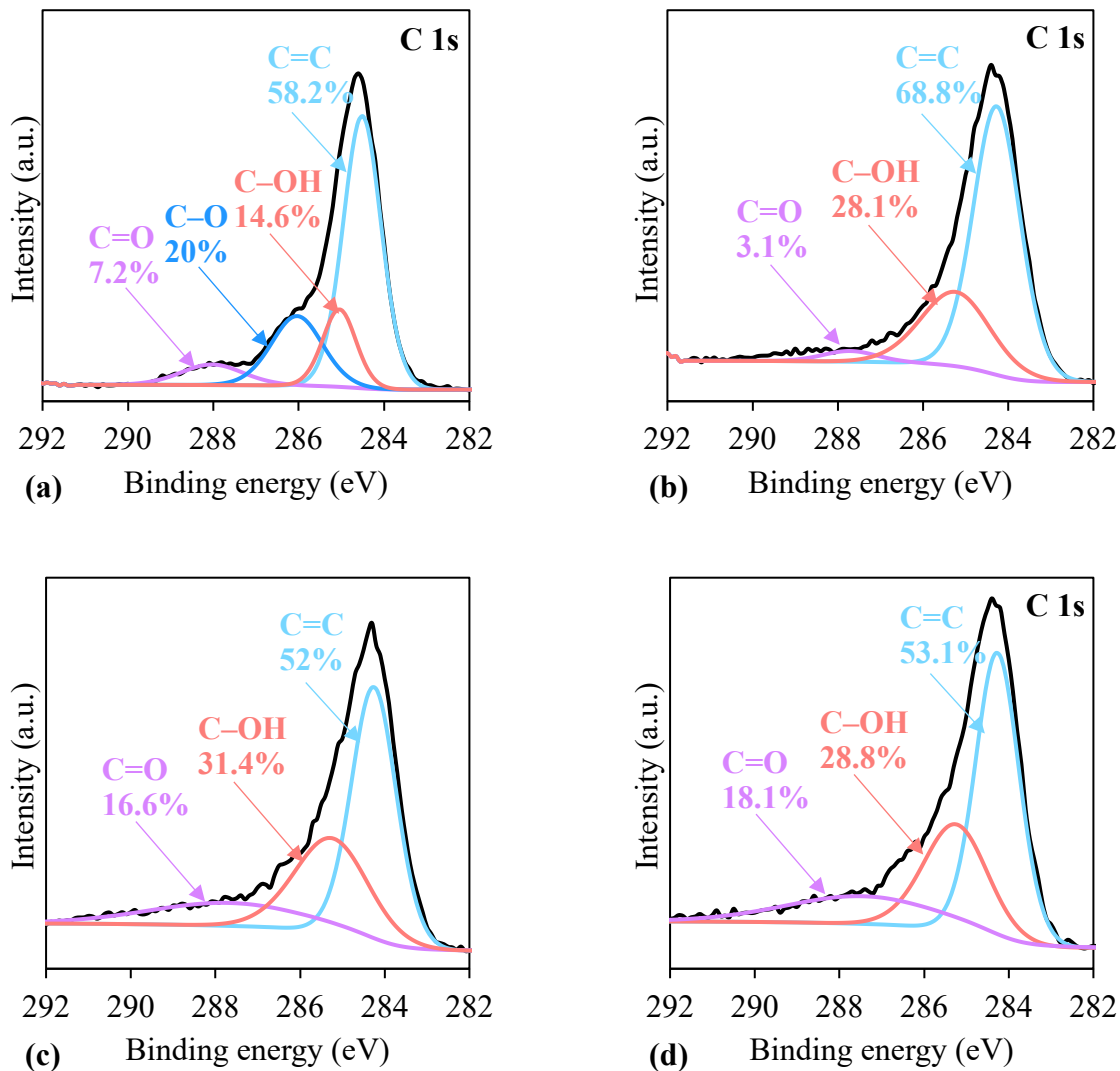


**Figure 4.2:** Deconvoluted C1s XPS spectra for (a) sludge, (b) SB-600, (c) SB-Zn, and (d) SB-Zn collected after adsorption.

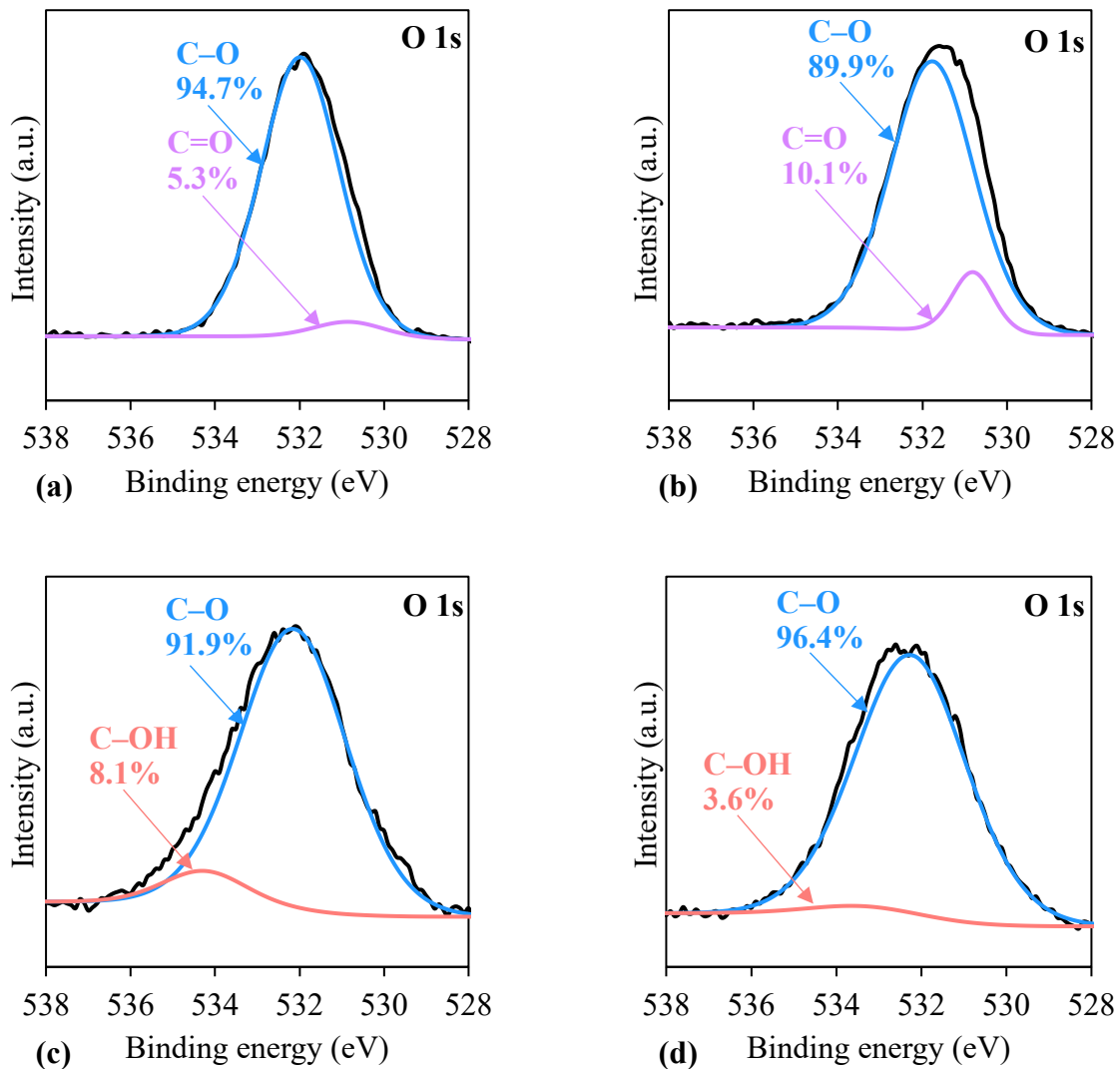


**Figure 4.3:** Deconvoluted O1s XPS spectra for (a) sludge, (b) SB-600, (c) SB-Zn, and (d) SB-Zn collected after adsorption.



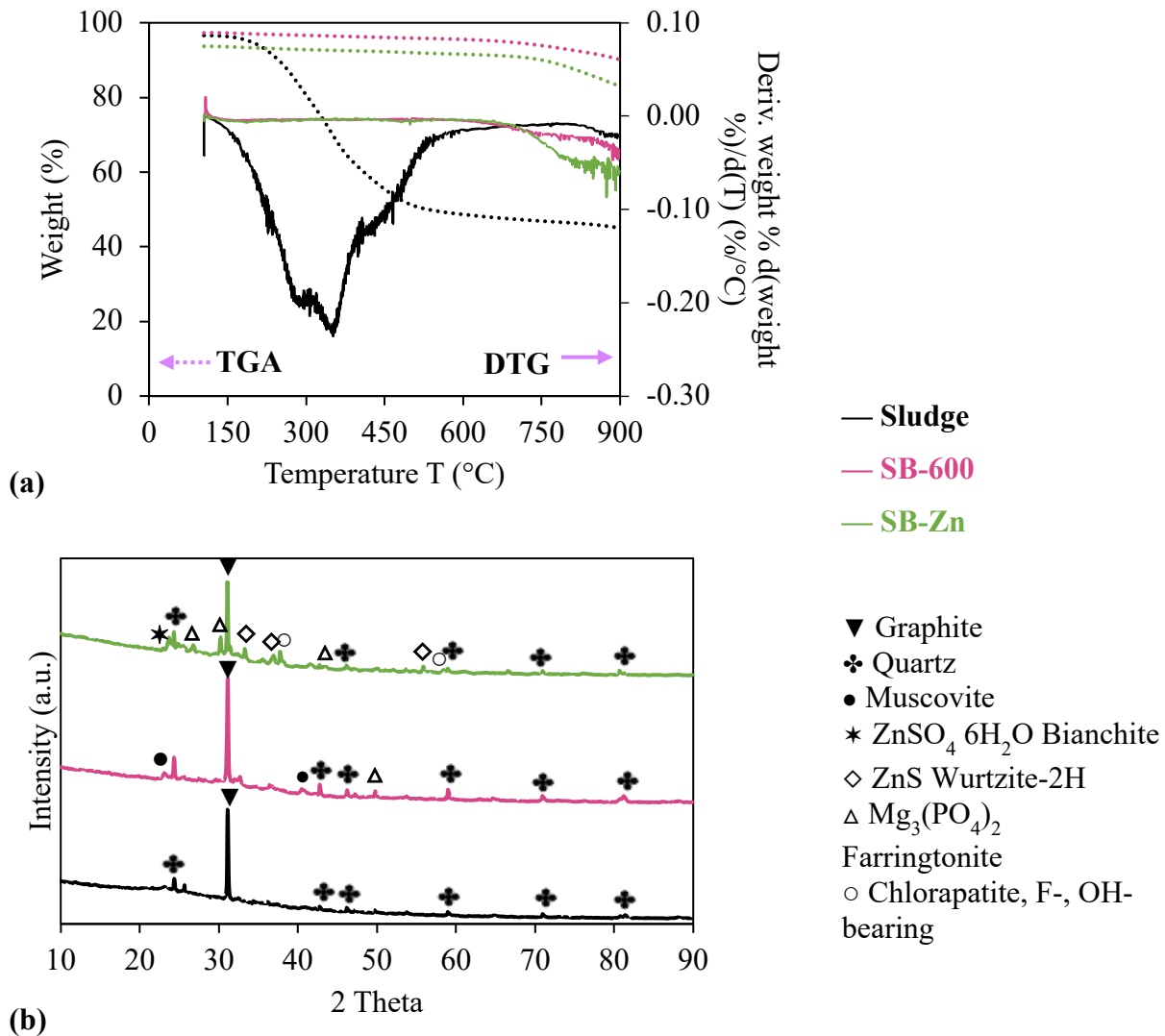


**Figure 4.4:** (a) Thermogravimetric (TGA) and the first derivative of thermogravimetric (DTG) curves and (b) XRD diffractograms of sludge, SB-600, and ZB-Zn.

#### 4.3.2 Performance of pristine and activated biochars in the adsorption of classical and oxidized NAs from OSPW

Pristine (SB-600) and activated biochars (SB-Zn) were applied in the adsorption of classical and oxidized species of NAs from raw OSPW at biochar dosage of 2 g L<sup>-1</sup> and 24 h and the results are presented in Figure 4.5. The total concentration of NAs in the raw OSPW was 61.8

mg L<sup>-1</sup>, from which 40.4 mg L<sup>-1</sup> was respective of classical NAs (O<sub>2</sub>-NAs). 7 and 86% of total NAs were adsorbed by the SB-600 and SB-Zn, respectively. In terms of adsorption capacity, SB-600 and SB-Zn presented total NAs adsorption capacity of 2.3 and 26.6 mg g<sup>-1</sup>, respectively. Specifically for classical NAs (O<sub>2</sub>-NAs), the adsorption capacity was 1.4 and 17.1 mg g<sup>-1</sup> for SB-Zn, respectively. The low removal by SB-600 can be associated directly to the biochar properties. The high surface area, the total pore volume, and the improvement of surface groups due to the ZnCl<sub>2</sub> activation already suggested that the removal of NAs would be better achieved by SB-Zn biochar. Due to the low removal of NAs by the pristine biochar, it was concluded that SB-600 was not an efficient adsorbent for the treatment of OSPW. All further adsorption studies were conducted using only SB-Zn.

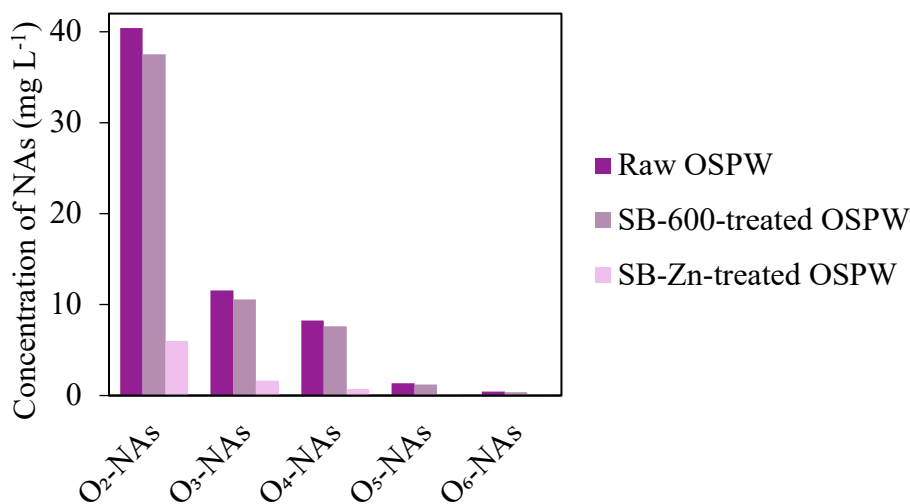


**Figure 4.5:** Final concentration of NAs in OSPW after adsorption on pristine (SB-600) and activated (SB-Zn) biochars.

#### 4.3.3 Adsorption kinetics of classical NAs from raw OSPW on activated biochar: Selectivity of NAs as a function of time

The kinetics study was performed between contact times 5 min and 24 h using 2 g L<sup>-1</sup> SB-Zn (Figure 4.6). In terms of removal of classical NAs in OSPW, the concentration in the OSPW decreased from 40.4 to 18 mg L<sup>-1</sup> (55% removal) by 5 min of contact time, and equilibrium was reached at 2 h with 86% removal of classical NAs from OSPW. The adsorption capacity at equilibrium was 17.1 mg classical NAs per g biochar. In comparison with a few other studies on the adsorption of O<sub>2</sub>-NAs from real process water, the adsorption capacity of SB-Zn was higher than that of carbon xerogel (7.8 mg g<sup>-1</sup>) (Benally et al., 2019) and lower than that of commercial granular activated carbon (GAC) (24 mg g<sup>-1</sup>) (Islam et al., 2018). There is only one study that reported biochar for adsorption of organics in real OSPW and the adsorption capacity of the acid extractable organics was 0.56 mg/g (Bhuiyan et al., 2017). For clarification, the acid extractable organics (AEO) in the OSPW are composed of naphthenic acids and other structurally similar organic compounds of unknown nature (Alberts et al., 2019; Frank et al., 2016), and the adsorption capacity of AEO is higher than the NAs, as presented in the work of Benally et al. (Benally et al., 2019).

The concentration profile of classical NAs as a function of carbon and DBE numbers in raw OSPW and OSPW treated with activated biochar at different adsorption times (Figure 4.6) shows that the classical NAs in the raw OSPW profile were in the range of carbon number 9–20 and DBE number 1–10. Most of NAs were found in the range of 12–19 (93% all classical NAs) and the highest peak was at carbon number 14 (7.2 mg L<sup>-1</sup>) represented by 17.9% of all classical NAs in the raw OSPW, followed by carbon numbers 13, 15, and 16. The concentration as function of DBE numbers indicated that the highest concentrations were obtained values of 3, 4, and 7,

representing 35, 21, and 11% of NAs, and most of classical NAs in this raw OSPW were bicyclic, tricyclic, and hexacyclic (Benally et al., 2019).

The removal of classical NAs increased up to 2 h, where equilibrium was reached. By 2 h of adsorption time, it was noticed that the removal increased with carbon number, in which there was removal of 46 to 74% from carbon numbers 10 to 13. Then, the removal increased from 83% (carbon number 14) to 100% (carbon numbers 20–22). In terms of DBE number, the removal increased as the DBE number increased (34 to 99% removal from 1 to 10). For the NAs remaining in the OSPW after adsorption, the peak concentrations occurred for carbon numbers 13, 12, and 14 with 1.7, 1.6, and 0.9 mg L<sup>-1</sup> and DBE numbers 3 and 4 with 2.9 and 1.5 mg L<sup>-1</sup> in the OSPW. These results suggest that the biochar has higher affinity for higher carbon and DBE numbers, therefore, more hydrophobic, recalcitrant, and with higher cyclicity (Islam et al., 2016; Zubot et al., 2012). Other carbon-based adsorbents also presented this trend, such as petroleum coke, carbon xerogel, and GAC (Benally et al., 2019; Islam et al., 2018; Pourrezaei et al., 2014).

Adsorption kinetics data were analyzed using the pseudo-first order (PFO) and pseudo-second order (PSO) kinetics models and the intraparticle diffusion (IPD) model. The concentration profile of classical NAs in the treated OSPW allows the evaluation of the kinetics for classical NAs as a total, and with specific carbon and DBE numbers. The adsorption capacity of SB-Zn over time was calculated for each carbon and DBE numbers (Figure S6). Four carbon numbers were evaluated (12, 14, 16, 18) aiming at different initial concentrations and adsorption capacities for analysis. Three DBE numbers with the peak concentrations (3, 4, 7) were selected for analysis. The fittings of PFO, PSO, and IPD models for classical NAs and specific NAs are presented in Figure 4.7 and Figure S7. The kinetics parameters are shown in Table 4.3. The PFO model had correlation coefficients ( $R^2$ ) between 0.77 and 0.93, while the PSO model had  $R^2$  of 0.99–1.00 for

the modelling of classical NAs and NAs with specific carbon and DBE numbers. Additionally, the  $q_e$  estimated by the PFO model ( $6.4 \text{ mg g}^{-1}$ ) was far from the  $q_e$  determined experimentally for classical NAs ( $17.1 \text{ mg g}^{-1}$ ), which deems the model unfit for the experimental data. Therefore, the adsorption of classical NAs from raw OSPW on SB-Zn followed the PSO model as the correlation coefficient was 1 and the  $q_e$  estimated by the PSO model was  $17.6 \text{ mg g}^{-1}$ . These findings are in accordance with other studies of carbon-based materials for NAs adsorption from raw OSPW (Benally et al., 2019; Islam et al., 2018).

The adsorption rate of classical NAs on SB-Zn was  $0.80 \text{ g mg}^{-1} \text{ h}^{-1}$ , which was higher than that of other carbon-based materials for adsorption of classical NAs from raw OSPW, such as carbon xerogel ( $0.418 \text{ g mg}^{-1} \text{ h}^{-1}$ ) and GAC ( $0.01 \text{ g mg}^{-1} \text{ h}^{-1}$ ). When the PSO adsorption rate ( $K_{\text{PSO}}$ ) is evaluated for the different carbon and DBE numbers, it is noticed that the  $K_{\text{PSO}}$  for classical NAs with  $n=14$  is  $14.9 \text{ g mg}^{-1} \text{ h}^{-1}$ , which is the highest among the carbon numbers 12, 14, and 16, and much higher than the  $K_{\text{PSO}}$  for total classical NAs ( $0.80 \text{ g mg}^{-1} \text{ h}^{-1}$ ). In terms of the DBE numbers, the  $K_{\text{PSO}}$  increased from  $1.75$  to  $10 \text{ g mg}^{-1} \text{ h}^{-1}$  when the DBE number increased from 3 to 7, and it seems to increase with the DBE number and/or initial concentration of NAs. From the data (Table 4.3), it seems like the  $K_{\text{PSO}}$  increased as carbon number increased or decreased away from carbon number 14 and that the  $K_{\text{PSO}}$  might be inversely proportional to the initial concentration as function of carbon numbers, while the  $K_{\text{PSO}}$  could be proportional to the initial concentration as function of DBE numbers.

To clarify whether the adsorption rates are related to the carbon and DBE numbers and/or initial concentration of NAs, the  $K_{\text{PSO}}$  was calculated for carbon numbers 12, 17, and 18, and DBE numbers 6 and 9 (Table S4). The initial NA concentration was  $3.4$ ,  $3.7$ , and  $3.5 \text{ mg L}^{-1}$  for carbon numbers 12, 17, and 18, respectively, so the effect of initial NA concentration on  $K_{\text{PSO}}$  was

minimized and the effect of carbon number could be assessed. The rate of adsorption was 2.5 times higher for carbon number 18 in comparison with carbon number 12. On the other hand, when the carbon number increased from 13 to 14, the initial concentration increased, as well as the  $K_{PSO}$ . In terms of DBE numbers, DBE numbers 6 and 9 had the same initial concentration ( $2.6 \text{ mg L}^{-1}$ ), but the  $K_{PSO}$  was 1.3 times higher for DBE = 9. These results indicate that  $K_{PSO}$  was directly proportional to both carbon and DBE numbers, and inversely proportional to initial NA concentration. This behavior was also noticed previously by Benally et al. (2019). Therefore, the SB-Zn biochar has higher affinity for higher carbon and DBE numbers, therefore, NAs with more hydrophobic, recalcitrant, and with higher cyclicality characteristics (Islam et al., 2016; Zubot et al., 2012).

The IPD model is the diffusion model used to understand the rate-limiting steps involved in the adsorption of NAs from OSPW on SB-Zn (Figure 4.5d, Figure S7e,f). As the plot of  $q_e$  versus  $t^{0.5}$  did not pass through the origin and there is more than one linear plot, then intraparticle diffusion is not the rate-limiting step of the adsorption process. Instead, more than one mass transfer process plays an important role in the adsorption process (Fan et al., 2011; Hao et al., 2018). Two linear regions respective of film and pore diffusions were identified (Figure 4.5d), meaning that the adsorption of classical NAs on SB-Zn was governed by both film and pore diffusion. The film diffusion rate ( $K_{IPD, \text{film}}$ ) was much higher than the pore diffusion rate ( $K_{IPD, \text{pore}}$ ). Therefore, the film diffusion was significant in the adsorption process, but the rate-limiting step seems to be the pore diffusion for classical NAs adsorption. This adsorption behaviour was also observed by Islam et al. (2018), which studied the adsorption of NAs from raw OSPW on GAC. Both film and pore diffusion rates tend to increase with the increase in initial concentration. However, when the effect of initial concentration is minimized (carbon numbers 12, 17, and 18

with slightly different initial concentrations), it was observed that lower pore diffusion rate was obtained for lower for carbon number, which indicates the preference of biochar for larger molecules (i.e., higher carbon numbers).

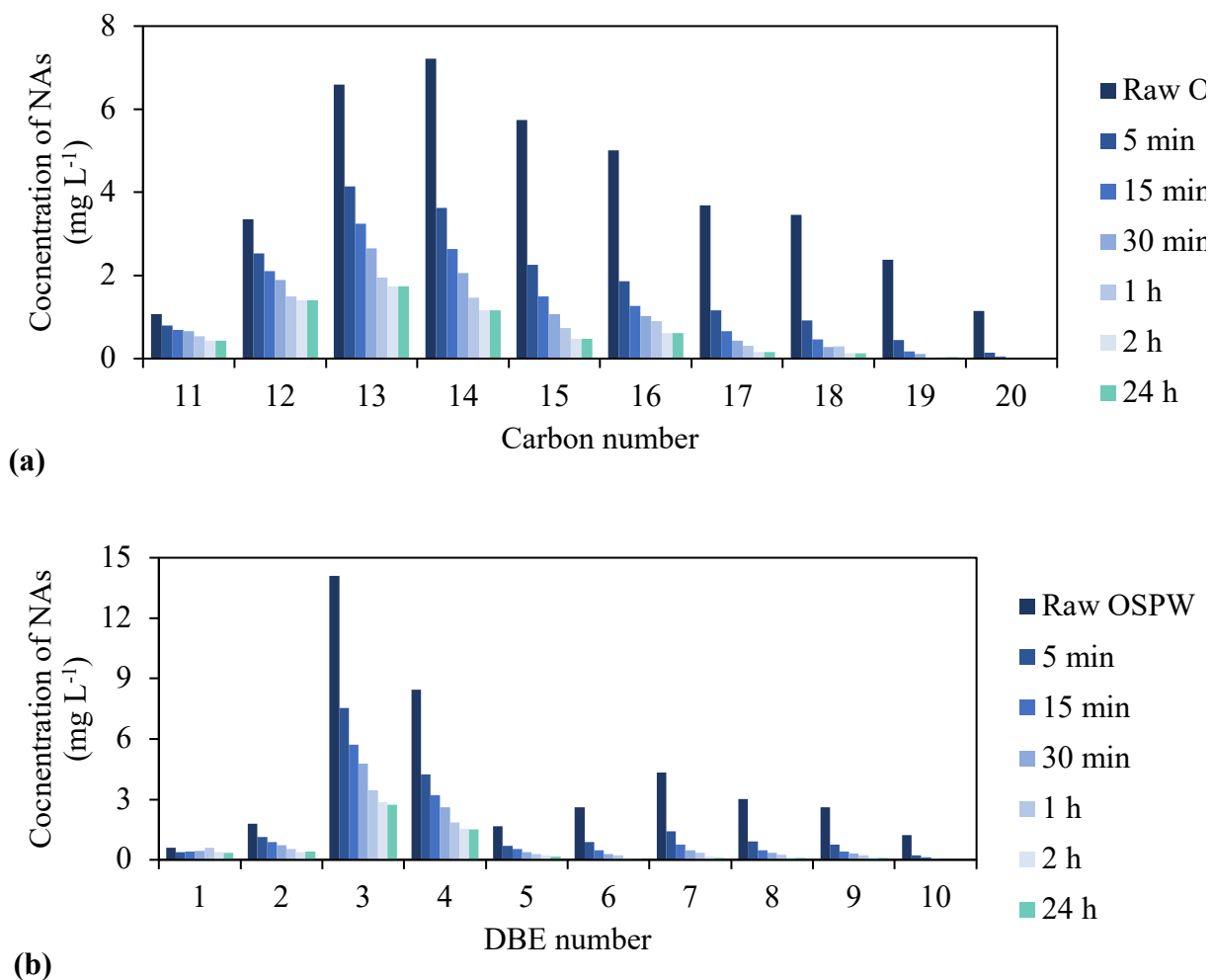


**Figure 4.6:** Concentration of classical NAs in raw OSPW and OSPW treated with 2 g L<sup>-1</sup> of SB-Zn for different times partitioned by (a) different carbon numbers and (b) different DBE numbers. Total classical NAs in the raw OSPW: 40.4 mg L<sup>-1</sup>.

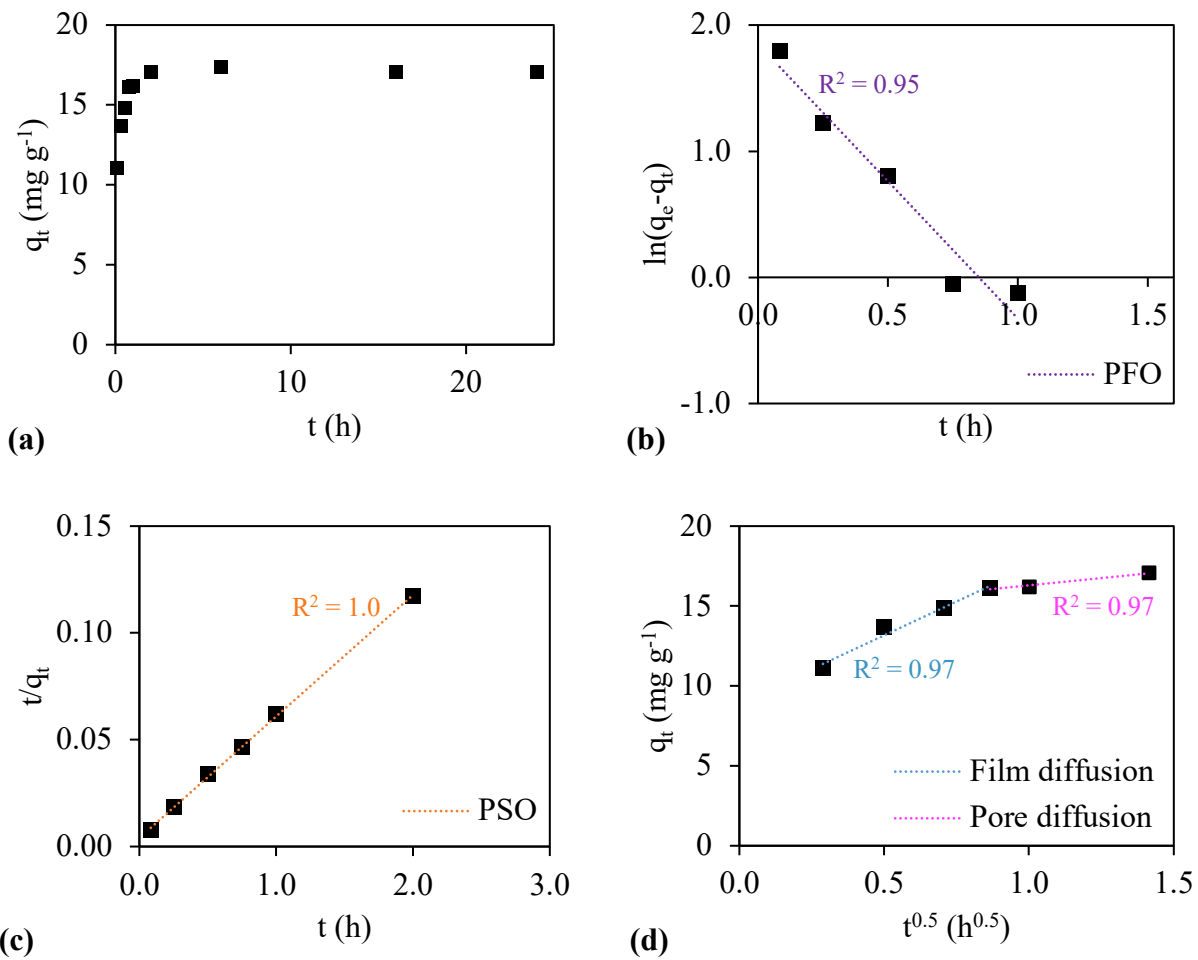


**Figure 4.7:** (a) Adsorption capacity of classical NAs from raw OSPW treated with 2 g L<sup>-1</sup> of SB-Zn for different times, and fittings of (b) intraparticle diffusion model, (c) pseudo-first order and (d) pseudo-second order kinetics models.



**Table 4.3:** Modeling kinetic parameters obtained for the adsorption of classical NAs from raw OSPW on SB-Zn.

Kinetics models and parameters	O <sub>2</sub> -NAs	Carbon number				DBE number			
		12	14	16	18	3	4	7	
<b>Initial concentration (mg L<sup>-1</sup>)</b>	40.4	3.4	7.2	5.0	3.5	14.1	8.5	4.3	
<b>q<sub>e.exp</sub> (mg g<sup>-1</sup>)</b>	17.1	1.0	3.0	2.2	1.7	5.6	3.4	2.1	
<b>PFO</b>	<b>q<sub>e.PFO</sub> (mg g<sup>-1</sup>)</b>	6.4	0.7	1.4	0.6	0.3	2.8	1.6	0.6
	<b>K<sub>PFO</sub> (h<sup>-1</sup>)</b>	2.18	2.87	2.42	1.61	1.58	2.36	2.40	2.18
	<b>R<sup>2</sup></b>	0.95	0.85	0.93	0.86	0.77	0.92	0.91	0.92
<b>PSO</b>	<b>q<sub>e.PSO</sub> (mg g<sup>-1</sup>)</b>	17.6	1.0	3.1	2.2	1.7	5.8	3.6	2.1
	<b>K<sub>PSO</sub> (g mg<sup>-1</sup> h<sup>-1</sup>)</b>	0.80	5.79	3.58	7.71	14.6	1.75	3.15	10.0
	<b>R<sup>2</sup></b>	1.00	0.99	1.00	1.00	1.00	1.00	1.82	1.00
<b>IDP</b>	<b>K<sub>IDP, film</sub> (mg g<sup>-1</sup> h<sup>-0.5</sup>)</b>	8.56	0.79	1.69	0.79	0.50	3.12	1.82	0.86
	<b>c<sub>i, film</sub></b>	8.94	0.19	1.34	1.38	1.16	2.42	1.61	1.26
	<b>R<sup>2</sup></b>	0.97	0.93	0.97	0.93	0.84	0.96	0.96	0.93
	<b>K<sub>IDP, pore</sub> (mg g<sup>-1</sup> h<sup>-0.5</sup>)</b>	1.82	0.09	0.31	0.26	0.18	0.61	0.34	0.17
	<b>c<sub>i, pore</sub></b>	14.5	0.84	2.56	1.80	1.39	4.70	2.94	1.82
	<b>R<sup>2</sup></b>	0.97	0.91	0.98	0.98	0.99	0.98	0.97	0.95

#### 4.3.1 Equilibrium modelling of classical NAs from raw OSPW on activated biochar

The adsorption process was evaluated at different biochar dosages for contact time of 24 h. The biochar dosages ranged from 0.25 to 2.5 g L<sup>-1</sup> and the removal is presented in Figure 4.8a. The removal of classical NAs increased with the increase in biochar dosage, reaching 89% with dosage of 2.5 g L<sup>-1</sup>. The Langmuir and Freundlich isotherms were applied to the experimental data to model the adsorption equilibrium (Figure 4.8b,c) and the fitted parameters of isotherms are presented in Table 4.4. The correlation coefficient for the Freundlich isotherm was 1, indicating

that this isotherm was the best one to describe the adsorption of NAs from raw OSPW on SB-Zn biochar. The Freundlich isotherm describes non-ideal reversible adsorption and assumes a multi-layer adsorption with different affinities at different adsorption sites (heterogeneous surface of adsorbent) (García-Zubiri et al., 2009). This result was expected because two carbon-based materials used as adsorbents of NAs also were represented by Freundlich isotherm (carbon xerogel and GAC) (Benally et al., 2019; Islam et al., 2018). From the fitted parameters of Freundlich isotherm, the  $K_f$  is indicative of the affinity between the adsorbents and the NAs and are important to compare adsorbents for the same purpose, considering that higher  $K_f$  values are desired. Comparing the adsorption of classical NAs on carbon-based materials, the SB-Zn biochar had  $K_f = 6.7 \text{ mg}^{0.5} \text{ L}^{0.5} \text{ g}^{-1}$ , while GAC had  $K_f = 7.35 \text{ mg}^{0.3} \text{ L}^{0.7} \text{ g}^{-1}$  (Islam et al., 2018). Considering that the GAC is a commercial activated carbon with almost double the surface area of SB-Zn, the Freundlich parameters were adequate. Additionally, the Freundlich heterogeneity parameter given by the parameter  $n$  indicates the heterogeneity of SB-Zn: as close as it is of zero, the greater the heterogeneity of biochar (Martins et al., 2015; Zeng & Kan, 2021). As the  $n$  for SB-Zn was 0.5, the biochar can be characterized as having a heterogeneous surface.

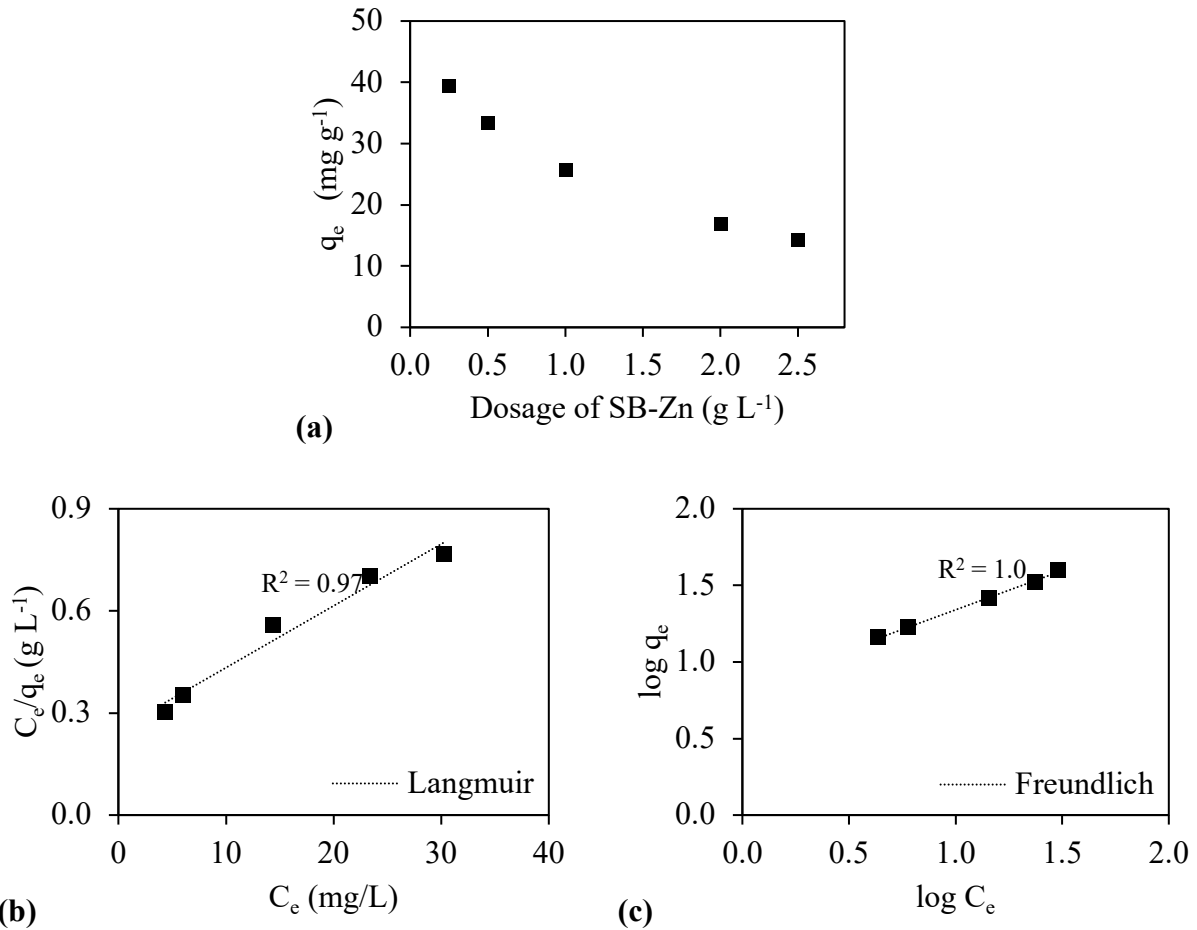


**Figure 4.8:** (a) Adsorption capacity of SB-Zn for adsorption of NAs from raw OSPW, and fittings of (b) Langmuir and (c) Freundlich isotherms.

**Table 4.4:** Modeling isotherm parameters obtained for the adsorption of classical NAs from raw OSPW on SB-Zn.

Isotherms and parameters		Value
Langmuir	$q_{\max}$ (mg g <sup>-1</sup> )	54.9
	$K_L$ (L mg <sup>-1</sup> )	0.07
	$R^2$	0.97
Freundlich	$K_f$ (mg <sup>1-n</sup> L <sup>n</sup> g <sup>-1</sup> )	6.7
	$n$	0.5
	$R^2$	1.0

#### 4.3.2 Adsorption mechanisms

The adsorption mechanisms were identified by comparing the FTIR and XPS spectra of SB-Zn before and after adsorption. For the FTIR spectra (Figure 4.1a), after the application of SB-Zn in the adsorption of NAs from OSPW, there was a shift in the peaks at 3202, 1567 and 1026 cm<sup>-1</sup>, which are associated with H bending vibrations (hydrogen bonding) and  $\pi$ - $\pi$  interactions (Chen et al., 2020a; Tran et al., 2017). For the deconvoluted C1s and O1s XPS spectra (Figure 4.2), it was noticed a shift of the peak respective to C=O after adsorption from 287.7 to 287.4 eV and 534.3 to 533.2 eV, and both are often associated with hydrogen bonding (Jing et al., 2014; Wu et al., 2022a). The enhancement of carboxyl group from 16.6 to 18.1% after adsorption might be related to the presence of the carboxyl groups from the pollutant on the surface of biochar (Li et al., 2022). This is expected, considering the carboxylic acid fraction of NAs.

Hydrogen bonding is considered the main mechanism of polar organic compound adsorption on biochar (Qiu et al., 2022). The SB-Zn has abundance of polar surface groups (hydroxyl, carboxyl). Considering that the NAs are amphipathic compounds, the interaction

between the polar functional groups of biochar and the hydrophilic region of NAs (carboxylic acid) led to the predominance of hydrogen bonding. On the other hand,  $\pi$ - $\pi$  interactions are characteristic of hydrophobic interactions between the aromatic groups of biochar and the aromatic side of NAs.

Pore filling might be one of the most important adsorption mechanisms for the adsorption of NAs on SB-Zn biochar considering that the biochar had large surface area (was composed of  $513.2 \text{ m}^2 \text{ g}^{-1}$ ) and 89% of total pore volume was respective of mesopores. The high porosity of biochar provides appropriate transport paths for the NAs (Cheng et al., 2021), leading to fast adsorption with high initial removal rates characteristic of pore-filling (Regkouzas & Diamadopoulos, 2019). This is in accordance with the conclusions of kinetics study, which indicated that by 5 min of contact time, 55% of classical NAs were already removed from the OSPW by the biochar. In addition, the study of GAC as adsorbent of classical NAs from OSPW could also clarify this, considering that the adsorption capacity was  $24 \text{ mg g}^{-1}$ , but its surface area was  $976 \text{ m}^2 \text{ g}^{-1}$ , in which 86% of surface area was respective to micropores (Islam et al., 2018). Even though the surface area of GAC is almost double the SB-Zn biochar, the adsorption capacity was still closer to SB-Zn biochar ( $17.1 \text{ mg g}^{-1}$ ), and this could suggest that the lack of mesopores in the GAC limited the adsorption of classical NAs.

The summary of the adsorption mechanisms observed for the adsorption of NAs on SB-Zn is illustrated in Figure 4.9.

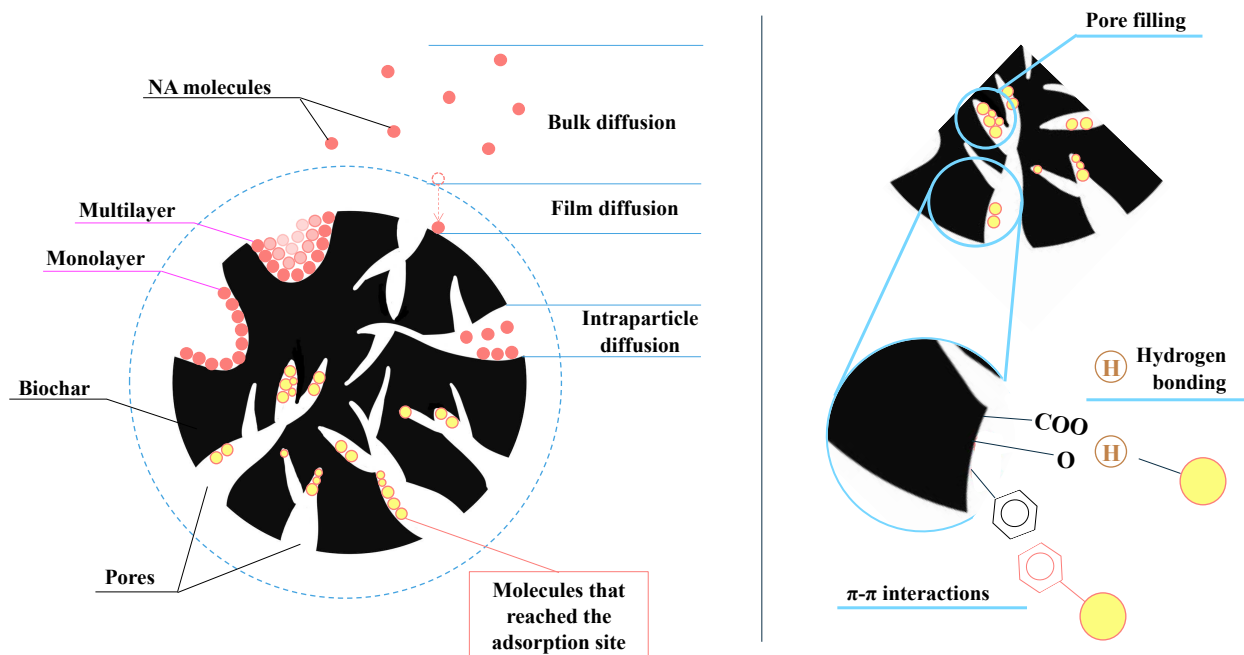


**Figure 4.9:** Adsorption of NAs from raw OSPW on activated biochar from sludge (SB-Zn).

#### 4.3.3 Regeneration and reuse ability of spent biochar

The regeneration of spent biochar had the purpose of breaking the bonds between the NAs and the biochar to allow reuse and reduce the risk of secondary pollution. The thermal regeneration is a straightforward technique to allow biochar reuse because (1) it can thermo-reactivate the surface of biochar for adsorption, (2) it does not produce contaminated wastewater because it does not use solvents or chemicals to promote desorption and regeneration, and (3) it can reduce the costs associated with the production of fresh biochar. In the thermal regeneration, the biochar is subjected to pyrolysis to be decomposed, and the pollutant molecules are either volatilized or released from the pores due to the shrinking effect.

The spent SB-Zn collected after reaching equilibrium was thermo-regenerated at 600°C and reused for adsorption of classical NAs from raw OSPW. Five cycles were performed, and the

results are presented in Figure 6a. The adsorption capacity of fresh SB-Zn was  $17.1 \text{ mg g}^{-1}$ . After the first regeneration and reuse, the adsorption capacity decreased to  $14.9 \text{ mg g}^{-1}$  (13% decrease) and kept steadily decreasing to  $12 \text{ mg g}^{-1}$  in the fourth cycle (30% decrease). Then, further decrease in the adsorption capacity was observed in the fifth cycle, reaching  $7.1 \text{ mg g}^{-1}$ . The possible reason for the decrease in the adsorption capacity after successive thermal regenerations includes the modification of chemical and pore structure of adsorbent during the regeneration through pyrolysis, as reported by Ledesma et al. (Ledesma et al., 2014). Nonetheless, the adsorption capacity obtained in the fifth cycle of regeneration was still 5 times higher than the one obtained for pristine biochar ( $1.4 \text{ mg g}^{-1}$ ), highlighting the SB-Zn potential to be reused efficiently.

The recovery, regeneration and reuse of spent biochar is important to reduce the secondary pollution often associated with the adsorption process. After the spent biochar is regenerated several times and the reuse is not possible, the spent biochar still needs to be disposed of properly. It is suggested that futures studies should evaluate:

- (1) The application of spent biochar on soil and introduce plants to promote the biodegradation of spent biochar and its adsorbed contaminants. Then, the plants can be used as feedstocks of new biochars.
- (2) The applicability of spent biochar as supporting media of degrading bacteria to promote biodegradation of organic contaminants.

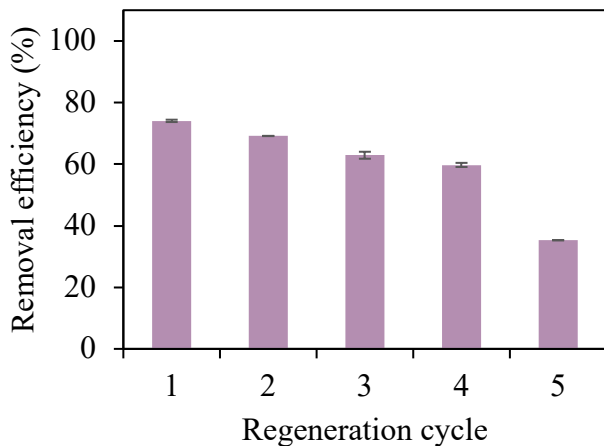


**Figure 4.10:** Adsorption efficiency of regenerated and reused SB-Zn for the removal of NAs from raw OSPW. Adsorption conditions: 2 g L<sup>-1</sup> biochar dosage; 24 h of contact time; raw OSPW.

#### 4.3.4 Leaching of metals from activated biochar to the OSPW during treatment

The leaching of metals from biochar could occur and it frequently depends on the feedstock characteristics and production techniques, as reported in the literature (Chen et al., 2019c; Zhang et al., 2020). Therefore, it is imperative to measure the content of metals in the raw OSPW and in the treated OSPW to identify possible leaching, if any. For the leaching study, the content of metals was determined for OSPW treated with SB-Zn at contact time of 2 h, that is respective of equilibrium time, and 30 days, aiming to evaluate the leaching from the biochar when it is in contact with the OSPW for an extended period of time (Table 4.5). The metals Ag, Be, Cd, Co, Cr, Cu, Fe, Ni, Pb, Sb, Se, Ti, and Tl were not detected in neither raw OSPW or treated OSPW (<LOD).

Based on the results, a minor leaching of Mo, P, S, and Si were observed in the treated OSPW at both 2 h and 30 days. The leaching can be associated with the nature of sludge. Mo, P,



S, and Si were detected in the raw feedstock (dried sludge) as follows: 0.014, 28.5, 9.5, and 2.1 g kg<sup>-1</sup>. Remarkably, the leaching of P was the only one that considerably increased when the contact time increased from 2 h to 30 days, and that can be associated with the high content of P in the raw feedstock. As P is considered an important nutrient, its release over time might be interesting from a fertilizing point of view (Yuan et al., 2016). The metals that are more concerning, such as Cd, Cr, and Pb did not leach from the SB-Zn biochar.

The leaching is often associated with the thermal-decomposition in the biochar production, which might lead to the formation of soluble metal compounds or metal compounds that can slightly dissolve in waters with higher pH, such as silica-containing mineral (quartz, muscovite) (Bagheri et al., 2022; Lammers et al., 2017). The XRD spectra of biochar might help in the identification of such compounds, leading to preventative steps to avoid the leaching, such as water and acid washing of biochar. In the case of SB-Zn biochar, the XRD spectra presented quartz and muscovite fractions, as well as the soluble zinc sulfate hexahydrate respective of bianchite (Figure 1b). The increase in pyrolysis temperature has been proven to minimize the leaching of metals from the biochar (Chen et al., 2019c; Zhang et al., 2020). Therefore, the minimal to no leaching of metals observed in the OSPW after treatment with SB-Zn biochar is probably due to the pyrolysis temperature used in this study (600°C).

Additionally, the treatment of OSPW with SB-Zn biochar for 2 h of contact time was able to remove some metals from the raw OSPW in the order of: Mg (7%), Ca (21%), Sr (27%), and Ba (60%). The concentrations further decreased when 30 days of contact time was applied. These results indicate that the SB-Zn biochar also has potential to decrease the concentration of some metals.

**Table 4.5:** Concentration of metals in the raw and SB-Zn-treated OSPW.

Metals	Units	Raw OSPW	OSPW treated with SB-Zn	
			2 h	30 days
Al	mg L <sup>-1</sup>	0.60	0.60	0.49
As	mg L <sup>-1</sup>	0.04	0.04	0.04
B	mg L <sup>-1</sup>	6.03	6.25	5.91
Ba	mg L <sup>-1</sup>	0.53	0.21	0.09
Ca	mg L <sup>-1</sup>	4.93	3.88	3.23
K	mg L <sup>-1</sup>	30.61	30.25	28.38
Li	mg L <sup>-1</sup>	0.27	0.28	0.26
Mg	mg L <sup>-1</sup>	5.29	4.91	4.73
Mn	mg L <sup>-1</sup>	0.12	<LOD	0.09
Mo	mg L <sup>-1</sup>	0.08	0.10	0.11
Na	mg L <sup>-1</sup>	1110.53	1168.19	1100.23
P	mg L <sup>-1</sup>	0.87	0.96	2.02
S	mg L <sup>-1</sup>	46.70	47.17	47.20
Si	mg L <sup>-1</sup>	1.76	1.77	1.87
Sr	mg L <sup>-1</sup>	0.44	0.32	0.24
V	mg L <sup>-1</sup>	0.02	0.02	0.02
Zn	mg L <sup>-1</sup>	<LOD	0.08	<LOD

LOD: limit of detection

#### 4.3.5 Water quality of raw OSPW after adsorption treatment with activated biochar

The water quality parameters obtained for the raw and SB-Zn-treated OSPW are presented in Table 4.6. The adsorption treatment with SB-Zn was able to decrease the organic matter contents effectively following the order of: DOD (63%) and COD (66%). The total NAs concentration in the OSPW decreased 86%. The presence of extractable petroleum hydrocarbons, polycyclic aromatic hydrocarbons, and volatile compounds was scarce, and some were not detected in the

OSPW. From the compounds that were detected, the SB-Zn biochar was able to decrease about 80% of the F1 and F2 fractions of the extractable petroleum hydrocarbons, and at least 44% of acridine considering that the concentration determined in the treated OSPW was below the limit of quantification.

The OSPW is recycled on-site in the bitumen extraction of oil sands. However, the continuous reuse of OSPW significantly decreases the water quality, impacting in the efficiency of process (Allen, 2008). Additionally, corrosion issues in the plant infrastructure are associated with the NAs in OSPW (Quinlan & Tam, 2015). Therefore, the purpose of this study is to present ZnCl<sub>2</sub>-activated biochar from sludge as part of the treatment of OSPW to reduce the concentration of NAs, allowing more efficient reuse of OSPW. Considering the decrease in NAs, COD and DOC, the SB-Zn biochar can be of assistance in achieving better quality of OSPW for reuse on-site. Should the OSPW be release to the environment, the surface water quality guidelines for the protection of freshwater aquatic life provided by the Government of Alberta would be used as a guideline (Government of Alberta, 2018). The guideline does not provide threshold for NAs, while limiting the concentrations of petroleum hydrocarbons F2 to 0.11 mg L<sup>-1</sup> and acridine to 0.004 mg L<sup>-1</sup>. Due to complexity of OSPW in terms of organics, the Water Quality Based Effluent Limits Procedures Manual acknowledges the effluent toxicity as an effective technique to account for the toxic effects of complex mixtures found in tailings waters (Alberta Environmental Protection, 1995).

**Table 4.6:** Water quality of raw OSPW and OSPW treated with SB-Zn at 2 g L<sup>-1</sup> for 24 h.

Water quality parameters		Units	Raw OSPW	SB-Zn-treated OSPW
pH		–	8.5	8.6
Dissolved organic carbon (DOC)		mg L <sup>-1</sup>	89.8	33.3
Chemical oxygen demand (COD)		mg L <sup>-1</sup>	355.5	121.5
Total NAs		mg L <sup>-1</sup>	61.8	8.5
O <sub>2</sub> -NAs		mg L <sup>-1</sup>	40.4	6.0
O <sub>3</sub> -NAs		mg L <sup>-1</sup>	11.5	1.7
O <sub>4</sub> -NAs		mg L <sup>-1</sup>	8.2	0.7
O <sub>5</sub> -NAs		mg L <sup>-1</sup>	1.3	0.1
O <sub>6</sub> -NAs		mg L <sup>-1</sup>	0.4	0.02
Extractable petroleum hydrocarbons	F2 (C10-C16 HC)	mg L <sup>-1</sup>	0.71	0.12
	F3 (C16-C34 HC)	mg L <sup>-1</sup>	0.51	<0.10
	F4 (C34-C50 HC)	mg L <sup>-1</sup>	<LOD	<LOD
Polycyclic aromatic hydrocarbons	Acridine	µg L <sup>-1</sup>	0.071	<0.04 (LOQ)
	Other PAHs	µg L <sup>-1</sup>	<LOD	<LOD
Volatile compounds	Benzene	µg L <sup>-1</sup>	<LOD	<LOD
	Toluene	µg L <sup>-1</sup>	<LOD	<LOD
	Ethylbenzene	µg L <sup>-1</sup>	<LOD	<LOD
	Xylenes	µg L <sup>-1</sup>	<LOD	<LOD
	F1 (C6-C10)	µg L <sup>-1</sup>	<LOD	<LOD

LOD: limit of detection

LOQ: limit of quantification

#### 4.3.6 Toxicity and bioavailability of organics in OSPW after adsorption treatment with activated biochar

The acute toxicity of raw and OSPW treated using SB-Zn biochar was assessed by means of the inhibition of the bioluminescence of Microtox® *V. fischeri*. The Microtox® bioassay is a simple and fast method to indicate the acute toxicity of OSPW (Islam et al., 2015; López-Vinent

et al., 2021; Suara et al., 2022). Based on the acute toxicity results (Figure 4.11a), the *V. fischeri* inhibition decreased from 46% to 15% after 5 min of exposure and 47% to 17% after 15 min of exposure to the treated samples. It was observed approximately 66% reduction of acute toxicity of OSPW after adsorption treatment using SB-Zn biochar. The reduction in acute toxicity of OSPW after adsorption treatment was also observed by Islam et al. (2015), in which GAC was used as adsorbent and a reduction of 77% of acute toxicity towards *V. fischeri* was achieved. The residual toxicity in the biochar treated OSPW could be due to the remaining organics in the OSPW, considering that the biochar treatment was responsible to reduce the COD and DOC by 66 and 63%.

The BE-SPME quantifies the bioavailability of hydrocarbons that contribute to toxicity, which refers to the hydrocarbons that target the lipid barrier of aquatic life (Redman et al., 2018). Based on the BE-SPME results obtained for the raw and biochar treated-OSPW (Figure 4.11b), there was approximately 91% reduction of bioavailability of organics in OSPW after adsorption treatment. Whale et al. (2022) characterized oil refinery wastewater using bioassays and BE-SPME, concluding that BE-SPME is a potential screening tool to be used with bioassays in the toxicity assessment of effluents. Therefore, the adsorption treatment using SB-Zn contributed to the remarkable reduction of toxicity of OSPW.

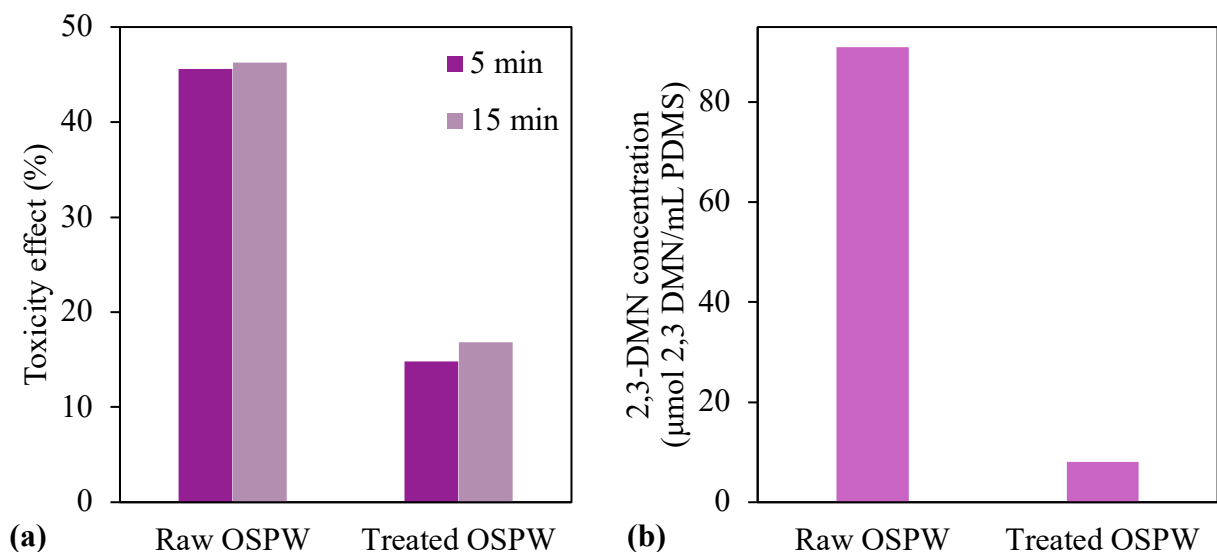


**Figure 4.11:** (a) Toxicity of raw and treated OSPW towards *Microtox*® *Vibrio fischeri* and (b) biomimetic extraction using solid-phase microextraction (BE-SPME) of OSPW before and after 24 h treatment with 2 g L<sup>-1</sup> activated-biochar.

#### 4.4 Conclusions

The treatment of OSPW is imperative to allow efficient recycling of OSPW on-site in the bitumen extraction of oil sands. Successive reuses of OSPW result in a decrease in water quality, impacting the recovery of bitumen and leading to corrosion issues in the plant infrastructure. The OSPW is treated through passive technologies, such as constructed wetlands, and adsorbents can be applied to assist in the OSPW treatment. Therefore, this study proposed the conversion of sludge from a municipal wastewater treatment plant into biochar to be applied in the adsorption treatment of OSPW. Figure 4.12 presents the circular economy concept envisioned for this project.

This is the first in-depth study of sludge-based biochar for advanced treatment of OSPW through adsorption of NAs, in which the knowledge gaps on biochars designed for adsorption of NAs from real OSPW were fully addressed. Such knowledge gaps included the assessment of the

adsorption selectivity by the biochar in the raw OSPW, the thermal-regeneration of spent biochar to avoid secondary pollution associated with adsorption, the leaching of metals from sludge-based biochars into the OSPW, and the toxicity indicators and water quality aspects of OSPW after adsorption treatment. High quality biochar was produced using  $\text{ZnCl}_2$  as chemical activation agent, achieving adsorption capacity of  $17.1 \text{ mg g}^{-1}$  for classical NAs and  $26.6 \text{ mg g}^{-1}$  for total NAs. The adsorption treatment using the  $\text{ZnCl}_2$ -activated biochar reduced the overall organic matter, some metals, and acute toxicity indicators in the raw OSPW, presenting as an effective and feasible adsorbent to be combined with passive treatment technologies. Further studies in biochar for adsorption treatment of OSPW should evaluate the life-cycle assessment of biochar systems and the advantages of applications of spent biochar in land reclamation in terms of phytoremediation of spent biochar and carbon sequestration abilities. In conclusion, the findings of this study are the first step towards circular economy by aligning the waste management of a biohazard and the efficient treatment of OSPW for reuse.

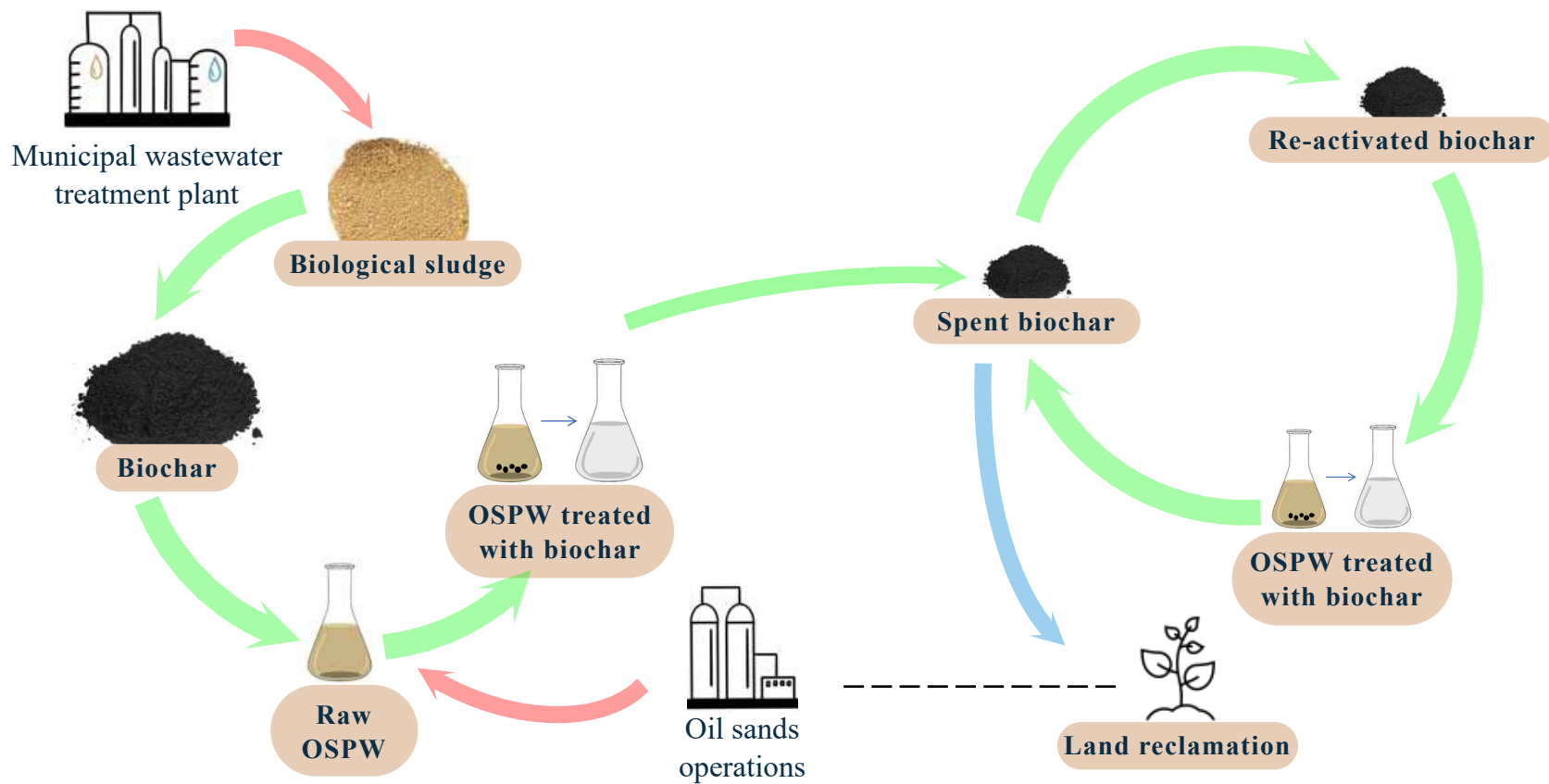


**Figure 4.12:** The circular economy concept envisioned for the waste management of sludge from municipal wastewater treatment plant and the treatment of OSPW from oil sands industries.



## 4.5 References

- Alberta Energy Regulator. (2021). *State of Fluid Tailings Management for Mineable Oil Sands, 2020* <https://static.aer.ca/prd/documents/reports/2020-State-Fluid-Tailings-Management-Mineable-OilSands.pdf>
- Alberta Environmental Protection. (1995). *Water Quality Based Effluent Limits Procedures Manual*.
- Alberts, M. E., Chua, G., & Muench, D. G. (2019). Exposure to naphthenic acids and the acid extractable organic fraction from oil sands process-affected water alters the subcellular structure and dynamics of plant cells. *Science of the Total Environment*, 651, 2830-2844. <https://doi.org/10.1016/j.scitotenv.2018.10.181>
- Allen, E. W. (2008). Process water treatment in Canada's oil sands industry: I. Target pollutants and treatment objectives. *Journal of Environmental Engineering & Science*, 7(2), 123-138. <https://doi.org/10.1139/S07-038>
- Bagheri, M., Lothenbach, B., Shakoorioskooie, M., & Scrivener, K. (2022). Effect of different ions on dissolution rates of silica and feldspars at high pH. *Cement and Concrete Research*, 152, 106644. <https://doi.org/10.1016/j.cemconres.2021.106644>
- Benally, C., Messele, S. A., & Gamal El-Din, M. (2019). Adsorption of organic matter in oil sands process water (OSPW) by carbon xerogel. *Water Research*, 154, 402-411. <https://doi.org/10.1016/j.watres.2019.01.053>
- Bhuiyan, T. I., Tak, J. K., Sessarego, S., Harfield, D., & Hill, J. M. (2017). Adsorption of acid-extractable organics from oil sands process-affected water onto biomass-based biochar: Metal content matters. *Chemosphere*, 168, 1337-1344. <https://doi.org/10.1016/j.chemosphere.2016.11.126>
- Brunauer, S., Emmett, P. H., & Teller, E. (1938). Adsorption of Gases in Multimolecular Layers. *Journal of the American Chemical Society*, 60(2), 309-319. <https://doi.org/10.1021/ja01269a023>
- Cancelli, A. M., & Gobas, F. A. P. C. (2022). Treatment of naphthenic acids in oil sands process-affected waters with a surface flow treatment wetland: mass removal, half-life, and toxicity-reduction. *Environmental Research*, 213, 113755. <https://doi.org/10.1016/j.envres.2022.113755>

- Cao, X., Meng, Z., Song, E., Sun, X., Hu, X., Wenbin, L., Liu, Z., Gao, S., & Song, B. (2022). Co-adsorption capabilities and mechanisms of bentonite enhanced sludge biochar for de-risking norfloxacin and Cu<sup>2+</sup> contaminated water. *Chemosphere*, 299, 134414. <https://doi.org/10.1016/j.chemosphere.2022.134414>
- Chakraborty, P., Banerjee, S., Kumar, S., Sadhukhan, S., & Halder, G. (2018). Elucidation of ibuprofen uptake capability of raw and steam activated biochar of Aegle marmelos shell: Isotherm, kinetics, thermodynamics and cost estimation. *Process Safety and Environmental Protection*, 118, 10-23. <https://doi.org/10.1016/j.psep.2018.06.015>
- Chen, C., Yan, X., Xu, Y., Yoza, B. A., Wang, X., Kou, Y., Ye, H., Wang, Q., & Li, Q. X. (2019a). Activated petroleum waste sludge biochar for efficient catalytic ozonation of refinery wastewater. *Science of the Total Environment*, 651, 2631-2640. <https://doi.org/10.1016/j.scitotenv.2018.10.131>
- Chen, D., Yu, X., Song, C., Pang, X., Huang, J., & Li, Y. (2016). Effect of pyrolysis temperature on the chemical oxidation stability of bamboo biochar. *Bioresource Technology*, 218, 1303-1306. <https://doi.org/10.1016/j.biortech.2016.07.112>
- Chen, H., Chen, D., & Hong, L. (2015). Influences of activation agent impregnated sewage sludge pyrolysis on emission characteristics of volatile combustion and De-NO<sub>x</sub> performance of activated char. *Applied Energy*, 156, 767-775. <https://doi.org/10.1016/j.apenergy.2015.05.098>
- Chen, X., Li, H., Liu, W., Meng, Z., Wu, Z., Wang, G., Liang, Y., & Bi, S. (2020a). Low-temperature constructing N-doped graphite-like mesoporous structure biochar from furfural residue with urea for removal of chlortetracycline from wastewater and hydrothermal catalytic degradation mechanism. *Colloids and Surfaces A: Physicochemical and Engineering Aspects*, 600, 124873. <https://doi.org/10.1016/j.colsurfa.2020.124873>
- Chen, X., Yang, L., Myneni, S. C. B., & Deng, Y. (2019c). Leaching of polycyclic aromatic hydrocarbons (PAHs) from sewage sludge-derived biochar. *Chemical Engineering Journal*, 373, 840-845. <https://doi.org/10.1016/j.cej.2019.05.059>
- Cheng, H., Ji, R., Bian, Y., Jiang, X., & Song, Y. (2020a). From macroalgae to porous graphitized nitrogen-doped biochars – Using aquatic biota to treat polycyclic aromatic hydrocarbons-

- contaminated water. *Bioresource Technology*, 303, 122947. <https://doi.org/10.1016/j.biortech.2020.122947>
- Cheng, L., Ji, Y., Liu, X., Mu, L., & Zhu, J. (2021). Sorption mechanism of organic dyes on a novel self-nitrogen-doped porous graphite biochar: Coupling DFT calculations with experiments. *Chemical Engineering Science*, 242, 116739. <https://doi.org/10.1016/j.ces.2021.116739>
- Cho, E.-J., Kang, J.-K., Moon, J.-K., Um, B.-H., Lee, C.-G., Jeong, S., & Park, S.-J. (2021). Removal of triclosan from aqueous solution via adsorption by kenaf-derived biochar: Its adsorption mechanism study via spectroscopic and experimental approaches. *Journal of Environmental Chemical Engineering*, 9(6), 106343. <https://doi.org/10.1016/j.jece.2021.106343>
- Crombie, K., Mašek, O., Sohi, S. P., Brownsort, P., & Cross, A. (2013). The effect of pyrolysis conditions on biochar stability as determined by three methods. *Gcb Bioenergy*, 5(2), 122-131. <https://doi.org/10.1111/gcbb.12030>
- Cybulak, M., Sokołowska, Z., Boguta, P., & Tomczyk, A. (2019). Influence of pH and grain size on physicochemical properties of biochar and released humic substances. *Fuel*, 240, 334-338. <https://doi.org/10.1016/j.fuel.2018.12.003>
- da Silva Souza, T., Lacerda, D., Aguiar, L. L., Martins, M. N. C., & Augusto de Oliveira David, J. (2020). Toxic potential of sewage sludge: Histopathological effects on soil and aquatic bioindicators. *Ecological Indicators*, 111, 105980. <https://doi.org/10.1016/j.ecolind.2019.105980>
- de Boer, J. H., Lippens, B. C., Linsen, B. G., Broekhoff, J. C. P., van den Heuvel, A., & Osinga, T. J. (1966). The curve of multimolecular N<sub>2</sub>-adsorption. *Journal of Colloid and Interface Science*, 21(4), 405-414. [https://doi.org/10.1016/0095-8522\(66\)90006-7](https://doi.org/10.1016/0095-8522(66)90006-7)
- De Gisi, S., Lofrano, G., Grassi, M., & Notarnicola, M. (2016). Characteristics and adsorption capacities of low-cost sorbents for wastewater treatment: A review. *Sustainable Materials and Technologies*, 9, 10-40. <https://doi.org/10.1016/j.susmat.2016.06.002>
- Ding, K., Zhou, X., Hadiatullah, H., Lu, Y., Zhao, G., Jia, S., Zhang, R., & Yao, Y. (2021). Removal performance and mechanisms of toxic hexavalent chromium (Cr(VI)) with ZnCl<sub>2</sub>

- enhanced acidic vinegar residue biochar. *Journal of Hazardous Materials*, 420, 126551. <https://doi.org/10.1016/j.jhazmat.2021.126551>
- dos Reis, G. S., Guy, M., Mathieu, M., Jebrane, M., Lima, E. C., Thyrel, M., Dotto, G. L., & Larsson, S. H. (2022). A comparative study of chemical treatment by MgCl<sub>2</sub>, ZnSO<sub>4</sub>, ZnCl<sub>2</sub>, and KOH on physicochemical properties and acetaminophen adsorption performance of biobased porous materials from tree bark residues. *Colloids and Surfaces A: Physicochemical and Engineering Aspects*, 642, 128626. <https://doi.org/10.1016/j.colsurfa.2022.128626>
- Fan, J., Li, Y., Yu, H., Li, Y., Yuan, Q., Xiao, H., Li, F., & Pan, B. (2020). Using sewage sludge with high ash content for biochar production and Cu(II) sorption. *Science of the Total Environment*, 713, 136663. <https://doi.org/10.1016/j.scitotenv.2020.136663>
- Fan, J., Zhang, J., Zhang, C., Ren, L., & Shi, Q. (2011). Adsorption of 2,4,6-trichlorophenol from aqueous solution onto activated carbon derived from loosestrife. *Desalination*, 267(2), 139-146. <https://doi.org/10.1016/j.desal.2010.09.016>
- Foo, K. Y., & Hameed, B. H. (2010). Insights into the modeling of adsorption isotherm systems. *Chemical Engineering Journal*, 156(1), 2-10. <https://doi.org/10.1016/j.cej.2009.09.013>
- Frank, R. A., Kavanagh, R., Kent Burnison, B., Arsenault, G., Headley, J. V., Peru, K. M., Van Der Kraak, G., & Solomon, K. R. (2008). Toxicity assessment of collected fractions from an extracted naphthenic acid mixture. *Chemosphere*, 72(9), 1309-1314. <https://doi.org/10.1016/j.chemosphere.2008.04.078>
- Frank, R. A., Milestone, C. B., Rowland, S. J., Headley, J. V., Kavanagh, R. J., Lengger, S. K., Scarlett, A. G., West, C. E., Peru, K. M., & Hewitt, L. M. (2016). Assessing spatial and temporal variability of acid-extractable organics in oil sands process-affected waters. *Chemosphere*, 160, 303-313. <https://doi.org/10.1016/j.chemosphere.2016.06.093>
- Frankel, M. L., Bhuiyan, T. I., Veksha, A., Demeter, M. A., Layzell, D. B., Helleur, R. J., Hill, J. M., & Turner, R. J. (2016). Removal and biodegradation of naphthenic acids by biochar and attached environmental biofilms in the presence of co-contaminating metals. *Bioresource Technology*, 216, 352-361. <https://doi.org/10.1016/j.biortech.2016.05.084>

- García-Zubiri, I. X., González-Gaitano, G., & Isasi, J. R. (2009). Sorption models in cyclodextrin polymers: Langmuir, Freundlich, and a dual-mode approach. *Journal of Colloid and Interface Science*, 337(1), 11-18. <https://doi.org/10.1016/j.jcis.2009.04.071>
- Government of Alberta. (2018). *Environmental Quality Guidelines for Alberta Surface Waters*.
- Grewer, D. M., Young, R. F., Whittal, R. M., & Fedorak, P. M. (2010). Naphthenic acids and other acid-extractables in water samples from Alberta: What is being measured? *Science of the Total Environment*, 408(23), 5997-6010. <https://doi.org/10.1016/j.scitotenv.2010.08.013>
- Guo, N., Lv, X., Yang, Q., Xu, X., & Song, H. (2021). Effective removal of hexavalent chromium from aqueous solution by ZnCl<sub>2</sub> modified biochar: Effects and response sequence of the functional groups. *Journal of Molecular Liquids*, 334, 116149. <https://doi.org/10.1016/j.molliq.2021.116149>
- Hao, C., Headley, J. V., Peru, K. M., Frank, R., Yang, P., & Solomon, K. R. (2005). Characterization and pattern recognition of oil-sand naphthenic acids using comprehensive two-dimensional gas chromatography/time-of-flight mass spectrometry. *Journal of Chromatography A*, 1067(1), 277-284. <https://doi.org/10.1016/j.chroma.2005.01.041>
- Hao, Z., Wang, C., Yan, Z., Jiang, H., & Xu, H. (2018). Magnetic particles modification of coconut shell-derived activated carbon and biochar for effective removal of phenol from water. *Chemosphere*, 211, 962-969. <https://doi.org/10.1016/j.chemosphere.2018.08.038>
- Huang, R., Chelme-Ayala, P., Zhang, Y., Changalov, M., & Gamal El-Din, M. (2017). Investigation of dissociation constants for individual and total naphthenic acids species using ultra performance liquid chromatography ion mobility time-of-flight mass spectrometry analysis. *Chemosphere*, 184, 738-746. <https://doi.org/10.1016/j.chemosphere.2017.06.067>
- Huang, R., Chen, Y., Meshref, M. N. A., Chelme-Ayala, P., Dong, S., Ibrahim, M. D., Wang, C., Klammerth, N., Hughes, S. A., Headley, J. V., Peru, K. M., Brown, C., Mahaffey, A., & Gamal El-Din, M. (2018). Characterization and determination of naphthenic acids species in oil sands process-affected water and groundwater from oil sands development area of Alberta, Canada. *Water Research*, 128, 129-137. <https://doi.org/10.1016/j.watres.2017.10.003>

- Huang, R., McPhedran, K. N., & Gamal El-Din, M. (2015a). Ultra Performance Liquid Chromatography Ion Mobility Time-of-Flight Mass Spectrometry Characterization of Naphthenic Acids Species from Oil Sands Process-Affected Water. *Environmental Science & Technology*, 49(19), 11737-11745. <https://doi.org/10.1021/acs.est.5b03178>
- Islam, M. S., McPhedran, K. N., Messele, S. A., Liu, Y., & Gamal El-Din, M. (2018). Isotherm and kinetic studies on adsorption of oil sands process-affected water organic compounds using granular activated carbon. *Chemosphere*, 202, 716-725. <https://doi.org/10.1016/j.chemosphere.2018.03.149>
- Islam, M. S., Zhang, Y., McPhedran, K. N., Liu, Y., & Gamal El-Din, M. (2015). Granular activated carbon for simultaneous adsorption and biodegradation of toxic oil sands process-affected water organic compounds. *Journal of Environmental Management*, 152, 49-57. <https://doi.org/10.1016/j.jenvman.2015.01.020>
- Islam, M. S., Zhang, Y., McPhedran, K. N., Liu, Y., & Gamal El-Din, M. (2016). Mechanistic investigation of industrial wastewater naphthenic acids removal using granular activated carbon (GAC) biofilm based processes. *Science of the Total Environment*, 541, 238-246. <https://doi.org/10.1016/j.scitotenv.2015.09.091>
- Jang, H. M., Yoo, S., Choi, Y.-K., Park, S., & Kan, E. (2018). Adsorption isotherm, kinetic modeling and mechanism of tetracycline on Pinus taeda-derived activated biochar. *Bioresource Technology*, 259, 24-31. <https://doi.org/10.1016/j.biortech.2018.03.013>
- Jerez, S., Ventura, M., Molina, R., Pariente, M. I., Martínez, F., & Melero, J. A. (2021). Comprehensive characterization of an oily sludge from a petrol refinery: A step forward for its valorization within the circular economy strategy. *Journal of Environmental Management*, 285, 112124. <https://doi.org/10.1016/j.jenvman.2021.112124>
- Jieying, Z., Zhao, Q., & Ye, Z. (2014). Preparation and characterization of activated carbon fiber (ACF) from cotton woven waste. *Applied Surface Science*, 299, 86-91. <https://doi.org/10.1016/j.apsusc.2014.01.190>
- Jing, X.-R., Wang, Y.-Y., Liu, W.-J., Wang, Y.-K., & Jiang, H. (2014). Enhanced adsorption performance of tetracycline in aqueous solutions by methanol-modified biochar. *Chemical Engineering Journal*, 248, 168-174. <https://doi.org/10.1016/j.cej.2014.03.006>

- Kong, L., Xiong, Y., Sun, L., Tian, S., Xu, X., Zhao, C., Luo, R., Yang, X., Shih, K., & Liu, H. (2014). Sorption performance and mechanism of a sludge-derived char as porous carbon-based hybrid adsorbent for benzene derivatives in aqueous solution. *Journal of Hazardous Materials*, 274, 205-211. <https://doi.org/10.1016/j.jhazmat.2014.04.014>
- Kumar, A., & Mohan Jena, H. (2015). High surface area microporous activated carbons prepared from Fox nut (*Euryale ferox*) shell by zinc chloride activation. *Applied Surface Science*, 356, 753-761. <https://doi.org/10.1016/j.apsusc.2015.08.074>
- Kumari, U., Behera, S. K., Siddiqi, H., & Meikap, B. C. (2020). Facile method to synthesize efficient adsorbent from alumina by nitric acid activation: Batch scale defluoridation, kinetics, isotherm studies and implementation on industrial wastewater treatment. *Journal of Hazardous Materials*, 381, 120917. <https://doi.org/10.1016/j.jhazmat.2019.120917>
- Lammers, K., Smith, M. M., & Carroll, S. A. (2017). Muscovite dissolution kinetics as a function of pH at elevated temperature. *Chemical Geology*, 466, 149-158. <https://doi.org/10.1016/j.chemgeo.2017.06.003>
- Ledesma, B., Román, S., Álvarez-Murillo, A., Sabio, E., & González, J. F. (2014). Cyclic adsorption/thermal regeneration of activated carbons. *Journal of Analytical and Applied Pyrolysis*, 106, 112-117. <https://doi.org/10.1016/j.jaap.2014.01.007>
- Lehmann, J., & Joseph, S. (2015). *Biochar for environmental management: science, technology and implementation*. Routledge.
- Lévesque, C. M. (2014). *Oil sands process water and tailings pond contaminant transport and fate : physical, chemical and biological processes*, University of British Columbia]. <https://open.library.ubc.ca/collections/24/items/1.0165952>
- Li, X., Xu, J., Luo, X., & Shi, J. (2022). Efficient adsorption of dyes from aqueous solution using a novel functionalized magnetic biochar: Synthesis, kinetics, isotherms, adsorption mechanism, and reusability. *Bioresource Technology*, 360, 127526. <https://doi.org/10.1016/j.biortech.2022.127526>
- Li, Y., Hu, B., Gao, S., Tong, X., Jiang, L., Chen, X., An, S., & Zhang, F. (2020a). Comparison of 17 $\beta$ -estradiol adsorption on soil organic components and soil remediation agent-biochar. *Environmental Pollution*, 263, 114572. <https://doi.org/10.1016/j.envpol.2020.114572>

- Li, Y.-h., Chang, F.-m., Huang, B., Song, Y.-p., Zhao, H.-y., & Wang, K.-j. (2020d). Activated carbon preparation from pyrolysis char of sewage sludge and its adsorption performance for organic compounds in sewage. *Fuel*, 266, 117053. <https://doi.org/10.1016/j.fuel.2020.117053>
- Lin, L., Song, Z., Khan, Z. H., Liu, X., & Qiu, W. (2019). Enhanced As(III) removal from aqueous solution by Fe-Mn-La-impregnated biochar composites. *Science of the Total Environment*, 686, 1185-1193. <https://doi.org/10.1016/j.scitotenv.2019.05.480>
- Liou, T.-H. (2010). Development of mesoporous structure and high adsorption capacity of biomass-based activated carbon by phosphoric acid and zinc chloride activation. *Chemical Engineering Journal*, 158(2), 129-142. <https://doi.org/10.1016/j.cej.2009.12.016>
- López-Vinent, N., Cruz-Alcalde, A., Ganiyu, S. O., Sable, S., Messele, S. A., Lilloco, D., Stafford, J., Sans, C., Giménez, J., Esplugas, S., & Gamal El-Din, M. (2021). Coagulation-flocculation followed by catalytic ozonation processes for enhanced primary treatment during wet weather conditions. *Journal of Environmental Management*, 283, 111975. <https://doi.org/10.1016/j.jenvman.2021.111975>
- Ma, Y., Li, M., Li, P., Yang, L., Wu, L., Gao, F., Qi, X., & Zhang, Z. (2021). Hydrothermal synthesis of magnetic sludge biochar for tetracycline and ciprofloxacin adsorptive removal. *Bioresource Technology*, 319, 124199. <https://doi.org/10.1016/j.biortech.2020.124199>
- Ma, Y., Li, P., Yang, L., Wu, L., He, L., Gao, F., Qi, X., & Zhang, Z. (2020). Iron/zinc and phosphoric acid modified sludge biochar as an efficient adsorbent for fluoroquinolones antibiotics removal. *Ecotoxicology and Environmental Safety*, 196, 110550. <https://doi.org/10.1016/j.ecoenv.2020.110550>
- Martins, A. C., Pezoti, O., Cazetta, A. L., Bedin, K. C., Yamazaki, D. A. S., Bandoch, G. F. G., Asefa, T., Visentainer, J. V., & Almeida, V. C. (2015). Removal of tetracycline by NaOH-activated carbon produced from macadamia nut shells: Kinetic and equilibrium studies. *Chemical Engineering Journal*, 260, 291-299. <https://doi.org/10.1016/j.cej.2014.09.017>
- Meshref, M. N. A., Chelme-Ayala, P., & Gamal El-Din, M. (2017). Fate and abundance of classical and heteroatomic naphthenic acid species after advanced oxidation processes: Insights and indicators of transformation and degradation. *Water Research*, 125, 62-71. <https://doi.org/10.1016/j.watres.2017.08.007>



- Mohanty, K., Das, D., & Biswas, M. N. (2005). Adsorption of phenol from aqueous solutions using activated carbons prepared from *Tectona grandis* sawdust by ZnCl<sub>2</sub> activation. *Chemical Engineering Journal*, 115(1), 121-131. <https://doi.org/10.1016/j.cej.2005.09.016>
- Nguyen, T.-B., Truong, Q.-M., Chen, C.-W., Doong, R.-a., Chen, W.-H., & Dong, C.-D. (2022). Mesoporous and adsorption behavior of algal biochar prepared via sequential hydrothermal carbonization and ZnCl<sub>2</sub> activation. *Bioresource Technology*, 346, 126351. <https://doi.org/10.1016/j.biortech.2021.126351>
- Niasar, H. S., Das, S., Xu, C., & Ray, M. B. (2019). Continuous column adsorption of naphthenic acids from synthetic and real oil sands process-affected water (OSPW) using carbon-based adsorbents. *Chemosphere*, 214, 511-518. <https://doi.org/10.1016/j.chemosphere.2018.09.078>
- Nzediegwu, C., Naeth, M. A., & Chang, S. X. (2022). Effects of nitric acid modification on hydrochar's combustion, fuel and thermal properties are dependent on feedstock type. *Bioresource Technology*, 354, 127245. <https://doi.org/10.1016/j.biortech.2022.127245>
- Peng, P., Lang, Y.-H., & Wang, X.-M. (2016). Adsorption behavior and mechanism of pentachlorophenol on reed biochars: pH effect, pyrolysis temperature, hydrochloric acid treatment and isotherms. *Ecological Engineering*, 90, 225-233. <https://doi.org/10.1016/j.ecoleng.2016.01.039>
- Pourrezaei, P., Alpatova, A., Chelme-Ayala, P., Perez-Estrada, L. A., Jensen-Fontaine, M., Le, X. C., & Gamal El-Din, M. (2014). Impact of petroleum coke characteristics on the adsorption of the organic fractions from oil sands process-affected water. *International Journal of Environmental Science and Technology*, 11(7), 2037-2050. <https://doi.org/10.1007/s13762-013-0406-x>
- Qiu, B., Shao, Q., Shi, J., Yang, C., & Chu, H. (2022). Application of biochar for the adsorption of organic pollutants from wastewater: Modification strategies, mechanisms and challenges. *Separation and Purification Technology*, 300, 121925. <https://doi.org/10.1016/j.seppur.2022.121925>
- Qu, J., Yuan, Y., Zhang, X., Wang, L., Tao, Y., Jiang, Z., Yu, H., Dong, M., & Zhang, Y. (2022). Stabilization of lead and cadmium in soil by sulfur-iron functionalized biochar:

- Performance, mechanisms and microbial community evolution. *Journal of Hazardous Materials*, 425, 127876. <https://doi.org/10.1016/j.jhazmat.2021.127876>
- Qu, J., Zhang, B., Tong, H., Liu, Y., Wang, S., Wei, S., Wang, L., Wang, Y., & Zhang, Y. (2023). High-efficiency decontamination of Pb(II) and tetracycline in contaminated water using ball-milled magnetic bone derived biochar. *Journal of Cleaner Production*, 385, 135683. <https://doi.org/10.1016/j.jclepro.2022.135683>
- Quinlan, P. J., & Tam, K. C. (2015). Water treatment technologies for the remediation of naphthenic acids in oil sands process-affected water. *Chemical Engineering Journal*, 279, 696-714. <https://doi.org/10.1016/j.cej.2015.05.062>
- Redman, A. D., Butler, J. D., Letinski, D. J., Di Toro, D. M., Leon Paumen, M., & Parkerton, T. F. (2018). Technical basis for using passive sampling as a biomimetic extraction procedure to assess bioavailability and predict toxicity of petroleum substances. *Chemosphere*, 199, 585-594. <https://doi.org/10.1016/j.chemosphere.2018.02.024>
- Regkouzas, P., & Diamadopoulou, E. (2019). Adsorption of selected organic micro-pollutants on sewage sludge biochar. *Chemosphere*, 224, 840-851. <https://doi.org/10.1016/j.chemosphere.2019.02.165>
- Rogers, V. V., Wickstrom, M., Liber, K., & MacKinnon, M. D. (2002). Acute and Subchronic Mammalian Toxicity of Naphthenic Acids from Oil Sands Tailings. *Toxicological Sciences*, 66(2), 347-355. <https://doi.org/10.1093/toxsci/66.2.347>
- Russell, J. D., & Fraser, A. R. (1994). Infrared methods. In M. J. Wilson (Ed.), *Clay Mineralogy: Spectroscopic and Chemical Determinative Methods* (pp. 11-67). Springer Netherlands. [https://doi.org/10.1007/978-94-011-0727-3\\_2](https://doi.org/10.1007/978-94-011-0727-3_2)
- Scarlett, A. G., Reinardy, H. C., Henry, T. B., West, C. E., Frank, R. A., Hewitt, L. M., & Rowland, S. J. (2013). Acute toxicity of aromatic and non-aromatic fractions of naphthenic acids extracted from oil sands process-affected water to larval zebrafish. *Chemosphere*, 93(2), 415-420. <https://doi.org/10.1016/j.chemosphere.2013.05.020>
- Singh, R., Naik, D. V., Dutta, R. K., & Kanaujia, P. K. (2020). Biochars for the removal of naphthenic acids from water: A prospective approach towards remediation of petroleum refinery wastewater. *Journal of Cleaner Production*, 266, 121986. <https://doi.org/10.1016/j.jclepro.2020.121986>

- Suara, M. A., Ganiyu, S. O., Paul, S., Stafford, J. L., & Gamal El-Din, M. (2022). Solar-activated zinc oxide photocatalytic treatment of real oil sands process water: Effect of treatment parameters on naphthenic acids, polyaromatic hydrocarbons and acute toxicity removal. *Science of the Total Environment*, *819*, 153029. <https://doi.org/10.1016/j.scitotenv.2022.153029>
- Tomczyk, B., Siatecka, A., Jędruchiewicz, K., Sochacka, A., Bogusz, A., & Oleszczuk, P. (2020). Polycyclic aromatic hydrocarbons (PAHs) persistence, bioavailability and toxicity in sewage sludge- or sewage sludge-derived biochar-amended soil. *Science of the Total Environment*, *747*, 141123. <https://doi.org/10.1016/j.scitotenv.2020.141123>
- Tran, H. N., Wang, Y.-F., You, S.-J., & Chao, H.-P. (2017). Insights into the mechanism of cationic dye adsorption on activated charcoal: The importance of  $\pi$ - $\pi$  interactions. *Process Safety and Environmental Protection*, *107*, 168-180. <https://doi.org/10.1016/j.psep.2017.02.010>
- Uçar, S., Erdem, M., Tay, T., & Karagöz, S. (2009). Preparation and characterization of activated carbon produced from pomegranate seeds by ZnCl<sub>2</sub> activation. *Applied Surface Science*, *255*(21), 8890-8896. <https://doi.org/10.1016/j.apsusc.2009.06.080>
- Ullah, F., Ji, G., Irfan, M., Gao, Y., Shafiq, F., Sun, Y., Ain, Q. U., & Li, A. (2022). Adsorption performance and mechanism of cationic and anionic dyes by KOH activated biochar derived from medical waste pyrolysis. *Environmental Pollution*, *314*, 120271. <https://doi.org/10.1016/j.envpol.2022.120271>
- Vaughn, S. F., Kenar, J. A., Eller, F. J., Moser, B. R., Jackson, M. A., & Peterson, S. C. (2015). Physical and chemical characterization of biochars produced from coppiced wood of thirteen tree species for use in horticultural substrates. *Industrial Crops and Products*, *66*, 44-51. <https://doi.org/10.1016/j.indcrop.2014.12.026>
- Wang, Y., Jiang, B., Wang, L., Feng, Z., Fan, H., & Sun, T. (2021). Hierarchically structured two-dimensional magnetic microporous biochar derived from hazelnut shell toward effective removal of p-arsanilic acid. *Applied Surface Science*, *540*, 148372. <https://doi.org/10.1016/j.apsusc.2020.148372>
- Whale, G. F., Hjort, M., Di Paolo, C., Redman, A. D., Postma, J. F., Legradi, J., & Leonards, P. E. G. (2022). Assessment of oil refinery wastewater and effluent integrating bioassays,

- mechanistic modelling and bioavailability evaluation. *Chemosphere*, 287, 132146. <https://doi.org/10.1016/j.chemosphere.2021.132146>
- Wu, C., De Visscher, A., & Gates, I. D. (2019). On naphthenic acids removal from crude oil and oil sands process-affected water. *Fuel*, 253, 1229-1246. <https://doi.org/10.1016/j.fuel.2019.05.091>
- Wu, J., Yang, J., Feng, P., Wen, L., Huang, G., Xu, C., & Lin, B. (2022a). Highly efficient and ultra-rapid adsorption of malachite green by recyclable crab shell biochar. *Journal of Industrial and Engineering Chemistry*, 113, 206-214. <https://doi.org/10.1016/j.jiec.2022.05.047>
- Wu, L., Li, B., & Liu, M. (2018). Influence of aromatic structure and substitution of carboxyl groups of aromatic acids on their sorption to biochars. *Chemosphere*, 210, 239-246. <https://doi.org/10.1016/j.chemosphere.2018.07.003>
- Xia, D., Tan, F., Zhang, C., Jiang, X., Chen, Z., Li, H., Zheng, Y., Li, Q., & Wang, Y. (2016). ZnCl<sub>2</sub>-activated biochar from biogas residue facilitates aqueous As(III) removal. *Applied Surface Science*, 377, 361-369. <https://doi.org/10.1016/j.apsusc.2016.03.109>
- Yuan, H., Lu, T., Wang, Y., Chen, Y., & Lei, T. (2016). Sewage sludge biochar: Nutrient composition and its effect on the leaching of soil nutrients. *Geoderma*, 267, 17-23. <https://doi.org/10.1016/j.geoderma.2015.12.020>
- Yusuff, A. S., Lala, M. A., Thompson-Yusuff, K. A., & Babatunde, E. O. (2022). ZnCl<sub>2</sub>-modified eucalyptus bark biochar as adsorbent: preparation, characterization and its application in adsorption of Cr(VI) from aqueous solutions. *South African Journal of Chemical Engineering*, 42, 138-145. <https://doi.org/10.1016/j.sajce.2022.08.002>
- Zeng, S., & Kan, E. (2021). Adsorption and regeneration on iron-activated biochar for removal of microcystin-LR. *Chemosphere*, 273, 129649. <https://doi.org/10.1016/j.chemosphere.2021.129649>
- Zhang, P., Zhang, X., Li, Y., & Han, L. (2020). Influence of pyrolysis temperature on chemical speciation, leaching ability, and environmental risk of heavy metals in biochar derived from cow manure. *Bioresource Technology*, 302, 122850. <https://doi.org/10.1016/j.biortech.2020.122850>

- Zhu, X., Liu, Y., Qian, F., Zhou, C., Zhang, S., & Chen, J. (2014). Preparation of magnetic porous carbon from waste hydrochar by simultaneous activation and magnetization for tetracycline removal. *Bioresource Technology*, *154*, 209-214. <https://doi.org/10.1016/j.biortech.2013.12.019>
- Zielińska, A., Oleszczuk, P., Charmas, B., Skubiszewska-Zięba, J., & Pasieczna-Patkowska, S. (2015). Effect of sewage sludge properties on the biochar characteristic. *Journal of Analytical and Applied Pyrolysis*, *112*, 201-213. <https://doi.org/10.1016/j.jaap.2015.01.025>
- Zubot, W., MacKinnon, M. D., Chelme-Ayala, P., Smith, D. W., & Gamal El-Din, M. (2012). Petroleum coke adsorption as a water management option for oil sands process-affected water. *Science of the Total Environment*, *427-428*, 364-372. <https://doi.org/10.1016/j.scitotenv.2012.04.024>

## **Chapter 5      The Role of Feedstock Type and Chemical Activation on Biochar Synthesis from Sludge and Peat for the Adsorption of Naphthenic Acids <sup>4</sup>**

### **5.1 Introduction**

Biochar is a carbon-based material resulted from the thermal decomposition of biomass under minimal or no oxygen conditions. The biochar production can assist in the energy generation, waste management, water treatment, and soil improvement (Lehmann & Joseph, 2015). Additionally, the biochar production from wastes can contribute to the circular economy when such biomass is converted into biochar to target compounds of interest in contaminated waters. Industrial sludge (Wu et al., 2022b), municipal sludge (Ma et al., 2021), food wastes such as coconut shell (Baharum et al., 2020), and agricultural wastes such as wheat and canola straws (Nzediegwu et al., 2021a) are examples of feedstocks studied to produce biochar. The biochar properties can be further improved by using chemical activation agents during production, aiming at further decomposing the feedstock to improve surface area and pore volume and add surface functional groups to assist in the adsorption. Ferric chloride ( $\text{FeCl}_3$ ) activation was reported as a graphitization catalyst and could add magnetic properties to the biochar. Additionally, it aids in the decomposition of hemicelluloses and celluloses into smaller hydrocarbons during the carbonization process (Wang et al., 2021). On the other hand, the combination of  $\text{ZnCl}_2$  and  $\text{FeCl}_3$

---

<sup>4</sup> A version of this chapter will be submitted to the Bioresource Technology as: Medeiros, D. C. C. S., Chelme-Ayala, P., and Gamal El-Din, M. The role of feedstock type and chemical activation on biochar synthesis for the adsorption of naphthenic acids: Implications in the tailoring of activated biochars.

as chemical activation agents allows superior pore-forming properties, resulting in significant improvement of mesopores (Cheng et al., 2020a).

The oil sands process water (OSPW) is generated during the bitumen extraction from the oil sands using the Clark caustic hot water extraction process and it is stored in on-site tailings ponds as required by the Alberta's zero discharge approach (Allen, 2008; Hao et al., 2005; Zubot et al., 2012). The extraction process involves the usage of 0.2 to 2.6 barrels of fresh water per barrel of bitumen (Natural Resources Canada, 2020), and the high volume of OSPW generated by the oil sands industries highlights the importance of treatment to secure efficient water reuse or safe discharge of OSPW. One of the main concerns of OSPW is the presence of naphthenic acids (NAs), which represents more than 50% of all organic compounds in OSPW (Grewer et al., 2010). Such compounds have been related to acute and chronic toxicity towards zebrafish (Scarlett et al., 2013), mammals (Rogers et al., 2002), and aquatic invertebrates (Bartlett et al., 2017). NAs are given by the general chemical formula  $C_nH_{2n+Z}O_x$ : "n" is the carbon number ( $7 \leq n \leq 26$ ), "Z" is the hydrogen deficiency number resulting from ring or double bond formation ( $0 \leq -Z \leq 24$ ) – also written in terms of the double bond equivalency (DBE) where  $DBE = 1 - Z/2$ , and "x" is the oxygen number, where classical NAs are characterized by  $x = 2$  and oxidized NAs are characterized by x number 3 – 6 (Huang et al., 2015a; Meshref et al., 2017). In terms of OSPW treatment for the removal of NAs, few studies reported the development of biochars for the adsorption of NAs, in which most studies focused on model compounds of NAs (Frankel et al., 2016; Singh et al., 2020) instead of real process water. The application of biochar in real OSPW for adsorption of organic matter was reported once (Bhuiyan et al., 2017).

Considering the lack of in-depth studies on biochar development and characteristics for adsorption of NAs from OSPW, the purpose of this study was to investigate how the type of

feedstock and the changes in the characteristics of resulting biochar affect the adsorption of NAs from OSPW, aiming at providing guidance for further studies in the field of biochar tailoring for adsorption treatment of OSPW. This exploratory study was conducted based on the biochar properties and the comparison of the adsorption efficiency obtained for surrogate compounds of NAs and NAs from real OSPW. The evaluation of the performance of biochars produced through same conditions but using different feedstocks is important to provide a reference for future applications and studies.

## **5.2 Methodology**

### **5.2.1 Chemicals and OSPW**

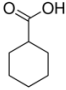
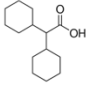
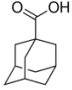
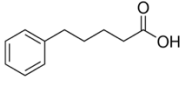
Analytical grade zinc chloride ( $\text{ZnCl}_2$ ), ferric chloride hexahydrate ( $\text{FeCl}_3 \cdot 6\text{H}_2\text{O}$ ), and hydrochloric acid (HCl) 37% were used in the production of activated biochars and purchased from Fisher Scientific (New Jersey, USA).

Cyclohexanecarboxylic acid (CHCA), dicyclohexylacetic acid (DCHA), 1-adamantanecarboxylic acid (ACA), and 5-phenylvaleric acid (PVA) purchased from Sigma Aldrich (Germany) were chosen as the surrogate compounds of NAs. Characteristics of NA compounds presented in Table 5.1. Solutions were prepared in 5 mM sodium bicarbonate ( $\text{NaHCO}_3$ , Fisher Scientific, New Jersey, USA) buffer (pH 8.5) to mimic pH of real OSPW.

Raw OSPW (Table 4.1) was collected from an oil sands tailing pond in Fort McMurray, Alberta, Canada and stored in a cold room at 4°C until use.



**Table 5.1:** Properties of model compounds of NAs.

Compound	CHCA	DCHA	ACA	PVA
Formula	C <sub>7</sub> H <sub>12</sub> O <sub>2</sub>	C <sub>14</sub> H <sub>24</sub> O <sub>2</sub>	C <sub>11</sub> H <sub>16</sub> O <sub>2</sub>	C <sub>11</sub> H <sub>14</sub> O <sub>2</sub>
Structure				
Molecular weight (g mol <sup>-1</sup> )	128.2	184.3	172.3	178.2
DBE <sup>1</sup>	2	3	4	5
-Z <sup>2</sup>	2	4	6	8
Solubility <sup>3,4</sup> (g L <sup>-1</sup> )	1000	79	234	779
pKa <sup>3</sup>	4.9	4.8	4.9	4.7
Log P <sup>3</sup>	1.6	4.5	2.6	3.0
Log D <sup>3,4</sup>	-1.35	1.40	-0.45	-0.12

<sup>1</sup>Double bond equivalency.

<sup>2</sup>Hydrogen deficiency.

<sup>3</sup>Data source: SciFinder Scholar, Calculated using Advanced Chemistry Development(ACD/Labs) Software V11.02 (© 1994–2022 ACD/Labs). Parameters determined at 25°C.

<sup>4</sup>Solubility (g L<sup>-1</sup>) and log D at pH 8.

### 5.2.2 Feedstock preparation

The sludge was received from a municipal wastewater treatment plant (Edmonton, Alberta, Canada) as a mixture of primary and secondary sludge collected from the anaerobic digester of biosolids. The peat-mineral mix was received from an oil and gas industry (Alberta, Canada) as a resulting material from the surface mining of oil sands (Alberta, Canada). Both feedstocks were dried completely and grinded using a ball milling process at 30 s<sup>-1</sup> frequency for 50 s operation time (MM400, Retsch, Germany) to obtain a homogeneous powder, and then stored in air-tight glass containers to be applied in the subsequent steps to produce the biochar.

### 5.2.3 Biochar synthesis

Pristine biochars (without chemical activation) were produced from sludge and peat at 800°C. Crucibles containing sludge or peat were carbonized at 800°C using a muffle furnace (Lindberg Blue M, Thermo Scientific™, USA) at the following conditions: 10°C min<sup>-1</sup> of heating rate, heating and cooling down under oxygen-free conditions achieved supplying 99% pure N<sub>2</sub> at 2 L min<sup>-1</sup>, and time at pyrolysis temperature of 2 h. Cool crucibles were taken out of the muffle furnace, and the sludge- and peat-based pristine biochars named SB-800 and PB-800, respectively, were stored in glass vials.

Activated biochars were produced using chemical activation agents FeCl<sub>3</sub> or a combination of ZnCl<sub>2</sub> and FeCl<sub>3</sub>. To obtain the activated biochars, 2 g of feedstock and 40 mL of the chemical activation agent solution (0.3 M FeCl<sub>3</sub> or 0.5 M ZnCl<sub>2</sub>+0.3 M FeCl<sub>3</sub>) were added to crucibles containing one magnetic stirring bar and placed in the stirrer platform at 400 rpm for 24 h. After 24 h, the crucibles were dried in the oven at 105°C for 24 h to ensure that all water has evaporated. Pyrolysis of crucibles were done in closed system using the muffle furnace at 800°C. Cool crucibles were taken out of the muffle furnace and the biochar was soaked in 20 mL 1 M HCl for 2 h. After acid soaking time, the contents of crucible were transferred to the vacuum filtration system equipped with hydrophilic polycarbonate membrane of 8.0 µm pore size (TETP04700, Isopore™, Millipore, Germany) to be washed several times using deionized water until the pH of the filtrate was between 6 and 8. Washed activated biochars were dried in the oven at 105°C for 24 h, followed by crushing using the mortar and pestle and storage in closed glass vials. Biochars were named as follows: SB-Fe (FeCl<sub>3</sub>-activated sludge-based biochar), SB-Fe/Zn (FeCl<sub>3</sub>/ZnCl<sub>2</sub>-activated sludge-based biochar), PB-Fe (FeCl<sub>3</sub>-activated peat-based biochar), and PB-Fe/Zn (FeCl<sub>3</sub>/ZnCl<sub>2</sub>-activated peat-based biochar).

#### 5.2.4 Characterization of feedstocks and biochars

The properties of the feedstocks and its respective pristine and activated biochars were evaluated by means of surface characteristics. Surface area and pore volume were evaluated by N<sub>2</sub> adsorption using a surface area analyzer (Autosorb-iQ, Quantachrome, USA) and the materials were outgassed at 120°C for 4 h prior to analysis. The surface area ( $S_{\text{BET}}$ ) and the total pore volume ( $V_{\text{TOT}}$ ) were calculated using the Brunauer–Emmett–Teller (BET) method (Brunauer et al., 1938), while the micropore surface area ( $S_{\text{MICRO}}$ ), mesopore surface area ( $S_{\text{MESO}}$ ), and the micropore volume ( $V_{\text{MICRO}}$ ) were calculated using the t-plot method (de Boer et al., 1966). The point of zero charge ( $\text{pH}_{\text{pzc}}$ ) of materials was determined based on the salt addition method (Jang et al., 2018). The moisture, volatile matter, ash, and fixed carbon contents were determined by weight loss using a thermogravimetric analyzer (Discovery TGA, TA Instruments, USA) equipped with platinum pan according to method presented by Crombie et al. (2013). The thermostability of materials between 105 and 900°C was evaluated using the thermogravimetric analyzer at heating rate of 20°C min<sup>-1</sup>. The ultimate analysis was performed using an elemental analyzer (2400 Series II CHNOS analyzer, PerkinElmer, USA), in which carbon (C), nitrogen (N), hydrogen (H), and sulphur (S) contents were determined, and the oxygen (O) content was estimated by difference ( $100 - \text{C}(\%) - \text{H}(\%) - \text{N}(\%) - \text{S}(\%) - \text{Ash}(\%)$ ) on a dry-mass basis. A Fourier transform infrared (FTIR) spectrometer (Nicolet™ 8700 FT-IR Spectrometer, Thermo Scientific, USA) was used to scan the surface of materials for functional groups between 600 and 4000 cm<sup>-1</sup> at 4 cm<sup>-1</sup> resolution. The crystallographic properties were evaluated by means of X-ray diffractometer (XRD, Ultima IV, Rigaku, Japan) at scanning rate of 3° min<sup>-1</sup> between 10 and 90° 2 $\theta$  angles using Cobalt tube at 38 kV and 38 mA.

### 5.2.5 Adsorption experiments

Pristine (SB-800 and PB-800) and activated biochars (SB-Fe, SB-Fe/Zn, PB-Fe, PB-Fe/Zn) were applied in single adsorption experiments at biochar dosage of  $2 \text{ g L}^{-1}$  and contact time of 24 h using four solutions of model compounds of NAs (Table 5.1) and raw OSPW. The objective is to evaluate the performance of activated biochars in controlled settings (surrogate compounds of NAs) and using a real process water.

30 mL of solution (model compound solution or raw OSPW) were added to flasks containing 0.06 g of biochar and the start time was recorded. The flasks were covered and agitated for 24 h in a platform shaker (New Brunswick™ Innova® 2100 platform shaker, Eppendorf Inc., USA) at agitation speed of 200 rpm and temperature of  $20^{\circ}\text{C}$ . After 24 h of contact time, the contents of the flasks were filtered using  $0.45 \mu\text{m}$  filters (Basix™ Nylon Syringe Filters, Fisher Scientific, USA) and samples were stored at  $4^{\circ}\text{C}$  until analysis. All experiments were performed in duplicates. The analytical methods for the measurement of the concentration of model compounds of NAs (CHCA, DCHA, ACA and PVA) and classical and oxidized NAs in OSPW are described in detail in the Supporting Information (Appendix).

### 5.2.6 Data analysis

The removal rate (Eq. 2.1) and the adsorption capacity (Eq. 2.2) were applied to evaluate any adsorption data. The Pearson correlation ( $r$ ) was applied to reveal the relationship between the properties of biochars and their adsorption capacity (Boskovic et al., 2020), and Microsoft Excel software was used to calculate the ( $r$ ) using the functions =PEARSON and =TDIST.

## 5.3 Results and discussion

### 5.3.1 $pH_{pzc}$ , surface area and pore volume of biochars from sludge and peat

The specific surface area and pore volume of the feedstocks (sludge and peat), pristine (SB-800 and PB-800), and activated biochars (SB-Fe, PB-Fe, SB-Fe/Zn, and PB-Fe/Zn) were determined based on the nitrogen adsorption, and the results are presented in Table 5.2. The pyrolysis of sludge and peat at 800°C was responsible to increase the surface area in approximately 187 times for SB-800 and 67 times for PB-800, in which 60-70% of the surface area was respective of mesopores. Since the biochars were produced using the same conditions, the difference observed in the porous properties is due to the different characteristics observed for their respective feedstock. The impressive increase in the surface area in the pristine biochars can be associated with the pyrolysis temperature that led to the decomposition of the carbon matrix and release of volatile matter, resulting in the pore formation (Wang et al., 2020; Wang et al., 2022). The biochars produced using chemical activation further helped in the improvement of surface area and pore volume of biochars. It was not noticed great difference between SB-Fe and SB-Fe/Zn surface areas. In fact, the surface area of SB-Fe/Zn increased only 1.4 times in comparison with SB-800. However, the addition of  $ZnCl_2$  to the chemical activation solution resulted in sludge and peat-based biochars composed of only mesopores, indicating that the association of  $FeCl_3$  and  $ZnCl_2$  allowed superior degradation of feedstock and development of pores (Feng et al., 2020), but without transformation of mesopores into micropores, which might be desirable for large organic molecules such as NAs. PB-Fe/Zn had the highest surface area ( $1070.2 \text{ m}^2 \text{ g}^{-1}$ ) observed in this study, and the surface area was 5.5 times higher than PB. However, PB-Fe had almost half of the surface area and pore volume of PB-Fe/Zn. The differences observed for the sludge- and peat-based biochars indicate that the nature of the feedstock plays also play a crucial role in the biochar

quality, even though the use of  $\text{FeCl}_3$  and  $\text{ZnCl}_2$  as chemical activation agents is important to enlarge the pores due to the metal impregnation in the pores (Wang et al., 2017b). The differences in feedstocks that most likely affected the porous properties will be further enlightened in the next sections.

According to the International Union of Pure and Applied Chemistry classification for nitrogen adsorption-desorption isotherm (IUPAC, 1982), the curve of the nitrogen adsorption-desorption isotherm for the biochars (Figure 5.1) provided isotherms consistent with the type IV adsorption isotherm, in which the isotherm is characteristic of mesoporous adsorbents, and also a type H4 hysteresis curve, indicating narrow slit-like pores in the adsorbent material. Those isotherm characteristics were also observed for biochars from biogas residue of pig manure (Xia et al., 2016) and corn straw (Feng et al., 2020).

The  $\text{pH}_{\text{pzc}}$  for the pristine biochars were higher than their respective activated biochar, that is because the presence negative functional groups on the surface of biochar can decrease the  $\text{pH}_{\text{pzc}}$  (Chen et al., 2008). Therefore, the activation with  $\text{FeCl}_3$  or  $\text{FeCl}_3$  and  $\text{ZnCl}_2$  combined helped the retention of some functional groups that would otherwise be released in the thermal degradation of feedstock. Among the biochars studied, the only biochar that presented  $\text{pH}_{\text{pzc}}$  higher than a typical pH of OSPW (pH~8.5) was PB-800, indicating that the PB-800 will have a positive charge in OSPW (Peng et al., 2016). That might benefit the electrostatic attraction in the adsorption of NAs in the OSPW as they are mostly in the deprotonated form (Huang et al., 2017). However, the negatively charged biochars could be neutralized due to metal ions present in the raw OSPW, reducing the repulsion due to similar charged biochars and NAs (Pourrezaei et al., 2014).

**Table 5.2:** Surface properties of the feedstocks and their respective biochars.

<b>Material</b>	<b>pH<sub>pzc</sub></b>	<b>Surface area (m<sup>2</sup> g<sup>-1</sup>)</b>			<b>Pore volume (cm<sup>3</sup> g<sup>-1</sup>)</b>		
		<b>S<sub>TOT</sub></b>	<b>S<sub>MESO</sub></b>	<b>S<sub>MICRO</sub></b>	<b>V<sub>TOT</sub></b>	<b>V<sub>MESO</sub></b>	<b>V<sub>MICRO</sub></b>
<b>Sludge</b>	–	1.4	1.4	–	0.02	0.02	–
<b>SB-800</b>	6.33	261.7	155.6	106.2	0.18	0.12	0.06
<b>SB-Fe</b>	3.99	350.2	330.7	19.4	0.38	0.36	0.02
<b>SB-Fe/Zn</b>	4.15	375.9	375.9	–	0.48	0.48	–
<b>Peat</b>	–	2.9	2.9	–	0.01	0.01	–
<b>PB-800</b>	10.98	193.7	132.5	61.2	0.14	0.08	0.05
<b>PB-Fe</b>	3.94	643.0	466.5	176.5	0.42	0.33	0.09
<b>PB-Fe/Zn</b>	5.48	1070.2	1070.2	–	0.79	0.79	–

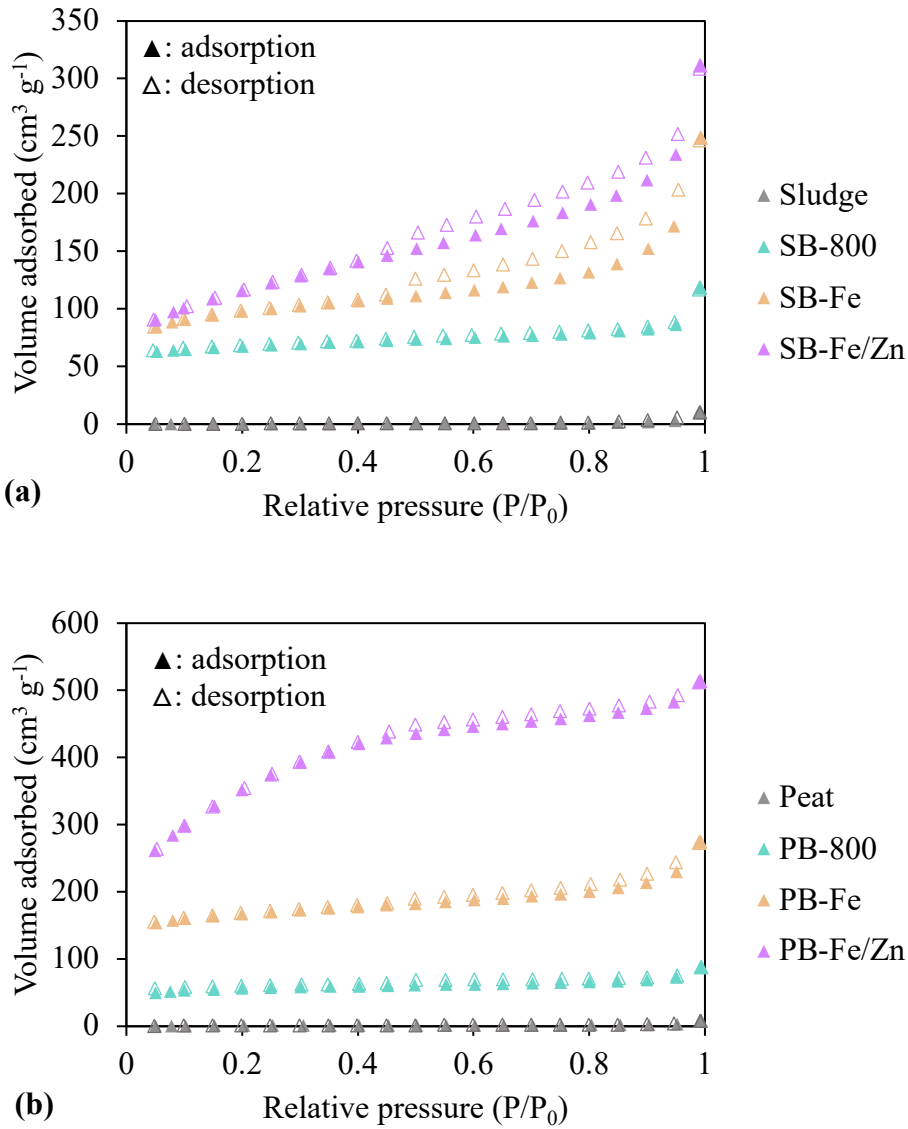


**Figure 5.1:** Nitrogen adsorption and desorption isotherms of **(a)** sludge and **(b)** peat, and their respective pristine and activated biochars.

### 5.3.2 Proximate analysis and elemental content of biochars from sludge and peat

The results of proximate analysis of feedstocks and biochars are presented in Table 5.3. The volatile matter of sludge and peat was similar, whereas the fixed carbon and ash contents were



crucial to differentiate the materials. Sludge has higher ash content, which is associated with high inorganic residue respective of minerals (Yusuff et al., 2022). The ash content tends to increase after carbonization due to the loss of volatile matter (Zielińska et al., 2015). However, SB-Fe and SB-Fe/Zn had almost double the ash content in comparison with PB-Fe and PB-Fe/Zn biochars. The presence of ash can cause the blockage of biochar pores, resulting in lower surface area and pore volume (Lu et al., 1995). This corroborates with the findings presented in Table 5.2, in which the  $\text{FeCl}_3$  and combination of  $\text{FeCl}_3$  and  $\text{ZnCl}_2$  as activation agents provided the biochars from sludge and peat unique characteristics, in which peat-based activated biochars had much higher values of  $S_{\text{BET}}$  and  $V_{\text{TOT}}$ . The carbonization of sludge and peat resulted and pristine and chemically-activated biochars with similar volatile matter content, considering that the carbonization process purges the volatile compounds from the surface, but different fixed carbon content was observed. The fixed carbon content increased after carbonization for peat-based biochars, indicating that biochar has more stable carbon (Yang et al., 2020), while it was noticed a decrease for the sludge-based biochars. This is usual for feedstocks with high ash content, such as sludge (Enders et al., 2012).

The elemental content of the sludge- and peat-based biochars were determined by ultimate analysis (Table 5.3), and they can be translated into the atomic ratios H/C, O/C, and (N+O)/C. H/C and O/C are inversely proportional to the degree of aromaticity and hydrophobicity of biochar, respectively, and (N+O)/C is proportional to the biochar polarity (Chen et al., 2016; Nzediegwu et al., 2022). The chemical activation of both sludge and peat in the biochar synthesis resulted in the increase of H/C ratio, leading to the decrease in biochar aromaticity. Nonetheless, comparing the  $\text{FeCl}_3$  and  $\text{FeCl}_3/\text{ZnCl}_2$  activations, the addition of  $\text{ZnCl}_2$  to the chemical activation solution allowed the increase of O/C and (N+O)/C ratios of peat-based biochars. On the other hand, the

chemical activations were responsible to further decrease the O/C ratio of sludge-based biochars, implying that the sludge-based biochars are more hydrophobic than peat-based biochars. That difference in the O/C ratio for sludge-based biochar might be due to the high temperature used. Maintaining elevated aromaticity of biochar and hydrophobicity that might benefit the adsorption of NAs.

The O/C ratio can indicate the stability of biochar in the environment over time. As the O/C ratio of biochars were lower than 0.2 – except for PB-Fe, it is estimated that the half-life of biochars will be greater than 1000 years (Spokas, 2010). For PB-Fe, the half-life would be between 100 and 1000 years. Therefore, these biochars have potential to be applied not only as adsorbents, but as carbon sequestration materials.

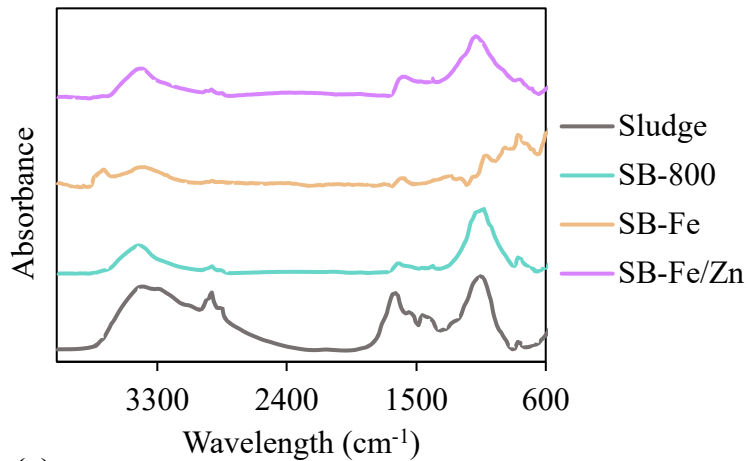
Even though the activation resulted in the same trend for both sludge- and peat-based biochars, the ratios differ greatly from sludge- and peat-based biochars produced at same conditions, yielding distinct properties that might affect the adsorption of NAs. As the pyrolysis temperature for biochar synthesis was considered high, it was expected a biochar with more hydrophobicity of biochar often associated with such temperatures (Abdoul Magid et al., 2021). That was observed for sludge-based biochars, but not for the activated peat-based biochars, which presented much higher O/C ratio. That resulted in biochars with different characteristics. Activated sludge-based biochars are more hydrophobic than activated peat-based biochars, and that will impact in the adsorption of NAs.

**Table 5.3:** Proximate, elemental composition, and atomic ratio properties of sludge and peat as feedstocks and their respective biochars.

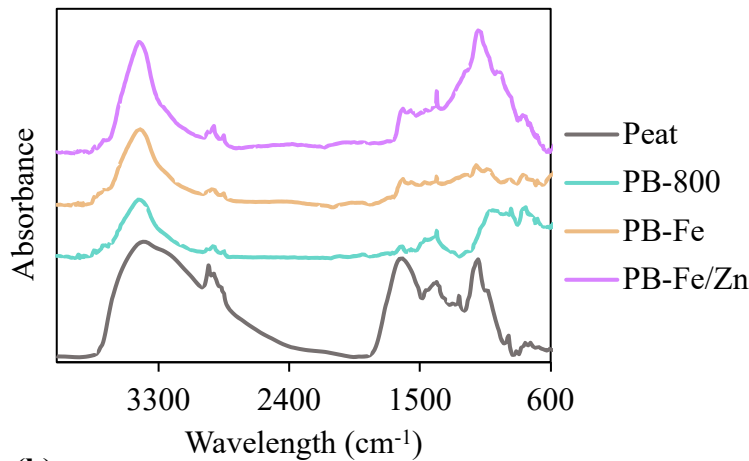
<b>Material</b>	<b>Proximate analysis (%)</b>				<b>Elemental composition (%)</b>					<b>Atomic ratio</b>		
	<b>Moisture</b>	<b>Volatile matter</b>	<b>Ash</b>	<b>Fixed carbon</b>	<b>C</b>	<b>H</b>	<b>N</b>	<b>O</b>	<b>S</b>	<b>H/C</b>	<b>O/C</b>	<b>(N+O)/C</b>
<b>Sludge</b>	3.4	53.3	35.6	7.7	32.9	4.9	5.3	20.7	0.6	1.78	0.47	0.61
<b>SB-800</b>	3.0	6.2	66.8	24.1	26.1	0.4	2.5	4.2	0.0	0.20	0.12	0.20
<b>SB-Fe</b>	9.7	12.4	71.9	6.0	24.1	1.3	1.6	1.1	0.0	0.64	0.03	0.09
<b>SB-Fe/Zn</b>	7.1	12.9	73.3	6.6	23.8	0.9	1.6	0.5	0.0	0.45	0.02	0.07
<b>Peat</b>	12.9	50.8	24.0	12.2	38.5	4.7	2.0	30.7	0.0	1.48	0.60	0.64
<b>PB-800</b>	4.7	13.8	42.9	38.7	52.5	0.9	0.8	3.0	0.0	0.21	0.04	0.05
<b>PB-Fe</b>	4.5	13.9	24.7	56.9	53.1	2.1	2.0	18.1	0.0	0.47	0.26	0.29
<b>PB-Fe/Zn</b>	9.7	12.4	27.3	50.6	56.0	1.9	2.3	12.5	0.0	0.40	0.17	0.20

### 5.3.3 Functional surface groups and crystallinity of biochars from sludge and peat

The differences and similarities between the surface functional groups of feedstocks and their resulting biochars are highlighted by the FTIR spectra (Figure 5.2). Peat and sludge have similar peaks respective of –OH stretching (around 3400 and 1050  $\text{cm}^{-1}$ ) and C=C stretching (around 1600  $\text{cm}^{-1}$ ) (Deng et al., 2022; Nzediegwu et al., 2021b). After carbonization, there was a significant decrease in the peaks, especially for the pristine biochars, indicating that the thermal degradation was responsible for the release of some functional groups, as evidenced by the elemental analysis (Table 5.3). Once  $\text{FeCl}_3$  was used as chemical activation agent, an enhancement of some peaks of  $\text{FeCl}_3$ -activated biochar was observed in comparison with its respective pristine biochar. Such peaks were –OH stretching group (around 3400  $\text{cm}^{-1}$  for PB-Fe and 3400 and 3600  $\text{cm}^{-1}$  for SB-Fe) and C=C of aromatic rings (around 1600  $\text{cm}^{-1}$ ). On the other hand, abundance of oxygen-containing surface groups was observed when a combination of  $\text{ZnCl}_2$  and  $\text{FeCl}_3$  were applied as activation agents of biochar. The peaks around 3400 and 1100  $\text{cm}^{-1}$  for both SB-Fe/Zn and PB-Fe/Zn had increased intensity. Additionally, the peak respective to C=C (1600  $\text{cm}^{-1}$ ) was also improved in comparison with pristine and  $\text{FeCl}_3$ -activated biochars.  $\text{ZnCl}_2$  is a pore-forming agent that can help retaining the oxygen-containing groups of feedstocks, while the  $\text{FeCl}_3$  helps in the formation of C=C due to the decomposition of hemicelluloses and celluloses into smaller hydrocarbons (Cheng et al., 2020a; Wang et al., 2021). The presence of –OH and C=C groups are beneficial for the adsorption of naphthenic acids through hydrogen bonding and  $\pi$ - $\pi$  interactions.



(a)



(b)

**Figure 5.2:** FTIR spectra of (a) sludge and (b) peat, and their respective pristine and activated biochars.

The XRD spectra were collected to identify the mineralogical phases presented in feedstocks and biochars. The sludge-based biochars (Figure 5.3a) had more mineral fractions than peat-based biochars (Figure 5.3b), which was expected considering the high ash content of sludge-based biochars (Table 5.3), characterizing the high inorganic residue due to minerals (Yusuff et al., 2022). Quartz (peak at  $2\theta$  of  $24.3^\circ$  and  $31.0^\circ$ ) was presented for the SB-800, SB-Fe, and SB-

Fe/Zn biochars, while barringerite (peak at  $2\theta$  47.1°, 51.8° and 55.5°) and schreibersite (peak at  $2\theta$  48.0° and 53.7°) were observed for SB-Fe and SB-Fe/Zn biochars. Barringerite and schreibersite are Fe-containing minerals that were formed due to the  $\text{FeCl}_3$  impregnation. The only peaks observed for peat-based biochars were quartz (peak at  $2\theta$  of 24.2° and 31.0°). It was noticed that the minerals formed in the biochars were not water-soluble minerals. Since the biochars were acid washed, the water-soluble minerals were most likely dissolved in the washing step, reducing the risk of leaching of metals from the biochars after production.

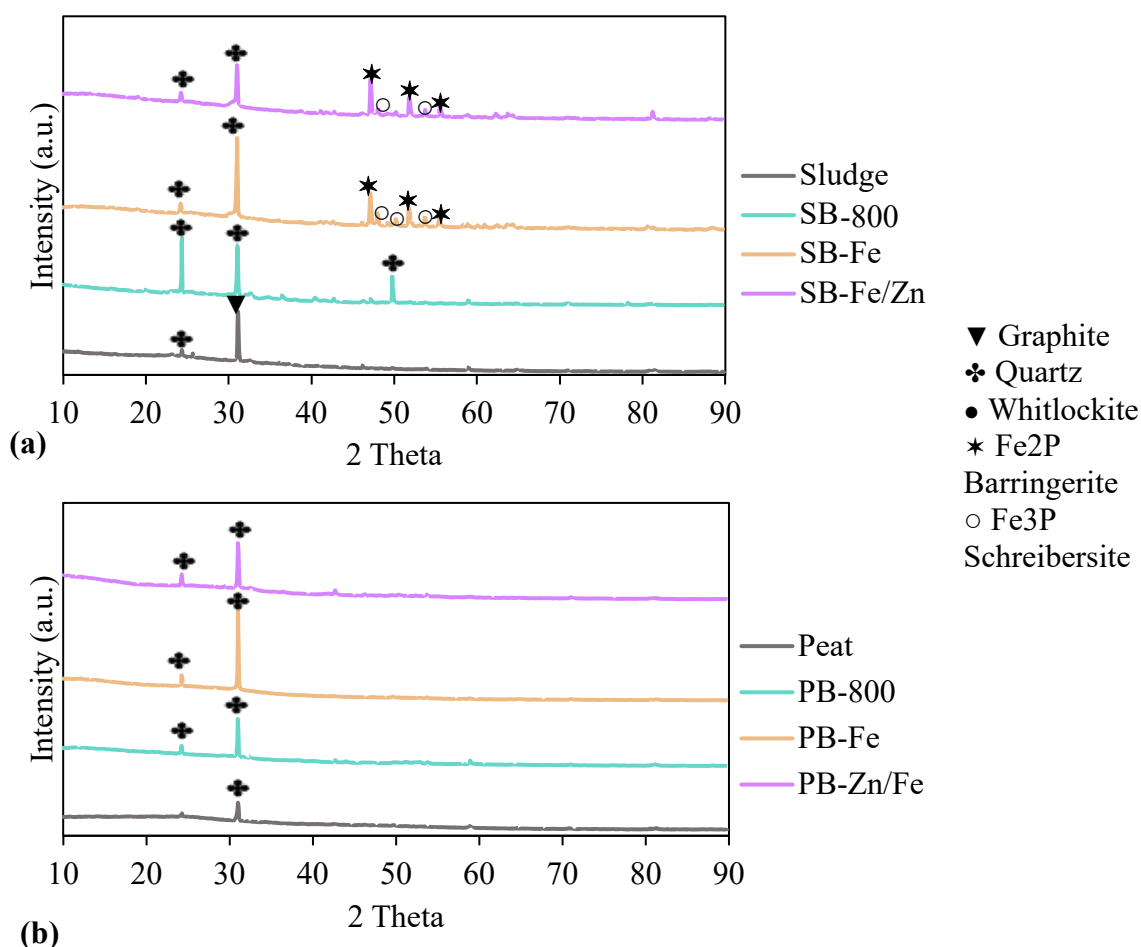
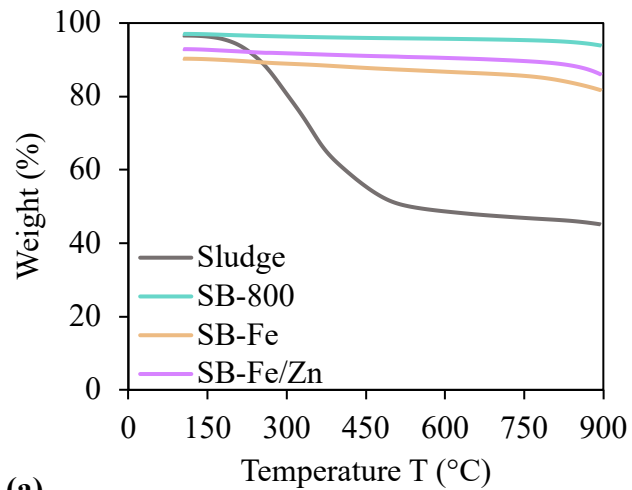


**Figure 5.3:** XRD diffractograms of (a) sludge and (b) peat, followed by their respective pristine and activated biochars.

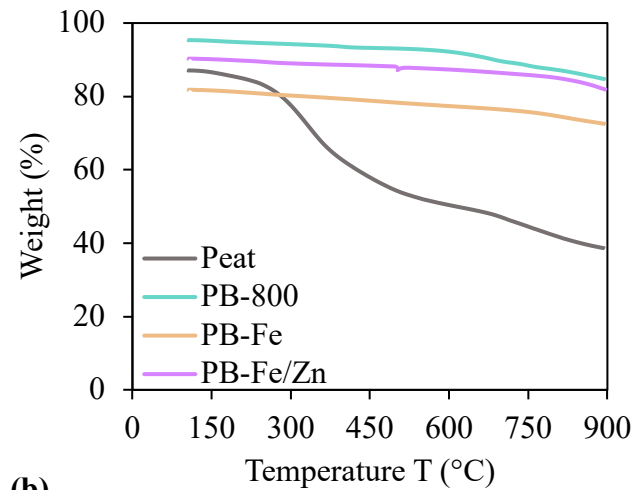
#### 5.3.4 Thermostability of biochars from sludge and peat

The thermostability of feedstocks and biochars was evaluated and the results (Figure 5.4a,b) indicated that the biochars were more thermostable than their respective feedstock. The weight loss was in the order of pristine biochar < Fe/Zn biochar < Fe biochar < feedstock. The peat and peat-based biochars had higher weight loss than sludge and sludge-based biochars caused by the lower ash content of the former (Xu & Chen, 2013).

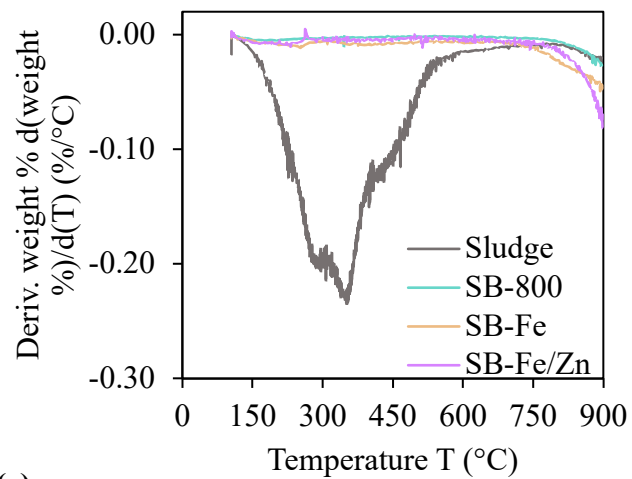
The DTG curves are valuable to assess the different thermal degradation pathways of the feedstocks (Nzediegwu et al., 2021b). The DTG curve of sludge (Figure 5.4c) and peat (Figure 5.4d) showed major degradation step between 250 and 600°C, indicating the degradation of volatile and organic compounds (Jerez et al., 2021; Xia et al., 2016), and contents of hemicellulose, cellulose, and lignin (Nzediegwu et al., 2021a). The biochars did not present such degradation steps because the compounds were successfully degraded in the carbonization process. Two smaller degradation steps around 700 and 750°C were observed in peat and its pristine biochar and it is associated with the decomposition of inorganic compounds (i.e. carbonates) (Liu et al., 2009). These degradation steps were not noticed for the activated biochars, indicating that the chemical activation played a role in the degradation of these compounds.



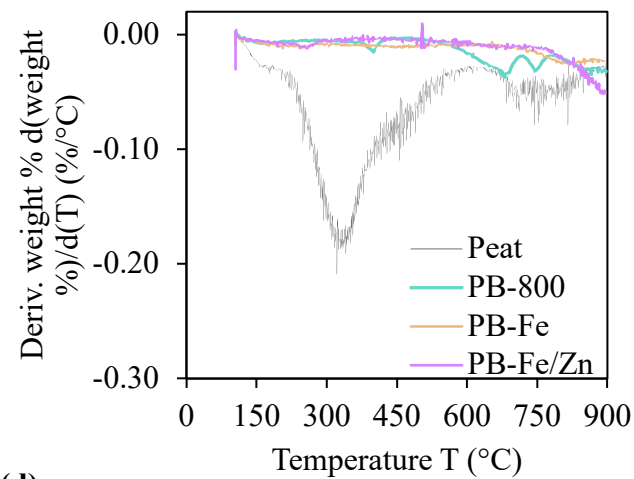
(a)



(b)



(c)



(d)

**Figure 5.4:** (a,b) Thermogravimetric (TGA) and (c,d) first derivative of thermogravimetric (DTG) curves of sludge and peat, and their respective biochars.



### 5.3.5 Adsorption performance of surrogate compounds of NAs on biochars from sludge and peat

The pristine and activated biochars produced from sludge and peat were applied in the adsorption of surrogate compounds of NAs to assess their performance in adsorbing NAs. Four different model compounds were studied in single-compound solution based on their different characteristics (Table 5.1), and the results are presented in terms of the final concentration after adsorption (Figure 5.5a) and adsorption capacity (Figure 5.5b).

Overall, the removal of surrogate compounds of NAs by activated biochars was better than the removal obtained by their respective pristine biochars. SB-800 did not adsorb any compound, except for DHCA (7% removal). PB-800 removed 42 and 44% of DCHA and PVA, respectively. Even though PB-800 performed well for these two compounds, the adsorption of CHCA and ACA was not effective, which might be related to the biochar characteristics. The chemical activation agents were applied to improve biochar characteristics and selectivity for NAs. Activated biochars performed better than pristine biochars. The adsorption of DCHA and PVA reached removal rates near 100% for activated biochars using sludge and peat. Among the four studied model compounds, CHCA and ACA were the most difficult to adsorb. Even though the adsorption of CHCA and ACA were greatly improved by using chemical activation agents, the activated biochar from peat performed better than sludge-based biochar. Based on the properties of the model compounds, the lipophilicity ( $\log D$ ) of model compounds at pH 8 (Table 5.1) indicated that CHCA and ACA are the first and the second most hydrophobic compounds in the list (Zhu et al., 2018). Therefore, the nature of peat-based biochars with lower H/C ratio than sludge-based biochars most likely affected the adsorption.

Nonetheless, the composition of real OSPW includes a wide range of NAs (Huang et al., 2018) that is not limited by the four model compounds studied. In fact, the classical NAs in OSPW usually have carbon numbers in the range from 11 to 20 and DBE numbers from 1 to 10, as presented previously. Therefore, it is imperative to evaluate the performance of biochars against real OSPW to determine the feasibility of biochar as adsorbents.

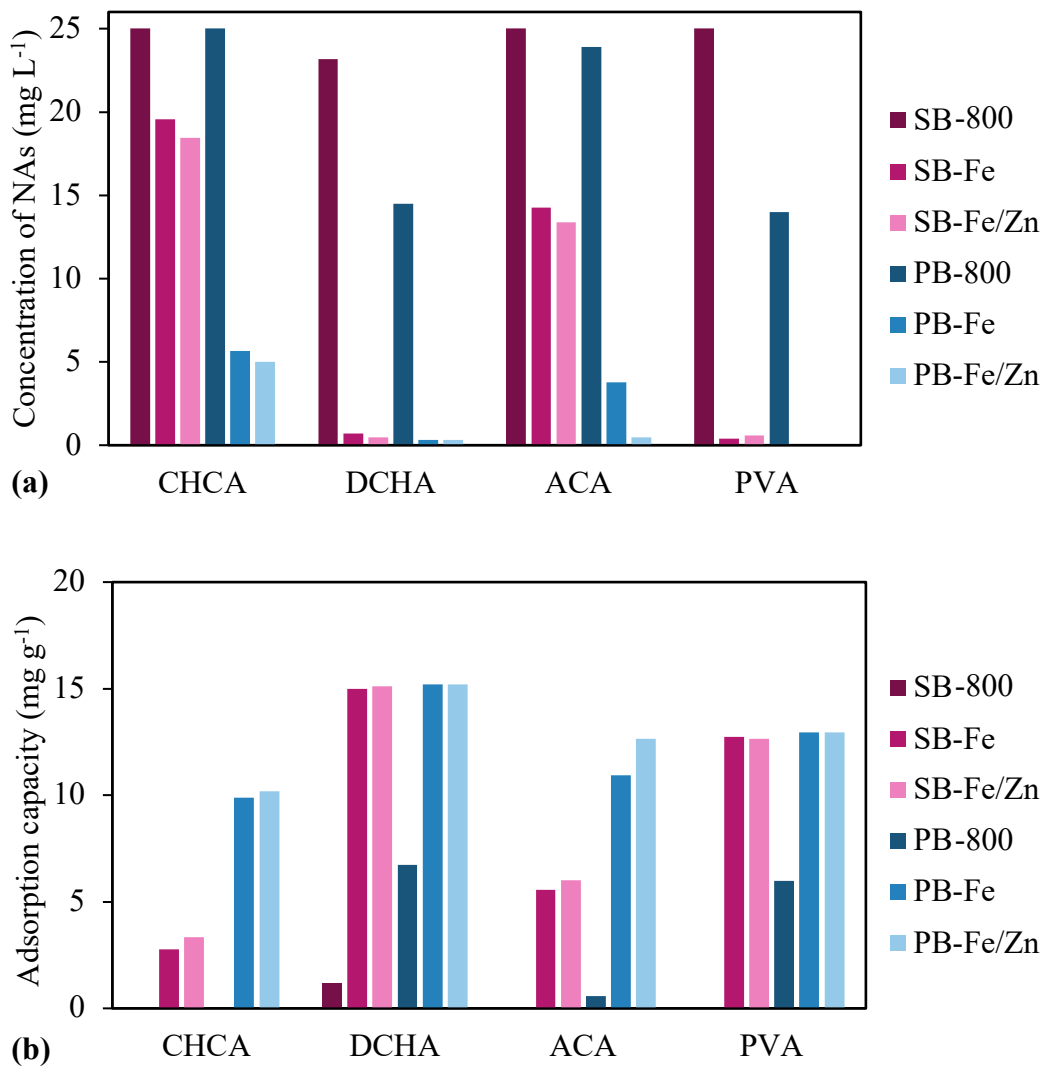


**Figure 5.5:** (a) Final concentration of model compound and (b) adsorption capacity of model compounds obtained for the adsorption using pristine and activated biochars from sludge and peat. Adsorption conditions: 2 g L<sup>-1</sup> biochar dosage; 24 h of contact time; 25 mg L<sup>-1</sup> initial concentration of NA.

### 5.3.6 Adsorption performance of NAs from raw OSPW on biochars from sludge and peat: Competitive adsorption in real process water

The biochars were further evaluated as adsorbents of NAs from real OSPW. The NAs in the OSPW are classified based on their oxygen number ( $O_x$ -NAs), in which  $x = 2$  is respective of classical NAs and  $3 \leq x \leq 6$  is respective of oxidized NAs (Huang et al., 2015a; Meshref et al., 2017). The raw OSPW used in this study had total concentration of NAs of  $61.8 \text{ mg L}^{-1}$  (Table 4.1) and the results of adsorption of NAs from raw OSPW on biochars are presented in Figure 5.6.

The highest concentration of NAs in the raw OSPW was  $40.4 \text{ mg L}^{-1}$  for classical NAs and the concentration decreased as the oxygen number increased. The pristine biochars SB-800 and PB-800 removed 12 and 27% of classical NAs and 13 and 23% of total NAs from raw OSPW, respectively. As indicated by the study using the model compounds, the PB-800 performs better than SB-800 because of some important differences between the two feedstocks, such as O/C and H/C ratios. On the other hand, the biochars produced through chemical activation accomplished very good removal rates, in which the activation agents ( $\text{FeCl}_3$  or combination of  $\text{FeCl}_3$  and  $\text{ZnCl}_2$ ) provided similar removal rates regardless of the feedstock. That supports the importance of evaluating adsorption of NAs from real OSPW instead of focusing on surrogate compounds, as the study using such compounds might not be accurate in the assessment of new adsorbents. The best adsorption capacities were achieved by SB-Fe/Zn and PB-Fe/Zn, in which the removal surpassed 90% for all NAs (classical and oxidized NAs).

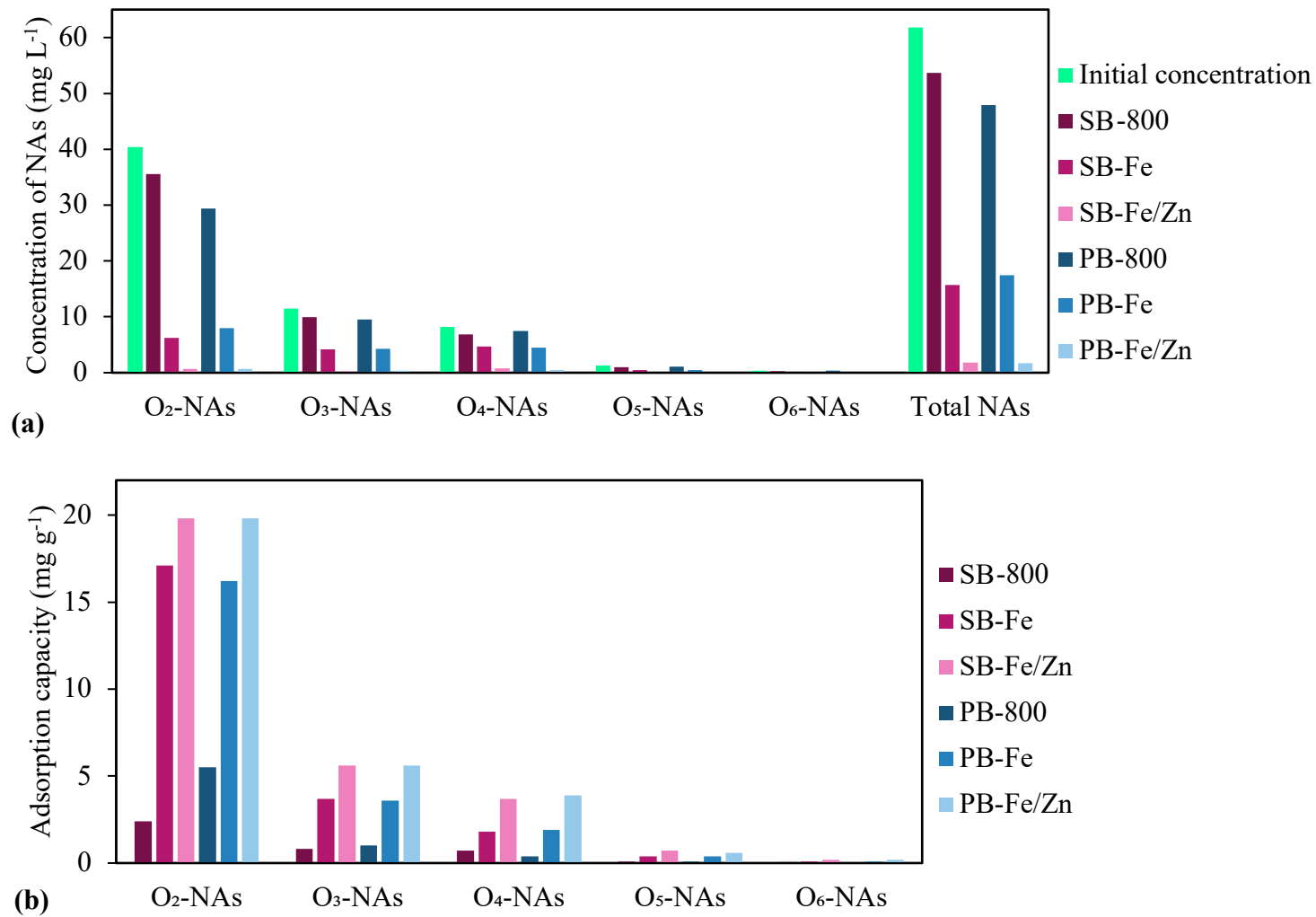
Based on the concentration profile of classical NAs as a function of carbon (Figure 5.7) and DBE (Figure 5.8) numbers in raw OSPW and OSPW treated with biochars from sludge and peat, the classical NAs in the raw OSPW profile were in the range of carbon number 9–20 and DBE number 1–10. The range of carbon numbers 12–19 represented 93% of all classical NAs, in

which carbon number 14 represented 17.9% of classical NAs in OSPW with concentration of 7.2 mg L<sup>-1</sup>. The highest concentrations in terms of DBE numbers were given by DBEs 3, 4, and 7 representing 35, 21, and 11% of NAs, respectively. Therefore, most classical NAs in this raw OSPW were bicyclic, tricyclic, and hexacyclic (Benally et al., 2019).

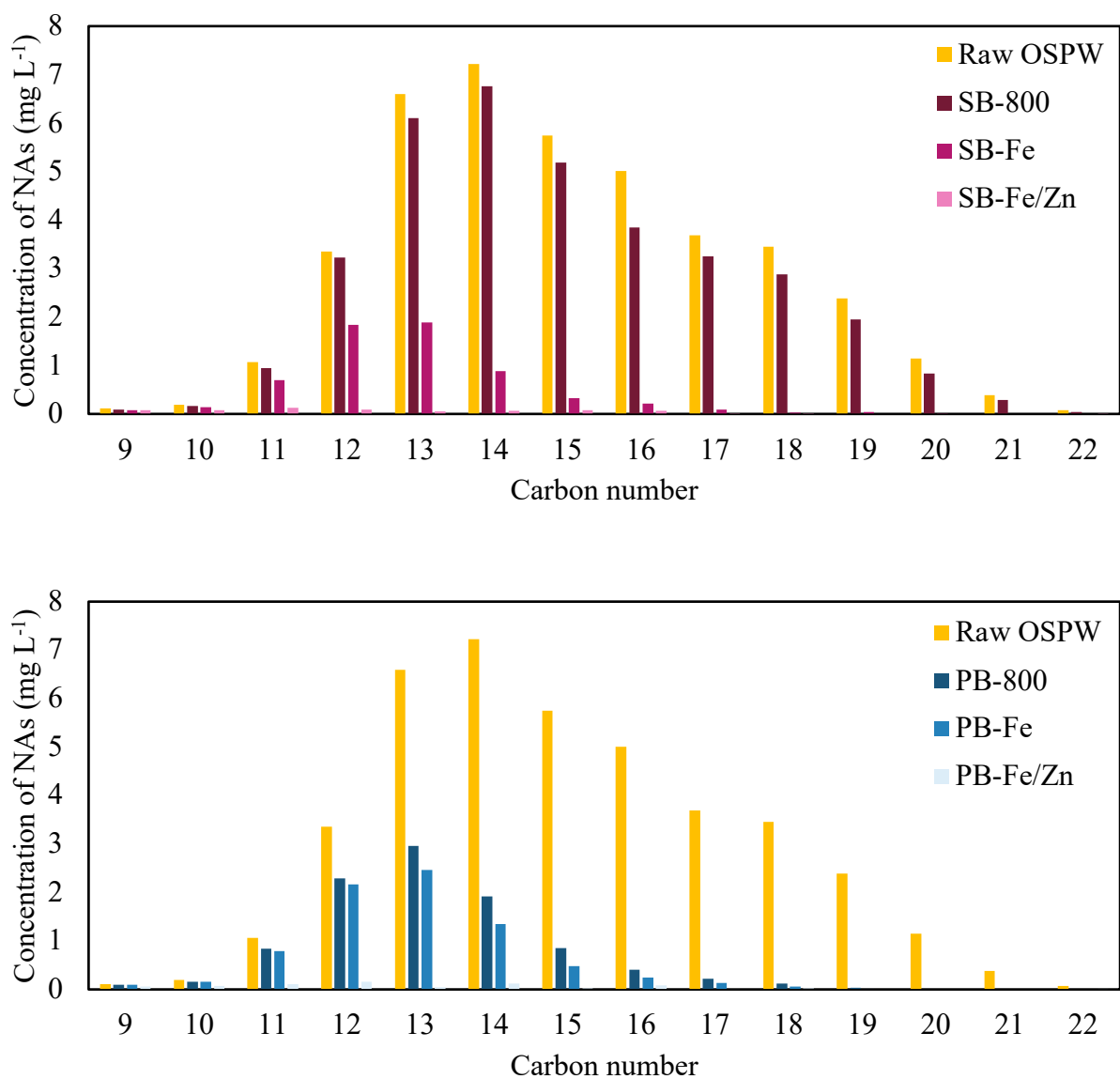
The adsorption capacity obtained for each carbon and DBE numbers is presented in Figure S8 (Appendix). In terms of the removal of classical NAs by the biochars, it was noticed that the adsorption capacity was slightly proportional to the initial concentration of NAs. To determine the role of initial concentration in the adsorption capacity, the adsorption capacity was compared between similar initial concentration, such as carbon numbers 13, 15, and 17 (3.4–3.7 mg L<sup>-1</sup>) and carbon numbers 11 and 20 (1.1 mg L<sup>-1</sup>). It was observed that the adsorption capacities of carbon numbers 11 and 13 were about 50% lower than the adsorption capacity determined for the carbon numbers with similar concentrations for the FeCl<sub>3</sub>-activated biochars, indicating that SB-Fe and PB-Fe might have more affinity with NAs with higher carbon number. However, when ZnCl<sub>2</sub> was added to the chemical activation agent to create SB-Fe/Zn and PB-Fe/Zn, that discrepancy between adsorption capacities for carbon numbers with similar initial concentrations was nullified. Therefore, among the biochars studied, the SB-Fe/Zn and PB-Fe/Zn were the best biochars in providing removal of a wider range of NAs.

Table 5.4 presents the previously reported adsorbents for the adsorption of NAs from OSPW. Pristine biochar produced from wheat straw at 600°C was applied in the adsorption of organics from OSPW and the adsorption capacity 0.56 mg g<sup>-1</sup>. On the other hand, pristine biochars from sludge and peat produced at 600°C achieved 6- and 11-times higher adsorption capacity. In comparison with other adsorbents, the activated biochars in this study accomplished higher adsorption capacity except for granular activated carbon, which was a commercial adsorbent.

Therefore, the biochars produced through chemical activation have potential to assist in the treatment NAs from OSPW.



**Figure 5.6:** (a) Final concentration and (b) adsorption capacity of NAs from OSPW on pristine and activated biochars. Adsorption conditions: 2 g L<sup>-1</sup> biochar dosage; 24 h of contact time; raw OSPW.



**Figure 5.7:** Concentration of classical NAs in terms of carbon number in raw OSPW and OSPW treated with biochars from (a) sludge and (b) peat. Adsorption conditions: 2 g L<sup>-1</sup> biochar dosage; 24 h of contact time; raw OSPW; total classical NAs in the raw OSPW: 40.4 mg L<sup>-1</sup>.



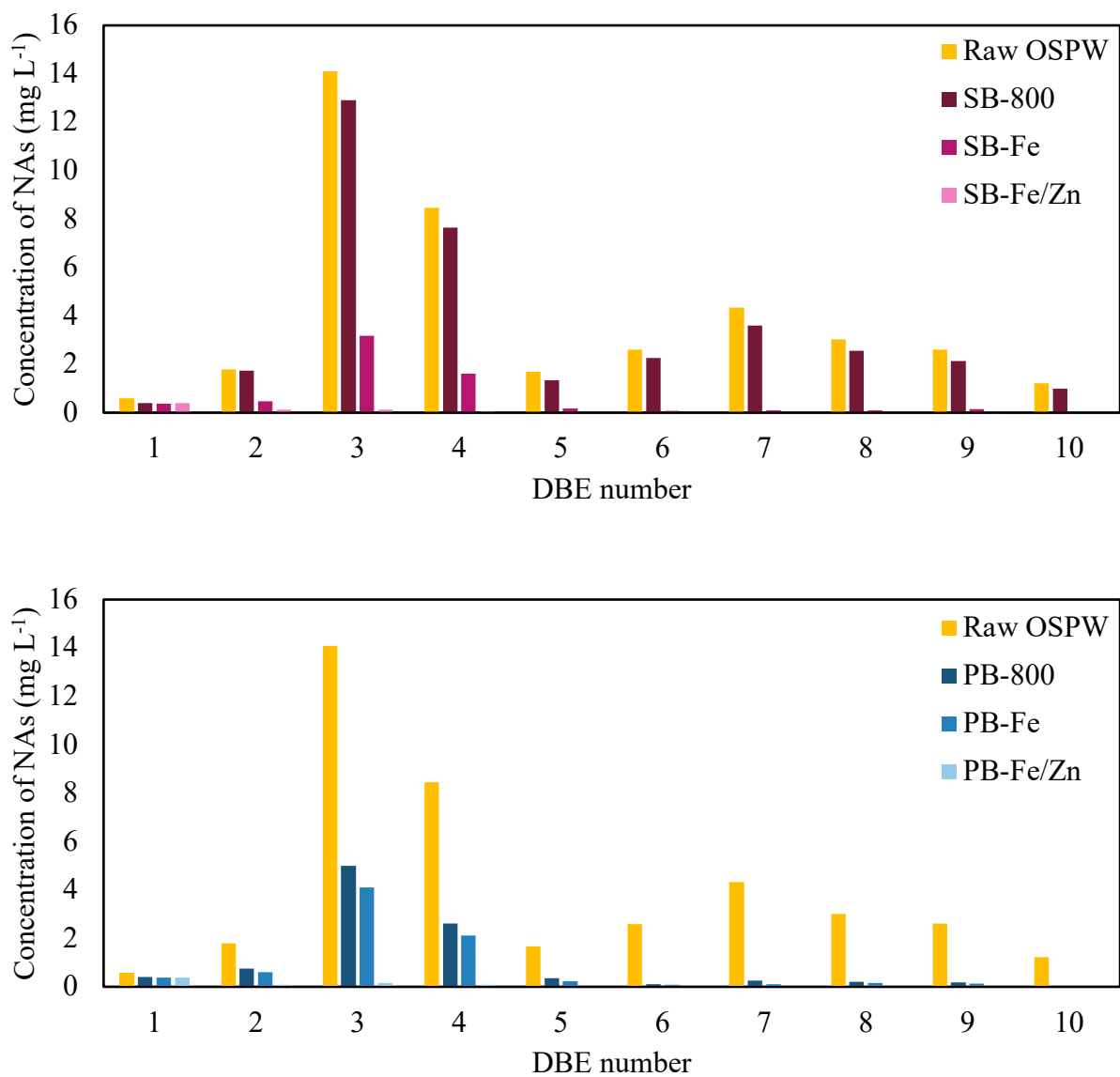


**Figure 5.8:** Concentration of classical NAs in terms of DBE number in raw OSPW and OSPW treated with biochars from (a) sludge and (b) peat. Adsorption conditions: 2 g L<sup>-1</sup> biochar dosage; 24 h of contact time; raw OSPW; total classical NAs in the raw OSPW: 40.4 mg L<sup>-1</sup>.

**Table 5.4:** Adsorption conditions and capacity for removal of naphthenic acids by different types of adsorbents.

Adsorbent	Source of NAs	Adsorption conditions	$q_t$ (mg g <sup>-1</sup> )	Reference
Granular activated carbon	Raw OSPW	Dosage: 0.4 g L <sup>-1</sup>	60	(Islam et al., 2018)
	Ozonated OSPW	Contact time: 24 h	37	
Biochar	Acid-extractable organics from OSPW	Dosage: 20 g L <sup>-1</sup> Contact time: 24 h	0.59	(Bhuiyan et al., 2017)
Biopolymer	OSPW	Dosage: 10 g L <sup>-1</sup> C <sub>i</sub> : 20.3 – 101.8 mg L <sup>-1</sup> Contact time: 24 h	–	(Arshad et al., 2016)
Carbon xerogel	Classical NAs from OSPW	Dosage: 3 g L <sup>-1</sup> C <sub>i</sub> : 26.3 mg L <sup>-1</sup> Contact time: 24 h	7.8	(Benally et al., 2019)
Petroleum coke	OSPW	Dosage: 200 g L <sup>-1</sup> C <sub>i</sub> : 60.3 mg L <sup>-1</sup> Contact time: 16 h	1	(Pourrezaei et al., 2014)
SB-800	OSPW	Dosage: 2 g L <sup>-1</sup>	4.0	<b>This study</b>
SB-Fe		C <sub>i</sub> : 61.8 mg L <sup>-1</sup>	23.1	
SB-Fe/Zn		Contact time: 24 h	30.0	
PB-800			7.0	
PB-Fe			22.2	
PB-Fe/Zn			30.1	

### 5.3.7 Effect of biochar properties on adsorption of NAs

According to the results presented previously, the adsorption of NAs on biochars is affected depending on the biochar properties, in which H/C ratio was suggested as one of the properties

that played a role in the differences observed in the removal of NAs. To further evaluate the relationship between the uptake of NAs and biochar properties, the Pearson correlation was applied to determine the correlation coefficient ( $r$ ) between the properties of the biochars and the adsorption capacities for surrogate compounds of NAs and NAs from OSPW. The Pearson correlation coefficients are presented in Table 5.5. It was confirmed that there is a positive correlation between the H/C ratio and the adsorption capacity of DCHA and PVA ( $r = 0.83\text{--}0.84$ ,  $p\text{-value} < 0.05$ ). As the H/C ratio increases, the aromaticity of biochar decreases (Nzediegwu et al., 2022). On the other hand, the adsorption of CHCA provided a positive correlation with H and O contents ( $r = 0.85\text{--}0.93$ ,  $p\text{-value} < 0.05$ ). Additionally, the total surface area, mesopore surface area, total pore volume, and mesopore volume provided a positive correlation with the adsorption capacities of CHCA and ACA ( $r = 0.82\text{--}0.91$ ,  $p\text{-value} < 0.05$ ). These findings suggest that the adsorption of NAs will not be dependent of a singular biochar property. To aim at the adsorption of a wide range of NAs from OSPW, such biochar should present a combination of properties. That is supported by the correlations obtained for classical NAs and total NAs in the OSPW. Based on the Pearson correlation, the total pore volume, the mesopore volume, and the H/C ratio had a positive correlation with the adsorption capacities of NAs in OSPW ( $r = 0.81\text{--}0.88$ ,  $p\text{ value} < 0.05$ ). Therefore, the importance of mesopores in the biochar is highlighted. Biochars with higher mesopore volume adsorbed more NAs, and that might be due to the pore filling. The high porosity of biochar supports the transport of NAs in the biochars, allowing fast adsorption associated with pore filling mechanism (Cheng et al., 2021; Regkouzas & Diamadopoulos, 2019).

**Table 5.5:** Pearson correlation coefficient between adsorption capacity ( $q_t$  values) obtained from the adsorption of model compounds of NAs and NAs in raw OSPW and physicochemical properties of pristine and activated biochars from sludge and peat.

Parameters	CHCA	DCHA	ACA	PVA	Classical NAs	Total NAs
$\text{pH}_{\text{pzc}}$	-0.52	-0.63	-0.60	-0.59	-0.70	-0.69
$S_{\text{BET}}$ ( $\text{m}^2 \text{g}^{-1}$ )	0.91*	0.57	0.91*	0.56	0.63	0.66
$S_{\text{MICRO}}$ ( $\text{m}^2 \text{g}^{-1}$ )	0.00	-0.47	-0.19	-0.48	-0.55	-0.58
$S_{\text{MESO}}$ ( $\text{m}^2 \text{g}^{-1}$ )	0.85*	0.64	0.88*	0.63	0.71	0.74
$V_{\text{TOT}}$ ( $\text{cm}^3 \text{g}^{-1}$ )	0.82*	0.75	0.90*	0.73	0.84*	0.88*
$V_{\text{MICRO}}$ ( $\text{cm}^3 \text{g}^{-1}$ )	-0.05	-0.41	-0.22	-0.40	-0.56	-0.61
$V_{\text{MESO}}$ ( $\text{cm}^3 \text{g}^{-1}$ )	0.76	0.74	0.85*	0.72	0.84*	0.88*
C (%)	0.58	0.15	0.47	0.19	0.05	0.04
H (%)	0.93*	0.75	0.92	0.76	0.67	0.62
N (%)	0.45	-0.03	0.39	-0.08	0.10	0.14
O (%)	0.85*	0.31	0.72	0.31	0.24	0.23
Ash (%)	-0.72	-0.23	-0.60	-0.25	-0.14	-0.12
Fixed C (%)	0.63	-0.04	0.48	0.06	-0.04	-0.05
H/C	0.43	0.84*	0.57	0.83*	0.81*	0.75
O/C	0.75	0.13	0.60	0.13	0.09	0.08
(N+O)/C	0.67	0.06	0.53	0.04	0.05	0.05

\*Statistically significant correlation ( $p$ -value < 0.05).

## 5.4 Conclusions

In this study, pristine,  $\text{FeCl}_3$ - and  $\text{FeCl}_3+\text{ZnCl}_2$ -activated biochars were developed from sludge obtained from a municipal wastewater treatment plant and peat obtained from the surface mining of oil sands. The biochars were studied as adsorbents of surrogate compounds of NAs and NAs from real OSPW. The main objective was to investigate how the type of feedstock and the

chemical activation affected the changes in the characteristics of biochar that led to the superior adsorption of NAs from OSPW. It was observed important differences in the biochars produced using the same techniques but different feedstocks. The ash content of sludge-based biochars were much higher than peat-based biochars due to the inorganic fraction of sludge. After activation, the peat-based biochars presented higher porous properties and O/C ratios than sludge-based biochars. The use of  $\text{FeCl}_3$  as chemical activation agent resulted in the enhancement of some functional groups, such as  $-\text{OH}$  stretching group and  $\text{C}=\text{C}$  of aromatic rings, and these groups were further improved by the combination of  $\text{ZnCl}_2$  and  $\text{FeCl}_3$ . The minerals formed in the biochars were not water-soluble minerals, most likely due to the acid washing step during biochar production, reducing the risk of leaching of metals. The adsorption of surrogate compounds of NAs was better achieved by activated biochars and it was suggested that the hydrophobicity of compound and H/C ratio of biochar played a role in the adsorption selectivity. However, when the biochars were applied in the adsorption of NAs from real OSPW, the removal was impressive. The pristine biochars performed with up to 23% removal of total NAs. The comparison of the removals obtained for SB-800 in the adsorption of surrogate compounds and NAs from OSPW, it was highlighted that SB-800 did not adsorb any compound, except for DHCA (7% removal), but achieved 13% removal of total NAs from raw OSPW. Therefore, the use of surrogate compounds for the study of development of biochars for this purpose might limit the research on this topic. The best adsorption capacities were achieved by SB-Fe/Zn and PB-Fe/Zn, in which the removal surpassed 90% for all NAs (classical and oxidized NAs). In terms of adsorption selectivity of NAs from OSPW, it was noticed that the  $\text{FeCl}_3$ -activated biochars had higher affinity for NAs with higher carbon number. In contrast, the SB-Fe/Zn and PB-Fe/Zn biochars provided removal of a wider range of NAs. The biochar properties were correlated with the adsorption capacities obtained

for surrogate compounds of NAs and NAs from OSPW, emphasizing the importance of the mesopore fraction of biochar and H/C ratio in the adsorption of such compounds.

Based on the discussion, the importance of tailoring the biochar properties to target a wide range of NAs in the OSPW is highlighted and must be addressed. The use of surrogate compounds to evaluate the tailoring of biochars might not be advantageous, considering that it can lead to biochars that are effective to a few compounds. Therefore, it is suggested that further studies on biochar as adsorbents of NAs from OSPW should focus on tailoring biochars to achieve pore volume with high fraction of mesopore and present appropriate H/C and O/C ratios to support the hydrophobicity and aromaticity of biochar.

## 5.5 References

- Abdoul Magid, A. S. I., Islam, M. S., Chen, Y., Weng, L., Li, J., Ma, J., & Li, Y. (2021). Enhanced adsorption of polystyrene nanoplastics (PSNPs) onto oxidized corncob biochar with high pyrolysis temperature. *Science of the Total Environment*, 784, 147115. <https://doi.org/10.1016/j.scitotenv.2021.147115>
- Allen, E. W. (2008). Process water treatment in Canada's oil sands industry: I. Target pollutants and treatment objectives. *Journal of Environmental Engineering & Science*, 7(2), 123-138. <https://doi.org/10.1139/S07-038>
- Arshad, M., Khosa, M. A., Siddique, T., & Ullah, A. (2016). Modified biopolymers as sorbents for the removal of naphthenic acids from oil sands process affected water (OSPW). *Chemosphere*, 163, 334-341. <https://doi.org/10.1016/j.chemosphere.2016.08.015>
- Baharum, N. A., Nasir, H. M., Ishak, M. Y., Isa, N. M., Hassan, M. A., & Aris, A. Z. (2020). Highly efficient removal of diazinon pesticide from aqueous solutions by using coconut shell-modified biochar. *Arabian Journal of Chemistry*, 13(7), 6106-6121. <https://doi.org/10.1016/j.arabjc.2020.05.011>

- Bartlett, A. J., Frank, R. A., Gillis, P. L., Parrott, J. L., Marentette, J. R., Brown, L. R., Hooey, T., Vanderveen, R., McInnis, R., Brunswick, P., Shang, D., Headley, J. V., Peru, K. M., & Hewitt, L. M. (2017). Toxicity of naphthenic acids to invertebrates: Extracts from oil sands process-affected water versus commercial mixtures. *Environmental Pollution*, *227*, 271-279. <https://doi.org/10.1016/j.envpol.2017.04.056>
- Benally, C., Messele, S. A., & Gamal El-Din, M. (2019). Adsorption of organic matter in oil sands process water (OSPW) by carbon xerogel. *Water Research*, *154*, 402-411. <https://doi.org/10.1016/j.watres.2019.01.053>
- Bhuiyan, T. I., Tak, J. K., Sessarego, S., Harfield, D., & Hill, J. M. (2017). Adsorption of acid-extractable organics from oil sands process-affected water onto biomass-based biochar: Metal content matters. *Chemosphere*, *168*, 1337-1344. <https://doi.org/10.1016/j.chemosphere.2016.11.126>
- Boskovic, N., Brandstätter-Scherr, K., Sedláček, P., Bílková, Z., Bielská, L., & Hofman, J. (2020). Adsorption of epoxiconazole and tebuconazole in twenty different agricultural soils in relation to their properties. *Chemosphere*, *261*, 127637. <https://doi.org/10.1016/j.chemosphere.2020.127637>
- Brunauer, S., Emmett, P. H., & Teller, E. (1938). Adsorption of Gases in Multimolecular Layers. *Journal of the American Chemical Society*, *60*(2), 309-319. <https://doi.org/10.1021/ja01269a023>
- Chen, B., Zhou, D., & Zhu, L. (2008). Transitional Adsorption and Partition of Nonpolar and Polar Aromatic Contaminants by Biochars of Pine Needles with Different Pyrolytic Temperatures. *Environmental Science & Technology*, *42*(14), 5137-5143. <https://doi.org/10.1021/es8002684>
- Chen, D., Yu, X., Song, C., Pang, X., Huang, J., & Li, Y. (2016). Effect of pyrolysis temperature on the chemical oxidation stability of bamboo biochar. *Bioresource Technology*, *218*, 1303-1306. <https://doi.org/10.1016/j.biortech.2016.07.112>
- Cheng, H., Ji, R., Bian, Y., Jiang, X., & Song, Y. (2020a). From macroalgae to porous graphitized nitrogen-doped biochars – Using aquatic biota to treat polycyclic aromatic hydrocarbons-contaminated water. *Bioresource Technology*, *303*, 122947. <https://doi.org/10.1016/j.biortech.2020.122947>

- Cheng, L., Ji, Y., Liu, X., Mu, L., & Zhu, J. (2021). Sorption mechanism of organic dyes on a novel self-nitrogen-doped porous graphite biochar: Coupling DFT calculations with experiments. *Chemical Engineering Science*, 242, 116739. <https://doi.org/10.1016/j.ces.2021.116739>
- Crombie, K., Mašek, O., Sohi, S. P., Brownsort, P., & Cross, A. (2013). The effect of pyrolysis conditions on biochar stability as determined by three methods. *Gcb Bioenergy*, 5(2), 122-131. <https://doi.org/10.1111/gcbb.12030>
- de Boer, J. H., Lippens, B. C., Linsen, B. G., Broekhoff, J. C. P., van den Heuvel, A., & Osinga, T. J. (1966). The t-curve of multimolecular N<sub>2</sub>-adsorption. *Journal of Colloid and Interface Science*, 21(4), 405-414. [https://doi.org/10.1016/0095-8522\(66\)90006-7](https://doi.org/10.1016/0095-8522(66)90006-7)
- Deng, X., Jiang, Y., Zhang, M. a., Nan, Z., Liang, X., & Wang, G. (2022). Sorption properties and mechanisms of erythromycin and ampicillin in loess soil: Roles of pH, ionic strength, and temperature. *Chemical Engineering Journal*, 434, 134694. <https://doi.org/10.1016/j.cej.2022.134694>
- Enders, A., Hanley, K., Whitman, T., Joseph, S., & Lehmann, J. (2012). Characterization of biochars to evaluate recalcitrance and agronomic performance. *Bioresource Technology*, 114, 644-653. <https://doi.org/10.1016/j.biortech.2012.03.022>
- Feng, D., Guo, D., Zhang, Y., Sun, S., Zhao, Y., Shang, Q., Sun, H., Wu, J., & Tan, H. (2020). Functionalized construction of biochar with hierarchical pore structures and surface O-/N-containing groups for phenol adsorption. *Chemical Engineering Journal*, 127707. <https://doi.org/10.1016/j.cej.2020.127707>
- Frankel, M. L., Bhuiyan, T. I., Veksha, A., Demeter, M. A., Layzell, D. B., Helleur, R. J., Hill, J. M., & Turner, R. J. (2016). Removal and biodegradation of naphthenic acids by biochar and attached environmental biofilms in the presence of co-contaminating metals. *Bioresource Technology*, 216, 352-361. <https://doi.org/10.1016/j.biortech.2016.05.084>
- Grewer, D. M., Young, R. F., Whittal, R. M., & Fedorak, P. M. (2010). Naphthenic acids and other acid-extractables in water samples from Alberta: What is being measured? *Science of the Total Environment*, 408(23), 5997-6010. <https://doi.org/10.1016/j.scitotenv.2010.08.013>
- Hao, C., Headley, J. V., Peru, K. M., Frank, R., Yang, P., & Solomon, K. R. (2005). Characterization and pattern recognition of oil-sand naphthenic acids using comprehensive



- two-dimensional gas chromatography/time-of-flight mass spectrometry. *Journal of Chromatography A*, 1067(1), 277-284. <https://doi.org/10.1016/j.chroma.2005.01.041>
- Huang, R., Chelme-Ayala, P., Zhang, Y., Changelov, M., & Gamal El-Din, M. (2017). Investigation of dissociation constants for individual and total naphthenic acids species using ultra performance liquid chromatography ion mobility time-of-flight mass spectrometry analysis. *Chemosphere*, 184, 738-746. <https://doi.org/10.1016/j.chemosphere.2017.06.067>
- Huang, R., Chen, Y., Meshref, M. N. A., Chelme-Ayala, P., Dong, S., Ibrahim, M. D., Wang, C., Klammerth, N., Hughes, S. A., Headley, J. V., Peru, K. M., Brown, C., Mahaffey, A., & Gamal El-Din, M. (2018). Characterization and determination of naphthenic acids species in oil sands process-affected water and groundwater from oil sands development area of Alberta, Canada. *Water Research*, 128, 129-137. <https://doi.org/10.1016/j.watres.2017.10.003>
- Huang, R., McPhedran, K. N., & Gamal El-Din, M. (2015a). Ultra Performance Liquid Chromatography Ion Mobility Time-of-Flight Mass Spectrometry Characterization of Naphthenic Acids Species from Oil Sands Process-Affected Water. *Environmental Science & Technology*, 49(19), 11737-11745. <https://doi.org/10.1021/acs.est.5b03178>
- Islam, M. S., McPhedran, K. N., Messele, S. A., Liu, Y., & Gamal El-Din, M. (2018). Isotherm and kinetic studies on adsorption of oil sands process-affected water organic compounds using granular activated carbon. *Chemosphere*, 202, 716-725. <https://doi.org/10.1016/j.chemosphere.2018.03.149>
- IUPAC. (1982). Reporting Physisorption Data for Gas/Solid Systems (*Handbook of Heterogeneous Catalysis* (Vol. 54, pp. 2201-2218). Pure and Applied Chemistry. <https://doi.org/https://doi.org/10.1002/9783527610044.hetcat0065>
- Jang, H. M., Yoo, S., Choi, Y.-K., Park, S., & Kan, E. (2018). Adsorption isotherm, kinetic modeling and mechanism of tetracycline on Pinus taeda-derived activated biochar. *Bioresource Technology*, 259, 24-31. <https://doi.org/10.1016/j.biortech.2018.03.013>
- Jerez, S., Ventura, M., Molina, R., Pariente, M. I., Martínez, F., & Melero, J. A. (2021). Comprehensive characterization of an oily sludge from a petrol refinery: A step forward

- for its valorization within the circular economy strategy. *Journal of Environmental Management*, 285, 112124. <https://doi.org/10.1016/j.jenvman.2021.112124>
- Lehmann, J., & Joseph, S. (2015). *Biochar for environmental management: science, technology and implementation*. Routledge.
- Liu, J., Jiang, X., Zhou, L., Han, X., & Cui, Z. (2009). Pyrolysis treatment of oil sludge and model-free kinetics analysis. *Journal of Hazardous Materials*, 161(2), 1208-1215. <https://doi.org/10.1016/j.jhazmat.2008.04.072>
- Lu, G. Q., Low, J. C. F., Liu, C. Y., & Lua, A. C. (1995). Surface area development of sewage sludge during pyrolysis. *Fuel*, 74(3), 344-348. [https://doi.org/10.1016/0016-2361\(95\)93465-P](https://doi.org/10.1016/0016-2361(95)93465-P)
- Ma, Y., Li, M., Li, P., Yang, L., Wu, L., Gao, F., Qi, X., & Zhang, Z. (2021). Hydrothermal synthesis of magnetic sludge biochar for tetracycline and ciprofloxacin adsorptive removal. *Bioresource Technology*, 319, 124199. <https://doi.org/10.1016/j.biortech.2020.124199>
- Meshref, M. N. A., Chelme-Ayala, P., & Gamal El-Din, M. (2017). Fate and abundance of classical and heteroatomic naphthenic acid species after advanced oxidation processes: Insights and indicators of transformation and degradation. *Water Research*, 125, 62-71. <https://doi.org/10.1016/j.watres.2017.08.007>
- Natural Resources Canada. (2020). *Crude oil facts*. <https://www.nrcan.gc.ca/science-data/data-analysis/energy-data-analysis/energy-facts/crude-oil-facts/20064#L4>
- Nzediegwu, C., Arshad, M., Ulah, A., Naeth, M. A., & Chang, S. X. (2021a). Fuel, thermal and surface properties of microwave-pyrolyzed biochars depend on feedstock type and pyrolysis temperature. *Bioresource Technology*, 320, 124282. <https://doi.org/10.1016/j.biortech.2020.124282>
- Nzediegwu, C., Naeth, M. A., & Chang, S. X. (2021b). Carbonization temperature and feedstock type interactively affect chemical, fuel, and surface properties of hydrochars. *Bioresource Technology*, 330, 124976. <https://doi.org/10.1016/j.biortech.2021.124976>
- Nzediegwu, C., Naeth, M. A., & Chang, S. X. (2022). Effects of nitric acid modification on hydrochar's combustion, fuel and thermal properties are dependent on feedstock type. *Bioresource Technology*, 354, 127245. <https://doi.org/10.1016/j.biortech.2022.127245>

- Peng, P., Lang, Y.-H., & Wang, X.-M. (2016). Adsorption behavior and mechanism of pentachlorophenol on reed biochars: pH effect, pyrolysis temperature, hydrochloric acid treatment and isotherms. *Ecological Engineering*, 90, 225-233. <https://doi.org/10.1016/j.ecoleng.2016.01.039>
- Pourrezaei, P., Alpatova, A., Chelme-Ayala, P., Perez-Estrada, L. A., Jensen-Fontaine, M., Le, X. C., & Gamal El-Din, M. (2014). Impact of petroleum coke characteristics on the adsorption of the organic fractions from oil sands process-affected water. *International Journal of Environmental Science and Technology*, 11(7), 2037-2050. <https://doi.org/10.1007/s13762-013-0406-x>
- Regkouzas, P., & Diamadopoulos, E. (2019). Adsorption of selected organic micro-pollutants on sewage sludge biochar. *Chemosphere*, 224, 840-851. <https://doi.org/10.1016/j.chemosphere.2019.02.165>
- Rogers, V. V., Wickstrom, M., Liber, K., & MacKinnon, M. D. (2002). Acute and Subchronic Mammalian Toxicity of Naphthenic Acids from Oil Sands Tailings. *Toxicological Sciences*, 66(2), 347-355. <https://doi.org/10.1093/toxsci/66.2.347>
- Scarlett, A. G., Reinardy, H. C., Henry, T. B., West, C. E., Frank, R. A., Hewitt, L. M., & Rowland, S. J. (2013). Acute toxicity of aromatic and non-aromatic fractions of naphthenic acids extracted from oil sands process-affected water to larval zebrafish. *Chemosphere*, 93(2), 415-420. <https://doi.org/10.1016/j.chemosphere.2013.05.020>
- Singh, R., Naik, D. V., Dutta, R. K., & Kanaujia, P. K. (2020). Biochars for the removal of naphthenic acids from water: A prospective approach towards remediation of petroleum refinery wastewater. *Journal of Cleaner Production*, 266, 121986. <https://doi.org/10.1016/j.jclepro.2020.121986>
- Spokas, K. A. (2010). Review of the stability of biochar in soils: predictability of O:C molar ratios. *Carbon Management*, 1(2), 289-303. <https://doi.org/10.4155/cmt.10.32>
- Wang, L., Bolan, N. S., Tsang, D. C. W., & Hou, D. (2020). Green immobilization of toxic metals using alkaline enhanced rice husk biochar: Effects of pyrolysis temperature and KOH concentration. *Science of the Total Environment*, 720, 137584. <https://doi.org/10.1016/j.scitotenv.2020.137584>

- Wang, L., Olsen, M. N. P., Moni, C., Dieguez-Alonso, A., de la Rosa, J. M., Stenrød, M., Liu, X., & Mao, L. (2022). Comparison of properties of biochar produced from different types of lignocellulosic biomass by slow pyrolysis at 600 °C. *Applications in Energy and Combustion Science*, 12, 100090. <https://doi.org/10.1016/j.jaecs.2022.100090>
- Wang, P., Tang, L., Wei, X., Zeng, G., Zhou, Y., Deng, Y., Wang, J., Xie, Z., & Fang, W. (2017b). Synthesis and application of iron and zinc doped biochar for removal of p-nitrophenol in wastewater and assessment of the influence of co-existed Pb(II). *Applied Surface Science*, 392, 391-401. <https://doi.org/10.1016/j.apsusc.2016.09.052>
- Wang, Y., Jiang, B., Wang, L., Feng, Z., Fan, H., & Sun, T. (2021). Hierarchically structured two-dimensional magnetic microporous biochar derived from hazelnut shell toward effective removal of p-arsanilic acid. *Applied Surface Science*, 540, 148372. <https://doi.org/10.1016/j.apsusc.2020.148372>
- Wu, Q., Zhang, Y., Cui, M.-h., Liu, H., Liu, H., Zheng, Z., Zheng, W., Zhang, C., & Wen, D. (2022b). Pyrolyzing pharmaceutical sludge to biochar as an efficient adsorbent for deep removal of fluoroquinolone antibiotics from pharmaceutical wastewater: Performance and mechanism. *Journal of Hazardous Materials*, 426, 127798. <https://doi.org/10.1016/j.jhazmat.2021.127798>
- Xia, D., Tan, F., Zhang, C., Jiang, X., Chen, Z., Li, H., Zheng, Y., Li, Q., & Wang, Y. (2016). ZnCl<sub>2</sub>-activated biochar from biogas residue facilitates aqueous As(III) removal. *Applied Surface Science*, 377, 361-369. <https://doi.org/10.1016/j.apsusc.2016.03.109>
- Xu, Y., & Chen, B. (2013). Investigation of thermodynamic parameters in the pyrolysis conversion of biomass and manure to biochars using thermogravimetric analysis. *Bioresource Technology*, 146, 485-493. <https://doi.org/10.1016/j.biortech.2013.07.086>
- Yang, X., Kang, K., Qiu, L., Zhao, L., & Sun, R. (2020). Effects of carbonization conditions on the yield and fixed carbon content of biochar from pruned apple tree branches. *Renewable Energy*, 146, 1691-1699. <https://doi.org/10.1016/j.renene.2019.07.148>
- Yusuff, A. S., Lala, M. A., Thompson-Yusuff, K. A., & Babatunde, E. O. (2022). ZnCl<sub>2</sub>-modified eucalyptus bark biochar as adsorbent: preparation, characterization and its application in adsorption of Cr(VI) from aqueous solutions. *South African Journal of Chemical Engineering*, 42, 138-145. <https://doi.org/10.1016/j.sajce.2022.08.002>

- Zhu, S., Li, M., & Gamal El-Din, M. (2018). The roles of pH and draw solute on forward osmosis process treating aqueous naphthenic acids. *Journal of Membrane Science*, 549, 456-465. <https://doi.org/10.1016/j.memsci.2017.12.029>
- Zielińska, A., Oleszczuk, P., Charmas, B., Skubiszewska-Zięba, J., & Pasieczna-Patkowska, S. (2015). Effect of sewage sludge properties on the biochar characteristic. *Journal of Analytical and Applied Pyrolysis*, 112, 201-213. <https://doi.org/10.1016/j.jaap.2015.01.025>
- Zubot, W., MacKinnon, M. D., Chelme-Ayala, P., Smith, D. W., & Gamal El-Din, M. (2012). Petroleum coke adsorption as a water management option for oil sands process-affected water. *Science of the Total Environment*, 427-428, 364-372. <https://doi.org/10.1016/j.scitotenv.2012.04.024>

## **Chapter 6      Conclusions and Recommendations**

### **6.1    Thesis overview**

The oil sands are composed of approximately 85% mineral solids, 10% bitumen and 5% water, in which the oil sands operations in Alberta are responsible for the fourth largest oil reserves in the world. To recover the bitumen from the mined oil sands, the process involves the usage of the Clark caustic hot water technique, and the consumption can go up to 2.6 barrels of fresh water per barrel of bitumen, generating high volume of OSPW. The OSPW is stored in on-site tailings ponds, as required by the Alberta's zero discharge approach, and after settling of solids, a portion of OSPW is recycled back into the bitumen extraction process. However, there is a decrease of process water quality after reuse, leading to concerns in terms of scaling and corrosion of extraction plant infrastructure and bitumen recovery efficiency. NAs are amphiphilic compounds that are a concern in the OSPW due to their corrosive properties and their contribution to the toxicity of OSPW. Several OSPW treatments were suggested over the years, including coagulation-flocculation, advanced oxidation processes, and adsorption. Previous adsorbents used to study the removal of NAs or organic fraction from OSPW include carbon xerogel, biochar, commercial activated carbon, and petroleum coke. The use of adsorption for treatment of OSPW can promote a circular economy if the development of efficient adsorbents is associated with management of hazardous wastes.

During the surface mining of oil sands there is a requirement to excavate the muskeg layers, located above the oil sands and closer to the surface, and the overburden layers, located between the muskeg and the oil sands layers. This results in high quantities of peat-like and sand materials, also referred to as reclamation materials, which are stored until application in oil sands land

reclamation. The study of such reclamation materials from an oil sands extraction site for use as adsorbents of NAs from OSPW can provide important data regarding the transport of NAs in oil sands reclamation landscape where these materials are used.

On the other hand, highly-efficient carbon-based materials can be used as adsorbents in the treatment of OSPW. These carbon-based materials can be biochars produced from biological wastes, such as sludge from municipal wastewater treatment plants, and they can be designed to target specific compounds during water treatment. Biological sludge from municipal wastewater treatment plants is a biohazard associated with high toxicity for some aquatic microorganisms and the disposal of the sludge is an issue around the world. The application of sludge as a biomass to produce biochar for adsorption treatment of OSPW can promote circular economy.

Therefore, this thesis addresses the study of reclamation materials and biochars as adsorbents of NAs in OSPW. Chapter 3 reported the investigation of three reclamation materials as adsorbents of naphthenic acids to evaluate the adsorption characteristics, aiming at the adsorption and desorption behaviors of two model compounds of NAs, the application of the reclamation materials in the adsorption of classical NAs from real OSPW, and the understanding of the effect of the properties of the reclamation materials and the adsorption distribution coefficients. This study provided important data on the transport of NAs in oil sands reclamation landscape where these materials are used. Chapter 4 provided a detailed study of the application of sludge-based biochars as adsorbents of NAs from raw OSPW. This is the first in-depth study of biochar for NAs adsorption from OSPW, in which several research gaps were filled. The adsorption selectivity of NAs by biochar was investigated, with special consideration given to the diverse NAs composition in OSPW. In addition, the adsorption of classical and oxidized species of NAs from OSPW, regeneration and reuse ability of spent biochars for NAs adsorption to reduce

the risk of secondary pollution, and leaching of metals from biochar to the OSPW often associated with sludge-based biochars. Chapter 5 delivered an exploratory study of the comparison between two feedstocks and three types of biochars from such feedstocks (pristine, FeCl<sub>3</sub>-activated and FeCl<sub>3</sub>+ZnCl<sub>2</sub>-activated biochars) and their performance in the adsorption of four surrogate compounds of NAs in single solution and NAs from raw OSPW. The biochar properties were evaluated extensively, the adsorption efficiency obtained for surrogate compounds of NAs and NAs from real OSPW were compared, and the properties affecting the adsorption were identified. This study paved the road for future studies on biochar tailoring for adsorption of NAs from OSPW.

## 6.2 Conclusions

The research presented in this thesis focused on the investigation of two types of adsorbents for the adsorption of naphthenic acids from OSPW. Based on the experimental results and analysis, the following main conclusions were made:

### *Investigation of reclamation materials from surface mining of oil sands*

- The PF-1 and PF-2 diverged in terms of pH<sub>pzc</sub>, sand and clay content. The PT had higher CEC and TOC content, with silt as the major component.
- The adsorption of NAs model compounds (DA and PVA) reached equilibrium at approximately 2 days using PT and 3 and 6 days for DA and PVA, respectively, using PF-1 and PF-2.



- The Elovich kinetic model best described the adsorption of DA on all three materials and PVA on PT, while the PFO kinetic model best described the adsorption of PVA on both PF materials.
- The adsorption equilibrium of DA and PVA on the reclamation materials followed the Langmuir isotherm, and the calculated range of the intensity parameters indicated that the adsorption of NAs on the studied materials was favorable and suggested a high degree of irreversibility (close to 0).
- Desorption of DA and PVA from post-adsorption materials was studied using three different solutions (buffer solution, CaCl<sub>2</sub> solution, and simulated soil solution) and desorption was not observed for up to 14 days of contact time.
- The adsorption mechanisms included hydrophobic interactions as  $\pi$ - $\pi$  interaction, and hydrogen bonding.
- The materials were applied in the adsorption of classical NAs from raw OSPW in the following concentrations: 5 g L<sup>-1</sup> PT, 500 g L<sup>-1</sup> PF-1, and 100 g L<sup>-1</sup> PF-2, in which the removal was 20, 39, and 27%, respectively.
- The materials partially removed classical NAs with  $-Z$  numbers of 0 to 18 and carbon numbers ranging from 8 to 23.
- The adsorption coefficients calculated for DA, PVA, and classical NAs (from OSPW) stressed lower values for classical NAs in comparison with DA and PVA, indicating that the materials have more affinity with the model compounds than the NAs from real wastewater, most likely because of OSPW composition.
- The Pearson correlation coefficient was determined using the physicochemical properties of the materials and the adsorption properties ( $K_d$ ,  $K_{OC}$ ,  $q_t$ ,  $q_{max}$ ) obtained for

both representative compounds and classical NAs to identify patterns or connections. TOC was found to be the property affecting adsorption of NAs the most.

- The importance of TOC in the adsorption highlighted the hydrophobic interaction as an important adsorption mechanism of NAs on the reclamation materials that were studied.

#### *Investigation of pristine and ZnCl<sub>2</sub>-activated sludge-based biochar*

- Pristine and ZnCl<sub>2</sub>-activated biochars were produced from sludge sourced from a municipal wastewater treatment. The adsorption capacity for total NAs (classical and oxidized species) from raw OSPW increased from 2.3 to 26.6 mg g<sup>-1</sup> when activated biochar was used.
- The superior adsorption performance observed for the ZnCl<sub>2</sub>-activated biochar was due to the abundance of mesopores and oxygen-containing surface groups with affinity for NAs in OSPW.
- The adsorption of classical NAs from raw OSPW on ZnCl<sub>2</sub>-activated biochar was very fast, and within 5 min of contact time, the concentration of classical NAs decreased by 55% from 40.4 to 18 mg L<sup>-1</sup>. The equilibrium was reached at 2 h of contact time with 85% removal, and the adsorption capacity at equilibrium was 17 mg g<sup>-1</sup>.
- The PSO kinetic model best described the adsorption process, in which the adsorption rate of classical NAs on SB-Zn was 0.80 g mg<sup>-1</sup> h<sup>-1</sup>.
- Use of the IPD model helped us to conclude that the adsorption was limited by pore diffusion, but film diffusion also played a role in the process.

- The adsorption equilibrium followed the Freundlich isotherm, characterizing the ZnCl<sub>2</sub>-activated biochar as a heterogeneous adsorbent and indicating that the adsorption of NAs occurs in multilayers.
- The adsorption mechanisms of NAs from OSPW on ZnCl<sub>2</sub>-activated biochar were determined to be pore-filling, hydrogen bonding, and  $\pi$ - $\pi$  interactions.
- In terms of adsorption selectivity of classical NAs by ZnCl<sub>2</sub>-activated biochar, it was revealed that the biochar has higher affinity for NAs with higher carbon and DBE numbers, in other words those NAs that may be considered more hydrophobic, recalcitrant, and having higher cyclicality.
- Thermal regeneration of spent biochar and reusability potential were studied to reduce the secondary pollution often associated with exhausted adsorbents. The adsorption capacity of fresh SB-Zn was 17.1 mg g<sup>-1</sup> and after the first regeneration and reuse, the adsorption capacity decreased to 14.9 mg g<sup>-1</sup> (13% decrease) and further decreased to 7.1 mg g<sup>-1</sup> in the fifth cycle. However, the adsorption capacity obtained in the fifth cycle was still 5 times higher than the one obtained for pristine biochar (1.4 mg g<sup>-1</sup>).
- The adsorption treatment of OSPW using ZnCl<sub>2</sub>-activated biochar resulted in a 66% reduction of the acute toxicity towards *V. fischeri* and a 91% reduction of the bioavailability of organics.
- The potential leaching of metals from the produced biochar into treated OSPW at 2 h and 30 days of contact time was studied, revealing a minor leaching of Mo, P, S, and Si in the treated OSPW, which is probably due to the nature of sludge. However, the activated biochar has potential to decrease the concentration of some metals in the raw OSPW, such as Mg (7%), Ca (21%), Sr (27%), and Ba (60%).

- In terms of the organic matter, the ZnCl<sub>2</sub>-activated biochar treatment provided a 63% reduction of DOC and a 66% reduction of COD in the treated OSPW.

*Investigation of the role of feedstock and chemical activation types on biochar performance*

- The ash content of sludge-based biochars was much higher than that of the peat-based biochars due to the inorganic fraction of the sludge.
- After activation, the peat-based biochars presented higher porous properties and O/C ratios than the sludge-based biochars, in which the FeCl<sub>3</sub>+ZnCl<sub>2</sub>-activated biochars were composed mainly of mesopores.
- The use of FeCl<sub>3</sub> as a chemical activation agent resulted in the enhancement of some functional groups, such as the –OH stretching group and C=C of aromatic rings. These functional groups were further improved by the combination of chemical activation agents, ZnCl<sub>2</sub> and FeCl<sub>3</sub>.
- The minerals formed in the biochars were not water-soluble minerals, most likely due to the acid washing step during biochar production, reducing the risk of leaching of metals during the adsorption treatment.
- Pristine and activated biochars were applied in the adsorption of four surrogate compounds of NAs. The best removal was achieved by the activated biochars.
- In terms of adsorption of NAs from real OSPW, adsorption with the pristine biochars resulted with up to 23% removal of total NAs, while more than 90% total NAs removal was achieved using the FeCl<sub>3</sub>+ZnCl<sub>2</sub>-activated biochars.
- An important result that was highlighted was that the study of biochar efficiency for adsorption of NAs should always focus on NAs from OSPW instead of surrogate

compounds considering the diverse composition of NAs in the OSPW. One example is the comparison of the removals obtained for pristine sludge biochar, which hardly adsorbed any model compound, except for DHCA (7% removal), but achieved 13% removal of total NAs from raw OSPW. Therefore, use of surrogate compounds for the development of biochars for NAs adsorption might limit the research on this topic.

- In terms of adsorption selectivity of NAs from OSPW, it was noticed that the FeCl<sub>3</sub>-activated biochars had higher affinity for NAs with higher carbon number, while FeCl<sub>3</sub>+ZnCl<sub>2</sub>-activated biochars provided removal of a wider range of NAs.
- Results of the Pearson correlation of biochar properties with the adsorption capacities obtained for the NAs model compounds and NAs from OSPW emphasize the importance of the mesopore fraction and the H/C ratio of the produced biochar in the adsorption of NAs compounds.

### **6.3 Recommendations**

The Athabasca oil sands region, covering several thousands of square kilometers in northern Alberta, has reached a volume of 1,360,000 ML of fluid tailings in 2020. From the point of view of water resources management, the treatment of OSPW is imperative to ensure that the water is reused efficiently to decrease the freshwater intake for bitumen extraction from oil sands and eventually the OSPW stored in the tailings ponds are returned safely to the environment, considering the growing concern of water scarcity in the world. In light of the large volume of OSPW, further studies should be conducted to accelerate the OSPW reclamation.

Even though the reclamation materials were studied to evaluate the adsorptive characteristics for application in oil sands reclamation landscapes, peat-mineral mix was

highlighted as the most promising reclamation material for adsorption of NAs from OSPW due to the high TOC content. Considering the large amounts of peat-mineral mix resulted from the surface mining of oil sands and the minimal processing of peat-mineral mix, future research should further address the applicability of such materials as part of treatment of OSPW. Column studies, such as fixed-bed column, and biological activity of peat-mineral mix in contact with OSPW for longer periods could highlight the efficiency of removal of organics and inorganics from raw OSPW, paving the way towards the application of peat-mineral mix in wetlands as a seepage control or passive treatment of OSPW.

The proof of concept for biochars for OSPW treatment was throughout demonstrated in this thesis and it was the first step towards the ultimate application of these carbon-based materials in passive treatments, such as pit lakes, or active systems to assist in OSPW reclamation. In addition to efficient treatment of OSPW, biochars can contribute to the carbon credits of the oil sands industries. Therefore, the carbon cycle of biochar (Figure 6.1) highlights the importance of further studies to lead to the implementation of such materials on-site. To advance to the industrial application, the following recommendations were made for future research:

- Scaling up the adsorption treatment process: Biochars in configurations respective of active systems (fixed-bed columns) and passive treatments (wetlands and pit lakes) should be evaluated to identify the best technology to suit the industry needs and requirements. The removal of organic and inorganic constituents, the effect of temperature considering the range of temperatures observed on-site, and the acute and chronic toxicity of treated OSPW, i.e. genotoxicity and immunotoxicity, should be fully addressed. For the passive treatment technology, the adsorption process should be studied in line with other treatments (biological, advanced oxidation).

- Investigation of spent biochar: Secondary pollution is often associated with adsorption treatment. Therefore, the spent biochar should be addressed considering the possibilities of application on-site for OSPW treatment. The spent biochar should be evaluated as (1) soil amendment for oil sands reclamation landscapes aiming at phytoremediation of spent biochar and (2) biofilm carrier to assist in the biological treatment of OSPW.
- Life-cycle assessment of biochar production and application in OSPW treatment to identify the environmental impacts.
- Biochar production: Exploration of co-pyrolysis and other types of feedstocks based on local availability to improve biochar characteristics and minimize usage of chemical activation agents or other modifications and investigation of spherical biochar, i.e., alginate beads, to produce a lightweight biochar to be used in wetlands.

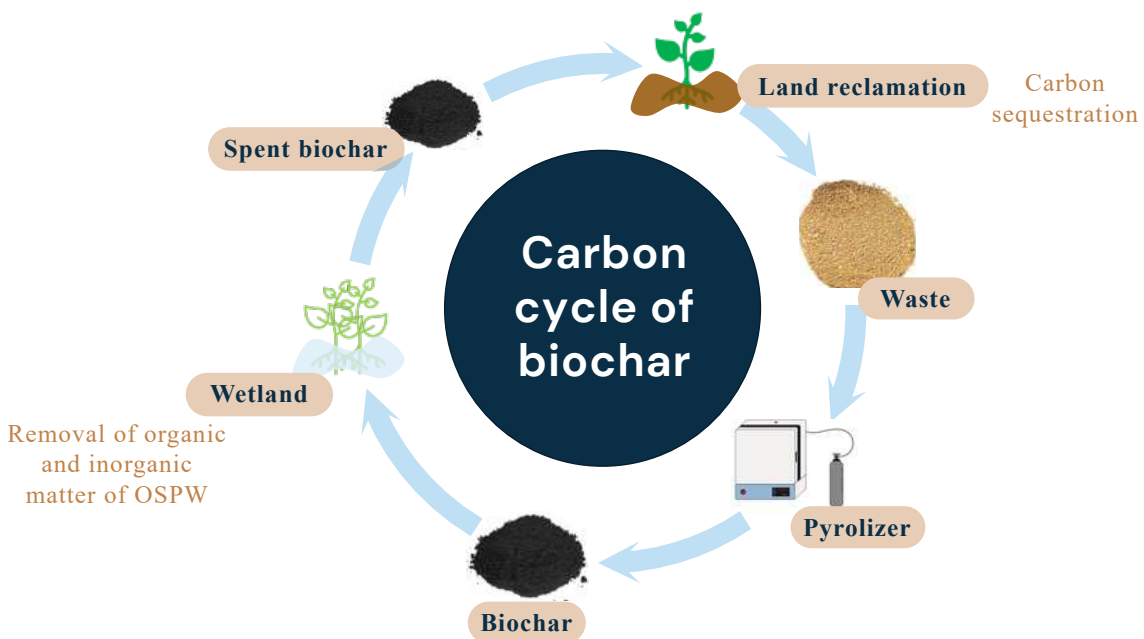


**Figure 6.1:** Carbon cycle of biochar for the OSPW treatment in the oil sands industries.

## BIBLIOGRAPHY

- Abdalrhman, A. S., Zhang, Y., Arslan, M., & Gamal El-Din, M. (2020). Low-current electro-oxidation enhanced the biodegradation of the recalcitrant naphthenic acids in oil sands process water. *Journal of Hazardous Materials*, 398, 122807. <https://doi.org/10.1016/j.jhazmat.2020.122807>
- Abdoul Magid, A. S. I., Islam, M. S., Chen, Y., Weng, L., Li, J., Ma, J., & Li, Y. (2021). Enhanced adsorption of polystyrene nanoplastics (PSNPs) onto oxidized corncob biochar with high pyrolysis temperature. *Science of the Total Environment*, 784, 147115. <https://doi.org/10.1016/j.scitotenv.2021.147115>
- Acevedo, B., Barriocanal, C., Lupul, I., & Gryglewicz, G. (2015). Properties and performance of mesoporous activated carbons from scrap tyres, bituminous wastes and coal. *Fuel*, 151, 83-90. <https://doi.org/10.1016/j.fuel.2015.01.010>
- Aghababaei, A., Ncibi, M. C., & Sillanpää, M. (2017). Optimized removal of oxytetracycline and cadmium from contaminated waters using chemically-activated and pyrolyzed biochars from forest and wood-processing residues. *Bioresource Technology*, 239, 28-36. <https://doi.org/10.1016/j.biortech.2017.04.119>
- Ahmed, M. B., Zhou, J. L., Ngo, H. H., Guo, W., & Chen, M. (2016). Progress in the preparation and application of modified biochar for improved contaminant removal from water and wastewater. *Bioresource Technology*, 214, 836-851. <https://doi.org/10.1016/j.biortech.2016.05.057>
- Alberta Energy Regulator. (2021). *State of Fluid Tailings Management for Mineable Oil Sands, 2020* <https://static.aer.ca/prd/documents/reports/2020-State-Fluid-Tailings-Management-Mineable-OilSands.pdf>
- Alberta Environmental Protection. (1995). *Water Quality Based Effluent Limits Procedures Manual*.
- Alberts, M. E., Chua, G., & Muench, D. G. (2019). Exposure to naphthenic acids and the acid extractable organic fraction from oil sands process-affected water alters the subcellular structure and dynamics of plant cells. *Science of the Total Environment*, 651, 2830-2844. <https://doi.org/10.1016/j.scitotenv.2018.10.181>



- Alhashimi, H. A., & Aktas, C. B. (2017). Life cycle environmental and economic performance of biochar compared with activated carbon: A meta-analysis. *Resources, Conservation and Recycling*, 118, 13-26. <https://doi.org/10.1016/j.resconrec.2016.11.016>
- Allen, E. W. (2008). Process water treatment in Canada's oil sands industry: I. Target pollutants and treatment objectives. *Journal of Environmental Engineering & Science*, 7(2), 123-138. <https://doi.org/10.1139/S07-038>
- Arshad, M., Khosa, M. A., Siddique, T., & Ullah, A. (2016). Modified biopolymers as sorbents for the removal of naphthenic acids from oil sands process affected water (OSPW). *Chemosphere*, 163, 334-341. <https://doi.org/10.1016/j.chemosphere.2016.08.015>
- Arslan, M., & Gamal El-Din, M. (2021). Bacterial diversity in petroleum coke based biofilters treating oil sands process water. *Science of the Total Environment*, 782, 146742. <https://doi.org/10.1016/j.scitotenv.2021.146742>
- Bagheri, M., Lothenbach, B., Shakoorioskooie, M., & Scrivener, K. (2022). Effect of different ions on dissolution rates of silica and feldspars at high pH. *Cement and Concrete Research*, 152, 106644. <https://doi.org/10.1016/j.cemconres.2021.106644>
- Baharum, N. A., Nasir, H. M., Ishak, M. Y., Isa, N. M., Hassan, M. A., & Aris, A. Z. (2020). Highly efficient removal of diazinon pesticide from aqueous solutions by using coconut shell-modified biochar. *Arabian Journal of Chemistry*, 13(7), 6106-6121. <https://doi.org/10.1016/j.arabjc.2020.05.011>
- Bakatula, E. N., Richard, D., Neculita, C. M., & Zagury, G. J. (2018). Determination of point of zero charge of natural organic materials. *Environmental Science and Pollution Research*, 25(8), 7823-7833. <https://doi.org/10.1007/s11356-017-1115-7>
- Banerjee, K., Cheremisinoff, P. N., & Cheng, S. L. (1997). Adsorption kinetics of o-xylene by flyash. *Water Research*, 31(2), 249-261. [https://doi.org/10.1016/S0043-1354\(96\)00003-6](https://doi.org/10.1016/S0043-1354(96)00003-6)
- Bartlett, A. J., Frank, R. A., Gillis, P. L., Parrott, J. L., Marentette, J. R., Brown, L. R., Hooey, T., Vanderveen, R., McInnis, R., Brunswick, P., Shang, D., Headley, J. V., Peru, K. M., & Hewitt, L. M. (2017). Toxicity of naphthenic acids to invertebrates: Extracts from oil sands process-affected water versus commercial mixtures. *Environmental Pollution*, 227, 271-279. <https://doi.org/10.1016/j.envpol.2017.04.056>

- Belkassa, K., Khelifa, M., Batonneau-Gener, I., Marouf-Khelifa, K., & Khelifa, A. (2021). Understanding of the mechanism of crystal violet adsorption on modified halloysite: Hydrophobicity, performance, and interaction. *Journal of Hazardous Materials*, 415, 125656. <https://doi.org/10.1016/j.jhazmat.2021.125656>
- Benally, C., Messele, S. A., & Gamal El-Din, M. (2019). Adsorption of organic matter in oil sands process water (OSPW) by carbon xerogel. *Water Research*, 154, 402-411. <https://doi.org/10.1016/j.watres.2019.01.053>
- Bhuiyan, T. I., Tak, J. K., Sessarego, S., Harfield, D., & Hill, J. M. (2017). Adsorption of acid-extractable organics from oil sands process-affected water onto biomass-based biochar: Metal content matters. *Chemosphere*, 168, 1337-1344. <https://doi.org/10.1016/j.chemosphere.2016.11.126>
- Bian, C., Wang, L., Cui, Z., Dong, Z., Shi, X., Li, Y., & Li, B. (2022). Adsorption-desorption and transport behavior of pydiflumetofen in eight different types of soil. *Ecotoxicology and Environmental Safety*, 234, 113378. <https://doi.org/10.1016/j.ecoenv.2022.113378>
- Bispo, M. D., Schneider, J. K., da Silva Oliveira, D., Tomasini, D., da Silva Maciel, G. P., Schena, T., Onorevoli, B., Bjerck, T. R., Jacques, R. A., Krause, L. C., & Caramão, E. B. (2018). Production of activated biochar from coconut fiber for the removal of organic compounds from phenolic. *Journal of Environmental Chemical Engineering*, 6(2), 2743-2750. <https://doi.org/10.1016/j.jece.2018.04.029>
- Boskovic, N., Brandstätter-Scherr, K., Sedláček, P., Bílková, Z., Bielská, L., & Hofman, J. (2020). Adsorption of epoxiconazole and tebuconazole in twenty different agricultural soils in relation to their properties. *Chemosphere*, 261, 127637. <https://doi.org/10.1016/j.chemosphere.2020.127637>
- Brunauer, S., Emmett, P. H., & Teller, E. (1938). Adsorption of Gases in Multimolecular Layers. *Journal of the American Chemical Society*, 60(2), 309-319. <https://doi.org/10.1021/ja01269a023>
- Cancelli, A. M., & Gobas, F. A. P. C. (2022). Treatment of naphthenic acids in oil sands process-affected waters with a surface flow treatment wetland: mass removal, half-life, and toxicity-reduction. *Environmental Research*, 213, 113755. <https://doi.org/10.1016/j.envres.2022.113755>

- Cao, X., Meng, Z., Song, E., Sun, X., Hu, X., Wenbin, L., Liu, Z., Gao, S., & Song, B. (2022). Co-adsorption capabilities and mechanisms of bentonite enhanced sludge biochar for de-risking norfloxacin and Cu<sup>2+</sup> contaminated water. *Chemosphere*, 299, 134414. <https://doi.org/10.1016/j.chemosphere.2022.134414>
- Carter, M. R., & Gregorich, E. G. (2007). *Soil sampling and methods of analysis. [electronic resource]* (2nd ed. ed. ed.). CRC Press. <https://www.taylorfrancis.com/books/9781420005271>
- Chakraborty, P., Banerjee, S., Kumar, S., Sadhukhan, S., & Halder, G. (2018). Elucidation of ibuprofen uptake capability of raw and steam activated biochar of Aegle marmelos shell: Isotherm, kinetics, thermodynamics and cost estimation. *Process Safety and Environmental Protection*, 118, 10-23. <https://doi.org/10.1016/j.psep.2018.06.015>
- Chapman, S. J., Campbell, C. D., Fraser, A. R., & Puri, G. (2001). FTIR spectroscopy of peat in and bordering Scots pine woodland: relationship with chemical and biological properties. *Soil Biology and Biochemistry*, 33(9), 1193-1200. [https://doi.org/10.1016/S0038-0717\(01\)00023-2](https://doi.org/10.1016/S0038-0717(01)00023-2)
- Chen, B., Zhou, D., & Zhu, L. (2008). Transitional Adsorption and Partition of Nonpolar and Polar Aromatic Contaminants by Biochars of Pine Needles with Different Pyrolytic Temperatures. *Environmental Science & Technology*, 42(14), 5137-5143. <https://doi.org/10.1021/es8002684>
- Chen, C., Yan, X., Xu, Y., Yoza, B. A., Wang, X., Kou, Y., Ye, H., Wang, Q., & Li, Q. X. (2019a). Activated petroleum waste sludge biochar for efficient catalytic ozonation of refinery wastewater. *Science of the Total Environment*, 651, 2631-2640. <https://doi.org/10.1016/j.scitotenv.2018.10.131>
- Chen, D., Yu, X., Song, C., Pang, X., Huang, J., & Li, Y. (2016). Effect of pyrolysis temperature on the chemical oxidation stability of bamboo biochar. *Bioresource Technology*, 218, 1303-1306. <https://doi.org/10.1016/j.biortech.2016.07.112>
- Chen, H., Chen, D., & Hong, L. (2015). Influences of activation agent impregnated sewage sludge pyrolysis on emission characteristics of volatile combustion and De-NO<sub>x</sub> performance of activated char. *Applied Energy*, 156, 767-775. <https://doi.org/10.1016/j.apenergy.2015.05.098>

- Chen, H., Zhang, Y., Li, J., Zhang, P., & Liu, N. (2019b). Preparation of pickling-reheating activated alfalfa biochar with high adsorption efficiency for p-nitrophenol: characterization, adsorption behavior, and mechanism. *Environmental Science and Pollution Research*, 26(15), 15300-15313. <https://doi.com/10.1007/s11356-019-04862-3>
- Chen, X., Gu, X., Bao, L., Ma, S., & Mu, Y. (2021). Comparison of adsorption and desorption of triclosan between microplastics and soil particles. *Chemosphere*, 263, 127947. <https://doi.org/10.1016/j.chemosphere.2020.127947>
- Chen, X., Li, H., Liu, W., Meng, Z., Wu, Z., Wang, G., Liang, Y., & Bi, S. (2020a). Low-temperature constructing N-doped graphite-like mesoporous structure biochar from furfural residue with urea for removal of chlortetracycline from wastewater and hydrothermal catalytic degradation mechanism. *Colloids and Surfaces A: Physicochemical and Engineering Aspects*, 600, 124873. <https://doi.org/10.1016/j.colsurfa.2020.124873>
- Chen, X., Yang, L., Myneni, S. C. B., & Deng, Y. (2019c). Leaching of polycyclic aromatic hydrocarbons (PAHs) from sewage sludge-derived biochar. *Chemical Engineering Journal*, 373, 840-845. <https://doi.org/10.1016/j.cej.2019.05.059>
- Chen, Y.-d., Wang, R., Duan, X., Wang, S., Ren, N.-q., & Ho, S.-H. (2020b). Production, properties, and catalytic applications of sludge derived biochar for environmental remediation. *Water Research*, 187, 116390. <https://doi.org/10.1016/j.watres.2020.116390>
- Cheng, H., Ji, R., Bian, Y., Jiang, X., & Song, Y. (2020a). From macroalgae to porous graphitized nitrogen-doped biochars – Using aquatic biota to treat polycyclic aromatic hydrocarbons-contaminated water. *Bioresource Technology*, 303, 122947. <https://doi.org/10.1016/j.biortech.2020.122947>
- Cheng, L., Ji, Y., Liu, X., Mu, L., & Zhu, J. (2021). Sorption mechanism of organic dyes on a novel self-nitrogen-doped porous graphite biochar: Coupling DFT calculations with experiments. *Chemical Engineering Science*, 242, 116739. <https://doi.org/10.1016/j.ces.2021.116739>
- Cheng, Y., Shiota, K., Kusakabe, T., Oshita, K., & Takaoka, M. (2020b). Characterizing the mechanisms of gas-phase elemental mercury adsorption with iodine-impregnated activated carbons using Brunauer-Emmett-Teller analysis, X-ray diffraction, X-ray photoelectron

- spectroscopy, and X-ray absorption near-edge structure analysis. *Chemical Engineering Journal*, 402, 126225. <https://doi.org/10.1016/j.cej.2020.126225>
- Cho, E.-J., Kang, J.-K., Moon, J.-K., Um, B.-H., Lee, C.-G., Jeong, S., & Park, S.-J. (2021). Removal of triclosan from aqueous solution via adsorption by kenaf-derived biochar: Its adsorption mechanism study via spectroscopic and experimental approaches. *Journal of Environmental Chemical Engineering*, 9(6), 106343. <https://doi.org/10.1016/j.jece.2021.106343>
- Chu, G., Zhao, J., Huang, Y., Zhou, D., Liu, Y., Wu, M., Peng, H., Zhao, Q., Pan, B., & Steinberg, C. E. W. (2018). Phosphoric acid pretreatment enhances the specific surface areas of biochars by generation of micropores. *Environmental Pollution*, 240, 1-9. <https://doi.org/10.1016/j.envpol.2018.04.003>
- Clark, K. A., & Pasternack, D. S. (1932). Hot Water Separation of Bitumen from Alberta Bituminous Sand. *Industrial and Engineering Chemistry*, 24(12), 1410-1416. <https://doi.org/10.1021/ie50276a016>
- Conde-Cid, M., Fernández-Calviño, D., Núñez-Delgado, A., Fernández-Sanjurjo, M. J., Arias-Estévez, M., & Álvarez-Rodríguez, E. (2020). Estimation of adsorption/desorption Freundlich's affinity coefficients for oxytetracycline and chlortetracycline from soil properties: Experimental data and pedotransfer functions. *Ecotoxicology and Environmental Safety*, 196, 110584. <https://doi.org/10.1016/j.ecoenv.2020.110584>
- Crittenden, J. C. (2012). *MWH's water treatment : principles and design* (3rd ed. / rev. by John C. Crittenden [and others]. ed.) [eBook]. John Wiley and Sons. <https://doi.org/10.1002/9781118131473>
- Crombie, K., Mašek, O., Sohi, S. P., Brownsort, P., & Cross, A. (2013). The effect of pyrolysis conditions on biochar stability as determined by three methods. *Gcb Bioenergy*, 5(2), 122-131. <https://doi.org/10.1111/gcbb.12030>
- Cybulak, M., Sokołowska, Z., Boguta, P., & Tomczyk, A. (2019). Influence of pH and grain size on physicochemical properties of biochar and released humic substances. *Fuel*, 240, 334-338. <https://doi.org/10.1016/j.fuel.2018.12.003>
- da Silva Souza, T., Lacerda, D., Aguiar, L. L., Martins, M. N. C., & Augusto de Oliveira David, J. (2020). Toxic potential of sewage sludge: Histopathological effects on soil and aquatic

- bioindicators. *Ecological Indicators*, *111*, 105980.  
<https://doi.org/10.1016/j.ecolind.2019.105980>
- Danish, M., & Ahmad, T. (2018). A review on utilization of wood biomass as a sustainable precursor for activated carbon production and application. *Renewable and Sustainable Energy Reviews*, *87*, 1-21. <https://doi.org/10.1016/j.rser.2018.02.003>
- de Boer, J. H., Lippens, B. C., Linsen, B. G., Broekhoff, J. C. P., van den Heuvel, A., & Osinga, T. J. (1966). The t-curve of multimolecular N<sub>2</sub>-adsorption. *Journal of Colloid and Interface Science*, *21*(4), 405-414. [https://doi.org/10.1016/0095-8522\(66\)90006-7](https://doi.org/10.1016/0095-8522(66)90006-7)
- De Gisi, S., Lofrano, G., Grassi, M., & Notarnicola, M. (2016). Characteristics and adsorption capacities of low-cost sorbents for wastewater treatment: A review. *Sustainable Materials and Technologies*, *9*, 10-40. <https://doi.org/10.1016/j.susmat.2016.06.002>
- de Jesus, J. H. F., da C. Cunha, G., Cardoso, E. M. C., Mangrich, A. S., & Romão, L. P. C. (2017). Evaluation of waste biomasses and their biochars for removal of polycyclic aromatic hydrocarbons. *Journal of Environmental Management*, *200*, 186-195. <https://doi.org/10.1016/j.jenvman.2017.05.084>
- Deng, X., Jiang, Y., Zhang, M. a., Nan, Z., Liang, X., & Wang, G. (2022). Sorption properties and mechanisms of erythromycin and ampicillin in loess soil: Roles of pH, ionic strength, and temperature. *Chemical Engineering Journal*, *434*, 134694. <https://doi.org/10.1016/j.cej.2022.134694>
- Ding, K., Zhou, X., Hadiatullah, H., Lu, Y., Zhao, G., Jia, S., Zhang, R., & Yao, Y. (2021). Removal performance and mechanisms of toxic hexavalent chromium (Cr(VI)) with ZnCl<sub>2</sub> enhanced acidic vinegar residue biochar. *Journal of Hazardous Materials*, *420*, 126551. <https://doi.org/10.1016/j.jhazmat.2021.126551>
- dos Reis, G. S., Guy, M., Mathieu, M., Jebrane, M., Lima, E. C., Thyrel, M., Dotto, G. L., & Larsson, S. H. (2022). A comparative study of chemical treatment by MgCl<sub>2</sub>, ZnSO<sub>4</sub>, ZnCl<sub>2</sub>, and KOH on physicochemical properties and acetaminophen adsorption performance of biobased porous materials from tree bark residues. *Colloids and Surfaces A: Physicochemical and Engineering Aspects*, *642*, 128626. <https://doi.org/10.1016/j.colsurfa.2022.128626>

- El-Naas, M. H., Surkatti, R., & Al-Zuhair, S. (2016). Petroleum refinery wastewater treatment: A pilot scale study. *Journal of Water Process Engineering*, 14, 71-76. <https://doi.org/10.1016/j.jwpe.2016.10.005>
- Enders, A., Hanley, K., Whitman, T., Joseph, S., & Lehmann, J. (2012). Characterization of biochars to evaluate recalcitrance and agronomic performance. *Bioresource Technology*, 114, 644-653. <https://doi.org/10.1016/j.biortech.2012.03.022>
- Entezari, I., Rivard, B., Geramian, M., & Lipsett, M. G. (2017). Predicting the abundance of clays and quartz in oil sands using hyperspectral measurements. *International Journal of Applied Earth Observation and Geoinformation*, 59, 1-8. <https://doi.org/10.1016/j.jag.2017.02.018>
- Fan, J., Li, Y., Yu, H., Li, Y., Yuan, Q., Xiao, H., Li, F., & Pan, B. (2020). Using sewage sludge with high ash content for biochar production and Cu(II) sorption. *Science of the Total Environment*, 713, 136663. <https://doi.org/10.1016/j.scitotenv.2020.136663>
- Fan, J., Zhang, J., Zhang, C., Ren, L., & Shi, Q. (2011). Adsorption of 2,4,6-trichlorophenol from aqueous solution onto activated carbon derived from loosestrife. *Desalination*, 267(2), 139-146. <https://doi.org/10.1016/j.desal.2010.09.016>
- Fang, Z., Huang, R., Chelme-Ayala, P., Shi, Q., Xu, C., & Gamal El-Din, M. (2019). Comparison of UV/Persulfate and UV/H<sub>2</sub>O<sub>2</sub> for the removal of naphthenic acids and acute toxicity towards *Vibrio fischeri* from petroleum production process water. *Science of the Total Environment*, 694, 133686. <https://doi.org/10.1016/j.scitotenv.2019.133686>
- Feng, D., Guo, D., Zhang, Y., Sun, S., Zhao, Y., Shang, Q., Sun, H., Wu, J., & Tan, H. (2020). Functionalized construction of biochar with hierarchical pore structures and surface O-/N-containing groups for phenol adsorption. *Chemical Engineering Journal*, 127707. <https://doi.org/10.1016/j.cej.2020.127707>
- Fernandes, A. N., Giovanella, M., Esteves, V. I., & Sierra, M. M. d. S. (2010). Elemental and spectral properties of peat and soil samples and their respective humic substances. *Journal of Molecular Structure*, 971(1), 33-38. <https://doi.org/10.1016/j.molstruc.2010.02.069>
- Foo, K. Y., & Hameed, B. H. (2010). Insights into the modeling of adsorption isotherm systems. *Chemical Engineering Journal*, 156(1), 2-10. <https://doi.org/10.1016/j.cej.2009.09.013>
- Frank, R. A., Kavanagh, R., Kent Burnison, B., Arsenault, G., Headley, J. V., Peru, K. M., Van Der Kraak, G., & Solomon, K. R. (2008). Toxicity assessment of collected fractions from

- an extracted naphthenic acid mixture. *Chemosphere*, 72(9), 1309-1314. <https://doi.org/10.1016/j.chemosphere.2008.04.078>
- Frank, R. A., Milestone, C. B., Rowland, S. J., Headley, J. V., Kavanagh, R. J., Lengger, S. K., Scarlett, A. G., West, C. E., Peru, K. M., & Hewitt, L. M. (2016). Assessing spatial and temporal variability of acid-extractable organics in oil sands process-affected waters. *Chemosphere*, 160, 303-313. <https://doi.org/10.1016/j.chemosphere.2016.06.093>
- Frankel, M. L., Bhuiyan, T. I., Veksha, A., Demeter, M. A., Layzell, D. B., Helleur, R. J., Hill, J. M., & Turner, R. J. (2016). Removal and biodegradation of naphthenic acids by biochar and attached environmental biofilms in the presence of co-contaminating metals. *Bioresource Technology*, 216, 352-361. <https://doi.org/10.1016/j.biortech.2016.05.084>
- Freundlich, H. (1906). *Über die Adsorption in Lösungen*. Wilhelm Engelmann.
- García-Zubiri, I. X., González-Gaitano, G., & Isasi, J. R. (2009). Sorption models in cyclodextrin polymers: Langmuir, Freundlich, and a dual-mode approach. *Journal of Colloid and Interface Science*, 337(1), 11-18. <https://doi.org/10.1016/j.jcis.2009.04.071>
- Genuino, D. A. D., de Luna, M. D. G., & Capareda, S. C. (2018). Improving the surface properties of municipal solid waste-derived pyrolysis biochar by chemical and thermal activation: Optimization of process parameters and environmental application. *Waste Management*, 72, 255-264. <https://doi.org/10.1016/j.wasman.2017.11.038>
- Gharedaghloo, B., & Price, J. S. (2021). Assessing benzene and toluene adsorption with peat depth: Implications on their fate and transport. *Environmental Pollution*, 274, 116477. <https://doi.org/10.1016/j.envpol.2021.116477>
- Godlewska, P., Siatecka, A., Kończak, M., & Oleszczuk, P. (2019). Adsorption capacity of phenanthrene and pyrene to engineered carbon-based adsorbents produced from sewage sludge or sewage sludge-biomass mixture in various gaseous conditions. *Bioresource Technology*, 280, 421-429. <https://doi.org/10.1016/j.biortech.2019.02.021>
- Government of Alberta. (2018). *Environmental Quality Guidelines for Alberta Surface Waters*.
- Government of Alberta. (2022). Oil sands facts and statistics. <https://www.alberta.ca/oil-sands-facts-and-statistics.aspx>



- Grewer, D. M., Young, R. F., Whittal, R. M., & Fedorak, P. M. (2010). Naphthenic acids and other acid-extractables in water samples from Alberta: What is being measured? *Science of the Total Environment*, 408(23), 5997-6010. <https://doi.org/10.1016/j.scitotenv.2010.08.013>
- Grube, M., Lin, J. G., Lee, P. H., & Kokorevicha, S. (2006). Evaluation of sewage sludge-based compost by FT-IR spectroscopy. *Geoderma*, 130(3), 324-333. <https://doi.org/10.1016/j.geoderma.2005.02.005>
- Guo, N., Lv, X., Yang, Q., Xu, X., & Song, H. (2021). Effective removal of hexavalent chromium from aqueous solution by ZnCl<sub>2</sub> modified biochar: Effects and response sequence of the functional groups. *Journal of Molecular Liquids*, 334, 116149. <https://doi.org/10.1016/j.molliq.2021.116149>
- Guo, W., Wang, S., Wang, Y., Lu, S., & Gao, Y. (2018). Sorptive removal of phenanthrene from aqueous solutions using magnetic and non-magnetic rice husk-derived biochars. *Royal Society Open Science*, 5(5), 172382. <https://doi.com/10.1098/rsos.172382>
- Gupta, V. K., Nayak, A., Agarwal, S., & Tyagi, I. (2014). Potential of activated carbon from waste rubber tire for the adsorption of phenolics: Effect of pre-treatment conditions. *Journal of Colloid and Interface Science*, 417, 420-430. <https://doi.org/10.1016/j.jcis.2013.11.067>
- Hagemann, N., Spokas, K., Schmidt, H.-P., Kägi, R., Böhler, M. A., & Bucheli, T. D. (2018). Activated Carbon, Biochar and Charcoal: Linkages and Synergies across Pyrogenic Carbon's ABCs. *Water*, 10(2), 182. <https://www.mdpi.com/2073-4441/10/2/182>
- Hairuddin, M. N., Mubarak, N. M., Khalid, M., Abdullah, E. C., Walvekar, R., & Karri, R. R. (2019). Magnetic palm kernel biochar potential route for phenol removal from wastewater. *Environmental Science and Pollution Research*, 26(34), 35183-35197. <https://doi.com/10.1007/s11356-019-06524-w>
- Hao, C., Headley, J. V., Peru, K. M., Frank, R., Yang, P., & Solomon, K. R. (2005). Characterization and pattern recognition of oil-sand naphthenic acids using comprehensive two-dimensional gas chromatography/time-of-flight mass spectrometry. *Journal of Chromatography A*, 1067(1), 277-284. <https://doi.org/10.1016/j.chroma.2005.01.041>
- Hao, Z., Wang, C., Yan, Z., Jiang, H., & Xu, H. (2018). Magnetic particles modification of coconut shell-derived activated carbon and biochar for effective removal of phenol from water. *Chemosphere*, 211, 962-969. <https://doi.org/10.1016/j.chemosphere.2018.08.038>

- Hendges, L. T., Costa, T. C., Temochko, B., Gómez González, S. Y., Mazur, L. P., Marinho, B. A., da Silva, A., Weschenfelder, S. E., de Souza, A. A. U., & de Souza, S. M. A. G. U. (2021). Adsorption and desorption of water-soluble naphthenic acid in simulated offshore oilfield produced water. *Process Safety and Environmental Protection*, 145, 262-272. <https://doi.org/10.1016/j.psep.2020.08.018>
- Ho, Y. S., & McKay, G. (1999). Pseudo-second order model for sorption processes. *Process Biochemistry*, 34(5), 451-465. [https://doi.org/10.1016/S0032-9592\(98\)00112-5](https://doi.org/10.1016/S0032-9592(98)00112-5)
- Hsieh, C.-T., & Teng, H. (2000). Influence of mesopore volume and adsorbate size on adsorption capacities of activated carbons in aqueous solutions. *Carbon*, 38(6), 863-869. [https://doi.org/10.1016/S0008-6223\(99\)00180-3](https://doi.org/10.1016/S0008-6223(99)00180-3)
- Hu, H., & Xu, K. (2020). Chapter 8 - Physicochemical technologies for HRP and risk control. In H. Ren & X. Zhang (Eds.), *High-Risk Pollutants in Wastewater* (pp. 169-207). Elsevier. <https://doi.org/10.1016/B978-0-12-816448-8.00008-3>
- Huang, R., Chelme-Ayala, P., Zhang, Y., Changalov, M., & Gamal El-Din, M. (2017). Investigation of dissociation constants for individual and total naphthenic acids species using ultra performance liquid chromatography ion mobility time-of-flight mass spectrometry analysis. *Chemosphere*, 184, 738-746. <https://doi.org/10.1016/j.chemosphere.2017.06.067>
- Huang, R., Chen, Y., Meshref, M. N. A., Chelme-Ayala, P., Dong, S., Ibrahim, M. D., Wang, C., Klammerth, N., Hughes, S. A., Headley, J. V., Peru, K. M., Brown, C., Mahaffey, A., & Gamal El-Din, M. (2018). Characterization and determination of naphthenic acids species in oil sands process-affected water and groundwater from oil sands development area of Alberta, Canada. *Water Research*, 128, 129-137. <https://doi.org/10.1016/j.watres.2017.10.003>
- Huang, R., McPhedran, K. N., & Gamal El-Din, M. (2015a). Ultra Performance Liquid Chromatography Ion Mobility Time-of-Flight Mass Spectrometry Characterization of Naphthenic Acids Species from Oil Sands Process-Affected Water. *Environmental Science & Technology*, 49(19), 11737-11745. <https://doi.org/10.1021/acs.est.5b03178>
- Huang, R., Sun, N., Chelme-Ayala, P., McPhedran, K. N., Changalov, M., & Gamal El-Din, M. (2015b). Fractionation of oil sands-process affected water using pH-dependent extractions:

- A study of dissociation constants for naphthenic acids species. *Chemosphere*, 127, 291-296. <https://doi.org/10.1016/j.chemosphere.2014.11.041>
- Huang, R., Yang, L., How, Z. T., Fang, Z., Bekele, A., Letinski, D. J., Redman, A. D., & Gamal El-Din, M. (2021). Characterization of raw and ozonated oil sands process water utilizing atmospheric pressure gas chromatography time-of-flight mass spectrometry combined with solid phase microextractionun. *Chemosphere*, 266, 129017. <https://doi.org/10.1016/j.chemosphere.2020.129017>
- Hughes, S. A., Mahaffey, A., Shore, B., Baker, J., Kilgour, B., Brown, C., Peru, K. M., Headley, J. V., & Bailey, H. C. (2017). Using ultrahigh-resolution mass spectrometry and toxicity identification techniques to characterize the toxicity of oil sands process-affected water: The case for classical naphthenic acids. *Environmental Toxicology and Chemistry*, 36(11), 3148-3157. <https://doi.org/10.1002/etc.3892>
- Iranmanesh, S., Harding, T., Abedi, J., Seyedeyn-Azad, F., & Layzell, D. B. (2014). Adsorption of naphthenic acids on high surface area activated carbons. *Journal of Environmental Science and Health, Part A*, 49(8), 913-922. <https://doi.org/10.1080/10934529.2014.894790>
- Islam, M. S., Kwak, J.-H., Nzediegwu, C., Wang, S., Palansuriya, K., Kwon, E. E., Naeth, M. A., El-Din, M. G., Ok, Y. S., & Chang, S. X. (2021). Biochar heavy metal removal in aqueous solution depends on feedstock type and pyrolysis purging gas. *Environmental Pollution*, 281, 117094. <https://doi.org/10.1016/j.envpol.2021.117094>
- Islam, M. S., McPhedran, K. N., Messele, S. A., Liu, Y., & Gamal El-Din, M. (2018). Isotherm and kinetic studies on adsorption of oil sands process-affected water organic compounds using granular activated carbon. *Chemosphere*, 202, 716-725. <https://doi.org/10.1016/j.chemosphere.2018.03.149>
- Islam, M. S., Zhang, Y., McPhedran, K. N., Liu, Y., & Gamal El-Din, M. (2015). Granular activated carbon for simultaneous adsorption and biodegradation of toxic oil sands process-affected water organic compounds. *Journal of Environmental Management*, 152, 49-57. <https://doi.org/10.1016/j.jenvman.2015.01.020>
- Islam, M. S., Zhang, Y., McPhedran, K. N., Liu, Y., & Gamal El-Din, M. (2016). Mechanistic investigation of industrial wastewater naphthenic acids removal using granular activated

- carbon (GAC) biofilm based processes. *Science of the Total Environment*, 541, 238-246. <https://doi.org/10.1016/j.scitotenv.2015.09.091>
- IUPAC. (1982). Reporting Physisorption Data for Gas/Solid Systems (*Handbook of Heterogeneous Catalysis* (Vol. 54, pp. 2201-2218). Pure and Applied Chemistry. <https://doi.org/https://doi.org/10.1002/9783527610044.hetcat0065>
- Jafarinejad, S. (2017). 2 - Pollutions and Wastes From the Petroleum Industry. In S. Jafarinejad (Ed.), *Petroleum Waste Treatment and Pollution Control* (pp. 19-83). Butterworth-Heinemann. <https://doi.org/https://doi.org/10.1016/B978-0-12-809243-9.00002-X>
- Janfada, A., Headley, J. V., Peru, K. M., & Barbour, S. L. (2006). A Laboratory Evaluation of the Sorption of Oil Sands Naphthenic Acids on Organic Rich Soils. *Journal of Environmental Science and Health, Part A*, 41(6), 985-997. <https://doi.org/10.1080/10934520600620105>
- Jang, H. M., Yoo, S., Choi, Y.-K., Park, S., & Kan, E. (2018). Adsorption isotherm, kinetic modeling and mechanism of tetracycline on Pinus taeda-derived activated biochar. *Bioresource Technology*, 259, 24-31. <https://doi.org/10.1016/j.biortech.2018.03.013>
- Jerez, S., Ventura, M., Molina, R., Pariente, M. I., Martínez, F., & Melero, J. A. (2021). Comprehensive characterization of an oily sludge from a petrol refinery: A step forward for its valorization within the circular economy strategy. *Journal of Environmental Management*, 285, 112124. <https://doi.org/10.1016/j.jenvman.2021.112124>
- Jieying, Z., Zhao, Q., & Ye, Z. (2014). Preparation and characterization of activated carbon fiber (ACF) from cotton woven waste. *Applied Surface Science*, 299, 86-91. <https://doi.org/10.1016/j.apsusc.2014.01.190>
- Jing, X.-R., Wang, Y.-Y., Liu, W.-J., Wang, Y.-K., & Jiang, H. (2014). Enhanced adsorption performance of tetracycline in aqueous solutions by methanol-modified biochar. *Chemical Engineering Journal*, 248, 168-174. <https://doi.org/10.1016/j.cej.2014.03.006>
- Karmacharya, M. S., Gupta, V. K., Tyagi, I., Agarwal, S., & Jha, V. K. (2016). Removal of As(III) and As(V) using rubber tire derived activated carbon modified with alumina composite. *Journal of Molecular Liquids*, 216, 836-844. <https://doi.org/10.1016/j.molliq.2016.02.025>
- Kazemi Shariat Panahi, H., Dehghani, M., Ok, Y. S., Nizami, A.-S., Khoshnevisan, B., Mussatto, S. I., Aghbashlo, M., Tabatabaei, M., & Lam, S. S. (2020). A comprehensive review of

- engineered biochar: Production, characteristics, and environmental applications. *Journal of Cleaner Production*, 270, 122462. <https://doi.org/10.1016/j.jclepro.2020.122462>
- Kiskira, K., Papirio, S., Mascolo, M. C., Fourdrin, C., Pechaud, Y., van Hullebusch, E. D., & Esposito, G. (2019). Mineral characterization of the biogenic Fe(III)(hydr)oxides produced during Fe(II)-driven denitrification with Cu, Ni and Zn. *Science of the Total Environment*, 687, 401-412. <https://doi.org/10.1016/j.scitotenv.2019.06.107>
- Kong, L., Xiong, Y., Sun, L., Tian, S., Xu, X., Zhao, C., Luo, R., Yang, X., Shih, K., & Liu, H. (2014). Sorption performance and mechanism of a sludge-derived char as porous carbon-based hybrid adsorbent for benzene derivatives in aqueous solution. *Journal of Hazardous Materials*, 274, 205-211. <https://doi.org/10.1016/j.jhazmat.2014.04.014>
- Kumar, A., & Jena, H. M. (2016). Removal of methylene blue and phenol onto prepared activated carbon from Fox nutshell by chemical activation in batch and fixed-bed column. *Journal of Cleaner Production*, 137, 1246-1259. <https://doi.org/10.1016/j.jclepro.2016.07.177>
- Kumar, A., & Mohan Jena, H. (2015). High surface area microporous activated carbons prepared from Fox nut (*Euryale ferox*) shell by zinc chloride activation. *Applied Surface Science*, 356, 753-761. <https://doi.org/10.1016/j.apsusc.2015.08.074>
- Kumar, A., Saini, K., & Bhaskar, T. (2020). Hydrochar and biochar: Production, physicochemical properties and techno-economic analysis. *Bioresource Technology*, 310, 123442. <https://doi.org/10.1016/j.biortech.2020.123442>
- Kumari, U., Behera, S. K., Siddiqi, H., & Meikap, B. C. (2020). Facile method to synthesize efficient adsorbent from alumina by nitric acid activation: Batch scale defluoridation, kinetics, isotherm studies and implementation on industrial wastewater treatment. *Journal of Hazardous Materials*, 381, 120917. <https://doi.org/10.1016/j.jhazmat.2019.120917>
- Kwon, S., Fan, M., DaCosta, H. F. M., Russell, A. G., Berchtold, K. A., & Dubey, M. K. (2011). Chapter 10 - CO<sub>2</sub> Sorption. In D. A. Bell, B. F. Towler, & M. Fan (Eds.), *Coal Gasification and Its Applications* (pp. 293-339). William Andrew Publishing. <https://doi.org/10.1016/B978-0-8155-2049-8.10010-5>
- Lagergren, S. (1898). Zur theorie der sogenannten adsorption geloster stoffe.

- Lammers, K., Smith, M. M., & Carroll, S. A. (2017). Muscovite dissolution kinetics as a function of pH at elevated temperature. *Chemical Geology*, 466, 149-158. <https://doi.org/10.1016/j.chemgeo.2017.06.003>
- Langmuir, I. (1918). The adsorption of gases on plane surfaces of glass, mica and platinum. *Journal of the American Chemical Society*, 40(9), 1361-1403. <https://doi.org/10.1021/ja02242a004>
- Lawal, A. A., Hassan, M. A., Ahmad Farid, M. A., Tengku Yasim-Anuar, T. A., Samsudin, M. H., Mohd Yusoff, M. Z., Zakaria, M. R., Mokhtar, M. N., & Shirai, Y. (2021). Adsorption mechanism and effectiveness of phenol and tannic acid removal by biochar produced from oil palm frond using steam pyrolysis. *Environmental Pollution*, 269, 116197. <https://doi.org/10.1016/j.envpol.2020.116197>
- Lawal, A. A., Hassan, M. A., Ahmad Farid, M. A., Yasim-Anuar, T. A. T., Mohd Yusoff, M. Z., Zakaria, M. R., Roslan, A. M., Mokhtar, M. N., & Shirai, Y. (2020). One-step steam pyrolysis for the production of mesoporous biochar from oil palm frond to effectively remove phenol in facultatively treated palm oil mill effluent. *Environmental Technology & Innovation*, 18, 100730. <https://doi.org/10.1016/j.eti.2020.100730>
- Ledesma, B., Román, S., Álvarez-Murillo, A., Sabio, E., & González, J. F. (2014). Cyclic adsorption/thermal regeneration of activated carbons. *Journal of Analytical and Applied Pyrolysis*, 106, 112-117. <https://doi.org/10.1016/j.jaap.2014.01.007>
- Lehmann, J., & Joseph, S. (2015). *Biochar for environmental management: science, technology and implementation*. Routledge.
- Lei, C., Hu, Y.-y., & He, M.-z. (2013). Adsorption characteristics of triclosan from aqueous solution onto cetylpyridinium bromide (CPB) modified zeolites. *Chemical Engineering Journal*, 219, 361-370. <https://doi.org/10.1016/j.cej.2012.12.099>
- Lévesque, C. M. (2014). *Oil sands process water and tailings pond contaminant transport and fate : physical, chemical and biological processes*, [University of British Columbia]. <https://open.library.ubc.ca/collections/24/items/1.0165952>
- Li, C., Fu, L., Stafford, J., Belosevic, M., & Gamal El-Din, M. (2017). The toxicity of oil sands process-affected water (OSPW): A critical review. *Science of the Total Environment*, 601-602, 1785-1802. <https://doi.org/10.1016/j.scitotenv.2017.06.024>

- Li, D.-C., & Jiang, H. (2017). The thermochemical conversion of non-lignocellulosic biomass to form biochar: A review on characterizations and mechanism elucidation. *Bioresource Technology*, 246, 57-68. <https://doi.org/10.1016/j.biortech.2017.07.029>
- Li, F., Fang, X., Zhou, Z., Liao, X., Zou, J., Yuan, B., & Sun, W. (2019). Adsorption of perfluorinated acids onto soils: Kinetics, isotherms, and influences of soil properties. *Science of the Total Environment*, 649, 504-514. <https://doi.org/10.1016/j.scitotenv.2018.08.209>
- Li, G., Zhu, W., Zhang, C., Zhang, S., Liu, L., Zhu, L., & Zhao, W. (2016). Effect of a magnetic field on the adsorptive removal of methylene blue onto wheat straw biochar. *Bioresource Technology*, 206, 16-22. <https://doi.org/10.1016/j.biortech.2015.12.087>
- Li, X., Xu, J., Luo, X., & Shi, J. (2022). Efficient adsorption of dyes from aqueous solution using a novel functionalized magnetic biochar: Synthesis, kinetics, isotherms, adsorption mechanism, and reusability. *Bioresource Technology*, 360, 127526. <https://doi.org/10.1016/j.biortech.2022.127526>
- Li, Y., Hu, B., Gao, S., Tong, X., Jiang, L., Chen, X., An, S., & Zhang, F. (2020a). Comparison of 17 $\beta$ -estradiol adsorption on soil organic components and soil remediation agent-biochar. *Environmental Pollution*, 263, 114572. <https://doi.org/10.1016/j.envpol.2020.114572>
- Li, Y., Wei, M., Liu, L., Xue, Q., & Yu, B. (2020b). Adsorption of toluene on various natural soils: Influences of soil properties, mechanisms, and model. *Science of the Total Environment*, 740, 140104. <https://doi.org/10.1016/j.scitotenv.2020.140104>
- Li, Y., Xing, B., Ding, Y., Han, X., & Wang, S. (2020c). A critical review of the production and advanced utilization of biochar via selective pyrolysis of lignocellulosic biomass. *Bioresource Technology*, 312, 123614. <https://doi.org/10.1016/j.biortech.2020.123614>
- Li, Y.-h., Chang, F.-m., Huang, B., Song, Y.-p., Zhao, H.-y., & Wang, K.-j. (2020d). Activated carbon preparation from pyrolysis char of sewage sludge and its adsorption performance for organic compounds in sewage. *Fuel*, 266, 117053. <https://doi.org/10.1016/j.fuel.2020.117053>
- Liang, X., Liu, L., Jiang, Y., Nan, Z., Deng, X., Ma, F., Wang, G., & Wu, Y. (2022). Study of the sorption/desorption behavior of chlortetracycline on sediments in the upper reaches of the

- Yellow River. *Chemical Engineering Journal*, 428, 131958. <https://doi.org/10.1016/j.cej.2021.131958>
- Lin, L., Song, Z., Khan, Z. H., Liu, X., & Qiu, W. (2019). Enhanced As(III) removal from aqueous solution by Fe-Mn-La-impregnated biochar composites. *Science of the Total Environment*, 686, 1185-1193. <https://doi.org/10.1016/j.scitotenv.2019.05.480>
- Liou, T.-H. (2010). Development of mesoporous structure and high adsorption capacity of biomass-based activated carbon by phosphoric acid and zinc chloride activation. *Chemical Engineering Journal*, 158(2), 129-142. <https://doi.org/10.1016/j.cej.2009.12.016>
- Liu, B.-L., Li, Y.-W., Xie, L.-S., Guo, J.-J., Xiang, L., & Mo, C.-H. (2022). Sorption of microcystin-RR onto surface soils: Characteristics and influencing factors. *Journal of Hazardous Materials*, 431, 128571. <https://doi.org/10.1016/j.jhazmat.2022.128571>
- Liu, H., Xu, G., & Li, G. (2021). Preparation of porous biochar based on pharmaceutical sludge activated by NaOH and its application in the adsorption of tetracycline. *Journal of Colloid and Interface Science*, 587, 271-278. <https://doi.org/10.1016/j.jcis.2020.12.014>
- Liu, J., Jiang, X., Zhou, L., Han, X., & Cui, Z. (2009). Pyrolysis treatment of oil sludge and model-free kinetics analysis. *Journal of Hazardous Materials*, 161(2), 1208-1215. <https://doi.org/10.1016/j.jhazmat.2008.04.072>
- Liu, J., Wang, L., Tang, J., & Ma, J. (2016). Photocatalytic degradation of commercially sourced naphthenic acids by TiO<sub>2</sub>-graphene composite nanomaterial. *Chemosphere*, 149, 328-335. <https://doi.org/10.1016/j.chemosphere.2016.01.074>
- López-Vinent, N., Cruz-Alcalde, A., Ganiyu, S. O., Sable, S., Messele, S. A., Lillico, D., Stafford, J., Sans, C., Giménez, J., Esplugas, S., & Gamal El-Din, M. (2021). Coagulation-flocculation followed by catalytic ozonation processes for enhanced primary treatment during wet weather conditions. *Journal of Environmental Management*, 283, 111975. <https://doi.org/10.1016/j.jenvman.2021.111975>
- Lu, G. Q., Low, J. C. F., Liu, C. Y., & Lua, A. C. (1995). Surface area development of sewage sludge during pyrolysis. *Fuel*, 74(3), 344-348. [https://doi.org/10.1016/0016-2361\(95\)93465-P](https://doi.org/10.1016/0016-2361(95)93465-P)
- Luo, J., Li, X., Ge, C., Müller, K., Yu, H., Huang, P., Li, J., Tsang, D. C. W., Bolan, N. S., Rinklebe, J., & Wang, H. (2018). Sorption of norfloxacin, sulfamerazine and



- oxytetracycline by KOH-modified biochar under single and ternary systems. *Bioresource Technology*, 263, 385-392. <https://doi.org/10.1016/j.biortech.2018.05.022>
- Lütke, S. F., Igansi, A. V., Pegoraro, L., Dotto, G. L., Pinto, L. A. A., & Cadaval, T. R. S. (2019). Preparation of activated carbon from black wattle bark waste and its application for phenol adsorption. *Journal of Environmental Chemical Engineering*, 7(5), 103396. <https://doi.org/10.1016/j.jece.2019.103396>
- Lv, S., Li, C., Mi, J., & Meng, H. (2020). A functional activated carbon for efficient adsorption of phenol derived from pyrolysis of rice husk, KOH-activation and EDTA-4Na-modification. *Applied Surface Science*, 510, 145425. <https://doi.org/10.1016/j.apsusc.2020.145425>
- Ma, Y., Li, M., Li, P., Yang, L., Wu, L., Gao, F., Qi, X., & Zhang, Z. (2021). Hydrothermal synthesis of magnetic sludge biochar for tetracycline and ciprofloxacin adsorptive removal. *Bioresource Technology*, 319, 124199. <https://doi.org/10.1016/j.biortech.2020.124199>
- Ma, Y., Li, P., Yang, L., Wu, L., He, L., Gao, F., Qi, X., & Zhang, Z. (2020). Iron/zinc and phosphoric acid modified sludge biochar as an efficient adsorbent for fluoroquinolones antibiotics removal. *Ecotoxicology and Environmental Safety*, 196, 110550. <https://doi.org/10.1016/j.ecoenv.2020.110550>
- Madejová, J., Gates, W. P., & Petit, S. (2017). Chapter 5 - IR Spectra of Clay Minerals. In W. P. Gates, J. T. Kloprogge, J. Madejová, & F. Bergaya (Eds.), *Developments in Clay Science* (Vol. 8, pp. 107-149). Elsevier. <https://doi.org/https://doi.org/10.1016/B978-0-08-100355-8.00005-9>
- Mahaffey, A., & Dubé, M. (2017). Review of the composition and toxicity of oil sands process-affected water. *Environmental Reviews*, 25(1), 97-114. <https://doi.org/10.1139/er-2015-0060>
- Marentette, J. R., Frank, R. A., Bartlett, A. J., Gillis, P. L., Hewitt, L. M., Peru, K. M., Headley, J. V., Brunswick, P., Shang, D., & Parrott, J. L. (2015). Toxicity of naphthenic acid fraction components extracted from fresh and aged oil sands process-affected waters, and commercial naphthenic acid mixtures, to fathead minnow (*Pimephales promelas*) embryos. *Aquatic Toxicology*, 164, 108-117. <https://doi.org/10.1016/j.aquatox.2015.04.024>
- Martins, A. C., Pezoti, O., Cazetta, A. L., Bedin, K. C., Yamazaki, D. A. S., Bandoch, G. F. G., Asefa, T., Visentainer, J. V., & Almeida, V. C. (2015). Removal of tetracycline by NaOH-

- activated carbon produced from macadamia nut shells: Kinetic and equilibrium studies. *Chemical Engineering Journal*, 260, 291-299. <https://doi.org/10.1016/j.cej.2014.09.017>
- Mary, G. S., Sugumaran, P., Niveditha, S., Ramalakshmi, B., Ravichandran, P., & Seshadri, S. (2016). Production, characterization and evaluation of biochar from pod (*Pisum sativum*), leaf (*Brassica oleracea*) and peel (*Citrus sinensis*) wastes. *International Journal of Recycling of Organic Waste in Agriculture*, 5(1), 43-53. <https://doi.com/10.1007/s40093-016-0116-8>
- Medeiros, D. C. C. d. S., Nzediegwu, C., Benally, C., Messele, S. A., Kwak, J.-H., Naeth, M. A., Ok, Y. S., Chang, S. X., & Gamal El-Din, M. (2022). Pristine and engineered biochar for the removal of contaminants co-existing in several types of industrial wastewaters: A critical review. *Science of the Total Environment*, 809, 151120. <https://doi.org/10.1016/j.scitotenv.2021.151120>
- Meshref, M. N. A., Chelme-Ayala, P., & Gamal El-Din, M. (2017). Fate and abundance of classical and heteroatomic naphthenic acid species after advanced oxidation processes: Insights and indicators of transformation and degradation. *Water Research*, 125, 62-71. <https://doi.org/10.1016/j.watres.2017.08.007>
- Messele, S. A., Chelme-Ayala, P., & Gamal El-Din, M. (2021). Catalytic ozonation of naphthenic acids in the presence of carbon-based metal-free catalysts: Performance and kinetic study. *Catalysis Today*, 361, 102-108. <https://doi.org/10.1016/j.cattod.2020.01.042>
- Mishra, S., Yadav, S. S., Rawat, S., Singh, J., & Koduru, J. R. (2019). Corn husk derived magnetized activated carbon for the removal of phenol and para-nitrophenol from aqueous solution: Interaction mechanism, insights on adsorbent characteristics, and isothermal, kinetic and thermodynamic properties. *Journal of Environmental Management*, 246, 362-373. <https://doi.org/10.1016/j.jenvman.2019.06.013>
- Mohammed, N. A. S., Abu-Zurayk, R. A., Hamadneh, I., & Al-Dujaili, A. H. (2018). Phenol adsorption on biochar prepared from the pine fruit shells: Equilibrium, kinetic and thermodynamics studies. *Journal of Environmental Management*, 226, 377-385. <https://doi.org/10.1016/j.jenvman.2018.08.033>

- Mohanty, K., Das, D., & Biswas, M. N. (2005). Adsorption of phenol from aqueous solutions using activated carbons prepared from *Tectona grandis* sawdust by ZnCl<sub>2</sub> activation. *Chemical Engineering Journal*, 115(1), 121-131. <https://doi.org/10.1016/j.cej.2005.09.016>
- Morris, J. C., Weber, W. J., Supply, U. S. D. o. W., & Control, P. (1966). *Adsorption of Biochemically Resistant Materials from Solution: 2*. Federal Water Pollution Control Administration, Basic and Applied Sciences Program. <https://books.google.ca/books?id=nDFSAQAAMAAJ>
- Mubarik, S., Saeed, A., Athar, M. M., & Iqbal, M. (2016). Characterization and mechanism of the adsorptive removal of 2,4,6-trichlorophenol by biochar prepared from sugarcane baggase. *Journal of Industrial and Engineering Chemistry*, 33, 115-121. <https://doi.org/10.1016/j.jiec.2015.09.029>
- Mutavdžić Pavlović, D., Ćurković, L., Blažek, D., & Župan, J. (2014). The sorption of sulfamethazine on soil samples: Isotherms and error analysis. *Science of the Total Environment*, 497-498, 543-552. <https://doi.org/10.1016/j.scitotenv.2014.08.018>
- Natural Resources Canada. (2020). *Crude oil facts*. <https://www.nrcan.gc.ca/science-data/data-analysis/energy-data-analysis/energy-facts/crude-oil-facts/20064#L4>
- Negara, D. N. K. P., Nindhia, T. G. T., Surata, I. W., Hidajat, F., & Sucipta, M. (2019). Nanopore structures, surface morphology, and adsorption capacity of tabah bamboo-activated carbons. *Surfaces and Interfaces*, 16, 22-28. <https://doi.org/10.1016/j.surfin.2019.04.002>
- Nguyen, T.-B., Truong, Q.-M., Chen, C.-W., Doong, R.-a., Chen, W.-H., & Dong, C.-D. (2022). Mesoporous and adsorption behavior of algal biochar prepared via sequential hydrothermal carbonization and ZnCl<sub>2</sub> activation. *Bioresource Technology*, 346, 126351. <https://doi.org/10.1016/j.biortech.2021.126351>
- Niasar, H. S., Das, S., Xu, C., & Ray, M. B. (2019). Continuous column adsorption of naphthenic acids from synthetic and real oil sands process-affected water (OSPW) using carbon-based adsorbents. *Chemosphere*, 214, 511-518. <https://doi.org/10.1016/j.chemosphere.2018.09.078>
- Niasar, H. S., Li, H., Kasanneni, T. V. R., Ray, M. B., & Xu, C. (2016). Surface amination of activated carbon and petroleum coke for the removal of naphthenic acids and treatment of

- oil sands process-affected water (OSPW). *Chemical Engineering Journal*, 293, 189-199. <https://doi.org/10.1016/j.cej.2016.02.062>
- Nzediegwu, C., Arshad, M., Ulah, A., Naeth, M. A., & Chang, S. X. (2021a). Fuel, thermal and surface properties of microwave-pyrolyzed biochars depend on feedstock type and pyrolysis temperature. *Bioresource Technology*, 320, 124282. <https://doi.org/10.1016/j.biortech.2020.124282>
- Nzediegwu, C., Naeth, M. A., & Chang, S. X. (2021b). Carbonization temperature and feedstock type interactively affect chemical, fuel, and surface properties of hydrochars. *Bioresource Technology*, 330, 124976. <https://doi.org/10.1016/j.biortech.2021.124976>
- Nzediegwu, C., Naeth, M. A., & Chang, S. X. (2022). Effects of nitric acid modification on hydrochar's combustion, fuel and thermal properties are dependent on feedstock type. *Bioresource Technology*, 354, 127245. <https://doi.org/10.1016/j.biortech.2022.127245>
- Otieno, A. O., Home, P. G., Raude, J. M., Murunga, S. I., Ngumba, E., Ojwang, D. O., & Tuhkanen, T. (2021). Pineapple peel biochar and lateritic soil as adsorbents for recovery of ammonium nitrogen from human urine. *Journal of Environmental Management*, 293, 112794. <https://doi.org/10.1016/j.jenvman.2021.112794>
- Park, K.-H., Balathanigaimani, M. S., Shim, W.-G., Lee, J.-W., & Moon, H. (2010). Adsorption characteristics of phenol on novel corn grain-based activated carbons. *Microporous and Mesoporous Materials*, 127(1), 1-8. <https://doi.org/10.1016/j.micromeso.2009.06.032>
- Pei, Z.-g., Shan, X.-q., Liu, T., Xie, Y.-n., Wen, B., Zhang, S., & Khan, S. U. (2007). Effect of lead on the sorption of 2,4,6-trichlorophenol on soil and peat. *Environmental Pollution*, 147(3), 764-770. <https://doi.org/10.1016/j.envpol.2006.09.001>
- Peng, J., Headley, J. V., & Barbour, S. L. (2002). Adsorption of single-ring model naphthenic acids on soils. *Canadian Geotechnical Journal*, 39(6), 1419-1426. <https://doi.org/10.1139/t02-098>
- Peng, P., Lang, Y.-H., & Wang, X.-M. (2016). Adsorption behavior and mechanism of pentachlorophenol on reed biochars: pH effect, pyrolysis temperature, hydrochloric acid treatment and isotherms. *Ecological Engineering*, 90, 225-233. <https://doi.org/10.1016/j.ecoleng.2016.01.039>

- Pourrezaei, P., Alpatova, A., Chelme-Ayala, P., Perez-Estrada, L. A., Jensen-Fontaine, M., Le, X. C., & Gamal El-Din, M. (2014). Impact of petroleum coke characteristics on the adsorption of the organic fractions from oil sands process-affected water. *International Journal of Environmental Science and Technology*, *11*(7), 2037-2050. <https://doi.org/10.1007/s13762-013-0406-x>
- Prasannamedha, G., Kumar, P. S., Mehala, R., Sharumitha, T. J., & Surendhar, D. (2021). Enhanced adsorptive removal of sulfamethoxazole from water using biochar derived from hydrothermal carbonization of sugarcane bagasse. *Journal of Hazardous Materials*, *407*, 124825. <https://doi.org/10.1016/j.jhazmat.2020.124825>
- Qiao, K., Tian, W., Bai, J., Dong, J., Zhao, J., Gong, X., & Liu, S. (2018). Preparation of biochar from *Enteromorpha prolifera* and its use for the removal of polycyclic aromatic hydrocarbons (PAHs) from aqueous solution. *Ecotoxicology and Environmental Safety*, *149*, 80-87. <https://doi.org/10.1016/j.ecoenv.2017.11.027>
- Qisse, N., El Alouani, M., El Azzouzi, L., El Fadil, I., Saufi, H., Alaoui El Belghiti, M., Zrineh, A., & El Azzouzi, M. (2020). Adsorption of Imazalil herbicide onto Moroccan agricultural soils: Kinetic and isotherm adsorption studies. *Groundwater for Sustainable Development*, *11*, 100468. <https://doi.org/10.1016/j.gsd.2020.100468>
- Qiu, B., Shao, Q., Shi, J., Yang, C., & Chu, H. (2022). Application of biochar for the adsorption of organic pollutants from wastewater: Modification strategies, mechanisms and challenges. *Separation and Purification Technology*, *300*, 121925. <https://doi.org/10.1016/j.seppur.2022.121925>
- Qu, J., Wang, Y., Tian, X., Jiang, Z., Deng, F., Tao, Y., Jiang, Q., Wang, L., & Zhang, Y. (2021). KOH-activated porous biochar with high specific surface area for adsorptive removal of chromium (VI) and naphthalene from water: Affecting factors, mechanisms and reusability exploration. *Journal of Hazardous Materials*, *401*, 123292. <https://doi.org/10.1016/j.jhazmat.2020.123292>
- Qu, J., Yuan, Y., Zhang, X., Wang, L., Tao, Y., Jiang, Z., Yu, H., Dong, M., & Zhang, Y. (2022). Stabilization of lead and cadmium in soil by sulfur-iron functionalized biochar: Performance, mechanisms and microbial community evolution. *Journal of Hazardous Materials*, *425*, 127876. <https://doi.org/10.1016/j.jhazmat.2021.127876>

- Qu, J., Zhang, B., Tong, H., Liu, Y., Wang, S., Wei, S., Wang, L., Wang, Y., & Zhang, Y. (2023). High-efficiency decontamination of Pb(II) and tetracycline in contaminated water using ball-milled magnetic bone derived biochar. *Journal of Cleaner Production*, 385, 135683. <https://doi.org/10.1016/j.jclepro.2022.135683>
- Quinlan, P. J., & Tam, K. C. (2015). Water treatment technologies for the remediation of naphthenic acids in oil sands process-affected water. *Chemical Engineering Journal*, 279, 696-714. <https://doi.org/10.1016/j.cej.2015.05.062>
- Radelyuk, I., Tussupova, K., Zhapargazinova, K., Yelubay, M., & Persson, M. (2019). Pitfalls of Wastewater Treatment in Oil Refinery Enterprises in Kazakhstan—A System Approach. *Sustainability*, 11(6). <https://doi.org/10.3390/su11061618>
- Rajapaksha, A. U., Vithanage, M., Ahmad, M., Seo, D.-C., Cho, J.-S., Lee, S.-E., Lee, S. S., & Ok, Y. S. (2015). Enhanced sulfamethazine removal by steam-activated invasive plant-derived biochar. *Journal of Hazardous Materials*, 290, 43-50. <https://doi.org/10.1016/j.jhazmat.2015.02.046>
- Rao, L., Luo, J., Zhou, W., Zou, Z., Tang, L., & Li, B. (2020). Adsorption–desorption behavior of benzobicyclon hydrolysate in different agricultural soils in China. *Ecotoxicology and Environmental Safety*, 202, 110915. <https://doi.org/10.1016/j.ecoenv.2020.110915>
- Rashed, Y., Messele, S. A., Zeng, H., & Gamal El-Din, M. (2020). Mesoporous carbon xerogel material for the adsorption of model naphthenic acids: structure effect and kinetics modelling. *Environmental Technology*, 41(27), 3534-3543. <https://doi.org/10.1080/09593330.2019.1615130>
- Rayment, G. E., & Lyons, D. J. (2011). *Soil chemical methods. [electronic resource] : Australasia*. CSIRO Pub. <https://doi.org/10.1071/9780643101364>
- Redman, A. D., Butler, J. D., Letinski, D. J., Di Toro, D. M., Leon Paumen, M., & Parkerton, T. F. (2018). Technical basis for using passive sampling as a biomimetic extraction procedure to assess bioavailability and predict toxicity of petroleum substances. *Chemosphere*, 199, 585-594. <https://doi.org/10.1016/j.chemosphere.2018.02.024>
- Regkouzas, P., & Diamadopoulou, E. (2019). Adsorption of selected organic micro-pollutants on sewage sludge biochar. *Chemosphere*, 224, 840-851. <https://doi.org/10.1016/j.chemosphere.2019.02.165>

- Ren, L., Zhang, J., Li, Y., & Zhang, C. (2011). Preparation and evaluation of cattail fiber-based activated carbon for 2,4-dichlorophenol and 2,4,6-trichlorophenol removal. *Chemical Engineering Journal*, 168(2), 553-561. <https://doi.org/10.1016/j.cej.2011.01.021>
- Rezanezhad, F., Price, J. S., & Craig, J. R. (2012). The effects of dual porosity on transport and retardation in peat: A laboratory experiment. *Canadian Journal of Soil Science*, 92(5), 723-732. <https://doi.org/10.4141/cjss2011-050>
- Roccaro, P., Lombardo, G., & Vagliasindi, F. G. A. (2015). Offline bioregeneration of spent activated carbon loaded with real Produced Water and its adsorption capacity for benzene and toluene. *Desalination and Water Treatment*, 55(3), 756-766. <https://doi.org/10.1080/19443994.2014.964328>
- Rodrigues, L. A., da Silva, M. L. C. P., Alvarez-Mendes, M. O., Coutinho, A. d. R., & Thim, G. P. (2011). Phenol removal from aqueous solution by activated carbon produced from avocado kernel seeds. *Chemical Engineering Journal*, 174(1), 49-57. <https://doi.org/10.1016/j.cej.2011.08.027>
- Rodríguez-Liévana, J. A., & Peña, A. (2020). Differences in the sorption kinetics of various non-ionisable pesticides in a limited number of agricultural soils from the Mediterranean basin. *Journal of Environmental Management*, 276, 111336. <https://doi.org/10.1016/j.jenvman.2020.111336>
- Rogers, V. V., Wickstrom, M., Liber, K., & MacKinnon, M. D. (2002). Acute and Subchronic Mammalian Toxicity of Naphthenic Acids from Oil Sands Tailings. *Toxicological Sciences*, 66(2), 347-355. <https://doi.org/10.1093/toxsci/66.2.347>
- Russell, J. D., & Fraser, A. R. (1994). Infrared methods. In M. J. Wilson (Ed.), *Clay Mineralogy: Spectroscopic and Chemical Determinative Methods* (pp. 11-67). Springer Netherlands. [https://doi.org/10.1007/978-94-011-0727-3\\_2](https://doi.org/10.1007/978-94-011-0727-3_2)
- Ruthven, D. M. (1984). *Principles of adsorption and adsorption processes*. John Wiley & Sons.
- Samara, F., Khamis, M., Sara, Z., & Elsayed, Y. (2017). Removal of benzo (a) anthracene from water using a novel UAE sludge-based activated adsorbent. *Desalination and Water Treatment*, 1-8. <https://doi.org/10.5004/dwt.2017.21422>
- Scarlett, A. G., Reinardy, H. C., Henry, T. B., West, C. E., Frank, R. A., Hewitt, L. M., & Rowland, S. J. (2013). Acute toxicity of aromatic and non-aromatic fractions of naphthenic acids

- extracted from oil sands process-affected water to larval zebrafish. *Chemosphere*, 93(2), 415-420. <https://doi.org/10.1016/j.chemosphere.2013.05.020>
- Schwarzenbach, R., Gschwend, P., & Imboden, D. (2005). Sorption I: General Introduction and Sorption Processes Involving Organic Matter ((pp. 275-330). <https://doi.org/10.1002/0471649643.ch9>
- Shabir, F., Sultan, M., Miyazaki, T., Saha, B. B., Askalany, A., Ali, I., Zhou, Y., Ahmad, R., & Shamshiri, R. R. (2020). Recent updates on the adsorption capacities of adsorbent-adsorbate pairs for heat transformation applications. *Renewable and Sustainable Energy Reviews*, 119, 109630. <https://doi.org/10.1016/j.rser.2019.109630>
- Shaheen, S. M., Tsadilas, C. D., & Rinklebe, J. (2013). A review of the distribution coefficients of trace elements in soils: Influence of sorption system, element characteristics, and soil colloidal properties. *Advances in Colloid and Interface Science*, 201-202, 43-56. <https://doi.org/10.1016/j.cis.2013.10.005>
- Shen, Y., Zhou, Y., Fu, Y., & Zhang, N. (2020). Activated carbons synthesized from unaltered and pelletized biomass wastes for bio-tar adsorption in different phases. *Renewable Energy*, 146, 1700-1709. <https://doi.org/10.1016/j.renene.2019.07.167>
- Shi, Q., Li, A., Zhu, Z., & Liu, B. (2013). Adsorption of naphthalene onto a high-surface-area carbon from waste ion exchange resin. *Journal of Environmental Sciences*, 25(1), 188-194. [https://doi.org/10.1016/S1001-0742\(12\)60017-5](https://doi.org/10.1016/S1001-0742(12)60017-5)
- Singh, N., & Balomajumder, C. (2016). Simultaneous removal of phenol and cyanide from aqueous solution by adsorption onto surface modified activated carbon prepared from coconut shell. *Journal of Water Process Engineering*, 9, 233-245. <https://doi.org/10.1016/j.jwpe.2016.01.008>
- Singh, R., Naik, D. V., Dutta, R. K., & Kanaujia, P. K. (2020). Biochars for the removal of naphthenic acids from water: A prospective approach towards remediation of petroleum refinery wastewater. *Journal of Cleaner Production*, 266, 121986. <https://doi.org/10.1016/j.jclepro.2020.121986>
- Smaranda, C., Popescu, M.-C., Bulgariu, D., Măluțan, T., & Gavrilăscu, M. (2017). Adsorption of organic pollutants onto a Romanian soil: Column dynamics and transport. *Process Safety and Environmental Protection*, 108, 108-120. <https://doi.org/10.1016/j.psep.2016.06.027>



- Speight, J. G. (2013). Chapter 3 - Oil Sand Mining. In J. G. Speight (Ed.), *Oil Sand Production Processes* (pp. 59-79). Gulf Professional Publishing. <https://doi.org/10.1016/B978-0-12-404572-9.00003-6>
- Spokas, K. A. (2010). Review of the stability of biochar in soils: predictability of O:C molar ratios. *Carbon Management*, 1(2), 289-303. <https://doi.org/10.4155/cmt.10.32>
- Statistics Canada. (2021). *Table 38-10-0271-01 Potable water use by sector and average daily use*. <https://doi.org/10.25318/3810027101-eng>
- Suara, M. A., Ganiyu, S. O., Paul, S., Stafford, J. L., & Gamal El-Din, M. (2022). Solar-activated zinc oxide photocatalytic treatment of real oil sands process water: Effect of treatment parameters on naphthenic acids, polyaromatic hydrocarbons and acute toxicity removal. *Science of the Total Environment*, 819, 153029. <https://doi.org/10.1016/j.scitotenv.2022.153029>
- Sullivan, G. L., Prigmore, R. M., Knight, P., & Godfrey, A. R. (2019). Activated carbon biochar from municipal waste as a sorptive agent for the removal of polyaromatic hydrocarbons (PAHs), phenols and petroleum based compounds in contaminated liquids. *Journal of Environmental Management*, 251, 109551. <https://doi.org/10.1016/j.jenvman.2019.109551>
- Sun, N., Chelme-Ayala, P., Klamerth, N., McPhedran, K. N., Islam, M. S., Perez-Estrada, L., Drzewicz, P., Blunt, B. J., Reichert, M., Hagen, M., Tierney, K. B., Belosevic, M., & Gamal El-Din, M. (2014). Advanced Analytical Mass Spectrometric Techniques and Bioassays to Characterize Untreated and Ozonated Oil Sands Process-Affected Water. *Environmental Science & Technology*, 48(19), 11090-11099. <https://doi.org/10.1021/es503082j>
- Swenson, H., & Stadie, N. P. (2019). Langmuir's Theory of Adsorption: A Centennial Review. *Langmuir*, 35(16), 5409-5426. <https://doi.org/10.1021/acs.langmuir.9b00154>
- Tang, L., Gudda, F. O., Wu, C., Ling, W., El-Ramady, H., Mosa, A., & Wang, J. (2022). Contributions of partition and adsorption to polycyclic aromatic hydrocarbons sorption by fractionated soil at different particle sizes. *Chemosphere*, 301, 134715. <https://doi.org/10.1016/j.chemosphere.2022.134715>

- Thang, P. Q., Jitae, K., Giang, B. L., Viet, N. M., & Huong, P. T. (2019). Potential application of chicken manure biochar towards toxic phenol and 2,4-dinitrophenol in wastewaters. *Journal of Environmental Management*, 251, 109556. <https://doi.org/10.1016/j.jenvman.2019.109556>
- Tomczyk, B., Siatecka, A., Jędruchiewicz, K., Sochacka, A., Bogusz, A., & Oleszczuk, P. (2020). Polycyclic aromatic hydrocarbons (PAHs) persistence, bioavailability and toxicity in sewage sludge- or sewage sludge-derived biochar-amended soil. *Science of the Total Environment*, 747, 141123. <https://doi.org/10.1016/j.scitotenv.2020.141123>
- Tran, H. N., Lima, E. C., Juang, R.-S., Bollinger, J.-C., & Chao, H.-P. (2021). Thermodynamic parameters of liquid-phase adsorption process calculated from different equilibrium constants related to adsorption isotherms: A comparison study. *Journal of Environmental Chemical Engineering*, 9(6), 106674. <https://doi.org/10.1016/j.jece.2021.106674>
- Tran, H. N., Wang, Y.-F., You, S.-J., & Chao, H.-P. (2017). Insights into the mechanism of cationic dye adsorption on activated charcoal: The importance of  $\pi$ - $\pi$  interactions. *Process Safety and Environmental Protection*, 107, 168-180. <https://doi.org/10.1016/j.psep.2017.02.010>
- Tseng, R.-L., Wu, F.-C., & Juang, R.-S. (2003). Liquid-phase adsorption of dyes and phenols using pinewood-based activated carbons. *Carbon*, 41(3), 487-495. [https://doi.org/10.1016/S0008-6223\(02\)00367-6](https://doi.org/10.1016/S0008-6223(02)00367-6)
- Turner, N. H. (1975). Kinetics of chemisorption: An examination of the Elovich equation. *Journal of Catalysis*, 36(3), 262-265. [https://doi.org/10.1016/0021-9517\(75\)90035-4](https://doi.org/10.1016/0021-9517(75)90035-4)
- Uçar, S., Erdem, M., Tay, T., & Karagöz, S. (2009). Preparation and characterization of activated carbon produced from pomegranate seeds by ZnCl<sub>2</sub> activation. *Applied Surface Science*, 255(21), 8890-8896. <https://doi.org/10.1016/j.apsusc.2009.06.080>
- Ullah, F., Ji, G., Irfan, M., Gao, Y., Shafiq, F., Sun, Y., Ain, Q. U., & Li, A. (2022). Adsorption performance and mechanism of cationic and anionic dyes by KOH activated biochar derived from medical waste pyrolysis. *Environmental Pollution*, 314, 120271. <https://doi.org/10.1016/j.envpol.2022.120271>
- Vaughn, S. F., Kenar, J. A., Eller, F. J., Moser, B. R., Jackson, M. A., & Peterson, S. C. (2015). Physical and chemical characterization of biochars produced from coppiced wood of

- thirteen tree species for use in horticultural substrates. *Industrial Crops and Products*, 66, 44-51. <https://doi.org/10.1016/j.indcrop.2014.12.026>
- Vimonses, V., Lei, S., Jin, B., Chow, C. W. K., & Saint, C. (2009). Kinetic study and equilibrium isotherm analysis of Congo Red adsorption by clay materials. *Chemical Engineering Journal*, 148(2), 354-364. <https://doi.org/10.1016/j.cej.2008.09.009>
- Volkov, D. S., Rogova, O. B., & Proskurnin, M. A. (2021). Organic Matter and Mineral Composition of Silicate Soils: FTIR Comparison Study by Photoacoustic, Diffuse Reflectance, and Attenuated Total Reflection Modalities. *Agronomy*, 11(9). <https://doi.org/10.3390/agronomy11091879>
- Wang, C., Alpatova, A., McPhedran, K. N., & Gamal El-Din, M. (2015). Coagulation/flocculation process with polyaluminum chloride for the remediation of oil sands process-affected water: Performance and mechanism study. *Journal of Environmental Management*, 160, 254-262. <https://doi.org/10.1016/j.jenvman.2015.06.025>
- Wang, F., Sun, H., Ren, X., & Zhang, K. (2017a). Sorption of naphthalene and its hydroxyl substitutes onto biochars in single-solute and bi-solute systems with propranolol as the co-solute. *Chemical Engineering Journal*, 326, 281-291. <https://doi.org/10.1016/j.cej.2017.05.159>
- Wang, J., & Guo, X. (2020). Adsorption isotherm models: Classification, physical meaning, application and solving method. *Chemosphere*, 258, 127279. <https://doi.org/10.1016/j.chemosphere.2020.127279>
- Wang, L., Bolan, N. S., Tsang, D. C. W., & Hou, D. (2020). Green immobilization of toxic metals using alkaline enhanced rice husk biochar: Effects of pyrolysis temperature and KOH concentration. *Science of the Total Environment*, 720, 137584. <https://doi.org/10.1016/j.scitotenv.2020.137584>
- Wang, L., Olsen, M. N. P., Moni, C., Dieguez-Alonso, A., de la Rosa, J. M., Stenrød, M., Liu, X., & Mao, L. (2022). Comparison of properties of biochar produced from different types of lignocellulosic biomass by slow pyrolysis at 600 °C. *Applications in Energy and Combustion Science*, 12, 100090. <https://doi.org/10.1016/j.jaecs.2022.100090>
- Wang, P., Tang, L., Wei, X., Zeng, G., Zhou, Y., Deng, Y., Wang, J., Xie, Z., & Fang, W. (2017b). Synthesis and application of iron and zinc doped biochar for removal of p-nitrophenol in

- wastewater and assessment of the influence of co-existed Pb(II). *Applied Surface Science*, 392, 391-401. <https://doi.org/10.1016/j.apsusc.2016.09.052>
- Wang, Y., Jiang, B., Wang, L., Feng, Z., Fan, H., & Sun, T. (2021). Hierarchically structured two-dimensional magnetic microporous biochar derived from hazelnut shell toward effective removal of p-arsanilic acid. *Applied Surface Science*, 540, 148372. <https://doi.org/10.1016/j.apsusc.2020.148372>
- Wang, Y., Qiu, L., Zhu, M., Sun, G., Zhang, T., & Kang, K. (2019). Comparative Evaluation of Hydrothermal Carbonization and Low Temperature Pyrolysis of *Eucommia ulmoides* Oliver for the Production of Solid Biofuel. *Scientific Reports*, 9(1), 5535. <https://doi.org/10.1038/s41598-019-38849-4>
- Wang, Z., Han, L., Sun, K., Jin, J., Ro, K. S., Libra, J. A., Liu, X., & Xing, B. (2016). Sorption of four hydrophobic organic contaminants by biochars derived from maize straw, wood dust and swine manure at different pyrolytic temperatures. *Chemosphere*, 144, 285-291. <https://doi.org/10.1016/j.chemosphere.2015.08.042>
- Wei, C., Song, X., Wang, Q., & Hu, Z. (2017). Sorption kinetics, isotherms and mechanisms of PFOS on soils with different physicochemical properties. *Ecotoxicology and Environmental Safety*, 142, 40-50. <https://doi.org/10.1016/j.ecoenv.2017.03.040>
- Whale, G. F., Hjort, M., Di Paolo, C., Redman, A. D., Postma, J. F., Legradi, J., & Leonards, P. E. G. (2022). Assessment of oil refinery wastewater and effluent integrating bioassays, mechanistic modelling and bioavailability evaluation. *Chemosphere*, 287, 132146. <https://doi.org/10.1016/j.chemosphere.2021.132146>
- Worch, E. (2012). *Adsorption Technology in Water Treatment*. De Gruyter. <https://doi.org/10.1515/9783110240238>
- Wu, C., De Visscher, A., & Gates, I. D. (2019). On naphthenic acids removal from crude oil and oil sands process-affected water. *Fuel*, 253, 1229-1246. <https://doi.org/10.1016/j.fuel.2019.05.091>
- Wu, J., Yang, J., Feng, P., Wen, L., Huang, G., Xu, C., & Lin, B. (2022a). Highly efficient and ultra-rapid adsorption of malachite green by recyclable crab shell biochar. *Journal of Industrial and Engineering Chemistry*, 113, 206-214. <https://doi.org/10.1016/j.jiec.2022.05.047>

- Wu, L., Li, B., & Liu, M. (2018). Influence of aromatic structure and substitution of carboxyl groups of aromatic acids on their sorption to biochars. *Chemosphere*, 210, 239-246. <https://doi.org/10.1016/j.chemosphere.2018.07.003>
- Wu, Q., Zhang, Y., Cui, M.-h., Liu, H., Liu, H., Zheng, Z., Zheng, W., Zhang, C., & Wen, D. (2022b). Pyrolyzing pharmaceutical sludge to biochar as an efficient adsorbent for deep removal of fluoroquinolone antibiotics from pharmaceutical wastewater: Performance and mechanism. *Journal of Hazardous Materials*, 426, 127798. <https://doi.org/10.1016/j.jhazmat.2021.127798>
- Wu, W., Miao, G., Yan, X., Xing, B., & Yang, K. (2020). Correlations and prediction of adsorption capacity and affinity of aromatic compounds on activated carbons. *Science of the Total Environment*, 704, 135457. <https://doi.org/10.1016/j.scitotenv.2019.135457>
- Xia, D., Tan, F., Zhang, C., Jiang, X., Chen, Z., Li, H., Zheng, Y., Li, Q., & Wang, Y. (2016). ZnCl<sub>2</sub>-activated biochar from biogas residue facilitates aqueous As(III) removal. *Applied Surface Science*, 377, 361-369. <https://doi.org/10.1016/j.apsusc.2016.03.109>
- Xiang, L., Wang, X.-D., Chen, X.-H., Mo, C.-H., Li, Y.-W., Li, H., Cai, Q.-Y., Zhou, D.-M., Wong, M.-H., & Li, Q. X. (2019). Sorption Mechanism, Kinetics, and Isotherms of Di-n-butyl Phthalate to Different Soil Particle-Size Fractions. *Journal of Agricultural and Food Chemistry*, 67(17), 4734-4745. <https://doi.org/10.1021/acs.jafc.8b06357>
- Xiang, L., Xiao, T., Mo, C.-H., Zhao, H.-M., Li, Y.-W., Li, H., Cai, Q.-Y., Zhou, D.-M., & Wong, M.-H. (2018). Sorption kinetics, isotherms, and mechanism of aniline aerofloat to agricultural soils with various physicochemical properties. *Ecotoxicology and Environmental Safety*, 154, 84-91. <https://doi.org/10.1016/j.ecoenv.2018.01.032>
- Xing, J., Xu, G., & Li, G. (2021). Comparison of pyrolysis process, various fractions and potential soil applications between sewage sludge-based biochars and lignocellulose-based biochars. *Ecotoxicology and Environmental Safety*, 208, 111756. <https://doi.org/10.1016/j.ecoenv.2020.111756>
- Xing, Z., Tian, K., Du, C., Li, C., Zhou, J., & Chen, Z. (2019). Agricultural soil characterization by FTIR spectroscopy at micrometer scales: Depth profiling by photoacoustic spectroscopy. *Geoderma*, 335, 94-103. <https://doi.org/10.1016/j.geoderma.2018.08.003>

- Xu, X.-R., & Li, X.-Y. (2010). Sorption and desorption of antibiotic tetracycline on marine sediments. *Chemosphere*, 78(4), 430-436. <https://doi.org/10.1016/j.chemosphere.2009.10.045>
- Xu, Y., & Chen, B. (2013). Investigation of thermodynamic parameters in the pyrolysis conversion of biomass and manure to biochars using thermogravimetric analysis. *Bioresource Technology*, 146, 485-493. <https://doi.org/10.1016/j.biortech.2013.07.086>
- Xue, J., Zhang, Y., Liu, Y., & Gamal El-Din, M. (2016). Effects of ozone pretreatment and operating conditions on membrane fouling behaviors of an anoxic-aerobic membrane bioreactor for oil sands process-affected water (OSPW) treatment. *Water Research*, 105, 444-455. <https://doi.org/10.1016/j.watres.2016.09.011>
- Yakout, S. M. (2015). Monitoring the Changes of Chemical Properties of Rice Straw–Derived Biochars Modified by Different Oxidizing Agents and Their Adsorptive Performance for Organics. *Bioremediation Journal*, 19(2), 171-182. <https://doi.org/10.1080/10889868.2015.1029115>
- Yang, K., Jiang, Y., Yang, J., & Lin, D. (2018). Correlations and adsorption mechanisms of aromatic compounds on biochars produced from various biomass at 700 °C. *Environmental Pollution*, 233, 64-70. <https://doi.org/10.1016/j.envpol.2017.10.035>
- Yang, X., Kang, K., Qiu, L., Zhao, L., & Sun, R. (2020). Effects of carbonization conditions on the yield and fixed carbon content of biochar from pruned apple tree branches. *Renewable Energy*, 146, 1691-1699. <https://doi.org/10.1016/j.renene.2019.07.148>
- Yuan, H., Lu, T., Wang, Y., Chen, Y., & Lei, T. (2016). Sewage sludge biochar: Nutrient composition and its effect on the leaching of soil nutrients. *Geoderma*, 267, 17-23. <https://doi.org/10.1016/j.geoderma.2015.12.020>
- Yusuff, A. S., Lala, M. A., Thompson-Yusuff, K. A., & Babatunde, E. O. (2022). ZnCl<sub>2</sub>-modified eucalyptus bark biochar as adsorbent: preparation, characterization and its application in adsorption of Cr(VI) from aqueous solutions. *South African Journal of Chemical Engineering*, 42, 138-145. <https://doi.org/10.1016/j.sajce.2022.08.002>
- Zeng, S., & Kan, E. (2021). Adsorption and regeneration on iron-activated biochar for removal of microcystin-LR. *Chemosphere*, 273, 129649. <https://doi.org/10.1016/j.chemosphere.2021.129649>

- Zhang, G., Yang, H., Jiang, M., & Zhang, Q. (2021). Preparation and characterization of activated carbon derived from deashing coal slime with ZnCl<sub>2</sub> activation. *Colloids and Surfaces A: Physicochemical and Engineering Aspects*, 128124. <https://doi.org/10.1016/j.colsurfa.2021.128124>
- Zhang, P., Zhang, X., Li, Y., & Han, L. (2020). Influence of pyrolysis temperature on chemical speciation, leaching ability, and environmental risk of heavy metals in biochar derived from cow manure. *Bioresource Technology*, 302, 122850. <https://doi.org/10.1016/j.biortech.2020.122850>
- Zheng, X., Lin, H., Tao, Y., & Zhang, H. (2018). Selective adsorption of phenanthrene dissolved in Tween 80 solution using activated carbon derived from walnut shells. *Chemosphere*, 208, 951-959. <https://doi.org/10.1016/j.chemosphere.2018.06.025>
- Zhou, W., Zhang, Y., Li, W., Jia, H., Huang, H., & Li, B. (2019). Adsorption isotherms, degradation kinetics, and leaching behaviors of cyanogen and hydrogen cyanide in eight texturally different agricultural soils from China. *Ecotoxicology and Environmental Safety*, 185, 109704. <https://doi.org/10.1016/j.ecoenv.2019.109704>
- Zhou, X. (2020). Comments on “Efficient adsorption of Mn(II) by layered double hydroxides intercalated with diethylenetriaminepentaacetic acid and the mechanistic study. *J. Environ. Sci.* 85, 56–65”. *Journal of Environmental Sciences*, 90, 409-410. <https://doi.org/10.1016/j.jes.2020.01.015>
- Zhou, X., & Zhou, X. (2014). The unit problem in the thermodynamic calculation of adsorption using the Langmuir equation. *Chemical Engineering Communications*, 201(11), 1459-1467. <https://doi.org/10.1080/00986445.2013.818541>
- Zhu, S., Li, M., & Gamal El-Din, M. (2018). The roles of pH and draw solute on forward osmosis process treating aqueous naphthenic acids. *Journal of Membrane Science*, 549, 456-465. <https://doi.org/10.1016/j.memsci.2017.12.029>
- Zhu, X., Liu, Y., Qian, F., Zhou, C., Zhang, S., & Chen, J. (2014). Preparation of magnetic porous carbon from waste hydrochar by simultaneous activation and magnetization for tetracycline removal. *Bioresource Technology*, 154, 209-214. <https://doi.org/10.1016/j.biortech.2013.12.019>

- Zhu, Y., & Kolar, P. (2014). Adsorptive removal of p-cresol using coconut shell-activated char. *Journal of Environmental Chemical Engineering*, 2(4), 2050-2058. <https://doi.org/10.1016/j.jece.2014.08.022>
- Zielińska, A., Oleszczuk, P., Charmas, B., Skubiszewska-Zięba, J., & Pasieczna-Patkowska, S. (2015). Effect of sewage sludge properties on the biochar characteristic. *Journal of Analytical and Applied Pyrolysis*, 112, 201-213. <https://doi.org/10.1016/j.jaap.2015.01.025>
- Zubot, W., MacKinnon, M. D., Chelme-Ayala, P., Smith, D. W., & Gamal El-Din, M. (2012). Petroleum coke adsorption as a water management option for oil sands process-affected water. *Science of the Total Environment*, 427-428, 364-372. <https://doi.org/10.1016/j.scitotenv.2012.04.024>



## **APPENDIX: SUPPORTING INFORMATION**

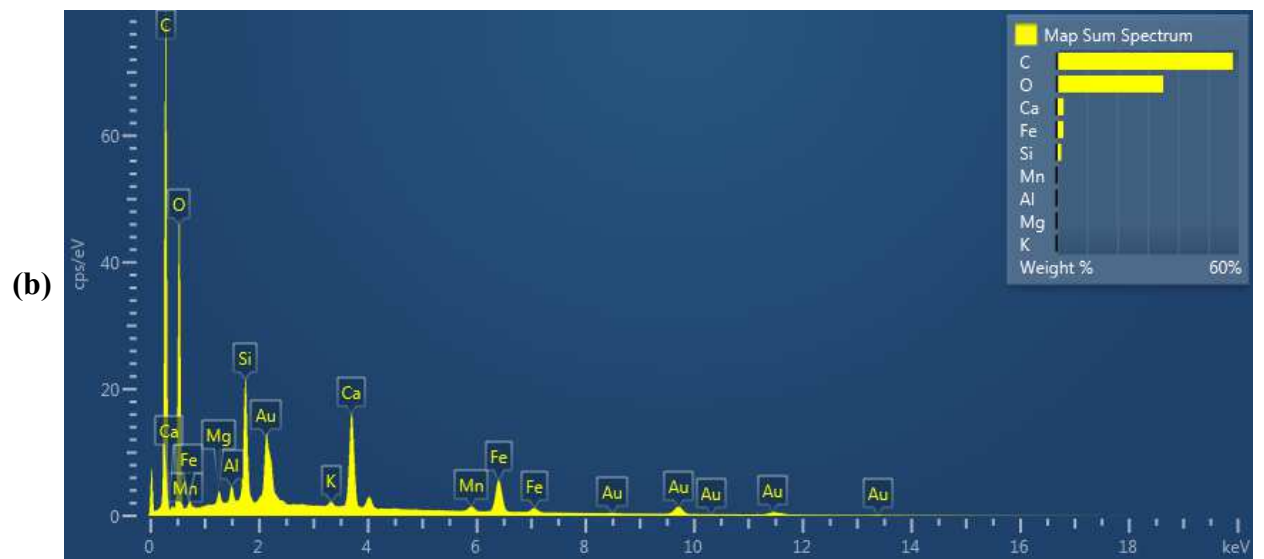
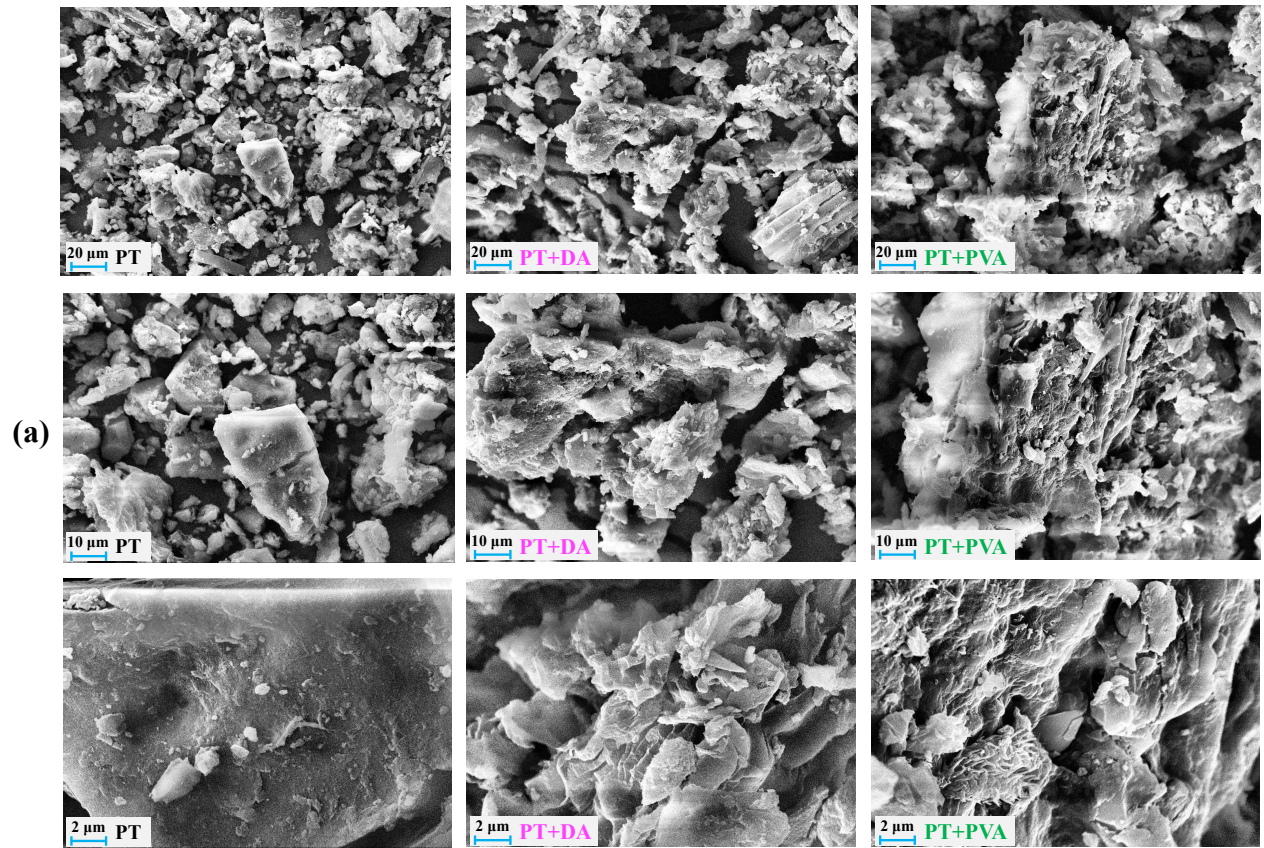
### **Analytical methods for the measurement of model compounds of NAs in solution and classical and oxidized NAs in OSPW**

Prior to analysis, all samples were filtered using 0.2  $\mu\text{m}$  filters (Basix™ Nylon Syringe Filters, Fisher Scientific, USA).

The concentrations of model compounds were determined with a liquid chromatography - mass spectrometry (LC-MS, Waters, USA) using a C18 column (1.7  $\mu\text{m}$ , 50 mm $\times$  2.1 mm) and column temperature was set at 40°C. The flow rate and injection volume were 0.4 mL min<sup>-1</sup> and 2  $\mu\text{L}$ , respectively. The analyzes were performed with a mobile phase of 4 mM ammonium acetate with 0.1% acetic acid and 100% acetonitrile.

The concentration of NAs in real OSPW was determined based on method presented by Huang et al. (2015b) using an ultra-high performance liquid chromatography-quadrupole time-of-flight mass spectrometry with electrospray ionization (ESI) in negative mode (UPLC-QTOF-MS, Synapt G2, Waters, USA). A UPLC Phenyl BEH column (1.7  $\mu\text{m}$ , 150 mm x 1 mm) (Waters, USA) was used to achieve chromatographic separation of samples. TOF analyzer was in high-resolution mode and an internal standard was employed to allow the calculation of NA concentrations based upon peak area.

# Figures



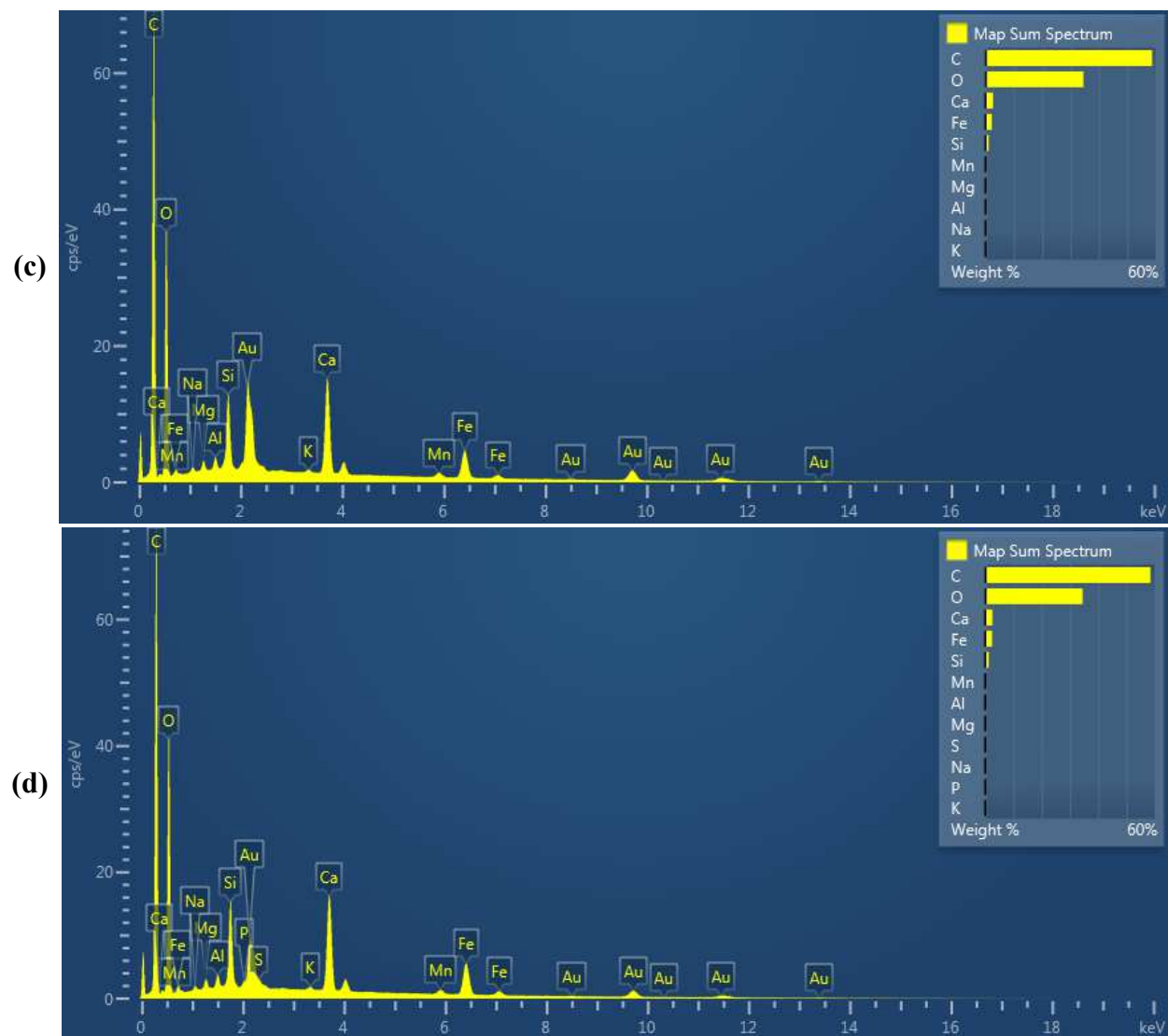
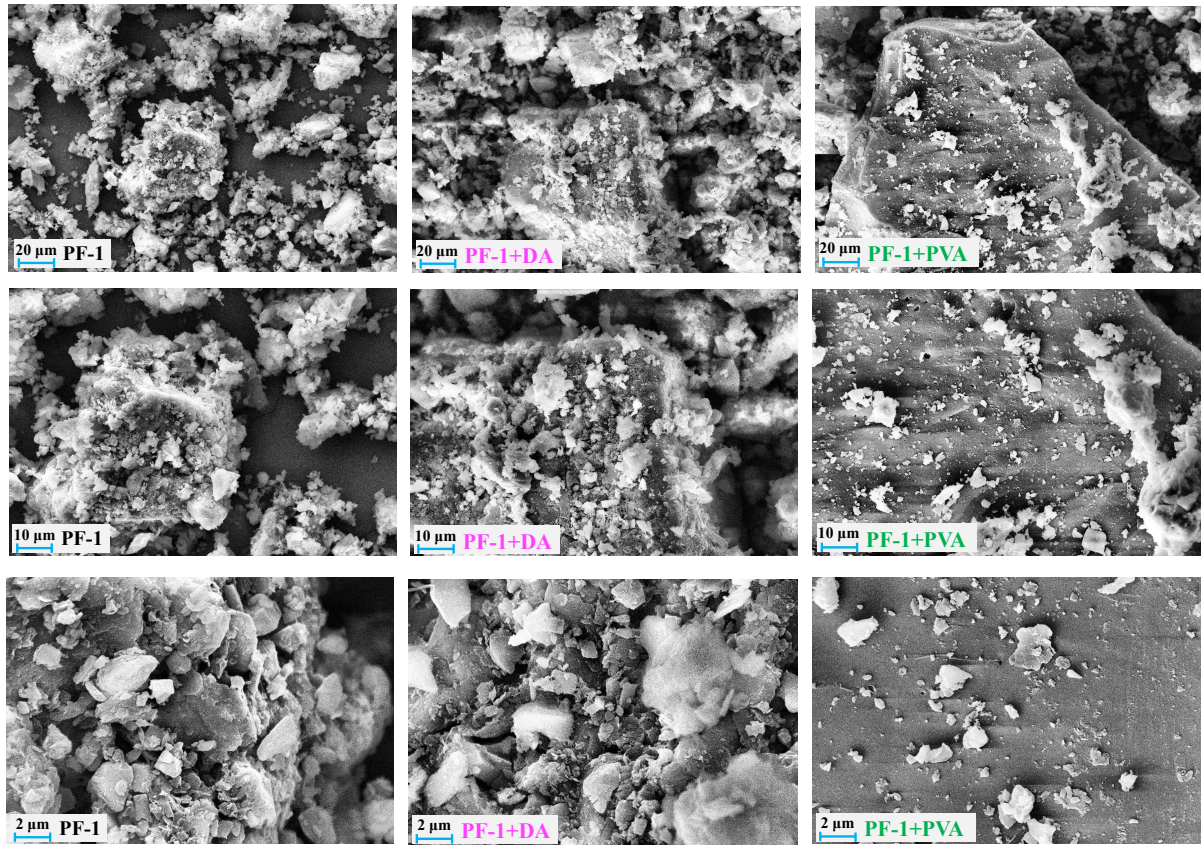
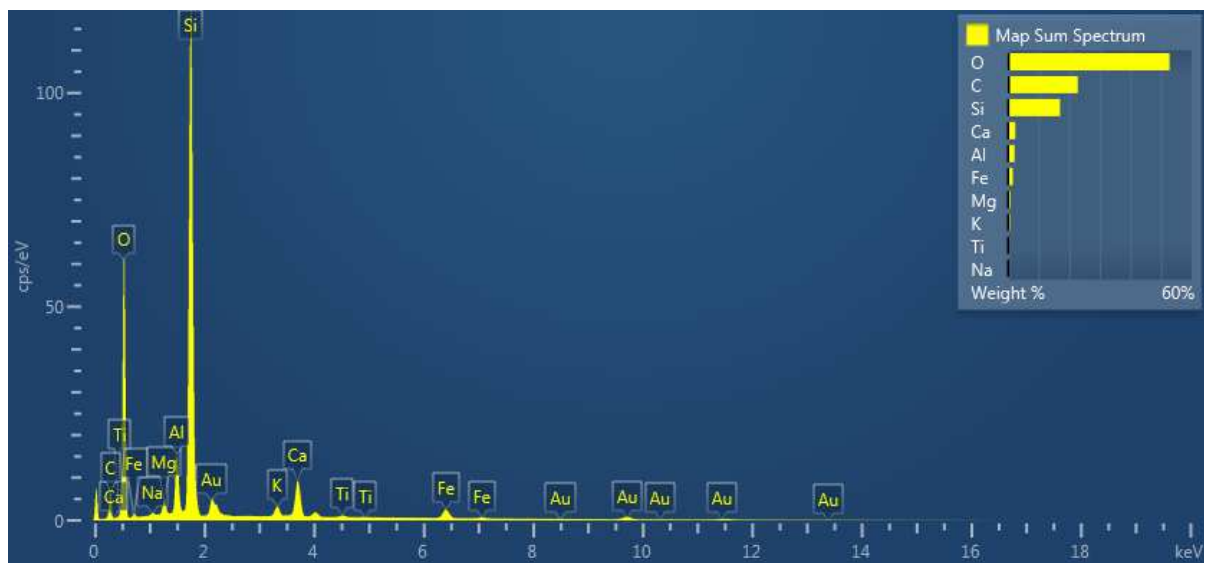


**Figure S1:** (a) SEM images of PT reclamation material before and after adsorption of model NA compounds at magnification from 500 to 5000 times. EDX spectra of PT reclamation material (b) before adsorption, and after adsorption of (c) DA and (d) PVA.

(a)



(b)



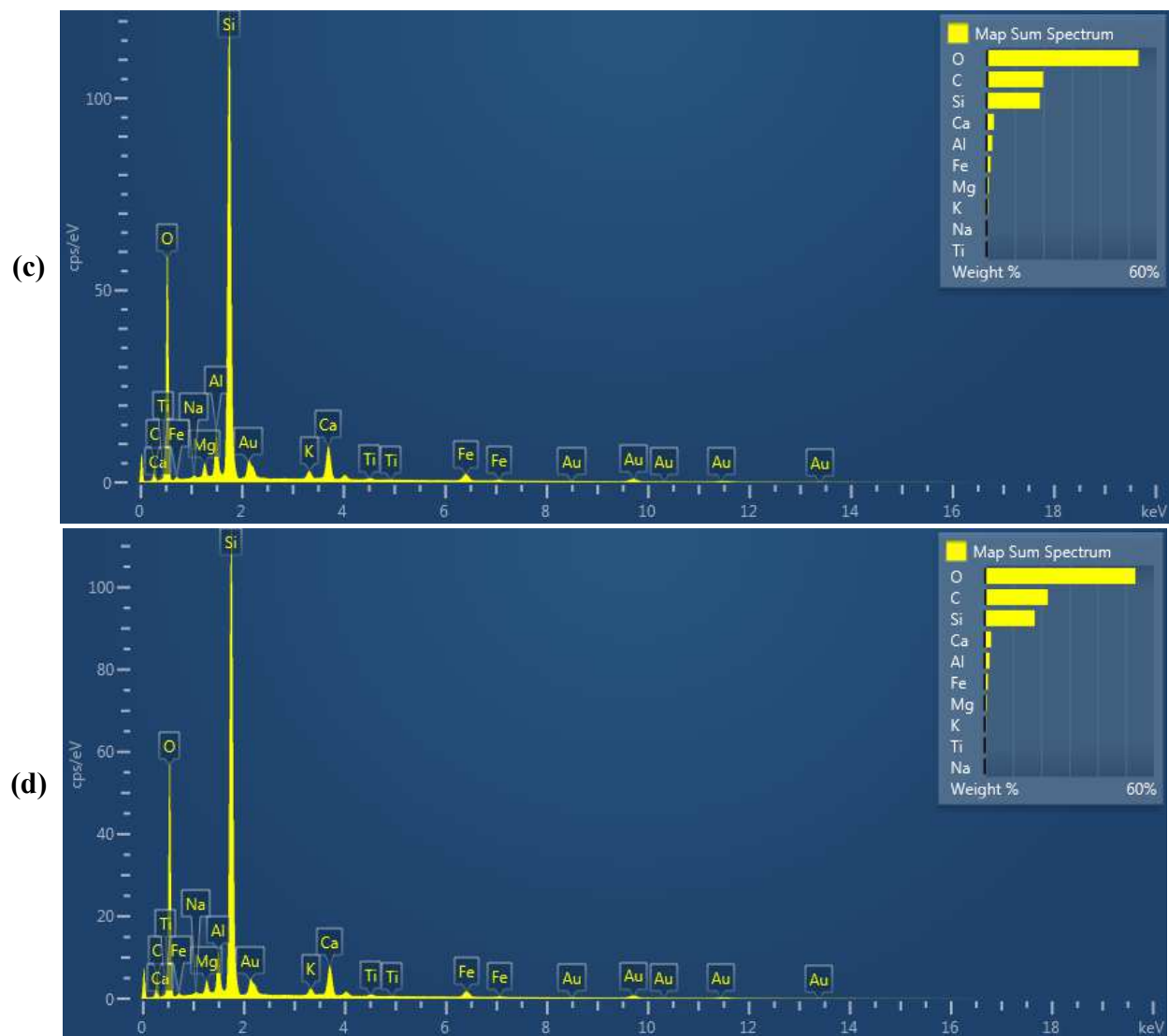
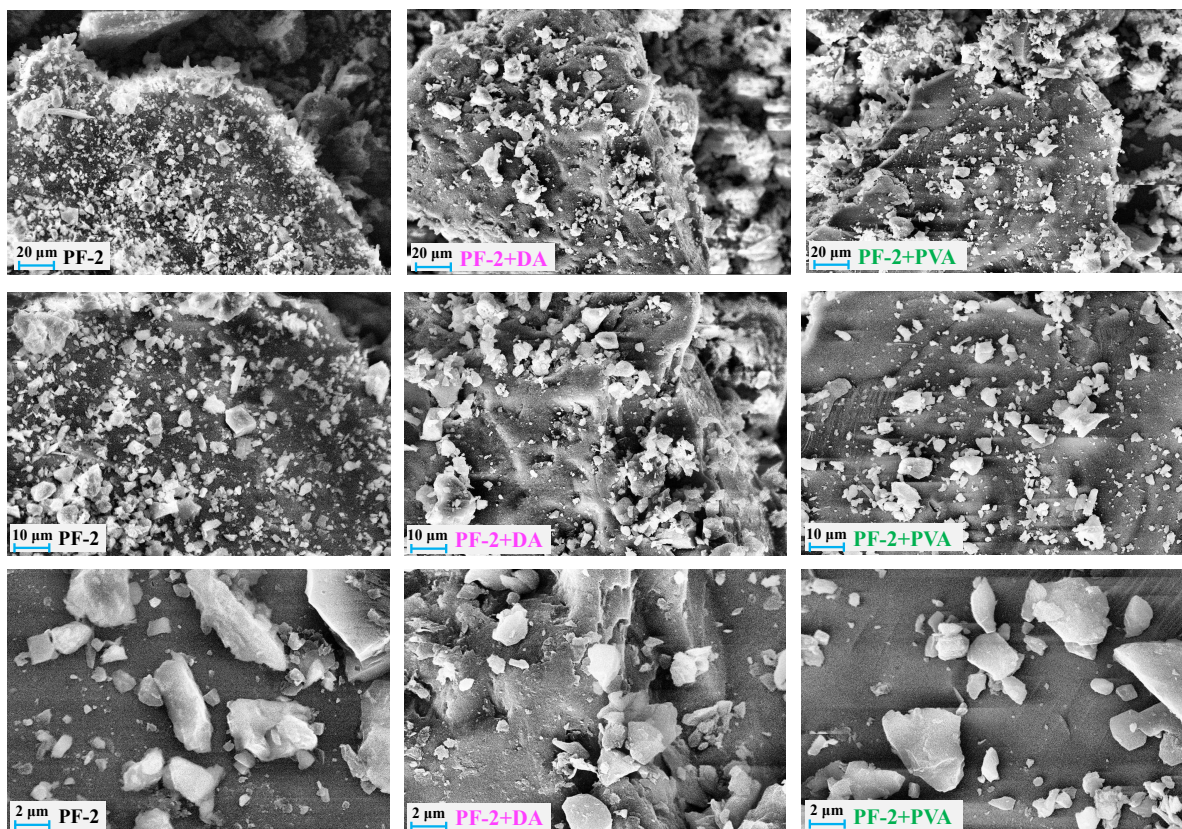
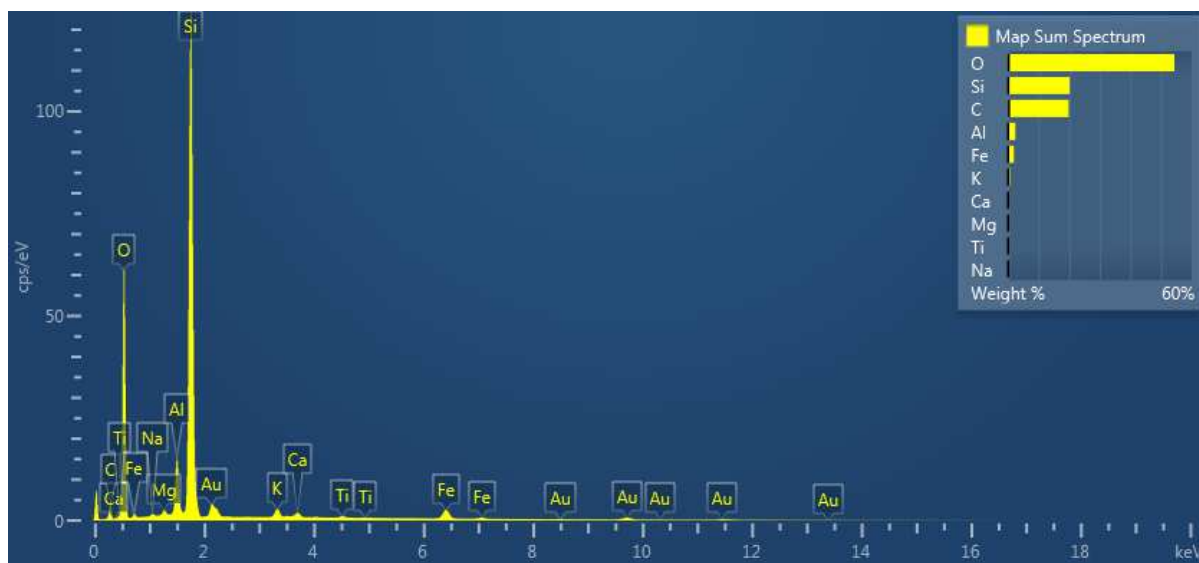


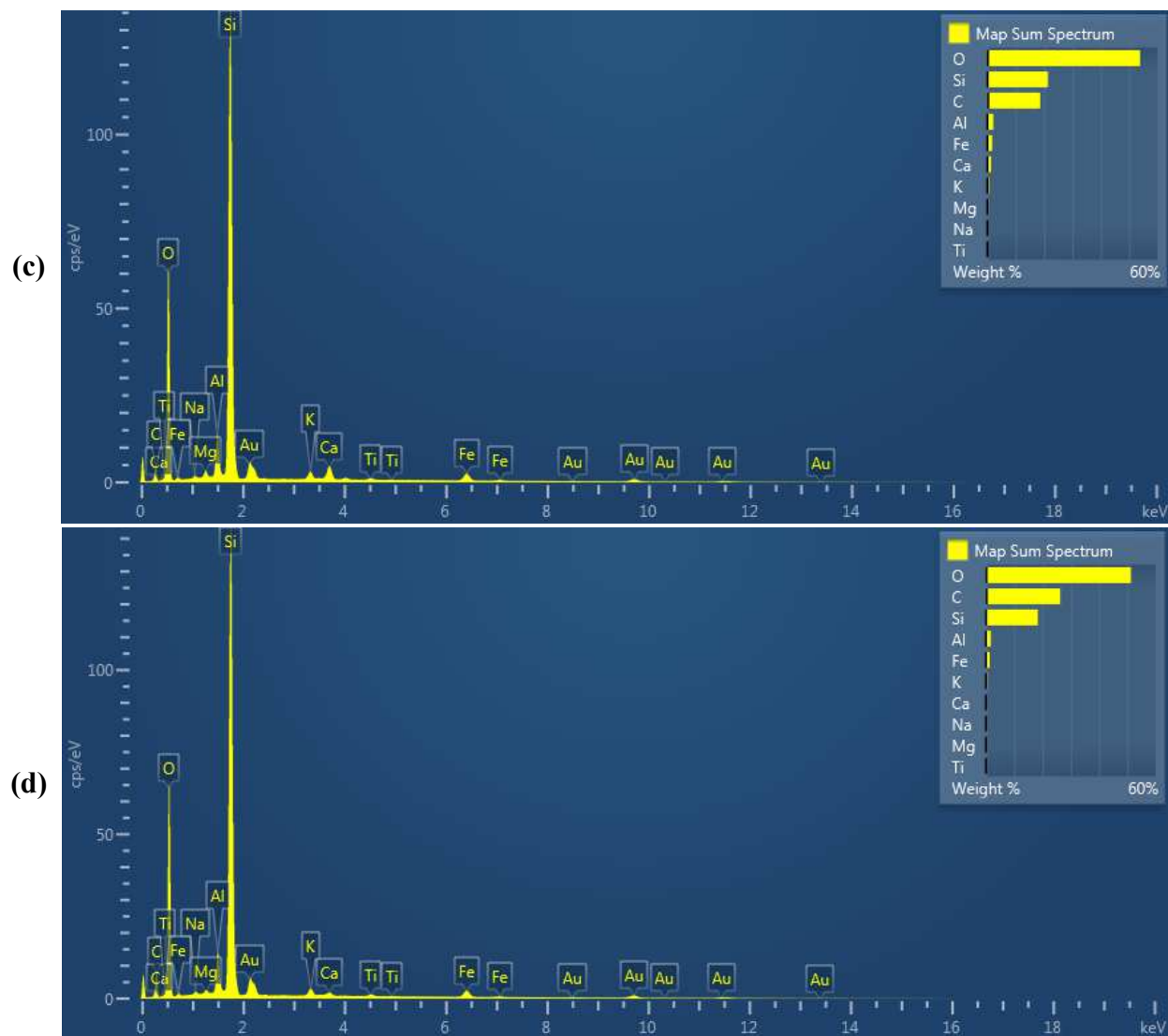
**Figure S2:** (a) SEM images of PF-1 reclamation material before and after adsorption of model NA compounds at magnification from 500 to 5000 times. EDX spectra of PF-1 reclamation material (b) before adsorption, and after adsorption of (c) DA and (d) PVA.

(a)

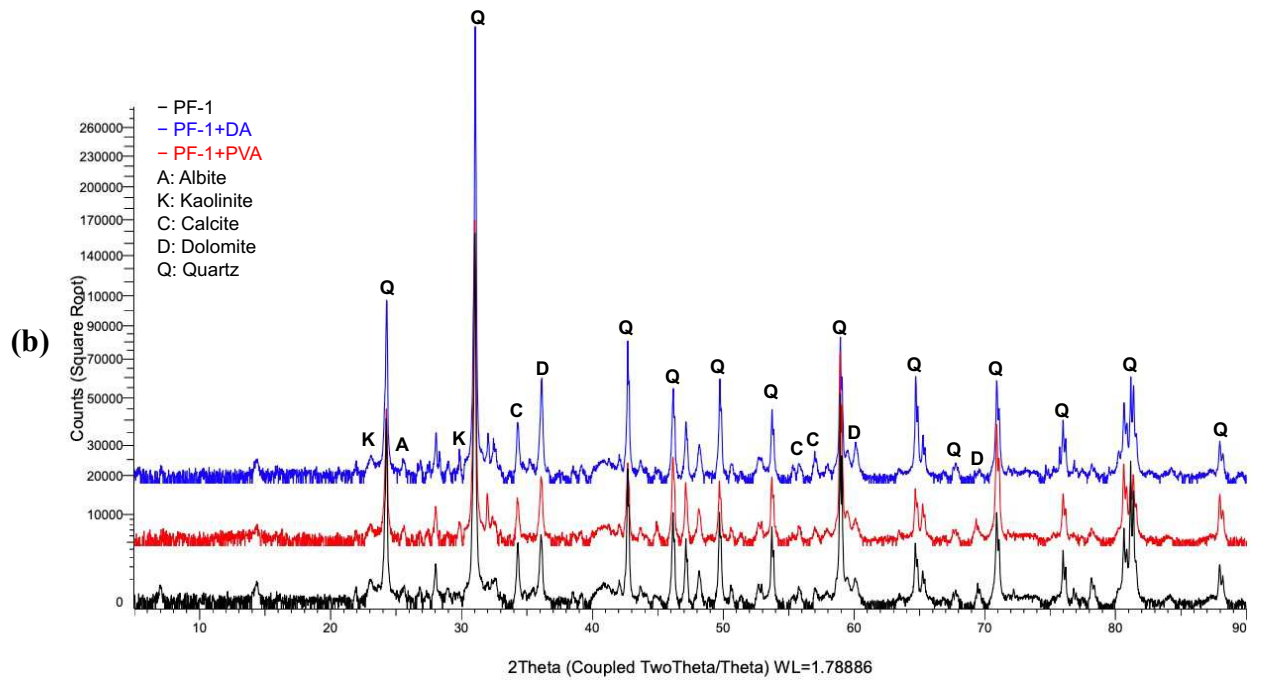
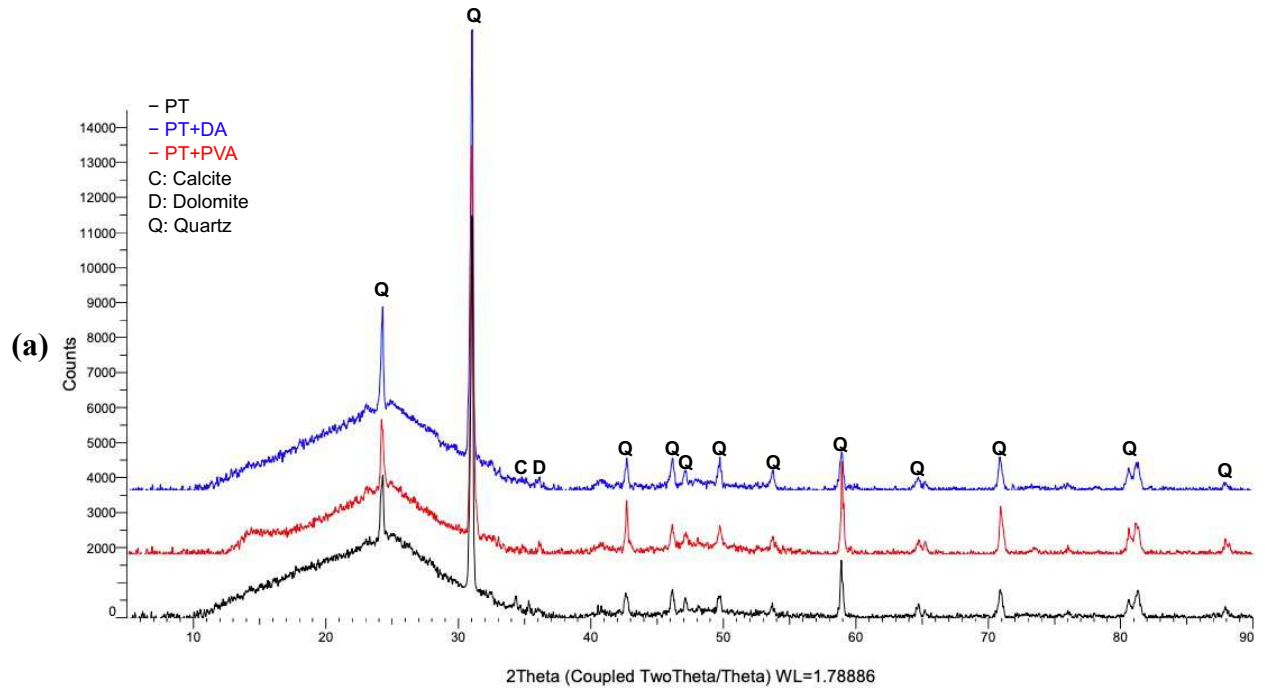


(b)





**Figure S3:** (a) SEM images of PF-2 reclamation material before and after adsorption of model NA compounds at magnification from 500 to 5000 times. EDX spectra of PF-2 reclamation material (b) before adsorption, and after adsorption of (c) DA and (d) PVA.





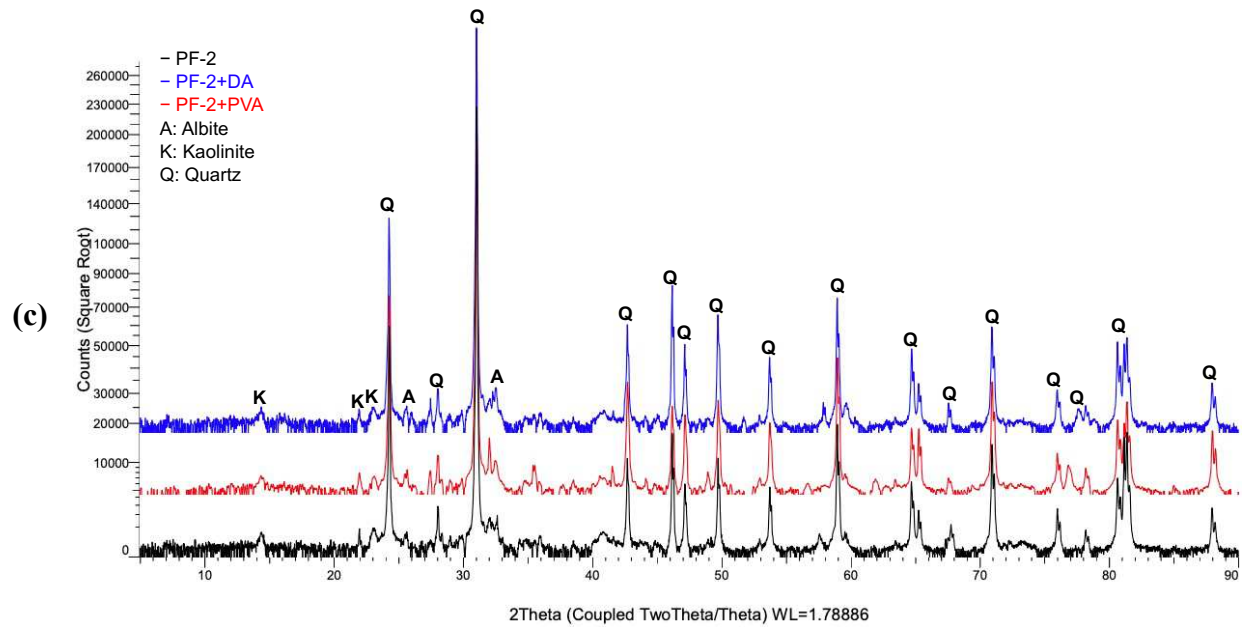


**Figure S4:** X-ray diffractograms obtained for (a) PT, (b) PF-1, and (c) PF-2 materials before and after adsorption.

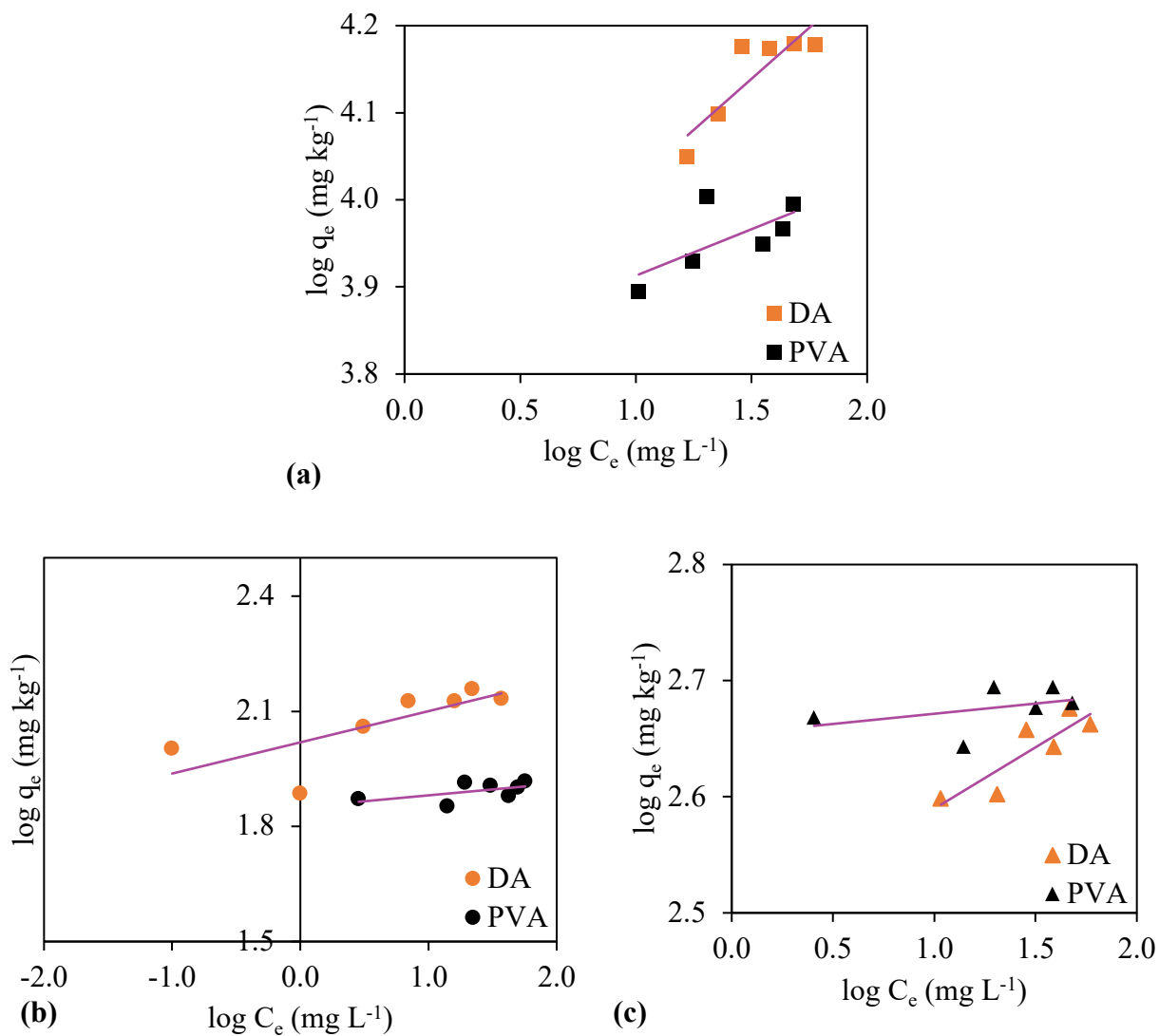


**Figure S5:** Fittings of the Freundlich isotherm for the adsorption of model NA compounds at different initial concentrations using reclamation materials (a) PT, (b) PF-1, and (c) PF-2.

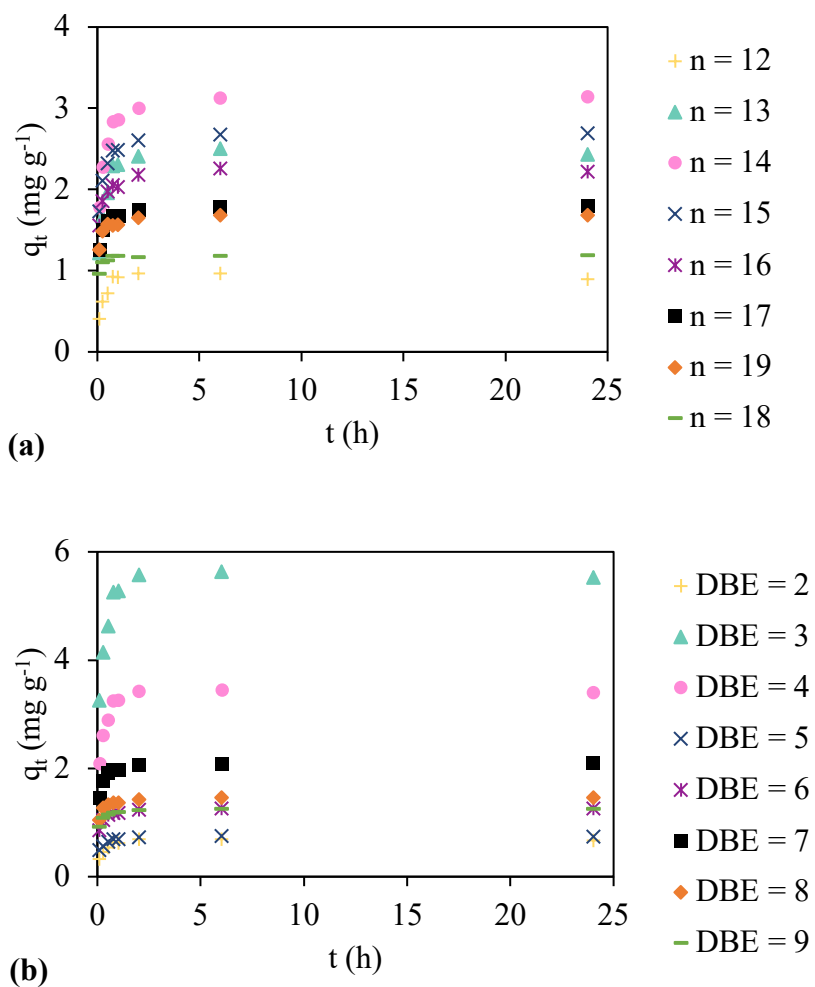


**Figure S6:** Adsorption capacity of classical NAs from raw OSPW treated with  $2 \text{ g L}^{-1}$  of SB-Zn for different times partitioned by (a) carbon and (b) DBE numbers.

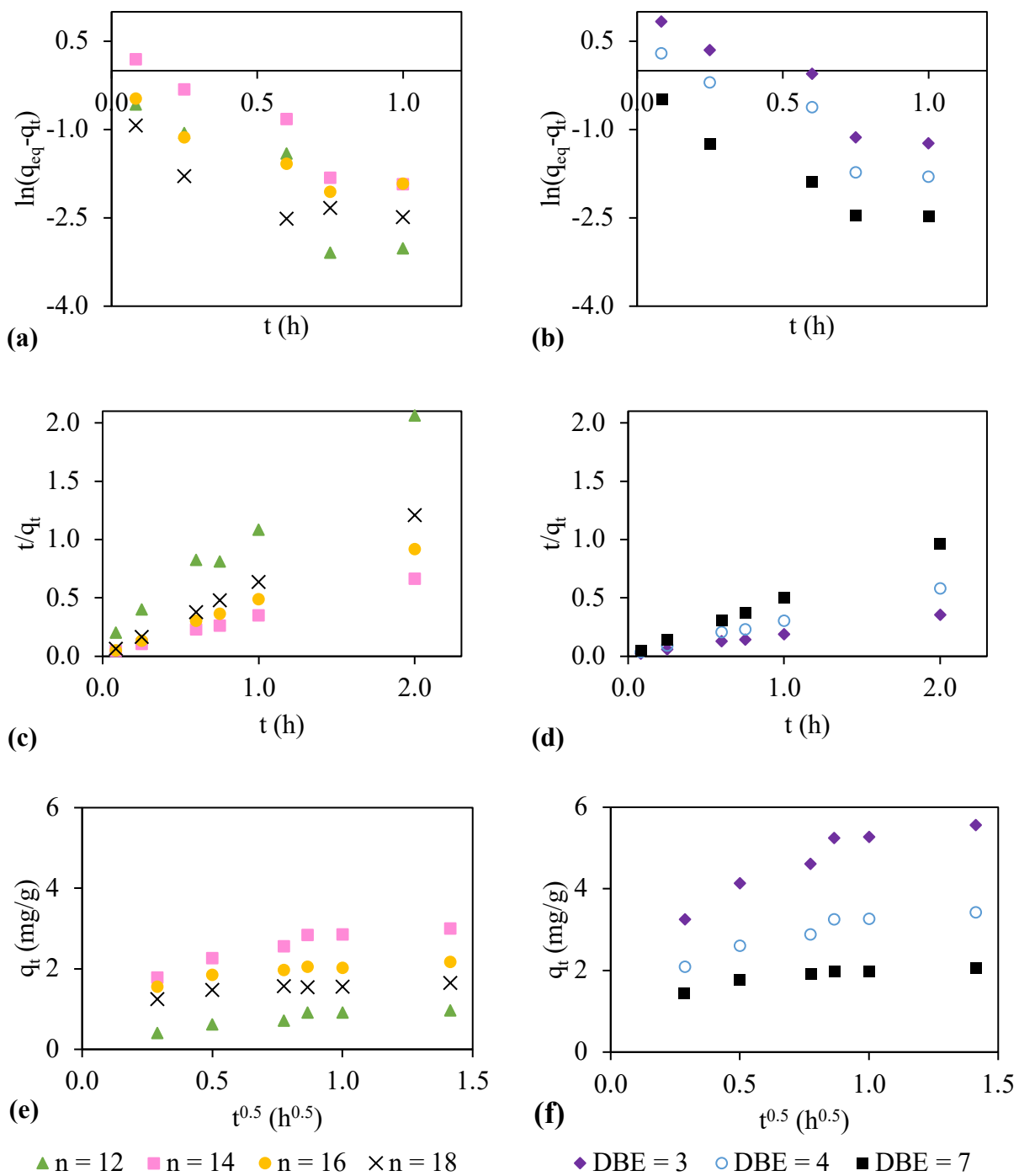
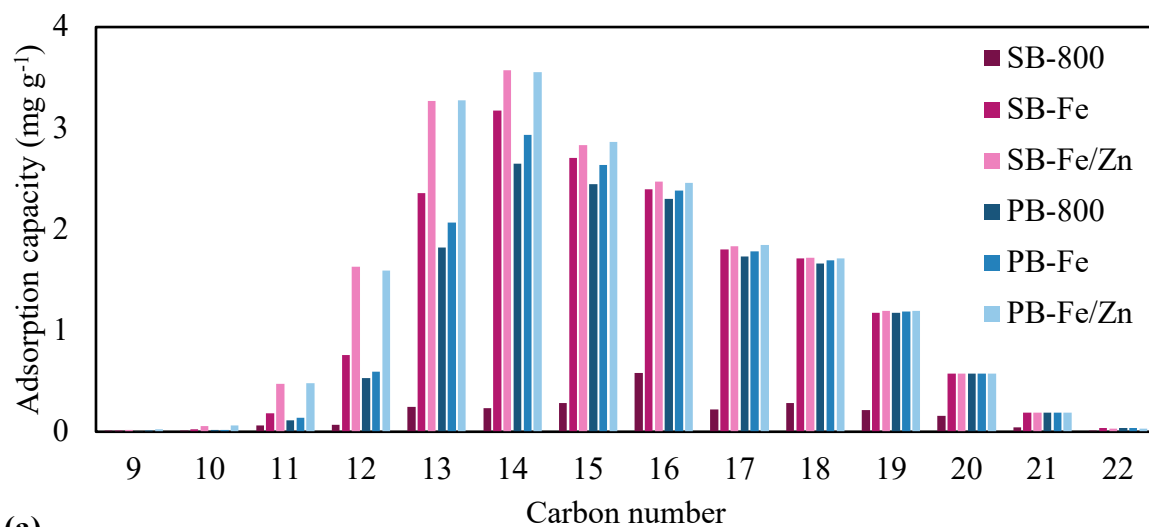
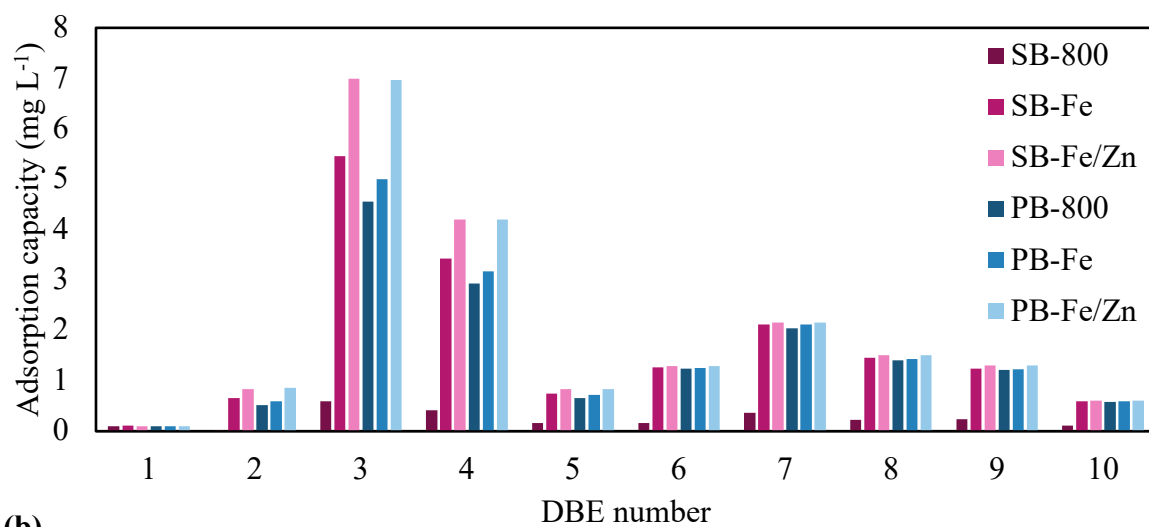


**Figure S7:** (a,b) PFO and (c,d) PSO kinetic modelling, and (e,f) IPD modelling for the adsorption of NAs on  $2 \text{ g L}^{-1}$  SB-Zn for different adsorption times as a function of carbon numbers ( $n$ ) 13 to 15 and DBE numbers 4, 6, and 12.



(a)



(b)

**Figure S8:** Adsorption capacity of classical NAs in terms of carbon and DBE numbers in raw OSPW and OSPW treated with biochars from sludge and peat.

## Tables

**Table S1:** Adsorption capacity of classical NAs from raw OSPW in terms of carbon and -Z numbers by the reclamation materials PT (5 g L<sup>-1</sup>), PF-1 (500 g L<sup>-1</sup>), and PF-2 (100 g L<sup>-1</sup>). Adsorption conditions: Initial concentration of classical NAs in OSPW: 46.3 mg L<sup>-1</sup>; contact time of 2 days for PT and 6 days for PF-1 and PF-2 materials.

Carbon number	Adsorption capacity (mg kg <sup>-1</sup> )			-Z	Adsorption capacity (mg kg <sup>-1</sup> )		
	PT	PF-1	PF-2		PT	PF-1	PF-2
8	0.93	0.01	0.07	0	12.79	0.13	0.41
9	4.47	0.06	0.30	2	55.56	0.39	4.28
10	3.89	0.08	0.45	4	778.84	8.69	40.30
11	38.99	0.30	2.43	6	259.92	6.03	18.69
12	77.49	0.24	3.24	8	75.48	1.74	7.66
13	482.50	2.44	25.72	10	108.30	1.80	12.25
14	178.19	4.31	13.46	12	125.79	3.07	16.46
15	292.40	5.37	15.58	14	186.81	3.68	10.79
16	192.42	4.61	19.45	16	175.92	3.44	8.33
17	146.19	2.96	12.89	18	96.04	2.13	8.19
18	136.51	3.44	11.72				
19	147.31	3.62	9.98				
20	96.28	2.27	7.50				
21	51.98	1.00	2.92				
22	21.24	0.34	1.41				
23	4.24	0.04	0.21				

**Table S2:** Pearson correlation coefficient between adsorption properties ( $K_d$ ,  $K_{OC}$ ,  $q_{max}$ , and  $q_t$  values) and physicochemical properties of reclamation materials obtained from an oil sands extraction site.

Parameters	$K_{d,50}^a$		$K_{d,100}^a$		$K_d^a$	$K_{OC,50}^a$		$K_{OC,100}^a$		$K_{OC}^a$	$q_{max}^b$		$q_t^b$
	DA	PVA	DA	PVA	O <sub>2</sub> -NAs	DA	PVA	DA	PVA	O <sub>2</sub> -NAs	DA	PVA	O <sub>2</sub> -NAs
pH	0.24	-0.98	-0.92	-0.93	-0.93	0.82	0.03	-0.65	-0.38	-0.04	-0.92	-0.93	-0.93
EC ( $\mu\text{S cm}^{-1}$ )	0.25	0.95	1.00	0.99	0.99	-0.46	-0.50	0.21	-0.11	-0.43	1.00	0.99	0.99
CEC ( $\text{cmol}(+) \text{kg}^{-1}$ )	0.18	0.97	1.00*	1.00*	1.00*	-0.52	-0.44	0.27	-0.04	-0.37	1.00*	1.00*	1.00*
pH <sub>pzc</sub>	0.76	-0.69	-0.52	-0.54	-0.55	1.00	-0.56	-0.97	-0.85	-0.62	-0.53	-0.54	-0.55
TOC (%)	0.18	0.97	1.00*	1.00*	1.00*	-0.51	-0.44	0.27	-0.04	-0.38	1.00*	1.00*	1.00*
Clay (%)	0.58	-0.85	-0.72	-0.73	-0.74	0.97	-0.34	-0.88	-0.69	-0.40	-0.72	-0.73	-0.74
Silt (%)	0.34	0.92	0.98	0.98	0.98	-0.36	-0.58	0.11	-0.21	-0.52	0.98	0.98	0.98
Sand (%)	-0.64	-0.73	-0.86	-0.85	-0.84	0.03	0.82	0.23	0.52	0.78	-0.86	-0.85	-0.85
Surface area ( $\text{m}^2 \text{g}^{-1}$ )	0.11	-1.00	-0.96	-0.97	-0.97	0.74	0.16	-0.54	-0.25	0.09	-0.96	-0.97	-0.97
Al ( $\text{g kg}^{-1}$ )	-0.15	-0.98	-1.00*	-1.00*	-1.00*	0.54	0.41	-0.30	0.01	0.35	-1.00*	-1.00*	-1.00*
Ca ( $\text{g kg}^{-1}$ )	0.71	0.66	0.81	0.79	0.79	0.07	-0.87	-0.33	-0.60	-0.84	0.80	0.79	0.79
Fe ( $\text{g kg}^{-1}$ )	0.19	0.97	1.00*	1.00*	1.00*	-0.51	-0.44	0.26	-0.05	-0.38	1.00*	1.00*	1.00*
Mg ( $\text{g kg}^{-1}$ )	0.97	-0.29	-0.08	-0.11	-0.11	0.89	-0.87	-0.98	-1.00	-0.90	-0.09	-0.10	-0.11
Si ( $\text{g kg}^{-1}$ )	0.18	-0.99	-0.94	-0.95	-0.95	0.78	0.09	-0.59	-0.31	0.02	-0.95	-0.95	-0.95

<sup>a</sup> Adsorption coefficients ( $\text{L kg}^{-1}$ ) for DA and PVA at 50 and 100  $\text{mg L}^{-1}$  and classical NAs obtained from experiments using real OSPW.

<sup>b</sup> Adsorption capacities ( $\text{mg kg}^{-1}$ ).

\*Statistically significant correlation ( $p\text{-value} < 0.05$ ).

**Table S3:** Properties of biological sludge.

<b>Parameters</b>	<b>Units</b>	<b>Sludge</b>
pH	–	7.5
Chemical oxygen demand (COD)	(g L <sup>-1</sup> )	24.4
Al	(g kg <sup>-1</sup> )	9.3
As	(g kg <sup>-1</sup> )	0.004
Ca	(g kg <sup>-1</sup> )	24.3
Cd	(g kg <sup>-1</sup> )	<0.001
Cr	(g kg <sup>-1</sup> )	0.07
Cu	(g kg <sup>-1</sup> )	0.4
Fe	(g kg <sup>-1</sup> )	10.4
K	(g kg <sup>-1</sup> )	13.3
Mg	(g kg <sup>-1</sup> )	8.4
Mn	(g kg <sup>-1</sup> )	0.2
Mo	(g kg <sup>-1</sup> )	0.01
Na	(g kg <sup>-1</sup> )	4.4
P	(g kg <sup>-1</sup> )	28.5
Pb	(g kg <sup>-1</sup> )	0.02
S	(g kg <sup>-1</sup> )	9.7
Si	(g kg <sup>-1</sup> )	2.0
Sr	(g kg <sup>-1</sup> )	0.2
Zn	(g kg <sup>-1</sup> )	0.6



**Table S4:** Summary of modeling kinetics parameters obtained for adsorption of classical NAs from raw OSPW on SB-Zn as a function of carbon and DBE numbers.

Models and parameters		Carbon number (n)						DBE number					
		12	13	14	15	16	17	18	3	4	6	7	9
<b>Initial concentration (mg L<sup>-1</sup>)</b>		3.4	6.6	7.2	5.7	5.0	3.7	3.5	14.1	8.5	2.6	4.3	2.6
<b>q<sub>e,exp</sub>(mg g<sup>-1</sup>)</b>		1.0	2.4	3.0	2.6	2.2	1.8	1.7	5.6	3.4	1.3	2.1	1.2
<b>PSO</b>	<b>K<sub>PSO</sub></b>	5.79	3.26	3.58	5.49	7.71	11.2	14.6	1.75	3.15	14.9	10.0	19.9
	<b>R<sup>2</sup></b>	0.99	1.00	1.00	1.00	1.00	1.00	1.00	1.00	1.00	1.00	1.00	1.00
<b>IPD</b>	<b>K<sub>IPD, film</sub></b>	0.79	1.70	1.69	1.22	0.79	0.69	0.50	3.12	1.82	0.54	0.86	0.41
	<b>R<sup>2</sup></b>	0.93	0.97	0.97	0.97	0.93	0.94	0.84	0.96	0.96	0.93	0.93	0.90
	<b>K<sub>IPD, pore</sub></b>	0.09	0.22	0.31	0.25	0.26	0.15	0.18	0.61	0.34	0.11	0.17	0.09
	<b>R<sup>2</sup></b>	0.91	0.99	0.98	0.95	0.98	0.97	0.99	0.98	0.97	0.95	0.95	0.99

K<sub>PSO</sub>: g mg<sup>-1</sup> h<sup>-1</sup>

K<sub>IPD</sub>: mg g<sup>-1</sup> h<sup>-0.5</sup>